Shifting To Renewable Furan Candidates: Synthesis and Study of New Optoelectronic Materials

Brandon Cigana

A Thesis

in the Department

of

Chemistry & Biochemistry

Presented in Partial Fulfillment of the Requirements

For the Degree of Master of Science (Chemistry) at

Concordia University

Montreal, Quebec, Canada

March 2024

CONCORDIA UNIVERSITY

School of Graduate Studies

This is to certify that the thesis prepared

By: Brandon Cigana

Entitled: Shifting To Renewable Furan Candidates: Synthesis and Study of New Optoelectronic Materials

and submitted in partial fulfillment of the requirements for the degree of

Master of Science (Chemistry)

complies with the regulations of the University and meets the accepted standards with respect to originality and quality.

Signed by the final examining committee:

_____ Chair

Dr. Rafik Naccache

_____ Examiner

Dr. Louis Cuccia

_____ Examiner

Dr. Rafik Naccache

_____ Thesis Supervisor

Dr. Pat Forgione

Approved by _____

Dr. Paul Joyce, Chair of Department

_____ 2024 _____

Dr. Pascale Sicotte, Dean of Faculty

Abstract

Shifting To Renewable Furan Candidates: Synthesis and Study of New Optoelectronic Materials

Brandon Cigana

With climate concerns consistently growing, the chemical industry must shift away from petrochemicals and turn to sustainable feedstocks derived from lignocellulosic biomass. There is urgency to develop new synthetic methodologies that effectively convert biomass-derived starting materials into useful consumer products. The production of multi-arylated furans and 2,5-furan-based oligomers, has gained popularity as organic candidates for light-emitting diodes or field-effect transistors, owing to their favourable optoelectronic properties found in highly conjugated furan-based materials. Hydroxymethylfurfural and furfural are biomass-derived platform chemicals that have received attention as raw materials due to their chemical functionality, renewability, and capability to produce various furan-containing building blocks. In this work, we aim to develop a synthetic methodology starting from biomass-derived chemicals to design potential optoelectronics. Hydroxymethylfurfural was studied to develop multi-arylated furans; however, a rigid diol monomer was synthesized instead. Working with methyl-5-bromofuran-2-carboxylate led to three different multi-arylated furans *via* regioselective halogenations followed by Pd-catalyzed cross-coupling reactions. 5-Bromofurfural, a close derivative of biomass-derived furfural, was an ideal candidate to produce ten 2,5-furan-based oligomers and one 2,5-furan-based push-pull chromophore. To rapidly extend the π-conjugation of each material, a double Pd-catalyzed decarboxylative cross-coupling (DCC) reaction was utilized. This strategy fuses two nucleophilic arylated furan acids with a dihalogenated aryl linker to produce highly planar furan-based oligomers. Regarding overall yields of the double DCC, electron-neutral and electron-donating furan acids exhibited higher yields (32 – 74%) than electron-withdrawing acid derivatives (18 – 21%). All furan-based compounds were then characterized by NMR and their absorbance, photoluminescence and quantum yields were studied in dilute solution.

Acknowledgements

This work could not have been made possible without the tremendous help and support from many individuals from Concordia University as well as my family and friends.

I would like to personally thank my supervisor, Dr. Pat Forgione, for his guidance, patience, and encouragement throughout this scientific journey. Being a member of this research group under his mentorship has not only deepened my scientific curiosity but has also equipped me with invaluable presentation skills which I intend to further utilize in my future endeavors. The most important measure Dr. Forgione values is the steady growth of his students. Beginning as an inexperienced undergrad in his group, I would ask graduate students to ensure I was doing a liquid-liquid extraction correctly. Where presently, I hope to publish a paper alongside him (currently in review). I am proud and honoured to have learned so much from him, thank you for allowing me to improve my organic chemistry abilities. I could not have grown as much as I have without you.

I am also wholly grateful to my committee members, Dr. Louis Cuccia and Dr. Rafik Naccache for their insightful feedback and perspective throughout each committee meeting. They have continuously kept me on my toes with their questions. It has been a privilege to have you both on this committee, you have given me great constructive criticism which has enhanced this thesis.

A big and sincere thank you to all fORGione lab members: Sevag Pilavdjian, Phil Prevost, Keegan Mckibbon, Venelin Petkov, Emma Shaver, Helena Braga, Sarah Taylor, Dipanjan Bhattacharyya and Rafael Hernandez. You have all helped me tremendously through this program, I could not have done it without you and your excellent feedback throughout my time here.

A special thank you to Dr. Cynthia Messina, who guided me as an undergraduate during their graduate studies. You have given me so much wisdom and guidance as a scientist, it was a pleasure to learn and work with you. Thank you to Dr. Gabi Mandl for proofreading this document and being exceptionally patient with my writing.

Thank you to my collaborators Victoria Lapointe and Dr. Marek Majewski of the Majewski research group. Victoria graciously performed all the optical spectroscopy properties of the final compounds. It has been a true delight to have worked with both of you during this process, you have expanded my interest in developing fluorescent organic compounds.

Finally, I'd like to thank my supporting family: my mother, my father, my sister Karina, my Nonnas, aunts, uncles, and cousins (James Paul Michael Montesi), as well as my loving girlfriend, Rose Marie Lecchino. Thank you for your encouragement throughout this academic journey. I love you all and am forever grateful to have you in my life. My parents always said to stay in school, and the smartest decision I ever made was to listen to them.

Dedications

This work is dedicated to my late nonno Marco who was able to watch me grow but has not seen what I have been able to accomplish.

Ci manchi ogni giorno. Ti amo sempre.

Table of Contents

List of figures ix

List of tables xiii

List of equations xiv

List of abbreviations xv

Chapter 1. Introduction 1

1.1 Consumption of Petrochemicals and its Impact on the Environment 1

1.1.1 Principles of Green Chemistry 5

1.1.2 Plant-Based Biomass-Derived Chemicals as a Renewable Feedstock 7

1.1.3 Furan Starting Chemicals Derived from Lignocellulosic Biomass 10

1.2 Comparing Heterocyclic Properties of Furans to Thiophenes 14

1.2.1 Highly Planar π-Conjugated 2,5-Furans as Optoelectronic Candidates 16

1.2.2 General Cross-Coupling Synthesis of π-Conjugated 2,5-Furans 18

1.2.3 Evaluation of Cyclization Synthesis on π-Conjugated Furans 21

1.3 Palladium-Catalyzed Cross-Coupling Reactions of Heterocycles 23

1.3.1 Stille Cross-Coupling Reactions of Heterocycles 25

1.3.2 Suzuki Cross-Coupling Reactions of Heterocycles 26

1.3.3 Decarboxylative Cross-Coupling Reactions of Heterocycles 28

1.4 Research Goals and Thesis Organization 32

Chapter 2. Synthesis of Multi-Arylated Furans *via* Pd-catalyzed Cross-Coupling Reactions 33

2.1 Introduction 33

2.2 Results and Discussion on HMF as a Starting Material 35

2.3 Results and Discussion on Methyl-5-bromofuran-2-carboxylate as a Starting Material 45

2.4 Spectroscopic Data of Multi-Arylated Furan Compounds 50

2.5 Conclusion 53

Chapter 3. Synthetic Methodology to Access 2,5-Furan-Based Phenylene/Thiophene Oligomers 54

3.1 Introduction 54

3.2 Previous Synthesis on Accessing Small Furan-Based Co-Oligomers 55

3.3 Results and Discussion 56

3.4 Spectroscopic Data of 2,5-Furan-Based Phenylene/Thiophene Oligomers 75

3.5 Conclusion 81
Chapter 4. General Conclusions and Future Work 82
Chapter 5. Experimental Information 83
5.1 General Conditions and Instrumentations 83
5.2 Atom Economy and E-factor Calculations 84
5.3 Experimental Procedures and Characterization of Compounds 87
5.4 ^{1}H NMR and ^{13}C NMR Spectra 112
References 158

List of figures

Figure 1. Graph depicting the monthly mean concentration of global CO_2 abundance over marine surface sites from 1980 to 2022.[4]……..2

Figure 2. Graph depicting yearly temperature anomalies from 1880 to 2020 with 1951 to 1980 as the baseline. Data was recorded by Met Office Hadley Centre, NOAA, Berkeley Earth, Cowtan & Way, and NASA.[5]……2

Figure 3. From oil to consumer goods, a generic representation of the petrochemical industry….3

Figure 4. Canadian consumption per barrel of oil (left)[9] and world demand for crude oil and liquid fuels (right).[10]……...4

Figure 5. Compositional breakdown of lignocellulose (taken from [18])……8

Figure 6. US Department of energy efficiency and renewable energy list of top 12 value-added chemicals from biomass…….10

Figure 7. **A**: Synthetic pathway to produce PEF (**3**) polymer through biomass-derived chemical HMF (**1**). **B**: Synthetic pathway to produce PET (**6**) polymer through petrochemicals *p*-xylene (**4**). **C**: Oxidation of HMF (**1**) to FDCA (**2**) using photocatalyst CoPz (**8**) under sunlight…….....12

Figure 8. General scheme of HMF (**1**) and furfural (**9**) production and their products…….12

Figure 9. Generalized synthetic pathways starting with biomass-derived HMF (**1**) and furfural (**9**) to produce a variety of high-value chemicals…….13

Figure 10. Generalized heterocyclic comparison between furan and thiophene…….15

Figure 11. **A**: Expected vs observed resonance for highly-conjugated furan derivatives. **B**: Solubility and PLQY differences between sexifuran (**26**) and sexithiophene (**27**)…….16

Figure 12. **A**: Oligofurans **F2 – F4** and their associated PLQY values performed in dioxanes. **B**: Photoluminescence emission spectra of oligofurans **F2 – F4** performed in acetonitrile at 293 K.[55] **C**: Oligofurans **3F – 9F** and their associated PLQY values performed in dioxanes. **D**: Normalized photoluminescence emission spectra of oligofurans **5F – 9F** performed in dioxane at 293 K.[47] **E**: Herringbone crystal structure of **6F** (grey, C; red, O) [47]……..17

Figure 13. Synthesis of 2,5-furan-based photovoltaic polymer *via* Stille cross-coupling……...19

Figure 14. Synthesis of push-pull 2,5-furan-based dye-sensitized solar cells *via* Suzuki cross-coupling……..20

Figure 15. Synthesis of a highly fluorescent 2,5-furan-based phenylene co-oligomer through double Stille and Suzuki cross-coupling…….20

Figure 16. Paul-Knorr cyclization to produce thiophene-furan alternative co-oligomers……...22

Figure 17. Cyclization of multi-arylated furans using bis-alkynylbenziodoxoles, carboxylic acids and imines through Pd-catalysis…….23

Figure 18. Generalized catalytic cycle for palladium-catalyzed cross-coupling reactions……..24

Figure 19. General Pd-catalyzed Stille cross-coupling reaction…….25

Figure 20. Catalytic cycle of the Suzuki cross-coupling reaction……...……27

Figure 21. Simplified pathway to reduce Pd(II) to Pd(0) and form homocoupling by-product through boronate anions…….27

Figure 22. Suzuki cross-coupling reaction of 5-bromofurfural (**33**) in water at room temperature.28

Figure 23. Proposed Pd-catalyzed DCC mechanism of pre-arylated furan carboxylic acids and aryl halides……30

Figure 24. Double cross-coupling comparison of thiophene trimer (**77**) highlighting the benefits of a double DCC…….31

Figure 25. Generalized synthesis starting with HMF (**1**) to synthesize 2,3,5 multi-arylated furan (**85**) in eight steps. Carbon numbering is also provided concerning the leftmost furan per compound……...34

Figure 26. Generalized synthesis starting with HMF (**1**) to synthesize 2,4,5 multi-arylated furan (**90**) in eight steps……...34

Figure 27. Pinnick oxidation of HMF (**1**) to HMFA (**81**)……..35

Figure 28. Double Pd-catalyzed DCC of HMFA (**81**) and 1,4-dibromobenzene (**38**) to diol (**82**)...36

Figure 29. From left to right: Entry 2, 3, 4, and 5 vials after microwave irradiation. Most right: Humin polymer by-product observed after microwave irradiation of vial 5……...37

Figure 30. Pd-catalyzed DCC of HMFA (**81**) and aryl-nitro (**91**) to form furan-nitro (**92**)…….39

Figure 31. Control EAS-bromination attempt of **93** to **93Br**……...40

Figure 32. Conversion of carboxylic acid (**93**) to methyl ester (**94**) *via* acidic or basic conditions..41

Figure 33. Selective EAS-bromination of ester (**94**) to 4-brominated ester (**94Br**)…….41

Figure 34. Suzuki cross-coupling reaction of 4-brominated ester (**94Br**) to diarylated ester (**96**)..42

Figure 35. Hydrolysis of ester (**96**) to carboxylic acid (**97**)…….42

Figure 36. Double DCC of acid (**97**) and 1,4-dibromobenzene (**38**) through Pd(0)/Pd(II) catalysts to produce 2,4,5-arylated-furan (**98**)……...43

Figure 37. Crude after workup ^{1}H NMR of 2,4,5-arylated-furan (**98**) in $CDCl_3$ ……43

Figure 38. Left: Normal phase column chromatography and fractions of 2,4,5-arylated furan (**98**) using silica gel (mobile phase: 97:1:2 Hexane:Toluene:EtOAc). Right: Fractions under 365nm UV-light……44

Figure 39. ^{1}H NMR of 2,4,5-arylated-furan (**98**) in $CDCl_3$ where each colour represents a different set of fractions pooled……45

Figure 40. Generalized synthesis starting with methyl-5-bromofuran-2-carboxylate (**99**) to synthesize various multi-arylated furans (**103**, **104**, **105**) in three to five steps……...46

Figure 41. Suzuki cross-coupling reaction of bromo-furan (**99**) with boronic acid (**41**, **106**) to produce diaryl-furan (**94**, **107**)……47

Figure 42. Path A: Hydrolysis of ester (**107**) to carboxylic acid (**108**)……47

Figure 43. Path A: Double DCC of acid (**108**) and dibromo-thiophene (**102**) to produce 2,5-diarylated-furan (**109**)……48

Figure 44. Purification of 2,5-diarylated-furan (**109**) through prepTLC. Left depicting TLC sheet developing through capillary action in 2:1 Hexane:$CHCl_3$ as mobile phase. Middle represents completed prepTLC, where **109** is found as a yellow band. Right showcasing completed prepTLC under 365nm UV-light……...48

Figure 45. Synthetic pathways *B* and *C* to access 2,3,5-furan esters (**110**) and 2,4,5-furan esters (**111**) respectively……...49

Figure 46. *Path B*: Hydrolysis followed by double Pd DCC to access 2,3,5-multi-arylated furan (**113**)……...50

Figure 47. *Path C*: Hydrolysis followed by double Pd DCC to access 2,4,5-multi-arylated furan (**115**)……...50

Figure 48. Normalized absorbance spectra of multi-arylated furans **109**, **113** and **115**……..51

Figure 49. Normalized photoluminescence spectra of multi-arylated furans **109**, **113** and **115**…..52

Figure 50. Photoluminescence of multi-arylated furans **109**, **113** and **115** in $CHCl_3$ solution [6×10^{-7} M] under 365 nm UV light……52

Figure 51. Synthesis of 2,5-furan-based phenylene co-oligomer (**42**) by Kazantsev *et al*……..55

Figure 52. Generalized synthesis starting with 5-bromofurfural (**33**) to produce varied 2,5-furan-based oligomers (**117**) in three steps……...56

Figure 53. Suzuki cross-coupling of 5-bromofufural (**33**) and thiophene boronic acid (**118**)…...57

Figure 54. Suzuki cross-coupling of 5-bromofufural (**33**) and phenylene boronic acids (**120**)…...58

Figure 55. TBAB test on the synthesis of 5-phenylfuran-2-carbaldehyde (**122**)…….59

Figure 56. Oxidation of aldehyde (**122**) to carboxylic acid (**140**) in one step…….60

Figure 57. Generalize scheme of furan aldehydes (**129**) to furan nitriles (**130**)……..61

Figure 58. Basic hydrolysis of nitrile (**130**) towards acid (**116**)……..63

Figure 59. Generalized Cannizzaro disproportionation of aldehyde (**122**) towards acid (**140**) and alcohol by-product (**140OH**)……..64

Figure 60. From left to right: Planetary ball miller. Stainless steel jar with starting reagents and 8mm steel balls with 1 gram reactants. Stainless steel jar after mixing at 60 Hz for 10 minutes….65

Figure 61. Ester by-product (**140Ester**) after treating alkoxide (**140OK**) with EtOAc immediately……66

Figure 62. Solvent-free Cannizzaro disproportionation of aldehyde (**129**) to acid (**116**) and alcohol (**116OH**)…….66

Figure 63. Double Pd-catalyzed DCC reaction of phenyl-furan acid (**140**) and dibromo-thiophene (**104**) to obtain alternating 2,5-furan-based oligomer (**148**)……68

Figure 64. Final double Pd-catalyzed DCC of acid (116) and dibromoaryl linker to access 2,5-furan-based oligomers……....69

Figure 65. Retrosynthetic comparison of **PFP** co-oligomer **42** from previous work[54] to this reported methodology starting with 5BF (**33**)…….71

Figure 66. Producing push-pull compound **156** by single DCC of furan acid (**146**) and bromo-thiophene (**155**)……..74

Figure 67. Normalized photoluminescence spectra of 2,5-furan-based phenylene/thiophene oligomers: **42** (**PFP**), **147** (**TFP**), **148** (**PFT**), and **44** (**TFT**)……..78

Figure 68. Normalized photoluminescence spectra of 2,5-furan-based phenylene oligomers: **149** (3,5-diMe**PFP**), **150** (4-*t*-Bu**PFP**), **153** (4-CF_3**PFP**), **151** (4-MeO**PFP**), **152** (4-TPA**PFP**), **154** (4-Nitro**PFP**) and 2,5-furan-based push-pull compound **156** (4-Nitro**PFT**)……...80

Figure 69. Photoluminescence of 2,5-furan-based oligomers in $CHCl_3$ solution [6×10^{-7} M] under 365 nm UV light. In order from most blue to most red emitting fluorescence for oligomers: **42** (**PFP**), **149** (3,5-diMe**PFP**), **150** (4-*t*-Bu**PFP**), **153** (4-CF_3**PFP**), **151** (4-MeO**PFP**), **147** (**TFP**), **148** (**PFT**), **152** (4-TPA**PFP**), **44** (**TFT**), **154** (4-Nitro**PFP**) and 2,5-furan-based push-pull compound **156** (4-Nitro**PFT**)…….80

List of tables

Table 1. First double Pd-catalyzed DCC with microwave vial test. 36

Table 2. Optimization of reaction conditions from Figure 30. 39

Table 3. Optical properties of final multi-arylated furan compounds in dilute $CHCl_3$ solution [2×10^{-7} M]; λ_{abs} and λ_{em} maxima and PLQY spectra. 52

Table 4. Optimization Table of Suzuki coupling on alternating heterocycles. 58

Table 5. Scope on Suzuki cross-couplings with diverse phenyl substrates. 59

Table 6. TBAB equivalent test results including ^{1}H NMR yields and *E-factor*. 60

Table 7. One-step oxidation of aldehyde to carboxylic acid results. 61

Table 8. Scope of aldehyde to nitrile synthesis with diverse substrates. 62

Table 9. Scope of hydrolysis of nitriles towards carboxylic acids. 63

Table 10. Optimization of solid-state Cannizaro disproportionation. 66

Table 11. Scope of Cannizzaro disproportionation with diverse substrates. 67

Table 12. Optimization of double Pd-catalyzed DCC reaction. 68

Table 13. Scope of alternating 2,5-furan-based oligomers *via* double Pd-catalyzed DCC reaction. 73

Table 14. Complete spectroscopic data for all final 2,5-furan-based oligomers and push-pull compound. 75

List of equations

Equation 1. Atom Economy Equation. 5

Equation 2. E-factor Equation..... 5

Equation 3. PLQY Equation. 16

List of abbreviations

5BF	5-Bromofurfural
ACN	Acetonitrile
ACS	American Chemical Society
$CHCl_3$	Chloroform
DCC	Decarboxylative Cross-Coupling
DCM	Dichloromethane
DMA	Dimethylacetamide
DMF	Dimethylformamide
ESI	Electrospray Ionization
EtOAc	Ethyl Acetate
EtOH	Ethanol
FDCA	2,5-Furandicarboxylic Acid
GCMS	Gas Chromatography-Mass Spectrometry
GHG	Greenhouse Gas
HMF	2,5-Hydroxymethyl Furfural
HRMS	High Resolution Mass Spectrometry
LC	Liquid Chromatography
MeOH	Methanol
NMR	Nuclear Magnetic Resonance
OFET	Organic Field-Effect Transistor
PLQY	Photoluminescent Quantum Yield
PTLC	Preparative Thin-Layer Chromatography
TBAB	Tetrabutylammonium Bromide
TBACl	Tetrabutylammonium Chloride
THF	Tetrahydrofuran
TLC	Thin-Layer Chromatography
TMB	(1,3,5)-Trimethoxybenzene
TOF	Time-Of-Flight

Chapter 1. Introduction

1.1 Consumption of Petrochemicals and its Impact on the Environment

In 1896, Svante Arrhenius, a Swedish scientist, published a pivotal paper that quantified the relationship between the concentration of CO_2 present in the atmosphere and how it alters the surface temperature of the planet. These calculations suggested that if the concentration of atmospheric CO_2 ever doubled, the earth's surface temperature would increase by 5 °C *via* the greenhouse effect.[1] If a change of temperature this extreme were to occur, it is speculated that environmental changes unprecedented since civilization would follow. These changes include record-high heat waves, food and water scarcity, additional devastating forest fires, polar ice caps fully melting causing global sea levels to rise, as well as other irreversible consequences towards vast ecosystems globally. Today, this phenomenon is known as global warming or climate change. Climate change is considered an ultimate threat to all human, animal as well as planetary health stated by the Intergovernmental Panel on Climate Change in 2023.[2] The European Environment Agency reports that atmospheric CO_2 levels were estimated to be at 294 ppm[3] during the time Arrhenius published his work, while current CO_2 levels are consistently breaking global records with reports stating the annual average of 417 ppm was reported in 2022 (by the National Oceanic and Atmospheric Administration, NOAA, see Figure 1).[4] With this 42% ppm increase in CO_2 (and additional gases), it is estimated and agreed from five different sources that the average planet temperature has increased by at least 1.1 °C since the 1880s (see Figure 2).[5] Fortunately for present life, Arrhenius's calculations have not correlated with observed global temperatures presently. However, his work still stands as the first scientific publishing to inform the public of the severe temperature changes being a direct result of increasing the concentration of greenhouse gases (GHGs) in the climate.

Since the late 1850s, CO_2, water vapor, O_3, CH_4, and N_2O, were all identified as GHGs after British physicist John Tyndall tested their infrared absorption.[6] Tyndall's findings revealed that GHGs have the characteristic to absorb and trap infrared radiation, unlike other abundant atmospheric gases such as nitrogen and oxygen. The high accumulation of GHGs in the atmosphere today is a direct cause of human activity due to our dependence on extracting, refining, and consuming finite resources like fossil fuels, which consist of crude oil, coal, and natural gas.

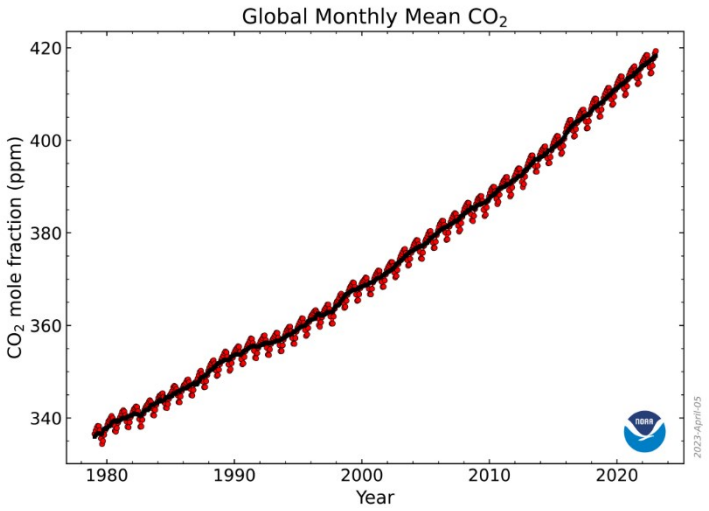

Figure 1. Graph depicting the monthly mean concentration of global CO_2 abundance over marine surface sites from 1980 to 2022.[4] (Image credit to NOAA Global Monitoring Laboratory)

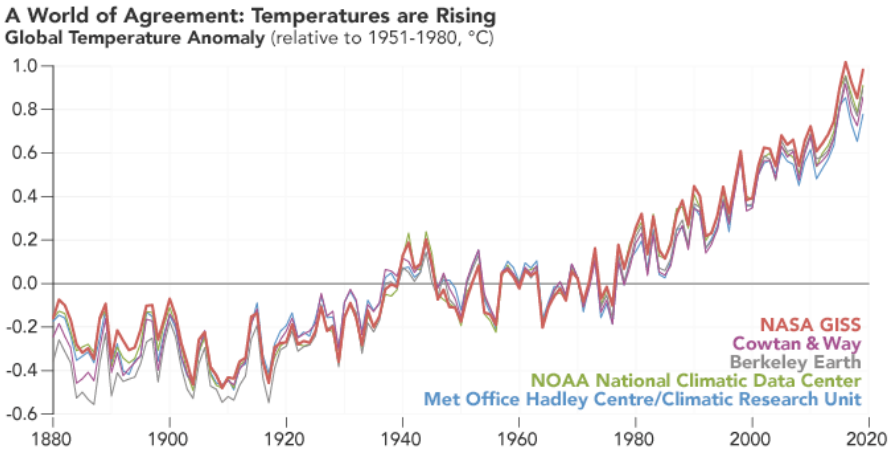

Figure 2. Graph depicting yearly temperature anomalies from 1880 to 2020 with 1951 to 1980 as the baseline. Data was recorded by Met Office Hadley Centre, NOAA, Berkeley Earth, Cowtan & Way, and NASA.[5]

For the past 150 years, the fossil fuel industry continues to lead the world as its primary source of energy. As of 2022, it is estimated that the energy consumption of fossil fuels encompasses 77% of the world's energy supply.[7] The fossil fuels industry has further expanded to lead other sectors such as the production of various petrochemicals for a multitude of final consumer goods. Understanding how the petrochemical industry functions is quite simple as it follows a straightforward path starting with oil and gas resources. Figure 3 depicts the general path of oil and gas toward final consumer goods. After refining, oil is isolated to its direct hydrocarbon

chemical feedstocks (small simple organic molecules like ethane and propane), and additional chemistry transforms these feedstocks into a variety of compounds known as petrochemicals. Common petrochemicals used in the chemical industry are classified into sectors: olefins (ethylene, propylene, 1,3-butadiene), aromatics (benzene, toluene, xylene), ammonia, and methanol. Petrochemicals are highly versatile hydrocarbons that can further produce more complex compounds (called high-value chemical derivatives) which are useful for the design of final products and consumer goods, petrochemicals are so popular they entail 90% of starting material demands globally in the chemical industry presently.[8]

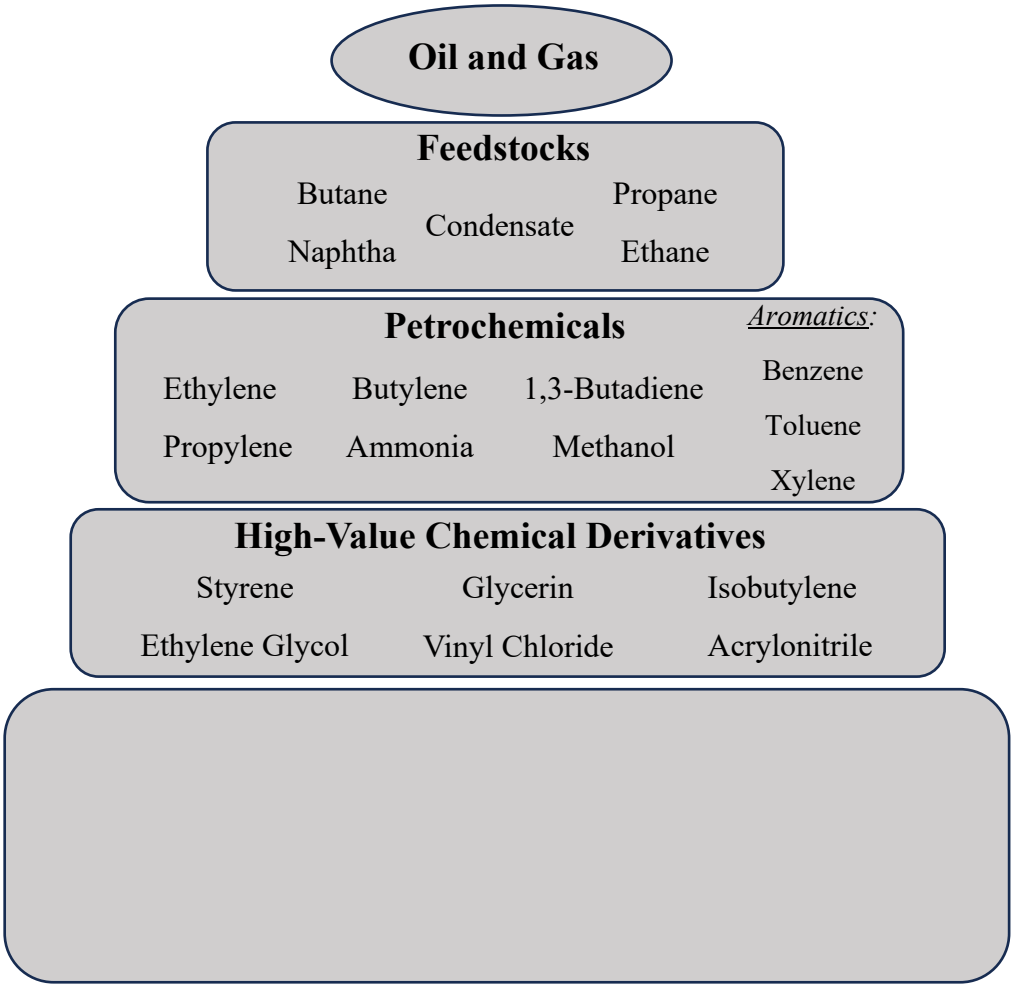

Figure 3. From oil to consumer goods, a generic representation of the petrochemical industry.

The oil sector is shared mostly between the transport and petrochemical sectors. To provide a visual representation of Canada's oil dependence (see left Figure 4), the Canadian Association of Petroleum Producers (CAPP) released data in 2022 indicating that 65% of oil per barrel goes towards transport, whereas 21% of oil per barrel is to produce petrochemicals.[9] According to CAPP, Canada consumes 1.5 million barrels a day. This means that 315,000 barrels are consumed daily to produce petrochemicals alone. Looking worldwide, reports from 2017 claim the total oil demand for petrochemicals is 12%.[8] Which may not seem like a lot; however, current world crude oil and liquid fuels production continue to increase annually (see right Figure 4), where quotas are met to meet 102 million barrels per day as of January 2024.[10] Meaning that roughly every day, ≈12.2 million barrels of oil are consumed daily from petrochemicals alone.

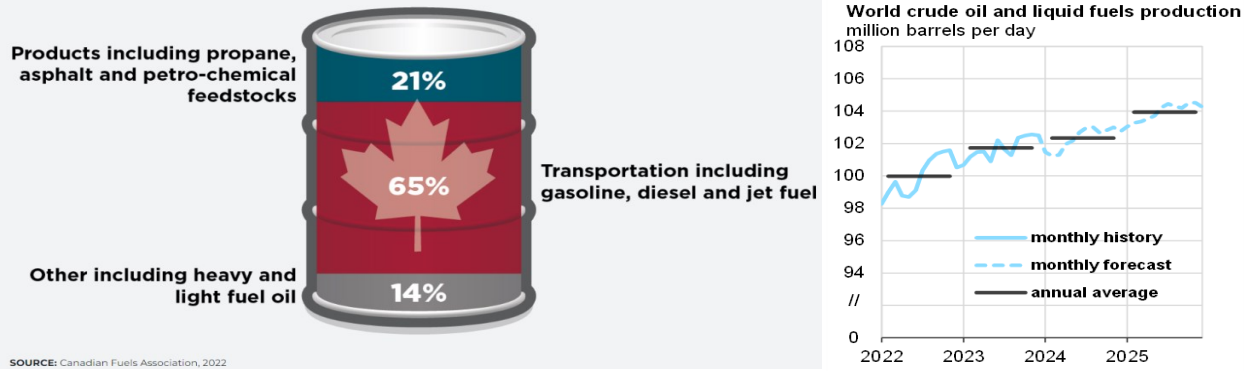

Figure 4. Canadian consumption per barrel of oil (left)[9] and world demand for crude oil and liquid fuels (right).[10]

The state of the climate has pushed countries and their governments to agree on signing the Paris Climate Agreement in 2015. These accords have been supported by the United Nations and 195 countries to maintain the global temperature under 2 °C when compared with preindustrial levels.[11] Many around the globe are focused on reducing GHG levels by improving today's transport and energy sectors by imploring renewable sources of energy (e.g. electric vehicles, nuclear energy, wind energy, and solar energy). The focus of this thesis is to shine additional light on the use of renewable starting materials from biomass to access new final products of interest as a method to reduce the usage of petrochemicals throughout a synthesis.

1.1.1 Principles of Green Chemistry

Since many agree it is in our best interest as a species to tackle the climate crisis, it will require many sustainable practices shared across many fields to make the Paris Climate Agreement goals a reality. In the field of chemistry, moving forward, all chemists presently have an environmental duty to design more benign chemical processes. This environmental framework was described in detail by the fathers of Green Chemistry, Paul Anastas and John Warner, who published these concepts in 1998.[12] This publication discusses specific principles to reduce the use of hazardous chemicals, promote the use of catalysis, include renewable materials for synthesis and minimize by-product waste or pollution. This can be accomplished by evaluating reactions based on environmental metrics like *Atom Economy* and *E-factor*. In 1991, American chemist Barry Trost introduced the first Green Chemistry term of *Atom Economy*, describing how atom-efficient a chemical reaction is by quantifying how many atoms from starting reagents are found in the desired product (Equation 1).[13]

Equation 1. Atom Economy Equation.

$$\boldsymbol{Atom\ Economy} = \frac{\boldsymbol{molecular\ mass\ of\ desired\ product}}{\boldsymbol{molecular\ mass\ of\ starting\ reactants}}\ \boldsymbol{x}\ \mathbf{100\%} \qquad \textbf{(1)}$$

A larger *atom economy* relates to a reaction being more green, having an *atom economy* of 100% suggests that all atoms of the reagents are found within the product. The next Green Chemistry term was provided a year later by British chemist Roger Sheldon. Sheldon introduced the *E-factor;* a quantitative metric used to calculate the overall waste generated in a reaction (equation 2).[14] A smaller *E-factor* relates to less theoretical waste generated assuming 90% of the solvent is recovered. The mass of solvents could also be negligible if a reaction could proceed under solvent-free conditions.

Equation 2. E-factor Equation.

$$\boldsymbol{E-factor} = \frac{\Sigma \boldsymbol{mass\ of\ (starting\ materials)} + \Sigma \boldsymbol{mass}(\mathbf{0.1}(\boldsymbol{solvent})) - \Sigma \boldsymbol{mass(product)}}{\Sigma \boldsymbol{mass\ of\ product}} \qquad \textbf{(2)}$$

These metrics paved the way for Anastas and Warner to design the fundamental principles of Green Chemistry. To this day these principles lay the groundwork for chemists to design safer

practices for humans, animals, and the planet. The 12 principles of Green Chemistry are stated below:

1. Prevention: It is better to prevent waste than to treat or clean up waste after it has been created.
2. Atom Economy: Synthetic methods should be designed to maximize the incorporation of all materials used in the process into the final product.
3. Less Hazardous Chemical Syntheses: Whenever practicable, synthetic methods should be designed to use and generate substances that possess little or no toxicity to human health and the environment.
4. Designing Safer Chemicals: Chemical products should be designed to preserve the efficacy of function while reducing toxicity.
5. Safer Solvents and Auxiliaries: The use of auxiliary substances (e.g., solvents, separation agents, etc.) should be made unnecessary wherever possible and, innocuous when used.
6. Design for Energy Efficiency: Energy requirements should be recognized for their environmental and economic impacts and should be minimized. Synthetic methods should be conducted at ambient temperature and pressure.
7. Use of Renewable Feedstocks: A raw material or feedstock should be renewable rather than depleting whenever technically and economically practicable.
8. Reduce Derivatives: Unnecessary derivatization (use of blocking groups, protection/deprotection, temporary modification of physical/chemical processes) should be avoided if possible.
9. Catalysis: Catalytic reagents (as selective as possible) are superior to stoichiometric reagents.
10. Design for Degradation: Chemical products should be designed so that at the end of their function they break down into innocuous degradation products and do not persist in the environment.
11. Real-Time Analysis for Pollution Prevention: Analytical methodologies need to be further developed to allow for real-time, in-process monitoring and control before the formation of hazardous substances.
12. Inherently Safer Chemistry for Accident Prevention: Substances and the form of a substance used in a chemical process should be chosen to minimize the potential for chemical accidents, including releases, explosions, and fires.

As stated in the very first principle, the primary focus of Green Chemistry is to develop synthetic approaches that reduce or eliminate chemical waste whenever possible. Following this concept, all

12 principles challenge synthetic chemists to develop innovative and more environmentally conscious strategies when designing high-value chemical targets. In a perfect world, chemists would naturally try to incorporate all principles mentioned to minimize waste and reduce environmental impact. Although this sounds promising, it is unfortunately quite difficult to incorporate all principles into practice simultaneously. However, it is highly encouraged to involve as many Green Chemistry principles in one's synthesis as possible. Henceforth, the main work reported from this thesis focuses primarily on the use of renewable feedstocks (principle 7) to build potential π-conjugated organic electronic candidates (more about these technologies and their synthesis in Chapter 1.2.1 and 1.2.2), while also including principles 2, 3, 6, 8 and 9 whenever applicable.

1.1.2 Plant-Based Biomass-Derived Chemicals as a Renewable Feedstock

To help mitigate the dependence on petroleum-derived chemicals, the decision to include renewable starting materials in the synthesis of high-value chemicals is a must. It is highly encouraged to use biomass-derived chemicals as a raw material due to their renewable nature and ability to replenish at a much faster rate than fossil fuels. Biomass itself encompasses a very broad class of naturally derived organic materials obtained from living organisms (e.g. plants, animals). Sectors sourcing forms of biomass presently vary differently from forestry residues to animal waste and sewage.[15] In its simple definition, biomass is a renewable organic mass, derived from animals or plants, with applications including its use for energy production, heat production, or as a sustainable raw material.[16]

While animal-based biomass is more commonly used for energy production in the form of biogas (a renewable natural gas), dry plant-based biomass (commonly known as lignocellulosic biomass) will be the focus of this research due to its vast global abundance (181.5 billion tonnes are produced annually)[17] and the range of starting chemicals obtained from this source. Lignocellulosic biomass can be sorted into four specific groups, including energy crops (e.g. switch grass, cotton stalk), agricultural residues (e.g. rice straw, rice husks, corn stover, sugar cane bagasse, and wheat bran), industrial residues (e.g. newspaper, pulp, wood residues) and agro-industrial residues (e.g. wood chips, potato, and orange peels, coffee grounds).[11] Composition of lignocellulosic biomass is

structurally based on three main biopolymers found in the plant cell wall: cellulose, hemicellulose, and lignin (as seen in Figure 5). While the percent composition of these biopolymers depends per species, cellulose is most common (40-80%), with fair amounts of hemicellulose (10-40%) and lignin (5-25%) present.[18] Cellulose is the most abundant polysaccharide on earth, found as the major biopolymer in plant cells, providing plants with a more stiff and rigid structure than animal cells.[18] Cellulose is chemically composed of D-glucose monomers bound by β-1,4-glycosidic bonds to produce polymer chain lengths made up of several monomer units long (hundreds to tens of thousands).[15,18] Hemicellulose is the second most abundant biopolymer found in nature. Unlike cellulose, hemicellulose is a much smaller heterogeneous polysaccharide (less than 200 monomer units long) and is derived from diverse monomeric sugars like pentose (D-xylose, L-arabinose) and hexoses (mannose, galactose, and rhamnose). Hemicellulose plays the adhesive role, strongly linking with the cellulose (and/or lignin) surface to prove additional support and structure.[19] Lastly, lignin is a complex phenolic-based polymer formed by the oxidation of aromatic alcohols (*p*-coumaryl, coniferyl, and sinapyl). Lignin is found to play an important role in plant growth by further enhancing the cell wall rigidity, provides hydrophobic properties, and is said to be a useful barrier to protect the plant from pests and pathogens.[20]

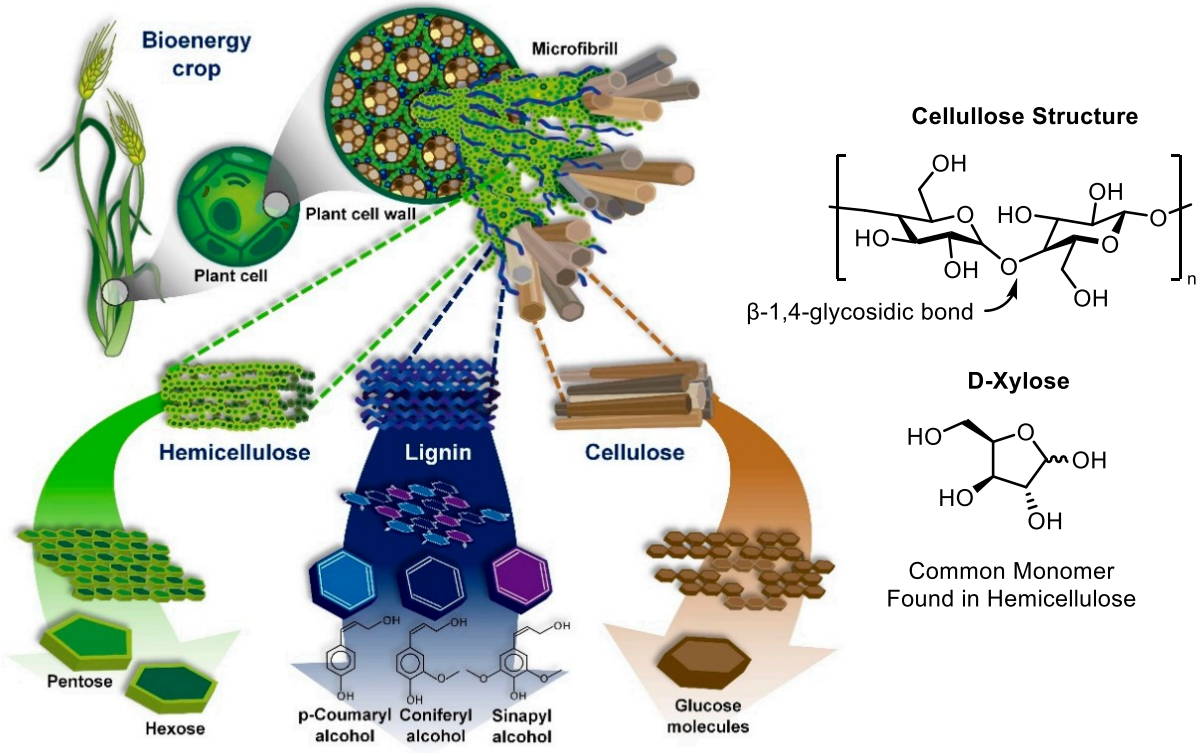

Figure 5. Compositional breakdown of lignocellulose (taken from [18]).

The most common sources of lignocellulosic biomass used presently include corn stover, sugarcane bagasse, pine, wheat straw, and rice straw.[21] These renewable resources are high in cellulose and hemicellulose, making them excellent feedstocks for obtaining a wide range of important organic starting building blocks. Industrial processes report the "pretreatment" procedure as a crucial step before transforming these feedstocks into useful building blocks. Pretreatment is a method to separate the biopolymers from their cellulose-hemicellulose-lignin matrix and/or enhance the reactivity of the isolated cellulose polymer. It is a necessary step to ensure maximum conversion of the feedstock. For example, physical mechanical pretreatment is performed whereby biomass is placed in a ball miller and the biomass is ground and crushed by using mechanical energy.[22,23] After pretreatment, the refined biomass can be transformed through chemical (acid catalyzed, ionic liquids, metal catalysis), physical (steam explosion) or even biological processes (microbes, enzymatic processes) have all been developed to obtain vast biomass-derived starting materials.[18,19,21,23] Impressively, over 200 valued starting materials can be synthesized from lignocellulosic biomass, and continued research to further advance this field is occurring at large chemical production companies such as DuPont, BASF, SABIC and Dow Chemical.[22,23] To emphasize the importance of renewable materials, in 2004, the United States Department of Energy Efficiency and Renewable Energy published a list of the top 12 value-added chemicals derived from polysaccharide biomass.[24] Deciding which compounds belong requires meticulous considerations, such as how facile it is to extract the material from biomass, and their potential use as a chemical building block. As depicted below, the chosen biomass-derived building blocks are fumaric acid, 2,5-furandicarboxylic acid (FDCA), 3-hydroxy propionic acid, aspartic acid, glucaric acid, glutamic acid, itaconic acid, levulinic acid, 3-hydroxybutyrolactone, glycerol, sorbitol, and xylitol (Figure 6).[24]

The chemicals listed in Figure 6 still carry significant importance today, especially since these renewable organic starting compounds are widely used in the production of other value-added chemicals with applications in many industries (e.g. food additives, medicine, resins, biopolymers, fertilizers, etc.). This list makes a great introduction to some of the most versatile biomass-derived molecules for organic synthesis presently. However, there exist many other building blocks derived from lignocellulosic biomass which also deserve attention for their diverse chemistry and chemical properties.

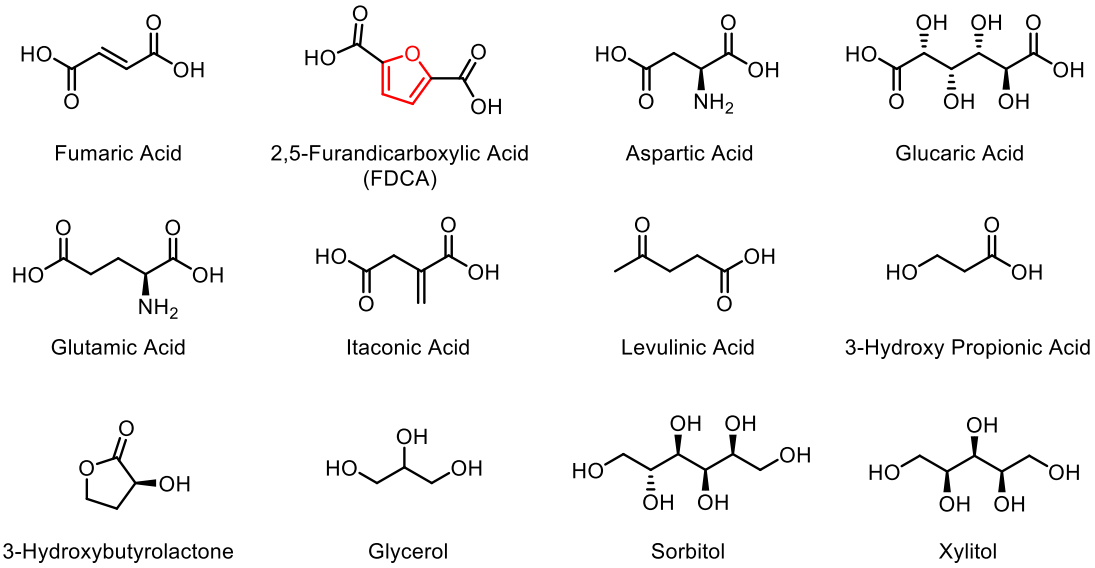

Figure 6. US Department of energy efficiency and renewable energy list of top 12 value-added chemicals from biomass (furan motif highlighted in red for clarity).

1.1.3 Furan Starting Chemicals Derived from Lignocellulosic Biomass

Furans (derived from the Latin word "*furfur*" meaning bran) are cyclic five-membered heteroaromatic organic compounds containing four carbon atoms and one oxygen atom (highlighted in red as seen in Figure 5). This chemical composition provides the furan motif with many useful chemical characteristics which will be further discussed in the following chapter. What is most notable about furans is that they are the most abundant heteroaromatic building blocks accessible from biomass.[25–27]

Being the only heteroaromatic compound found in the "Top 12 Value-Added Chemicals from Biomass", FDCA (**2**) is a renewable furan building block that contains two carboxylic acid functional groups, mimicking a similar chemical structure as petroleum-based monomer terephthalic acid (**5**) derived from petrochemical, *p*-xylenes (**4**). Both diacids are very useful for the synthesis of aromatic polyesters, in which the diacid undergoes polycondensation with ethylene glycol producing polymers like polyethylene 2,5-furanoate (PEF, **3**) and polyethylene terephthalate (PET, **6**) from FDCA and terephthalic acid respectively (Figure 7A & 7B). While petroleum-based polymer PET is a popular material presently, biopolymer PEF possesses superior plastic properties and is a strong candidate to replace polymer **6** as a commercial plastic used for

textiles and packaging.[28–30] Unfortunately, producing FDCA from a one-pot reaction from biomass is not the most efficient process to obtain monomer **2**. Instead, FDCA is best produced when oxidized from another biomass-derived furan called 5-hydroxymethyl furfural (HMF, **1**).[30] Unlike FDCA, HMF has an aldehyde and primary alcohol group on the 2,5-positions of the furan core. These functional groups make HMF a versatile starting chemical with researchers, claiming it as a "sleeping giant" for its synthetic capabilities.[26,31] Oxidation of HMF under basic conditions with Pd, Pt, Au, and Ru metals favourably converts HMF into FDCA (Figure 7A).[32,33] Alternatively, HMF can be oxidized to FDCA in ambient air, pressures, and temperatures without the need for expensive metals by using cobalt thioporphyrazine (CoPz, **8**) as a recyclable photocatalyst (dispensed on graphitic carbon nitride, g-C_3N_4).[34] Reported by Xu *et al.* in 2017, this selective oxidation can sustainably convert HMF to achieve high yields of FDCA (96%) under simulated sunlight in the appropriate buffer (Figure 7C).[34] This methodology can help visualize a more sustainable world where packaging plastics no longer must be derived from petrochemicals exclusively, and instead, biomass-derived chemicals can be converted to high-value monomers using sunlight.

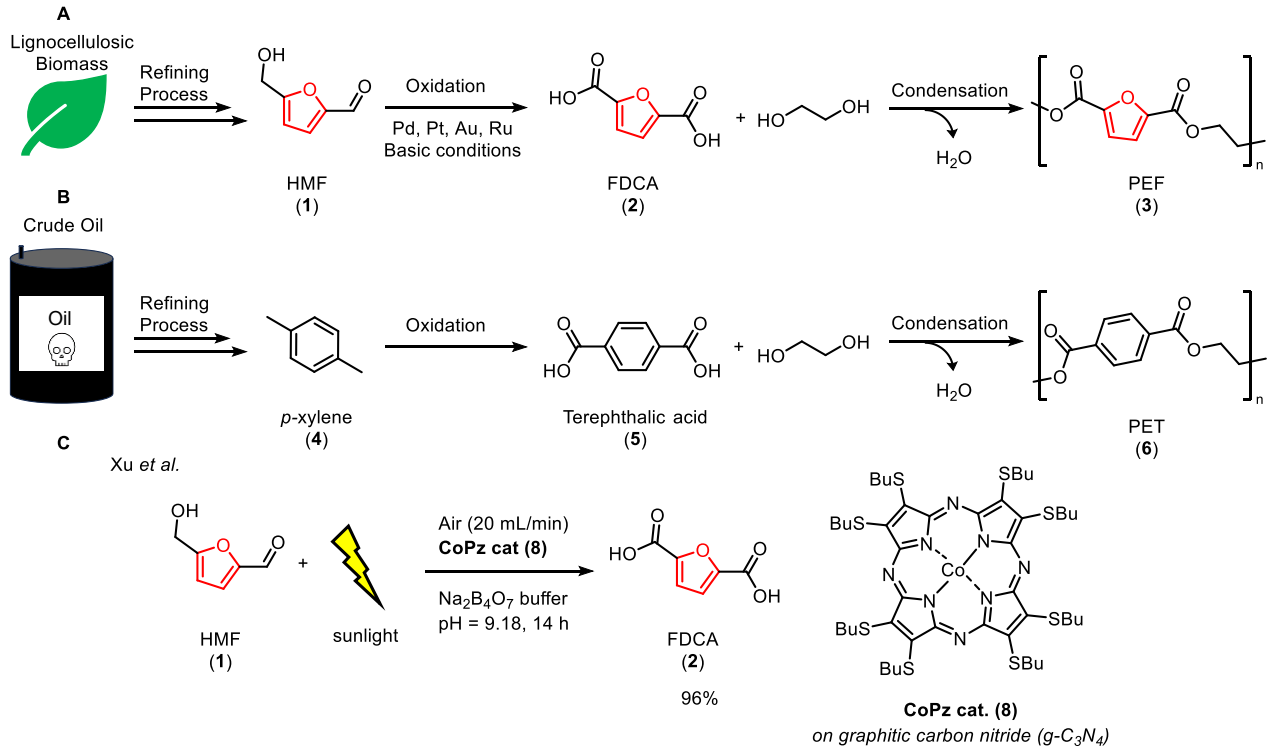

Figure 7. **A**: Synthetic pathway to produce PEF (**3**) polymer through biomass-derived chemical HMF (**1**). **B**: Synthetic pathway to produce PET (**6**) polymer through petrochemicals *p*-xylene (**4**). **C**: Oxidation of HMF (**1**) to FDCA (**2**) using photocatalyst CoPz (**8**) under sunlight

Over the past two decades, research has published synthetic methodologies from different fields of chemistry to incorporate HMF (and its close derivatives) into the production of high-value drugs, biopolymers, and nanomaterials.[35] Pertaining to a similar chemical structure as HMF, furfural (**9**) is another important biomass-derived chemical with its own methodologies to access other valued chemicals. Furfural is composed of a furan body with a single aldehyde group. In the chemical industry, furfural is used as a solvent and chemical to access additional furan resins and polymers.[36] Due to their natural ability to convert into a multitude of consumer goods or high-valued chemicals, both furans **1** & **9** are coined with the term "biomass-derived platform chemical" for their impressive chemical versatility.[37] Unsurprisingly, both derivatives are directly linked to lignocellulosic biomass as its starting source. Specific compositions of biomass relate to their production respectively. As shown below (Figure 8), when cellulose and hemicellulose are broken down (after pre-treatment) into their respectful monomers, HMF is directly converted from hexose sugars (polysaccharides derived from cellulose), whereas furfural production occurs from the transformation of pentose molecules (such as xylose monomer). Both furfurals are classically formed after selective thermal dehydration steps in acidic media with their selective monomer.[31]

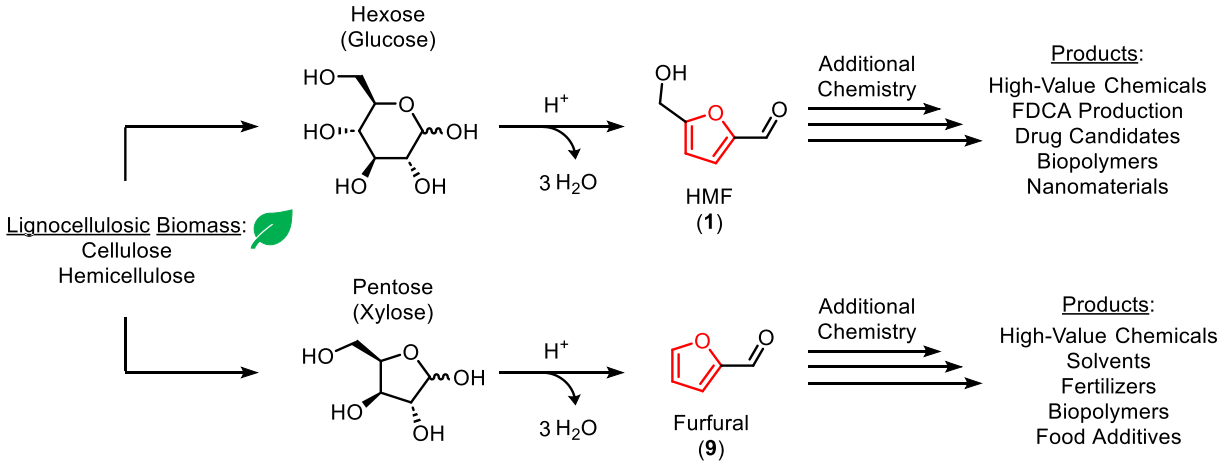

Figure 8. General scheme of HMF (**1**) and furfural (**9**) production and their products.

Furfural is claimed to be the most common industrial chemical derived from lignocellulosic biomass; in 2013, annual volume productions were estimated between 200,000 and 300,000 tons.[38] In 1921, the Quaker Oats Company was the first to produce furfural at industrial scales by converting hemicellulose feedstocks (from leftover oat hulls) using dilute sulfuric acid and steam pressure.[39] From an organic chemistry perspective, both biomass-derived platform chemicals

discussed are important starting candidates that access a variety of chemical feedstocks with different functionalized groups.

Both HMF (**1**) and furfural (**9**) can transform into functionally different furan sources or be converted to other useful aliphatic diacids, diols, furans (Figure 9).[23,26,37,40] HMF under the presence of strong acids cleaves the furan ring producing another "Top 12 Value-Added Chemicals from Biomass", levulinic acid (**10**), a key high-value chemical with applications in herbicides, cosmetics, perfumes, resins (etc.). While producing acid **10** may not always be the primary goal of an experiment, HMF is conveniently designed to degrade over time, further following Green Chemistry principles. Strong oxidation reactions convert either aldehyde into of variety of furan-based carboxylic acid motifs (**2**, **11**, **12**). Depending on the conditions of the oxidation, four to five carbon-containing diacids (**13**, **14**, **15**) or anhydride (**16**) can be produced as well. Hydrogenation reactions with palladium or platinum catalysts are methodologies to reduce either aldehyde, reducing furfural to produce furfuryl alcohol (**17**), an excellent monomer for furan resins. Further hydrogenation produces diol furan (**18**), saturated furans (**19**, **20**) as well as tetrahydrofuran (**21**) and 1,6-hexanediol (**22**). Interestingly, if ever a simple furan (**23**) ring is required, it cannot be directly available from biomass. Instead, two well-known methodologies exist to produce furan.

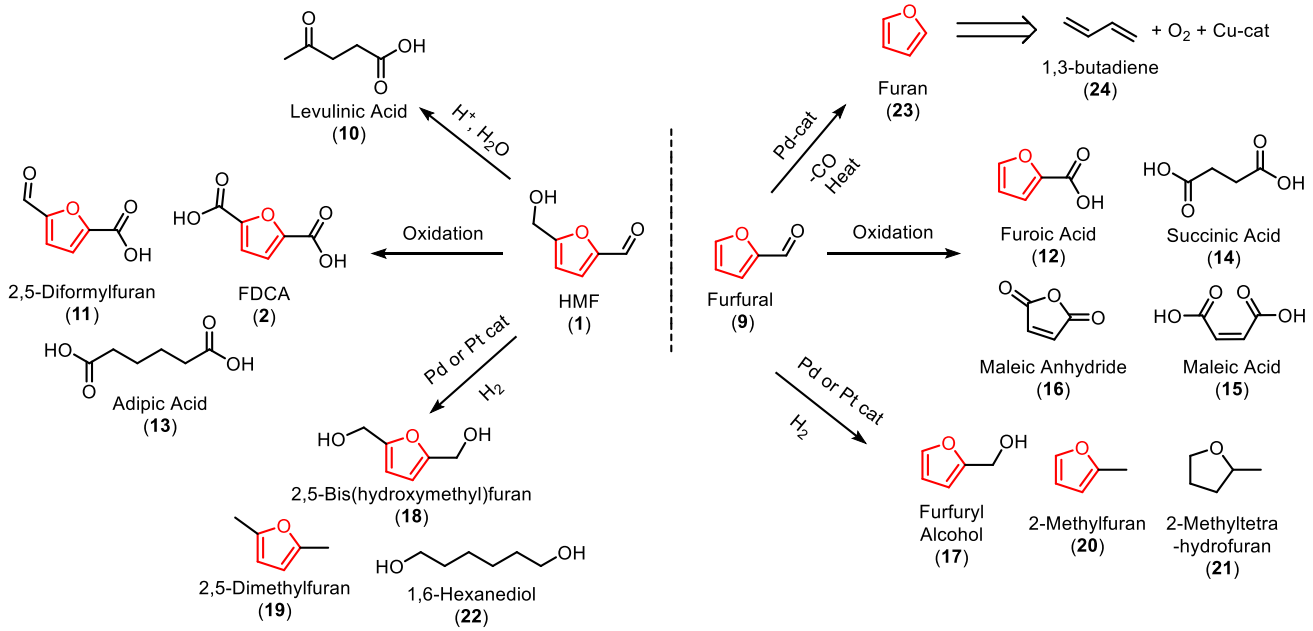

Figure 9. Generalized synthetic pathways starting with biomass-derived HMF (**1**) and furfural (**9**) to produce a variety of high-value chemicals.

Either furfural is subjected to a decarbonylation with a palladium catalyst under heat (~200 °C), where carbon monoxide leaves as a gaseous by-product, producing the furan ring. Or using petrochemicals, 1,3-butadiene (**24**) can be catalytically oxygenated under an oxygen atmosphere with a copper catalyst, however, this approach has been criticized for being economically inefficient.[37] This further highlights the chemical importance of producing and working with furans from biomass instead of petrochemicals.

1.2 Comparing Heterocyclic Properties of Furans to Thiophenes

As previously mentioned, furans are heterocyclic planar organic compounds composed of a five-membered ring, containing a sp_2-oxygen atom and four conjugated sp_2-carbon atoms. This single oxygen atom contributes towards the many useful properties and reactivity of this heterocycle. Oxygen is the second most electronegative element, providing a strong tendency to attract shared electrons towards itself. As oxygen continues to pull electrons, it also provides a lone pair of electrons (found in the 2p-orbital) towards the delocalization of the ring. With furans (**23**) being planar, cyclic rings with delocalized electrons (following Hückel's rule of $4n + 2$, where n is any whole integer), furans are heteroaromatic organic compounds, as they follow the traditional definition of aromaticity. Being a heteroaromatic compound comes with the need to compare to other similar heterocycles for application use. Hence, furans are most comparable to their ubiquitous heteroaromatic congener thiophenes (sulfur-containing heterocycle, **25**), since both elemental oxygen and sulfur are chalcogens found in group 16 of the periodic table, with sulfur found directly below oxygen. Because sulfur is a larger atom than oxygen (sulfur atomic radii is 1Å, oxygen atomic radii is 0.6Å)[41], thiophenes are found to have a larger covalent radius (covalent radius of 1.80Å between sulfur-carbon in thiophenes, covalent radius of 1.52Å between oxygen-carbon in furans)[42], and thus furans are more tightly packed heterocycles. Sulfur also contains eight more electrons and protons than oxygen, making sulfur more polarizable, as it has access to additional electron orbitals. Because of these differences in electronegativity, atomic radius, and polarizability found between these chalcogens, sulfur's electron density allows for more delocalization to occur on the thiophene motif, further stabilizing the ring through resonance. For these reasons, thiophenes are considerably more aromatic compared to furans.[43,44] The differences discussed directly relate to the heterocyclic properties of furans, which differ notably

from thiophenes reactivity, resonance structures, solubility, and spectroscopy. Figure 10 depicts these generalized differences.

The increased reactivity associated with furans can be viewed as a double-edged sword. While high reactivity can be favourable because it would require less overall energy to perform a transformation, it can also lead to the occurrence of unwanted side reactions. Synthetic limitations of furans come from their low stability in acidic environments (e.g. HMF (**1**) producing levulinic acid (**10**) in Figure 8)[26] and their sensitivity to light.[44] For these reasons alone, furans have been vastly understudied compared to thiophenes, especially in the field of developing highly π-conjugated organic electronic candidates.[42,44]

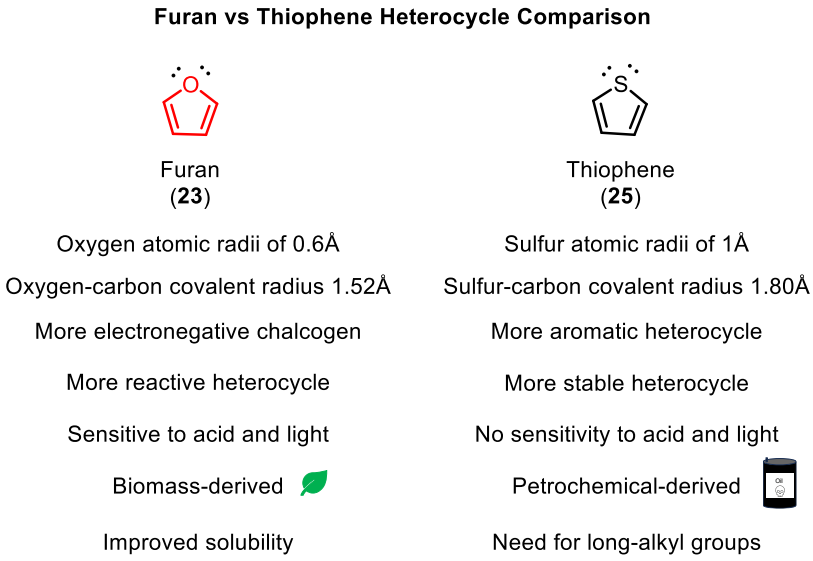

Figure 10. Generalized heterocyclic comparison between furan and thiophene.

The strong electronegativity of furans causes them to exhibit different properties than traditional heteroaromatics when their conjugation is extended. Instead, when highly conjugated groups are bonded to furan, a furan quinoidal resonance is observed (Figure 11A).[42,44] Quinoidal resonance ignores delocalization from the oxygen atom, benefiting the overall planar conformation of conjugated systems by shortening intermolecular π-π stacking distances, a useful characteristic to produce conjugated materials with more effective charge transport.[42] Oxygen's polarity also enables furans to be much more soluble than thiophenes in organic solvents.[42,45,46] A perfect example demonstrating the difference in solubility is seen with the comparison of α-oligomers of sexifuran (**26**, 0.7 mg/mL in $CHCl_3$) and sexithiophene (**27**, 0.05 mg/mL in $CHCl_3$) seen in Figure

11B.[47] Oligomeric furans do not require long-alkyl soluble chains, whereas oligomeric thiophenes need long-alkyl chains to further enhance their solubility for accessible transformations or their application of solution-processable semiconductors.[45]

Lastly, conjugated furans exhibit naturally high photoluminescent quantum yields (PLQY) than thiophenes (e.g. **26**, PLQY = 69%, **27**, PLQY = 41% both tested in dioxane, Figure 11B) in both solid-state and solution.[42,44,47] PLQY is defined as the ratio of the number of photons being emitted to the number of photons absorbed (Equation 3), describing how efficiently a fluorophore converts excited light into fluorescence.

Equation 3. PLQY Equation.

$$\boldsymbol{PLQY = \frac{Number\ of\ photons\ emitted}{Number\ of\ photons\ absorbed}} \qquad \textbf{(3)}$$

High PLQY values for organic materials are important for select applications, such as molecular fluorophores for bioimaging[48] and increasing the efficiency of organic optoelectronic devices.[49]

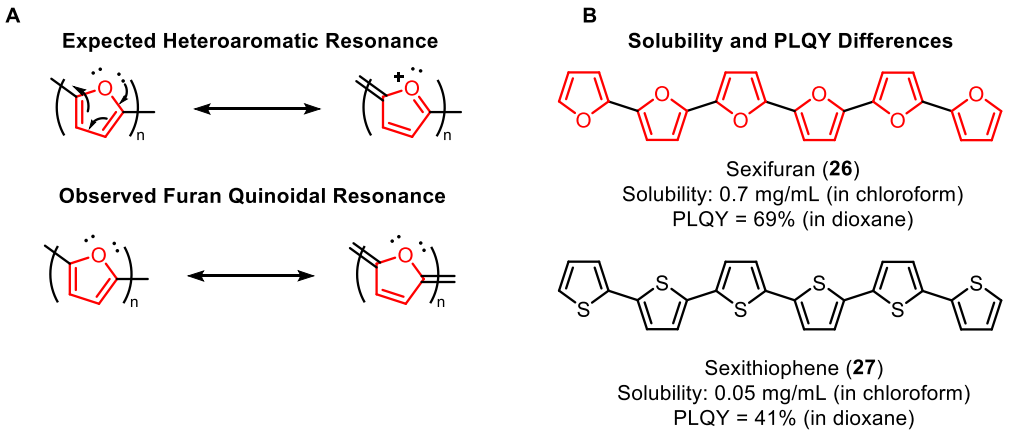

Figure 11. **A**: Expected vs observed resonance for highly-conjugated furan derivatives. **B**: Solubility and PLQY differences between sexifuran (**26**) and sexithiophene (**27**).

1.2.1 Highly Planar π-Conjugated 2,5-Furans as Optoelectronic Candidates

Optoelectronics devices are an established field of photoelectronic semiconducting devices that emit, detect, and/or control light, bridging the technologies of electronics and light together. Well-known optoelectronic devices that encompass this technology today include photovoltaics (solar cells), laser diodes, optical fibres, and light-emitting diodes. In the past two decades, highly

planar π-conjugated 2,5-furan-based compounds, oligomers and polymers have gained popularity as potential organic optoelectronic candidates, these candidates include organic photovoltaics,[50] dye-sensitized solar cells,[51] organic light-emitting diodes,[52] and organic field-effect transistors (OFETs).[53,54] The field of synthesizing and studying the photophysical properties of highly conjugated furans is relatively new. It begins with the investigation of very short chained oligofurans (from 2 – 4 conjugated furan rings, **F2** – **F4**) reported by Seixas de Melo *et al.* in 2000.[55] Their findings describe oligofurans as a highly planar molecule, where the photoluminescence maxima red shifts, whereas the PLQY increases with extended furan conjugation at 293 K (Figure 12A and 12B). Ten years later, new investigations into longer oligofurans (from 3 – 9 conjugated furan rings, **3F** – **9F**) reported by Gidron, Diskin-Posner and Bendikov further acknowledged the useful properties of conjugated oligofurans as organic electronic candidates presently.[47] Their PLQY data agrees with previous work, and interestingly found that further conjugating furans after **4F** causes a slight decrease in PLQY with increasing chain lengths (Figure 12C and 12D). Single crystal X-ray diffraction studies on **6F** additionally confirmed the high planarity structure hypothesized from previous reports demonstrating a "herringbone" structure in **6F** (Figure 12E), a common crystal structure observed in the field of aromatic hydrocarbons.[47,56]

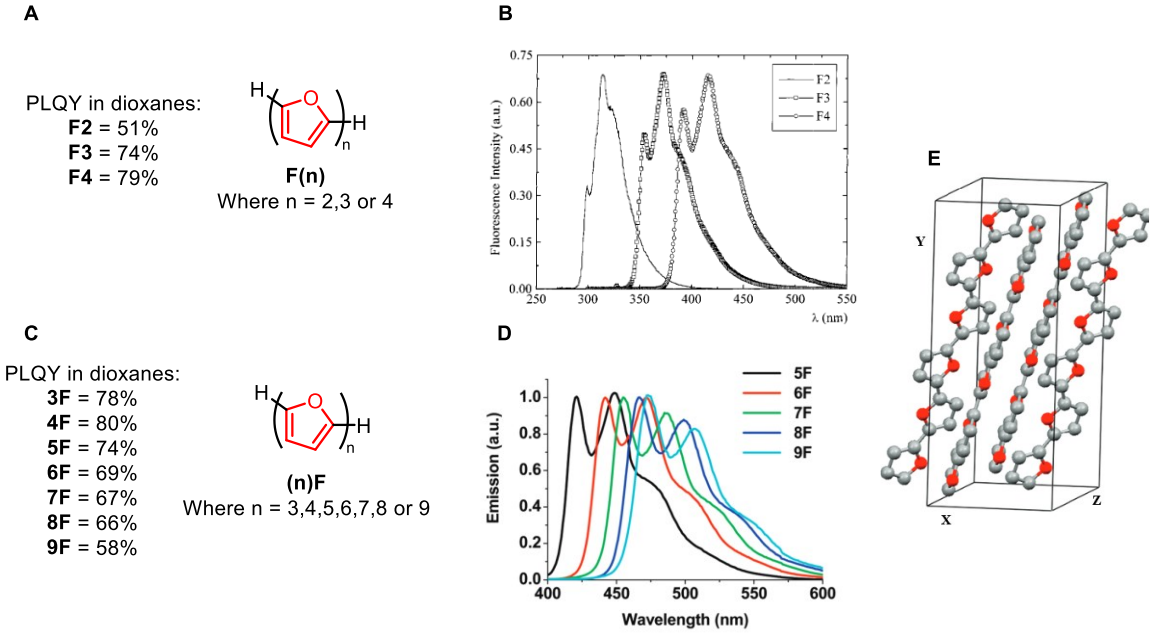

Figure 12. A: Oligofurans **F2 – F4** and their associated PLQY values performed in dioxanes. **B**: Photoluminescence emission spectra of oligofurans **F2 – F4** performed in acetonitrile at 293 K.[55]

C: Oligofurans **3F – 9F** and their associated PLQY values performed in dioxanes. **D**: Normalized photoluminescence emission spectra of oligofurans **5F – 9F** performed in dioxane at 293 K.[47] **E**: Herringbone crystal structure of **6F** (grey, C; red, O).[47]

1.2.2 General Cross-Coupling Synthesis of π-Conjugated 2,5-Furans

Oligofurans express high PLQYs and tunable photoluminescent maxima depending on their extended conjugation, which are useful photophysical properties to design various optoelectronic devices. Recall that working with furans also comes with synthetic limitations when compared to their more stable congener thiophenes (as discussed in Chapter 1.2). However, since furan-based materials are gaining in popularity in applications of optoelectronic devices, this indicates that problems associated with the stability of furans can be overcome with strategic synthetic decisions. Good practices include avoiding very strong acidic conditions, instead basic or neutral pH are more ideal environments for synthesis, as well as storing furan products in dark environments under inert gas for long-term storage. In this section, the synthesis of π-conjugated 2,5-furan-based derivatives that were briefly mentioned in Chapter 1.2.1 as potential organic optoelectronic candidates will be presented.

The majority of literature reports presently offer two synthetic approaches to construct conjugated furan materials: this is accomplished by Pd-catalyzed cross-coupling reactions[50,51,53,54] or achieved *via* cyclization methods.[52,57] Pd-catalyzed cross-coupling reactions (discussed in Chapter 1.3) are a synthetic class of reactions that couple aryl, vinyl, or alkyl halide substrates with organometallic nucleophiles, forming new carbon-carbon bonds using catalytic amounts of palladium metal. For the simplicity of this thesis, Pd-catalyzed cross-coupling reactions described herein will entail aryl halides reacting with aryl nucleophiles to produce new sp_2-sp_2 carbon-carbon bonds. Each named Pd-catalyzed cross-coupling reaction is distinguished by the organometallic nucleophile of choice and the scientist who developed its chemistry. Named Pd-catalyzed cross-coupling reactions for the arylation of furans often include the Stille cross-coupling (more details in Chapter 1.3.1), a reaction named after American chemist John Kenneth Stille, where organostannanes are coupled to aryl halides.[58] The Suzuki cross-coupling (more details in Chapter 1.3.2) is named after Japanese chemist Akira Suzuki, where aryl boronic acids replace the need for organometallics as the nucleophile under basic conditions.[59]

Developing polymeric photovoltaics with the incorporation of furan heterocycles was first reported by Woo *et al*. where a double Pd-catalyzed Stille cross-coupling polymerization of an aryl halide and an organometallic nucleophile was used to produce furan containing low band-gap semiconducting polymers as solar cells (Figure 13).[50] Dihalide (**28**) was coupled with either furan (**29**) or thiophene (**30**) organotin compounds producing polyfuran (**31**) and alternating heterocyclic polymer (**32**) respectively. The group's goal was to evaluate the potential for furans to replace thiophenes within solar cells, and their conclusions discuss that both polymers **31** and **32** not only require shorter solubilizing groups than polythiophene derivatives (due to the installation of the furan) but both polymers exhibit nearly interchangeable optical and electronic properties, making furans a particularly useful heterocyclic alternative to thiophenes for low band-gap polymers.[50]

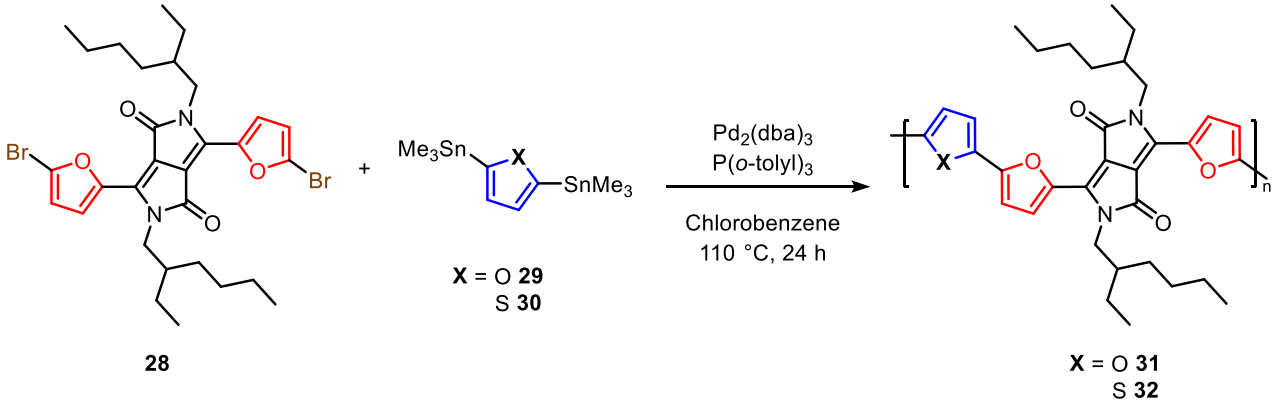

Figure 13. Synthesis of 2,5-furan-based photovoltaic polymer *via* Stille cross-coupling.

Small furan-based molecules also find potential as dye-sensitized solar cells as reported by Lin *et al.* where their group constructed a metal-free furan-containing push-pull compound (**36**).[51] This synthesis was accomplished by starting with a close halogenated derivative of furfural (**9**), 5-bromofurfural (**33**). 5-Bromofurfural **33** participated as the aryl halide coupling partner for a Pd-catalyzed Suzuki cross-coupling reaction with triphenylamine boronic acid (**34**), producing the newly arylated aldehyde (**35**). Aldehyde **35** was then reacted with cyanoacetic acid and NH_4OAc resulting in the final small push-pull compound **36** (Figure 14). Push-pull molecules are systems that include electron donor (D) and electron acceptor (A) groups which co-exist in the compound, providing a more facile route for electrons to flow (from D to A). These types of compounds are useful for the development of more efficient solar cells as they tune optical properties, electronic properties, and provide efficient intramolecular charge transfer of said devices.[60] Furans, on the other hand, are introduced in this material to play the role of π-spacer, an important mediator within

the complex that modifies the molecular conformation, photoelectric properties and/or the micromorphology of the device.[42] The dye-sensitized solar cell **36** can be described as a D-π-A compound where triphenylamine is the donor (highlighted in blue), furan is the mediating π-spacer (highlighted in green) and 2-cyanoacrylic acid acts as the electron acceptor (highlighted in red).[51]

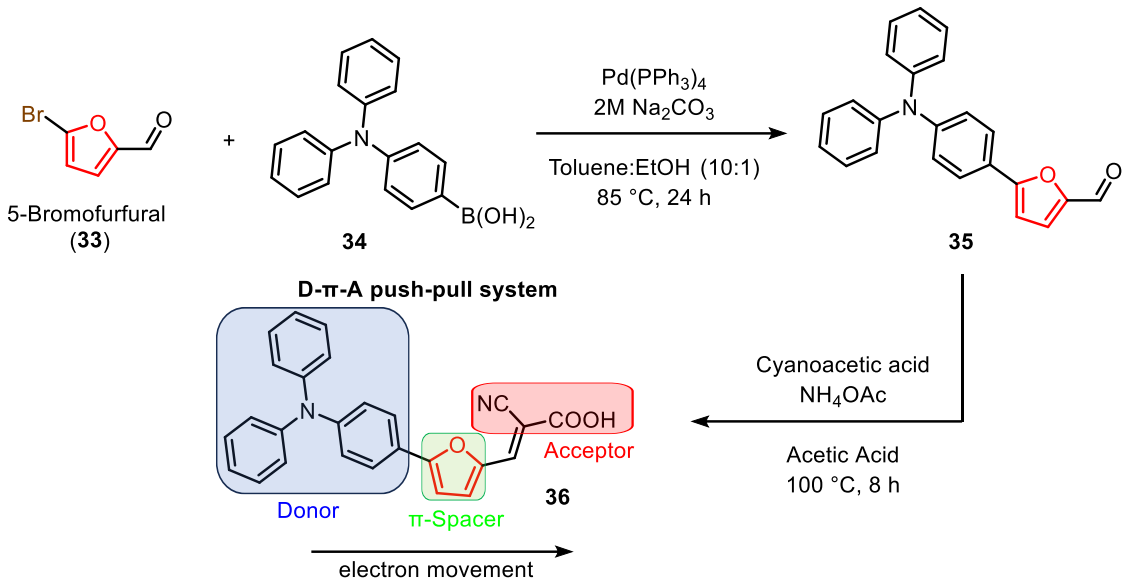

Figure 14. Synthesis of push-pull 2,5-furan-based dye-sensitized solar cells *via* Suzuki cross-coupling.

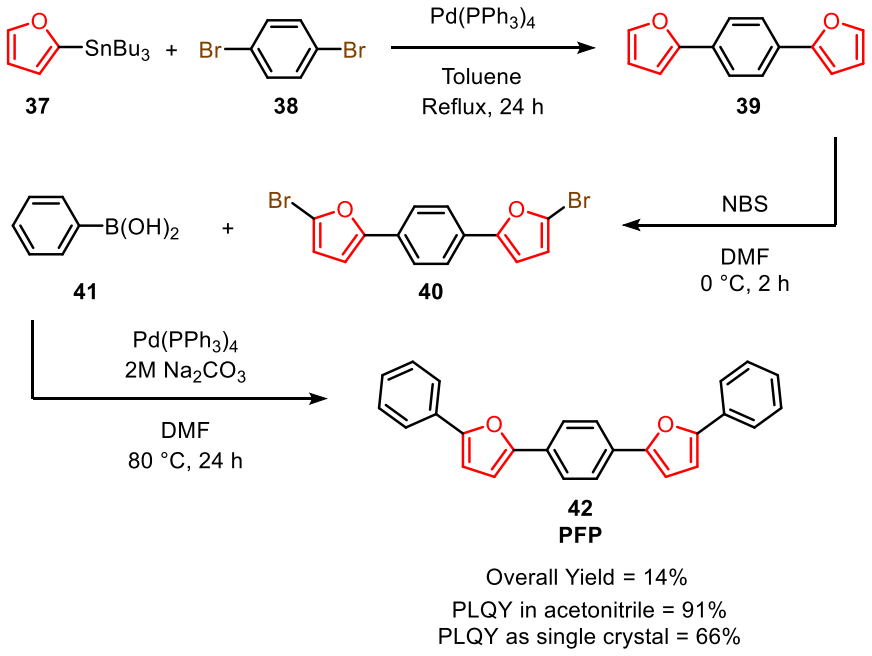

Figure 15. Synthesis of a highly fluorescent 2,5-furan-based phenylene co-oligomer through double Stille and Suzuki cross-coupling.

Lastly, regarding the synthesis of potential furan-based OFETs, Kazantsev *et al.* report a four-step synthesis to produce furan/phenylene co-oligomer crystals (**42**, **PFP**, see Figure 15).[54] Co-oligomers are defined as oligomers that incorporate more than one type of monomer within the structure. The highlighted synthesis will be discussed generally here, and in more detail in Chapter 3.2. Their synthesis begins with producing the furan organotin complex (**37**) derived from simple furan **23** (not shown in Figure 15). Organotin **37** is then directly consumed for a double Pd-catalyzed Stille cross-coupling with dihalide (**38**) to produce the furan-phenylene-furan core (**39**), this core is immediately dibrominated using NBS in DMF solvent. The newly formed dihalogenated complex (**40**) is coupled with phenylboronic acid (**41**) twice through a double Suzuki cross-coupling reaction in DMF solvent to produce the furan/phenylene co-oligomer crystal (**42, PFP**) in an overall yield of 14%. Final co-oligomer **PFP** (**42**) is impressive as a potential OFET candidate as it demonstrates good charge mobilities (0.12 $cm^2\ V^{-1}\ s^{-1}$) and reports an exceptionally high PLQY of 91% in acetonitrile and 66% as a single crystal, making it a valued optoelectronic candidate.[54] Despite these impressive results, it is important to note that the synthetic route to access product **42** requires substantial changes due to the high use of DMF. DMF is a polar aprotic amide molecule said to be a universal solvent for various chemical reactions, however, due to its high reproductive toxicity the European Union has restricted its use as of December 2023.[61] This means that chemists must find new alternative solvents, and substitute DMF to practice safer chemistry procedures moving forward.

1.2.3 Evaluation of Cyclization Synthesis on π-Conjugated Furans

Synthetic cyclization methodologies are also effective approaches to produce furan-based materials for optoelectronic devices. The primary benefits of this approach are that these methods require less reaction times, often including a one-pot synthetic step, and can produce multi-arylated heterocycles; a useful chemical tool when designing new push-pull systems. However, their drawbacks are quite noticeable as they cannot incorporate biomass-derived heterocycles into synthesis, meaning they are limited to petrochemicals. Starting reagents used in these methods are often not commercially available and are not always bench-stable due to their chemical complexity. Although designing multi-arylated compounds is possible and primarily performed using this method, there lacks the accessibility for late-stage functionalization.[62] Therefore,

developing a Pd-catalyzed cross-coupling route to produce multi-arylated furans can overcome these limitations mentioned (further discussed in Chapter 2).

The first highlighted cyclization is reported by Parakka and Cava, who demonstrated an effective cyclization methodology to produce a small library of sequential heterocyclic pentamers, such as thiophene-furan alternating co-oligomer (**44, TFT**) in high yields.[63] This is accomplished through a two-step process involving the Paul-Knorr synthesis to cyclize the diketone motif (**43**) into heterocyclic furans for the final step (Figure 16). Their method derives five conjugated heterocyclic co-oligomers quite quickly without the formation of any organometallic waste (a drawback in classical Pd-catalyzed cross-coupling reactions). Limitations here include the restriction to a heteroaromatic motif with unfunctionalized heterocycles and the use of petrochemicals solely.

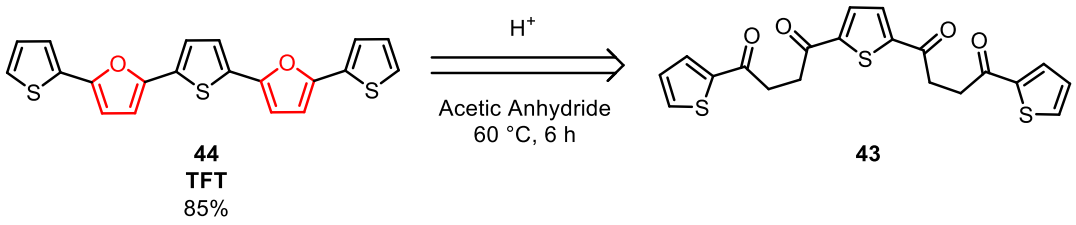

Figure 16. Paul-Knorr cyclization to produce thiophene-furan alternative co-oligomers.

More complex cyclization reactions accessing multi-arylated furan derivatives can be approached in various ways.[64,65] One example to highlight this field comes from Wu and Yoshikai who report a [2+2+1]-type cyclization per furan synthesized under Pd-catalysis using three specific reagents: hypervalent bis-alkynylbenziodoxole (**45**), aryl carboxylic acid (**46**) and an N-aryl imine (**47**, PMP = *p*-MeOC$_6$H$_4$).[66] 2,3,5-Multi-arylated furan (**48**) was made in one-pot yields of 38%, reported with a fair PLQY of 31% (Figure 17). However, the drawbacks of this approach are the same as those previously mentioned.

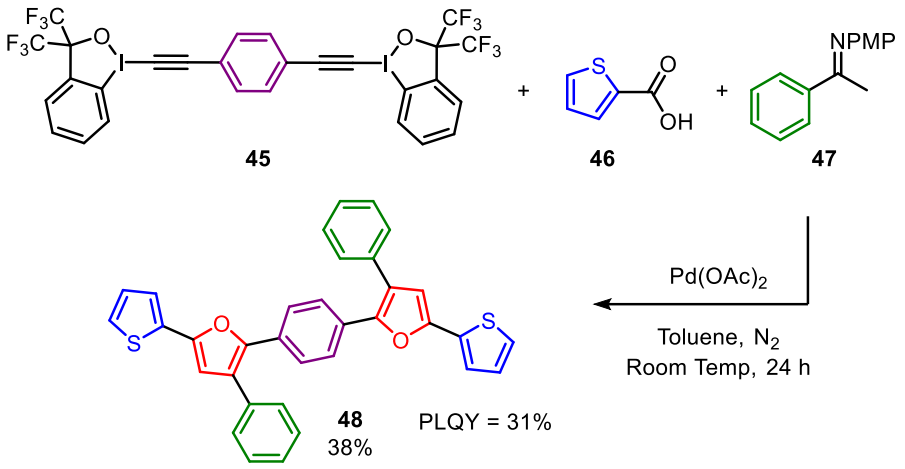

Figure 17. Cyclization of multi-arylated furans using bis-alkynylbenziodoxoles, carboxylic acids and imines through Pd-catalysis (colours added for aryl clarity).

1.3 Palladium-Catalyzed Cross-Coupling Reactions of Heterocycles

As discussed in Chapter 1.2.2, Pd-catalyzed cross-coupling reactions are extremely useful methods to produce new carbon-carbon bonds. These reactions are often utilized for the development of pharmaceutical candidates, agrochemicals, organic electronics, and many other fields of chemistry.[67] The importance of carbon-carbon bond formation *via* Pd-catalysis was acknowledged by providing scientists Richard F. Heck, Ei-ichi Negishi and Akira Suzuki a Nobel prize in 2010 for their work in developing "palladium-catalyzed cross-couplings in organic synthesis".[59] Palladium itself is a transition metal found in the 10th group of the periodic table with an atomic number of 46. What makes palladium special as a metal catalyst, is its ability to efficiently shuffle oxidation states from Pd(0)/Pd(II) and Pd(II)/Pd(IV), making two electron transfer processes possible. Pd(0) is considered the active oxidation species in catalytic cycles (often written as L_2Pd), this oxidation state exists with coordinating phosphine ligands (a common example being $Pd(PPh_3)_4$) making an 18-electron complex. Once in solution, phosphine ligands can dissociate forming reactive 16, 14 and 12 electron-counted complexes. However, due to its high reactivity, Pd(0) complexes must be stored under inert gas and at cool temperatures for preservation. To avoid the need for these protective measures, a more accessible Pd(II) pre-catalyst (common examples being $Pd(OAc)_2$ and $PdCl_2$) can be used instead due to its higher stability in ambient conditions. However, Pd(II) pre-catalysts must undergo reduction *in situ* to form the more

reactive Pd(0) species for the catalytic cycle to proceed. Reduction of the pre-catalyst is possible through high thermal conditions, reduction by organometallic coupling partners or reduction by the associated phosphine ligands.[68] It is noted that the reduction of palladium is not well understood, but the catalytic cycle of Pd-catalyzed cross-couplings has been extensively investigated.

After the catalyst is reduced to Pd(0), the generalized catalytic cycle of palladium cross-coupling reactions begins with an oxidative addition of the catalyst inserting itself into the carbon-halide bond of the electrophilic aryl halide (**49**) as seen in Figure 18.

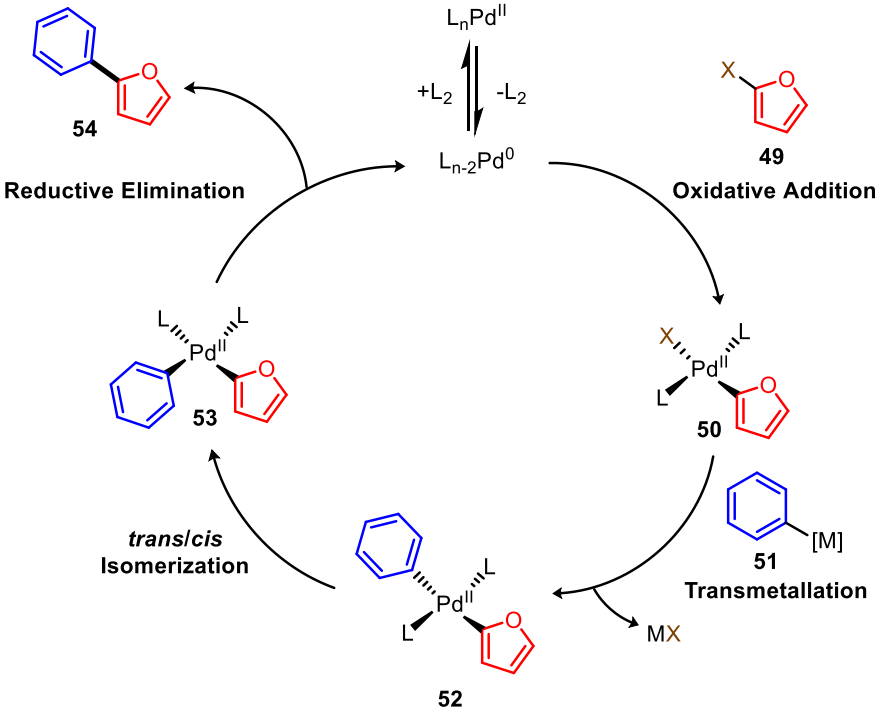

Figure 18. Generalized catalytic cycle for palladium-catalyzed cross-coupling reactions.

In doing so, this insertion oxidizes the palladium from a Pd(0) to Pd(II) species, where the metal forms a square planar molecular geometry (**50**). The next step occurs with the nucleophilic aryl coupling partner (**51**) as it undergoes a transmetallation with palladium-complex **50**, forming a diarylated palladium intermediate (**52**) with a trans conformation and a metal salt. This formation of salt is stoichiometric and considered a limitation of these reactions depending on the overall toxicity of these by-products, especially seen with Stille cross-coupling discussed in the next

subchapter. The trans intermediate **52** must then isomerize to its cis conformation (**53**) where the diaryl organic rings are now in closer proximity for a reductive elimination step, fusing the two aryls (**54**) to form a new sp_2-sp_2 carbon-carbon bond and simultaneously reduce the Pd catalyst back into its active Pd(0) species.

While many variations of these reactions exist based on the organometallic of choice, this thesis will focus on classical Stille and Suzuki Pd-catalyzed cross-coupling reactions, as they are some of the most utilized methods to form new sp_2-sp_2 carbon-carbon bonds for furan containing compounds as π-conjugated electronic candidates presently. Decarboxylative Pd-catalyzed cross-coupling will also be discussed as an alternative cross-coupling approach to traditional methods.

1.3.1 Stille Cross-Coupling Reactions of Heterocycles

In 1978, Milstein and Stille published their first work on ketone synthesis starting from acyl chlorides and organotin reagents with catalytic amounts of palladium.[69] Stille was named for this reaction after his cumulative work and mechanistic studies on the catalytic cycle of this reaction.[58] The catalytic cycle follows Figure 18 quite well as the Stille cross-coupling does not require additional additives, making this coupling quite mild to perform. It simply utilizes an organotin nucleophilic coupling partner (**56**) and an electrophilic aryl halide (**55**) for the reaction to proceed (Figure 19). Hence, this coupling methodology is quite a popular choice amongst chemists for the design of organic optoelectronics. For conjugated furan optoelectronic candidates specifically, the Stille cross-coupling is the most popular methodology to further conjugate furan rings, since the coupling is an effective high-yielding reaction that is also sensitive towards the reactive nature of furans.[45–47,50,53,54,70–74] The main limitation of this reaction is the subsequent organostannane-salt (**58**), a stochiometric by-product that is considered biocidal, and highly toxic to all life as it directly attacks the liver, nervous system, and reproductive system.[75,76]

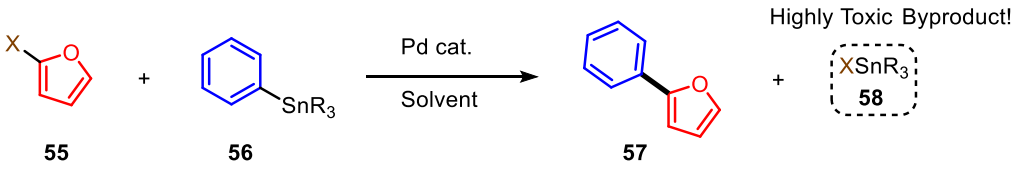

Figure 19. General Pd-catalyzed Stille cross-coupling reaction.

1.3.2 Suzuki Cross-Coupling Reactions of Heterocycles

The Suzuki cross-coupling (often referred to as Suzuki-Miyaura cross-coupling) reaction introduced the first coupling of an aryl halide and a phenylboronic acid in 1981.[77] Their work was extraordinarily impressive as it reported the use of organometalloids instead of organometallics in basic conditions to form new sp_2-sp_2 carbon-carbon bonds. Boronic acids are much less toxic than their organometallic counterparts, making them more environmentally friendly. These compounds are also considered bench stable, as they are less sensitive to air and moisture, making them easier to handle during synthesis. Another key feature of this reaction is the ability to work in mild aqueous conditions which was unheard of with organometallic coupling partners. For these reasons alone, researchers over the years have continuously used this methodology as the leading cross-coupling reaction.[67] Discussing its mechanism, it does follow the same principles as traditional Pd-catalyzed cross-couplings from Figure 18. However, there is an additional step as the requirement of a base is necessary for two roles (Figure 20). Firstly, the base can undergo a ligand substitution with the halogenated palladium complex (**60**) forming a new complex (**61**) which is important for the transmetallation step. Secondly, the base converts the less reactive boronic acid (**62**) to its more activated boronate anion (**63**). Forming anion **63** increases the overall nucleophilicity to initiate the transmetallation step with complex **61**. Complex **61** is necessary as it produces the relatively stable boronate by-product (**64**). After isomerization, the reductive elimination step occurs, providing the desired product (**66**).

What is very interesting to note about the Suzuki cross-coupling is how its Pd(II) pre-catalyst gets reduced to Pd(0) to enter the catalytic cycle. Since this reaction can be performed in water and at room temperature, reports have theorized that this reduction occurs from the reductive nature of the boronate anion *via* transmetallation with a labile ligand.[78] This occurs twice, coordinating two R groups (R = aryl) onto the palladium metal. Reductive elimination then occurs and what is

observed is an R-R minor by-product, known as the homocoupling product, as well as the reduction of Pd(II) to Pd(0) allowing the catalytic cycle to properly commence (Figure 21).[78]

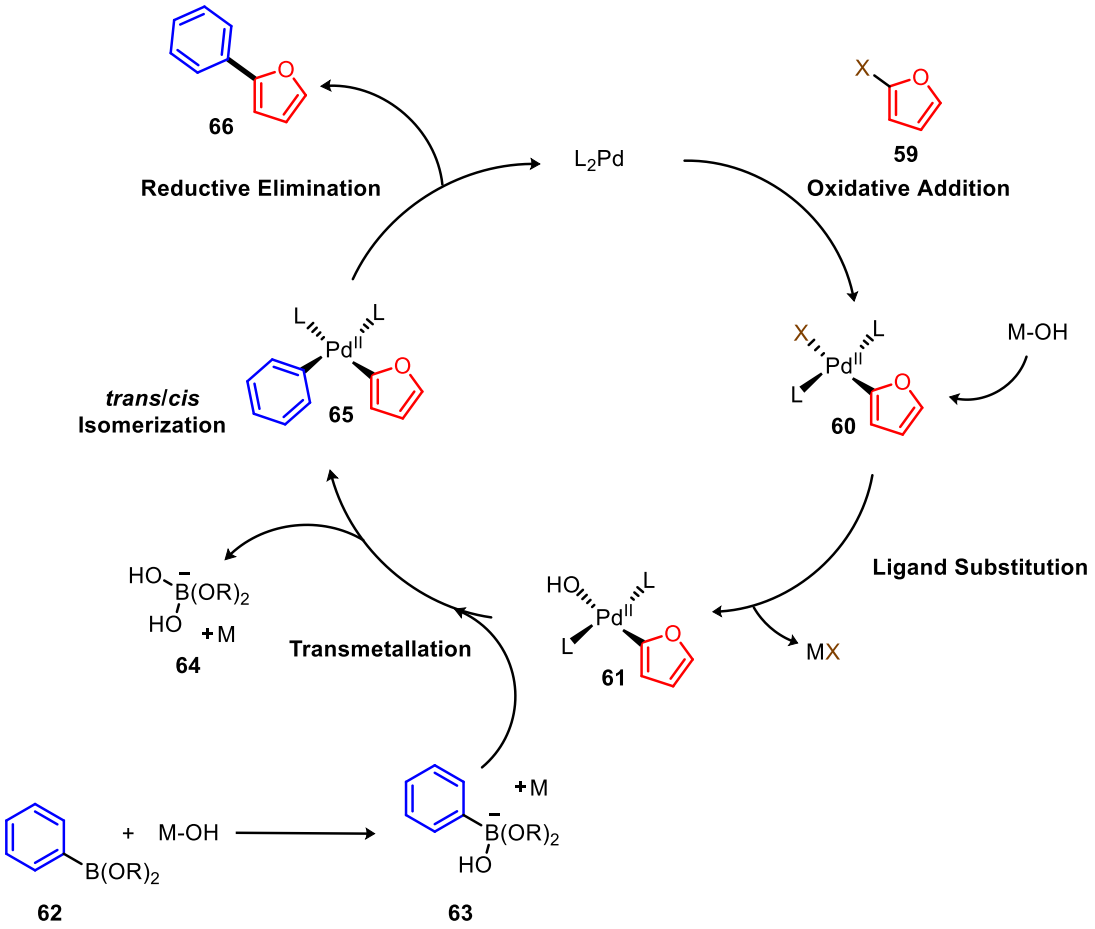

Figure 20. Catalytic cycle of the Suzuki cross-coupling reaction.

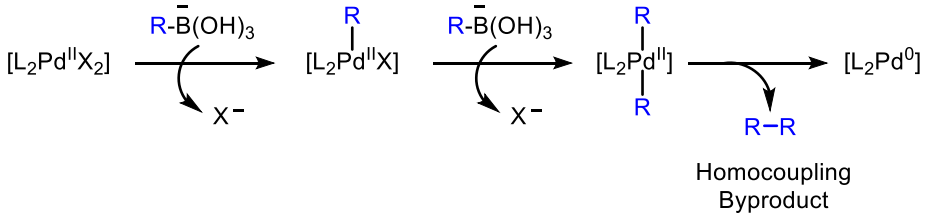

Figure 21. Simplified pathway to reduce Pd(II) to Pd(0) and form homocoupling by-product through boronate anions.

To highlight just how mild these reactions are performed with furans specifically, in 1999, Bussolari and Rehborn demonstrated a very mild Suzuki cross-coupling of 5-bromofurfural (**33**) (a very close derivative of biomass-derived furfural, **9**) and phenylboronic acid (**62**) using a cheap Pd(II) pre-catalyst ($Pd(OAc)_2$) with K_2CO_3 and tetrabutylammonium bromide (TBAB) in water at room temperature (Figure 22).[79] TBAB is necessary to solubilize the organics into water and after 1.75 hours they reported an impressive 74% yield of product (**67**). This reaction also touches on green chemistry principles: as it requires a catalyst, ignores the use of volatile solvents, utilizes biomass-derived starting materials, and requires no external energy source to heat the reaction.

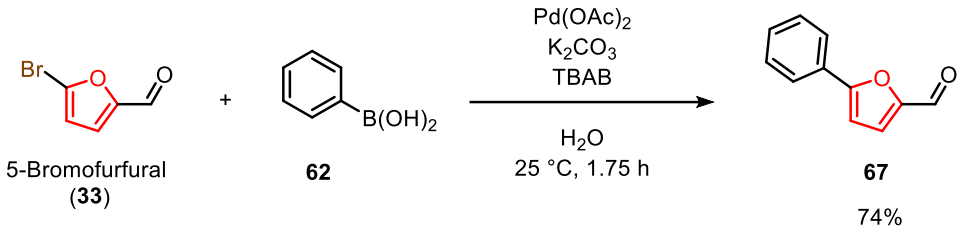

Figure 22. Suzuki cross-coupling reaction of 5-bromofurfural (**33**) in water at room temperature.

1.3.3 Decarboxylative Cross-Coupling Reactions of Heterocycles

The main limitations associated with classical Pd-catalyzed cross-couplings relate to their stoichiometric organometallic by-products, as mentioned previously. As seen based on their mechanism, it is not possible to avoid these wasteful and potentially dangerous unwanted products. Therefore, researchers have devoted efforts developing new methodologies to form selective sp_2-sp_2 carbon-carbon bonds while minimizing overall waste. An alternative synthetic approach to couple heterocyclic compounds such as furans while limiting the total amount of waste, begins with reported work by Forgione, Bilodeau *et al.* in 2010.[80] Their methodology introduced a Pd-catalyzed decarboxylative cross-coupling (DCC) on heterocyclic carboxylic acids nucleophiles coupling with electrophilic aryl halides through Pd-catalysis and basic conditions, releasing stoichiometric amounts of CO_2 as a gas by-product. This work highlights the optimization process including a detailed discussion on the effects different bases, catalysts and solvents have on facilitating the reaction under microwave conditions. Regarding yields, Cs_2CO_3 is the most effective base, DMF, DMA, NMP, and THF also report great yields as the chosen solvents and a variety of both Pd(0) and Pd(II) catalysts can be utilized. Microwave conditions drastically benefit

this reaction as well since the microwave can achieve high temperatures (170-190 °C) in a short time (a necessary condition to provide enough activation energy to decarboxylate the carboxylic acid). What is also impressive with this approach is the quick total reaction times required, often seen at 8 – 15 minutes. Lastly, minimizing the overall waste is made possible due to the swap of organometallic partners with ubiquitous carboxylic acids. Various carboxylic acids are commonly found in nature and are highly bench stable. Biomass-derived furans make especially ideal Pd-catalyzed DCC coupling partners due to their common carbonyl handle (seen with HMF **1** and furfural **9**) which can be oxidized to the desired acid and be readily used whenever required.

Regarding its mechanism, Pd-catalyzed DCC has been reported to follow three different pathways.[80] However, regarding pre-arylated furans specifically, it has been discussed that one of these pathways is more plausible than the others (Figure 23, where Ar = aryl).[80,81]

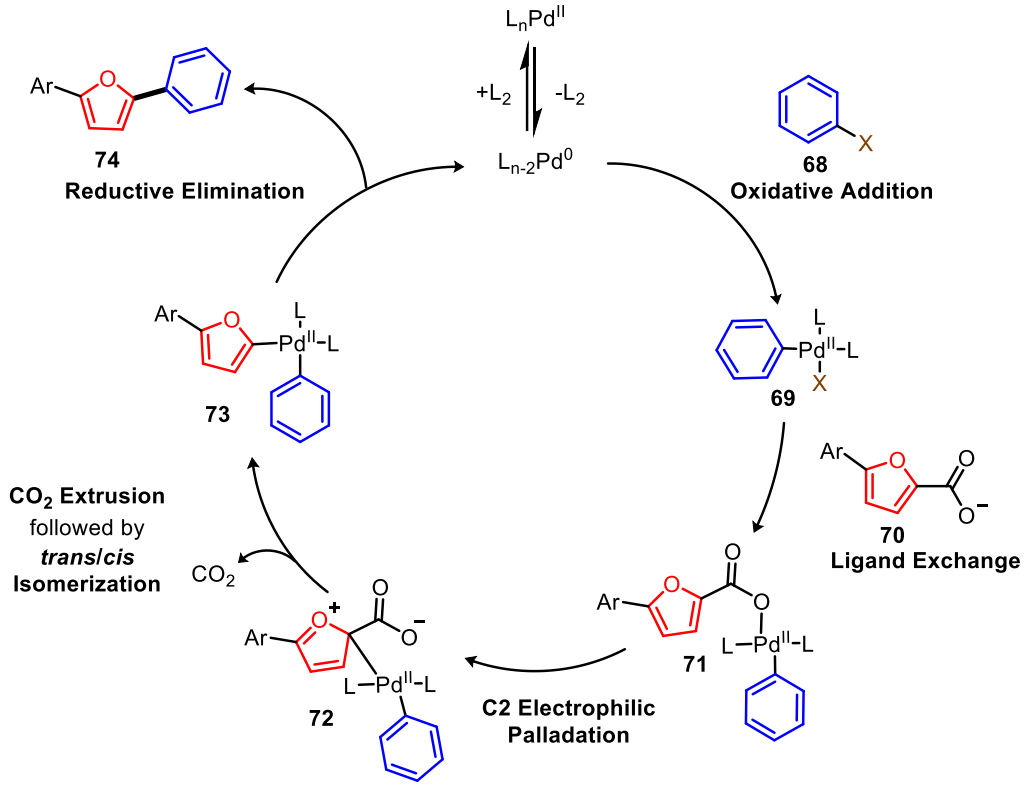

Figure 23. Proposed Pd-catalyzed DCC mechanism of pre-arylated furan carboxylic acids and aryl halides.

After the pre-catalyst is reduced to the active $L_2Pd(0)$, the metal begins with an oxidative addition inserting itself into the aryl-halide bond of compound **68** forming an oxidized Pd-complex (**69**).

The arylated heterocyclic carboxylic acid is then deprotonated (**70**) by a base further increasing its nucleophilicity towards the metal. Through a ligand exchange with Pd-complex **69** the labile ligand leaves and forms the newly made metal complex (**71**). Having an electron-rich heterocycle like a conjugated furan with a carboxylate directing group promotes the C2 electrophilic palladation to form Pd-intermediate (**72**). Having broken aromaticity to accomplish this palladation, CO_2 extrusion occurs, producing CO_2 gas while rearomatizing the furan ring, followed by isomerization to form the cis isomer (**73**). Lastly, reductive elimination occurs to produce the desired compound (**74**) while reforming the active catalyst.

To this day, the Forgione research group continues to lead the field of Pd-catalyzed DCC of heterocyclic carboxylic acid compounds to access drug candidates[81] and highly conjugated organic materials.[62,82]

Developing strategic methods to access desirable materials (such as oligomers) while minimizing total waste should be a priority for all organic chemists. In the field of Pd-catalyzed cross-coupling reactions, performing a double reaction minimizes the total steps required when designing two new carbon-carbon bonds. On paper, double cross-coupling reactions require 2:1 starting materials to produce these desired bonds. Performing this reaction twice using classical approaches produces twice the amount of waste. For this reason, Pd-catalyzed DCC are a useful synthetic tool for double cross-coupling reactions. For example, in 2020, Liu (a former Forgione research group student) developed a double cross-coupling approach to make various oligothiophenes for potential optoelectronic candidates.[82] Naturally, classical Pd-catalyzed cross-coupling methods like Stille and Suzuki were utilized to make said products due to their well-known chemistry. Liu opted to develop a new approach through a double Pd-catalyzed DCC reaction using carboxylate starting material (**80**), avoiding the production of such wasteful organometallic/metalloid by-products while promoting more green chemistry practices with his synthesis. Figure 24 illustrates three different double cross-coupling approaches to access thiophene trimer (**77**) (a short-chained material to produce longer conjugated oligothiophenes) and highlights the differences with their conditions, yields and green metrics (*E-factor* and *Atom Economy* from Chapter 1.1.1). Not only does the DCC method require less time and have a slightly better yield, but it also minimizes overall waste (*E-factor*) and provides a slightly better *Atom Economy* than traditional methods.

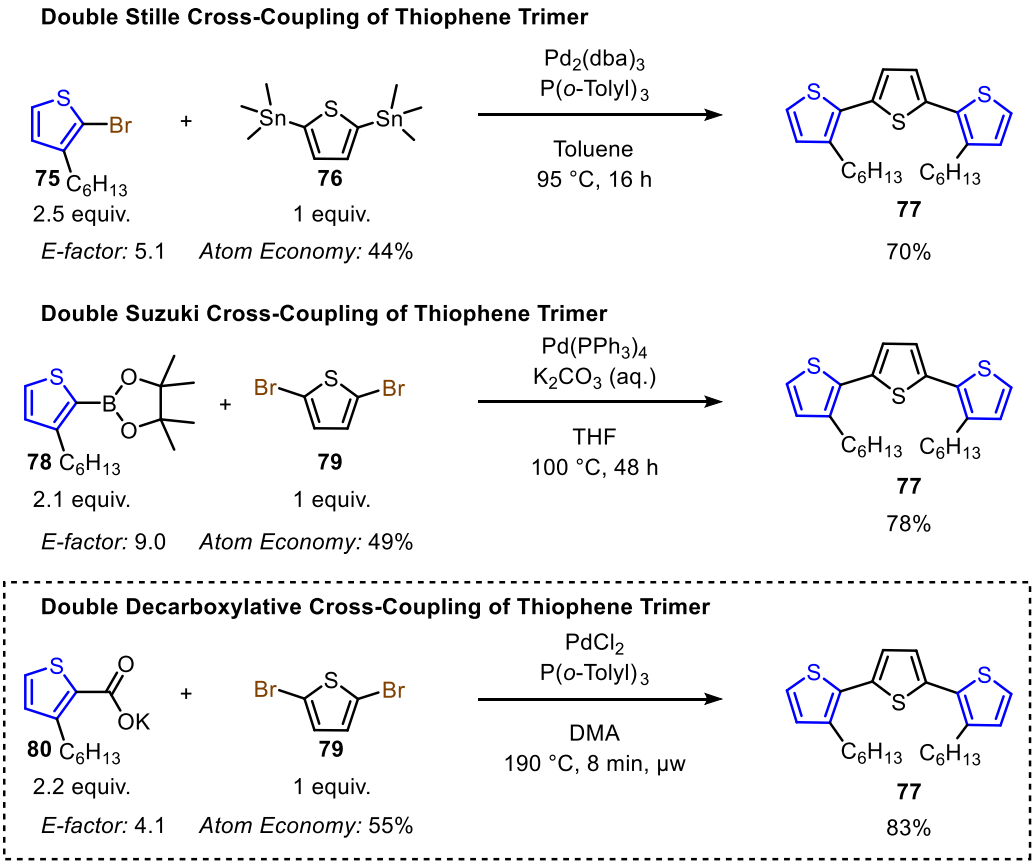

Figure 24. Double cross-coupling comparison of thiophene trimer (**77**) highlighting the benefits of a double DCC.

To our knowledge, no other researchers have attempted to develop a double DCC approach with arylated-furan carboxylic acids (derived from lignocellulosic biomass), specifically to access small furan-based oligomers with potential applications into optoelectronic candidates.

1.4 Research Goals and Thesis Organization

The focus of this thesis is to develop a synthetic methodology to access high π-conjugated materials derived from (or a close derivative of) lignocellulosic biomass through a double DCC reaction. Chapter 1 introduces the dependence of petrochemical starting materials and how biomass-derived starting materials such as furans should be further incorporated into synthesis. Additional chemical characteristics explain how furans can behave as thiophene replacements for the design of optoelectronic candidates, as they naturally exhibit higher PLQY than thiophenes. Lastly, we present a discussion of how furan-based electronic materials are commonly made through classical Pd-catalysis or cyclization methods and that more green principles should be applied when developing such materials.

Chapter 2 will focus on developing multi-arylated furans (without the use of cyclization methods) with HMF and methyl 5-bromofuran-2-carboxylate as starting materials. The small library of multi-arylated products is accessed through a double Pd-catalyzed DCC reaction and then studied in dilute $CHCl_3$ solution to investigate their spectroscopic characteristics, including their PLQY.

Chapter 3 focuses on using the close furfural derivative 5-bromofurfural to design small 2,5-furan-based phenylene/thiophene oligomers through a double Pd-catalyzed DCC reaction and will evaluate how environmentally benign this synthesis is than current methods. The developed oligomers were then studied in dilute $CHCl_3$ solution to investigate their spectroscopic characteristics, including their PLQY. Discussions of their tunable absorbance and photoluminescence maxima are also presented.

Chapter 4 concludes this research and will provide an outlook for future work related to the use of biomass-derived starting materials into possible optoelectronic candidates.

Chapter 2. Synthesis of Multi-Arylated Furans *via* Pd-catalyzed Cross-Coupling Reactions

2.1 Introduction

The goal of this chapter is to develop a synthetic methodology to produce multi-arylated furans (such as compound **48** in Figure 17) using a Pd-catalyzed cross-coupling methodology with biomass-derived, HMF (**1**), or a close derivative, methyl 5-bromofuran-2-carboxylate (**99**) as starting materials. Incorporating furan heterocycles directly into synthesis avoids the need for cyclization methods (which use non-commercially available starting materials derived from petrochemicals) and offers the potential for late-stage functionalization by picking and choosing where extended aryl groups bond onto the furan heterocycle. A potential route to develop 2,3,5 (**85**) or 2,4,5 (**90**) multi-arylated furans from HMF (**1**) is depicted in Figure 25 and Figure 26 respectively. Notable transformations from either method include oxidation of HMF to develop carboxylic acid, HMFA (**81**), regioselective electrophilic aromatic bromination to bond halogens onto the furan core and the Suzuki cross-coupling reaction to install aryl groups onto the furan ring. Having access to carboxylic acids (**81**, **89**) provides the possibility of a double Pd-catalyzed DCC reaction, as seen by fusing a dihalide (**38**) central linker to effectively extend conjugation. Solid arrows seen in Figures 25 and 26 depict transformations that have been completed and will be discussed, whereas dotted arrows represent theoretical transformations that have not been studied.

Additionally, furan-containing starting material, methyl 5-bromofuran-2-carboxylate (**99**), was also used to develop 2,5/2,3,5/2,4,5-multi-arylated furan compounds with a thiophene central linker (see Figure 40 in Chapter 2.3). This methodology is quite robust and modular as it takes advantage of the directing methyl ester group to regioselectivity arylate at any position on the furan.

The Pd-catalyzed cross-coupling methodology utilizing HMF is discussed throughout Chapter 2.2, where advantages and limitations are highlighted, while the methyl 5-bromofuran-2-carboxylate approach is further discussed in Chapter 2.3. All multi-arylated furans produced are spectroscopically investigated to study their optical properties, including their absorbance, photoluminescence and PLQY in dilute $CHCl_3$ solution (Chapter 2.4).

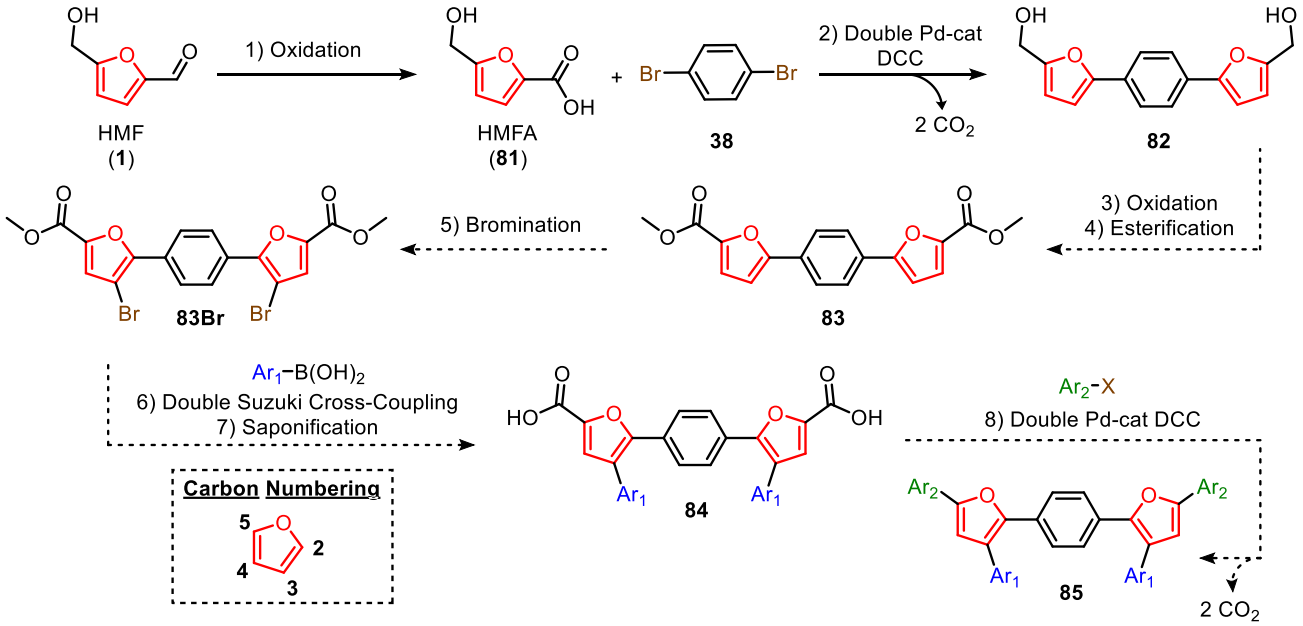

Figure 25. Generalized synthesis starting with HMF (**1**) to synthesize 2,3,5 multi-arylated furan (**85**) in eight steps. Carbon numbering is also provided concerning the leftmost furan per compound.

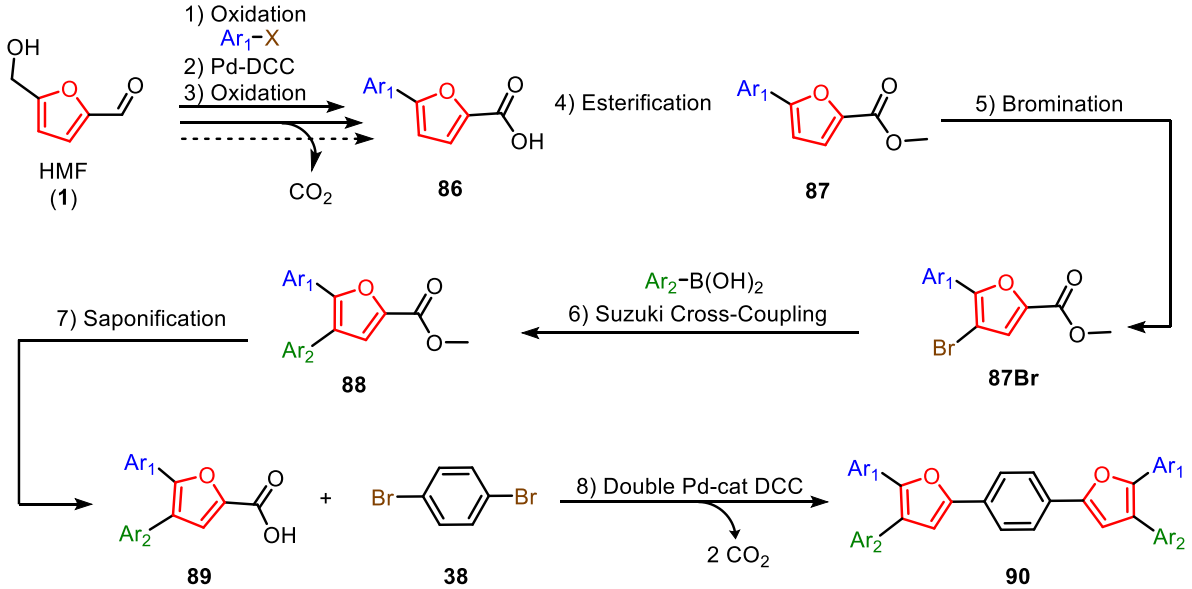

Figure 26. Generalized synthesis starting with HMF (**1**) to synthesize 2,4,5 multi-arylated furan (**90**) in eight steps.

2.2 Results and Discussion on HMF as a Starting Material

Methodology starting with HMF to attempt 2,3,5-multi-arylated furans as shown in Figure 25:

Our journey to access 2,3,5-multi-arylated furans begins with the oxidation of HMF (**1**) into its carboxylic acid derivative (**81**) through selective Pinnick oxidation (Figure 27). The Pinnick oxidation is mild (can be performed in water and at room temperature) and is commonly used to selectively convert an aldehyde into a carboxylic acid using inexpensive and easily accessible sodium chlorite ($NaClO_2$).[83] Unfortunately, once sodium chlorite reacts with the electrophilic carbonyl, it produces a more reactive oxidant called hypochlorous acid (HOCl) which can undergo unwanted side reactions. A sacrificial scavenger (2-methyl-2-butene, hydrogen peroxide or sulfamic acid) is often added to this reaction to consume HOCl and allow the reaction to proceed as intended. Sulfamic acid was chosen since it is reported to be a good candidate for the oxidation of hydroxylated aromatic aldehydes (such as HMF).[83] Repeated experiments provided yields between 55-62% where on average a 1:4 ratio of HMF(**1**):HMFA(**81**) was observed by ^{1}H NMR. We suspect that the remaining yield is lost in the workup due to the high solubility of both HMF and HMFA in water.[84]

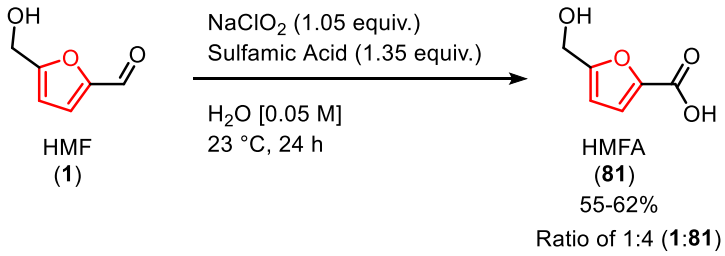

Figure 27. Pinnick oxidation of HMF (**1**) to HMFA (**81**).

Obtaining a fair yield of starting carboxylic acid (**81**) through this method enabled the opportunity to directly attempt a double Pd-catalyzed DCC reaction with 1,4-dihalide (**38**) as the central linker. This approach would extend conjugation quickly since a double cross-coupling reaction is performed, fusing two HMFA compounds to form a conjugated diol (**82**), as seen in Figure 28. Presently, the only work to report a single Pd-catalyzed DCC on HMFA (**81**) was reported from Chacón-Huete *et al.* who converted biomass-derived materials into a muscle relaxant known as Dantrolene.[81] That work highlighted the importance of the hydroxymethyl handle found in HMFA

to help coordinate the Pd-catalyst and potentially ease the C2 electrophilic palladation step (as discussed in Chapter 1.3.3) to push the cross-coupling reaction forward.[81] The double Pd-catalyzed DCC begins by mimicking these conditions and investigating their yields.

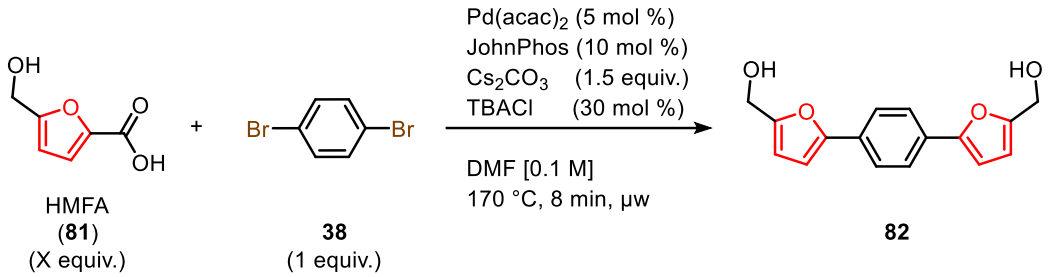

Figure 28. Double Pd-catalyzed DCC of HMFA (**81**) and 1,4-dibromobenzene (**38**) to diol (**82**).

Table 1. First double Pd-catalyzed DCC with microwave vial test.

Entry	81 X equiv.	Vial Type	82 Yield %	C-C bond formation%
1[a]	2	Conical (0.5-2 mL)	18	42
2	4	Conical (0.5-2 mL)	21[c]	46
3	4	Round (2-5 mL)	40[c]	63
4[b]	4	Conical (0.5-2 mL)	6[c]	25
5[b]	4	Round (2-5 mL)	0[c]	N/A
			Humin Formation	

[a] Performed literature conditions. [b] Reagents added to vial and reaction performed under argon gas. [c] Yield determined by ^{1}H NMR with 1,3,5-Trimethoxybenzene (TMB) as internal standard.

Table 1, entry 1 depicts these conditions in a 2:1 ratio of HMFA (**81**) to 1,4-dihalide (**38**) providing an 18% isolated yield after column chromatography. Since all double reactions form two new carbon-carbon bonds, another metric to consider is the product of bond formation per coupling reaction. This is measured by calculating the square root of the total yield. For example, an 18% yield was obtained using a double reaction, hence $\sqrt{0.18} \approx 0.42$. This means that the initial cross-coupling reaction (between acid and the first bromine of dihalogenated aryl) had approximately 42% carbon-carbon bond formation, as well as the second cross-coupling reaction (between another acid and the second bromine of halogenated aryl bonded to a single hydroxymethyl furan), which also had 42% bond formation. Mathematically this be expressed as such: 0.42% × 0.42% = 0.18% yield total. This was a promising first result as it indicated that HMFA (**81**) can undergo a

double Pd-catalyzed DCC reaction using microwave irradiation to produce the conjugated diol (**82**). To further optimize the reaction, a 4:1 ratio of acid to dihalide was reattempted, however, the yield did not change significantly (Table 1, entry 2). A change in the microwave vial (from conical 0.5-2mL to round 2-5mL) did noticeably increase the yield to 40% (entry 3, 63% bond-formation per coupling reaction) possibly due to more effective stirring in the larger vial. Additional headspace is also provided; however, this was not further investigated and is uncertain what role that would play in the reaction. These exact procedures were then retested in an inert environment (under argon) using both vials (entries 4 and 5). Entry 4 performed much worse in terms of yield compared to entry 2. The most interesting observation came from entry 5, which did not produce any diol (**82**) and instead formed insoluble polymeric "humin" after a workup. Humins are dark-coloured carbon-based macromolecular clusters that can form after HMF or close derivatives begin to polymerize in acidic environments or at high temperatures, primarily due to the hydroxyl and carbonyl functional groups present.[85,86] Figure 29 depicts all samples after irradiation and the humin polymer that is produced.

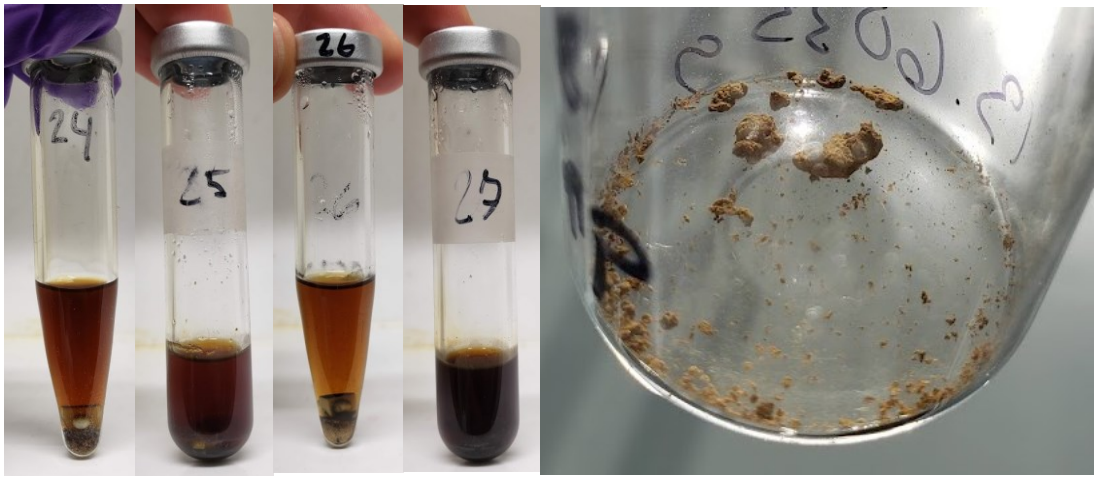

Figure 29. From left to right: Entry 2, 3, 4, and 5 vials after microwave irradiation. Most right: Humin polymer by-product observed after microwave irradiation of vial 5.

At this stage, the entire synthesis of 2,3,5-multi-arylated-furans from Figure 5 was under evaluation from a synthetic point of view since potential problems were more evident. Firstly, by forming a highly conjugated diol (**82**), more polar aprotic solvents like DMF would be required to further dissolve and perform necessary transformations. Recall that DMF is restricted under the

EU presently and is best to avoid it whenever possible. Additionally, the selective bromination step (step 5 of Figure 25) is quite ambitious and difficult to predict that a double bromination would behave as anticipated. Therefore, it seemed best to attempt another method to produce multi-arylated furans from HMF.

It is worth noting that π-conjugated diol (**82**) could potentially be an interesting monomer candidate to produce polyesters or epoxy resins. Other groups have shown the benefits of synthesizing diol monomers directly from HMF (**1**) before, including flexible to more rigid diols used in the production of polyesters.[87,88] Not only would those polymers use a biomass-derived starting material, but this motif could potentially enhance the strength of said polymer due to its highly planar and rigid furan-phenylene-furan core.[54,89] The furan-phenylene-furan core is a fascinating structural motif as it often expresses naturally high fluorescence in solution or as a crystal, exhibiting more intense luminescence than similar heterocycle oligothiophenes.[54,71,90] Further discussions regarding this structure will be discussed in Chapter 3.

Methodology starting with HMF to attempt 2,4,5-multi-arylated furans as shown in Figure 26:

Another method to access multi-arylated furans from HMFA (**81**) could occur after a single Pd-catalyzed DCC reaction followed by the oxidation of the hydroxymethyl handle into a carboxylic acid (Steps 2 and 3 from Figure 26). The acid can then be converted to an activated ester, perfect for electrophilic aromatic substitution (EAS) to selectively provide a bromine atom on the C4 position of the furan ring. The newly halogenated furan is then susceptible to a Suzuki cross-coupling to install an aryl group onto the furan core. The remaining diarylated furan ester (**88**, Figure 26) is then saponified to its carboxylic acid (**89**) species where it can undergo a double Pd-catalyzed DCC reaction with a dihalide (**38**) to produce the desired 2,4,5-multi-arylated furan.

Firstly, HMFA (**81**) underwent a single Pd-catalyzed as reported by Chacón-Huete *et al.* with 1-bromo-4-nitro benzene (**91**) (Figure 30).[81] 1-bromo-4-nitro benzene (**91**) is a suitable aryl halide cross-coupling partner as it contains a strong electron-withdrawing group (nitro) which increases the reactivity of the halogen-carbon bond facilitating the oxidative addition step.[91] Table 2 represents a small optimization table to see which parameters best suit the single DCC step. Anhydrous TBACl preferably increased the yields by 10%, suggesting that excess water may

hinder the reaction (entries 1 and 2). Entries 3 and 4 retested the round microwave vials with either JohnPhos or MePhos ligand respectively, interestingly a reduction in yield is observed. Entries 5 and 6 used freshly crushed Cs_2CO_3 and tested at different temperatures (170 and 180 °C), however, no improved yields were found. Thermal conditions were also tested but ultimately performed worse than their microwave counterpart (entry 7). Entries 8 and 9 were tested on a newly purchased microwave (Biotage Initiator™ +) and were consistent with the previous microwave (Biotage Initiator™) conditions.

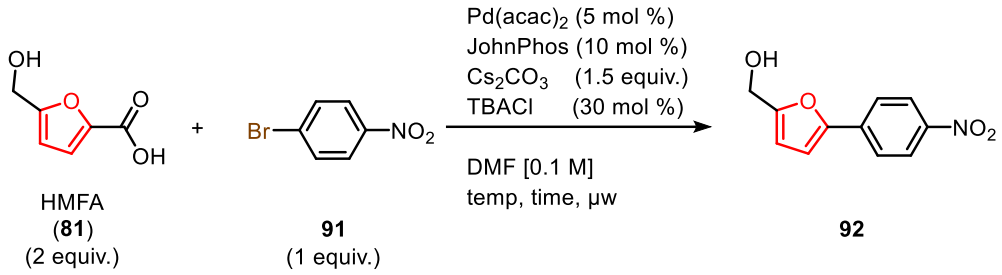

Figure 30. Pd-catalyzed DCC of HMFA (**81**) and aryl-nitro (**91**) to form furan-nitro (**92**).

Table 2. Optimization of reaction conditions from Figure 30.

Entry	Vial Type	Temp (°C)	Time (min)	94 ^{1}H NMR Yield %
1[a]	Conical (0.5-2 mL)	170	8	51
2	Conical (0.5-2 mL)	170	8	61
3	Round (2-5 mL)	170	8	35
4[b]	Round (2-5 mL)	170	8	39
5[c]	Conical (0.5-2 mL)	170	8	23
6[c]	Conical (0.5-2 mL)	180	8	54
7[d]	Conical (0.5-2 mL)	170	45	37
8[e]	Conical (0.5-2 mL)	170	8	63
9[e]	Conical (0.5-2 mL)	180	8	50

[a] Used hydrous TBACl. [b] Replaced ligand with MePhos. [c] Crushed Cs_2CO_3 before adding to vial. [d] Thermal conditions on silicon oil bath. [e] Performed on Biotage Initiator™ + (400 W magnetron) as opposed to Biotage Initiator™ (400 W magnetron).

After their first DCC reaction was performed, Chacón-Huete *et al.* reported that the remaining hydroxymethyl handle could be immediately oxidized into the required carboxylic acid for the last

DCC reaction to produce 2,5-diarylated furans.[81] Given their success, we decided to immediately work with phenyl furan acid (**93**) directly since its synthesis was reported prior.

To further increase the overall conjugation onto the furan ring, a halogenation reaction is necessary to install a bromine atom on the C4 position of the furan, followed by a Suzuki cross-coupling reaction. Carbonyl groups (like carboxylic acids and esters) are π-accepting deactivating groups for EAS reactions due to their electron-withdrawing characteristics. Meaning they favour *meta*-positions on aromatic species since there is a greater separation of partial positive charges. With the carbonyl on C2 of the furan, the *meta*-position is considerably more active than the *ortho*-position, hence, a bromination should occur on C4. A control experiment in Figure 31 represents an EAS bromination reaction on acid (**93**) to brominated acid (**93Br**) using conditions from previous work on arylated thiophene esters,[62] however, no conversion occurred and only the starting material was recovered. Due to the labile proton of the carboxylic acid (**93**), it is speculated that if this proton were to deprotonate, leaving a carboxylate ion, it would hinder the reaction and not proceed. Therefore, to test this hypothesis, the starting acid (**93**) was converted to a methyl ester by Fischer esterification using a catalytic amount of sulfuric acid in methanol or by a reported basic S_N2 like alkylation at lower temperatures (Figure 32).[92]

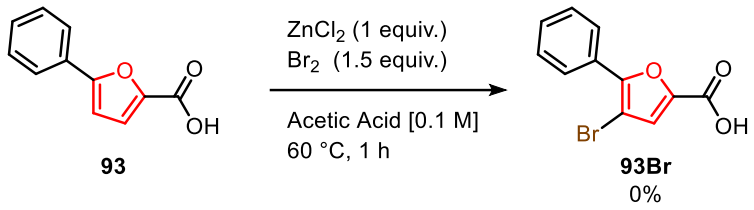

Figure 31. Control EAS-bromination attempt of **93** to **93Br**.

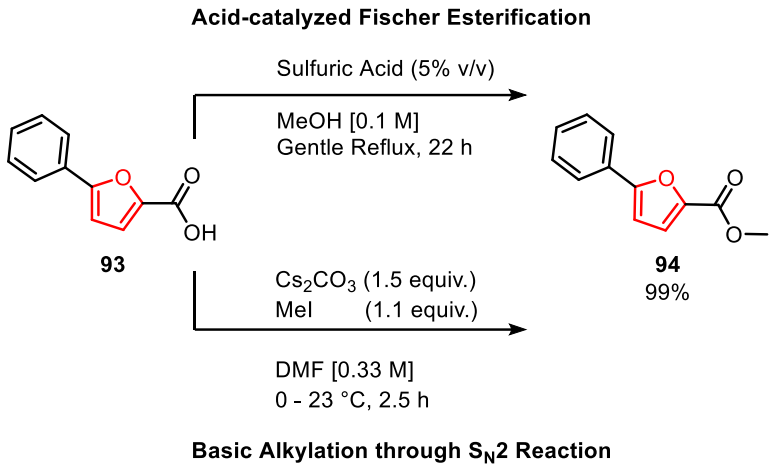

Figure 32. Conversion of carboxylic acid (**93**) to methyl ester (**94**) *via* acidic or basic conditions.

Both methods are equally effective in terms of yield to produce ester (**94**), instead, they vary on reagents, temperature, and time. The Fischer esterification seems more environmentally green from a reagent point of view, however, if this ester is required in shorter times, the basic approach is viable as well. After obtaining the newly made ester (**94**), the bromination began to perform as expected from previous conditions.[62] However, due to the acetic acid being wet, we speculate that water may hinder the reaction. Many tests were constructed with different bromine sources (Br_2 and NBS) and solvents (acetic acid, acetic acid:DCM, DCM, $CHCl_3$). Ultimately, anhydrous $CHCl_3$ provided the best conversion to obtain 4-bromo-ester (**94Br**) in 67% isolated yield after 1 hour (Figure 33). Afterwards, 4-bromo-ester (**94Br**) is immediately prepared for a Suzuki cross-coupling in MeOH:H_2O mixture with phenylboronic acid (**95**) as seen with 4-bromothiophene-esters from previous work to produce diarylated-furan ester (**96**) in high yields (Figure 34).[62] The diarylated-furan ester (**96**) is then subjected to basic hydrolysis to produce the nucleophilic carboxylic acid (**97**) in 30 minutes at close to quantitative yields (Figure 35).

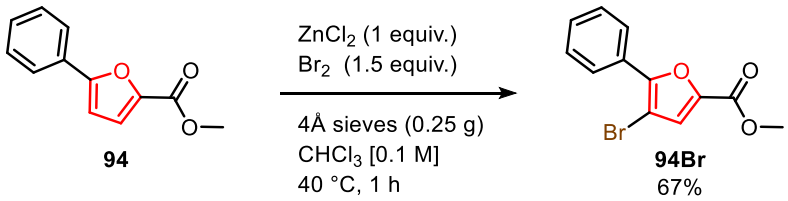

Figure 33. Selective EAS-bromination of ester (**94**) to 4-brominated ester (**94Br**).

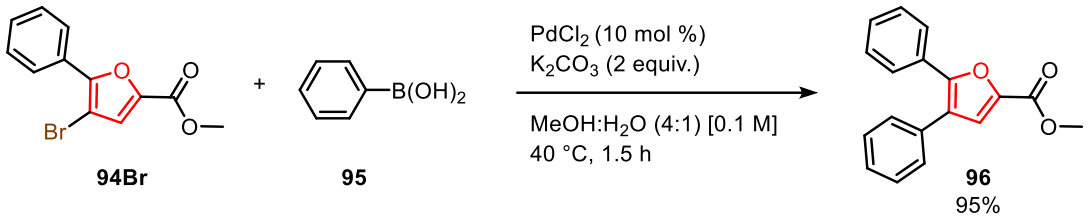

Figure 34. Suzuki cross-coupling reaction of 4-brominated ester (**94Br**) to diarylated ester (**96**).

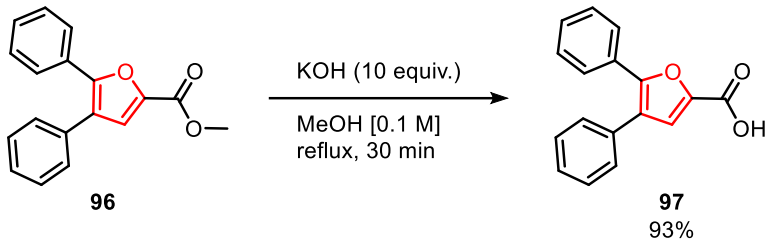

Figure 35. Hydrolysis of ester (**96**) to carboxylic acid (**97**).

With a more convenient way to produce the necessary 4,5-diarylated-furan acid (**97**), it was then appropriate to reattempt the double Pd-catalyzed DCC to finalize the structure and produce 2,4,5-multi-arylated furans (**98**) to complete the objectives of this project. At this stage it was still unknown what conditions were best to use for a double Pd-catalyzed DCC, therefore, both conditions from previous work were tested (by Chacón-Huete *et al.* and Messina *et al.* respectively as seen in Figure 36).[62,81] The major differences between the two reactions were the use of a pre-catalyse Pd(II) versus an active Pd(0) catalyst, the choice of ligand and the use of anhydrous TBACl. Unfortunately, it was difficult to evaluate which method performed better from a conversion or a yield perspective since the isolation of 2,4,5-multi-arylated furan (**98**) was incredibly challenging and both crude ^{1}H NMR looked very similar. Product (**98**) has aromatic protons exclusively within its structure, meaning that all required protons can be seen within 6.7 – 8.0 ppm using ^{1}H NMR. Figure 37 depicts the crude ^{1}H NMR of 2,4,5-multi-arylated furan (**98**) after a workup. Due to the high symmetry of this final compound, we speculate that protons found at 6.86 ppm refer to the two furan protons, whereas the four protons of the central phenylene linker are observed at 7.81 ppm. After integration, we do see a 2:4 area peak between the two mentioned proton species further agreeing with the previous assessment. The remaining protons (from 7.33 –

7.63 ppm) account for more than the expected amount, which is normal given the fact that it is a crude sample where other aromatic by-products co-exist.

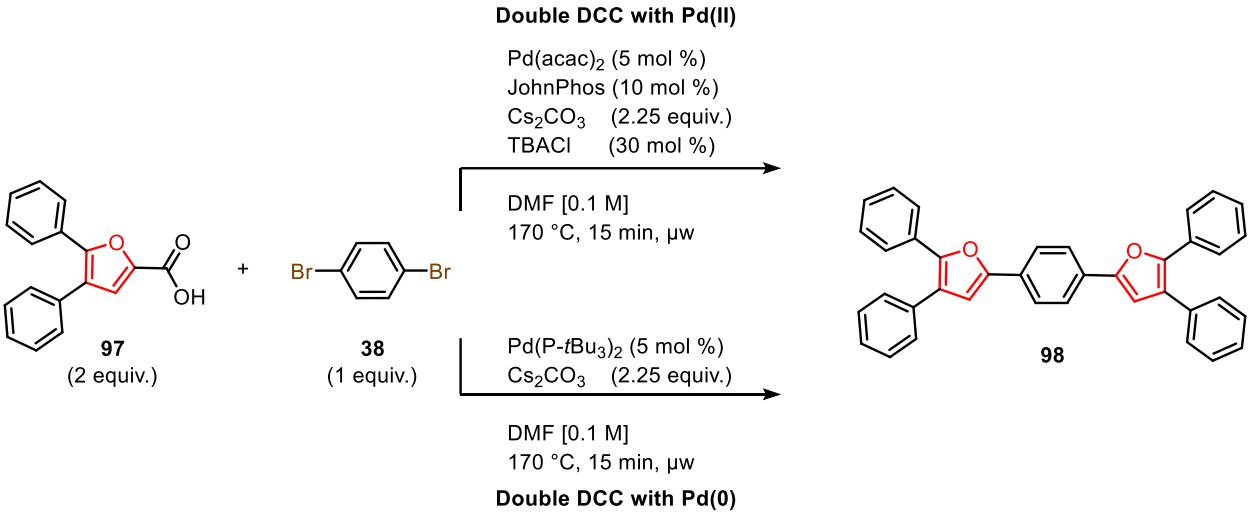

Figure 36. Double DCC of acid (**97**) and 1,4-dibromobenzene (**38**) through Pd(0)/Pd(II) catalysts to produce 2,4,5-arylated-furan (**98**).

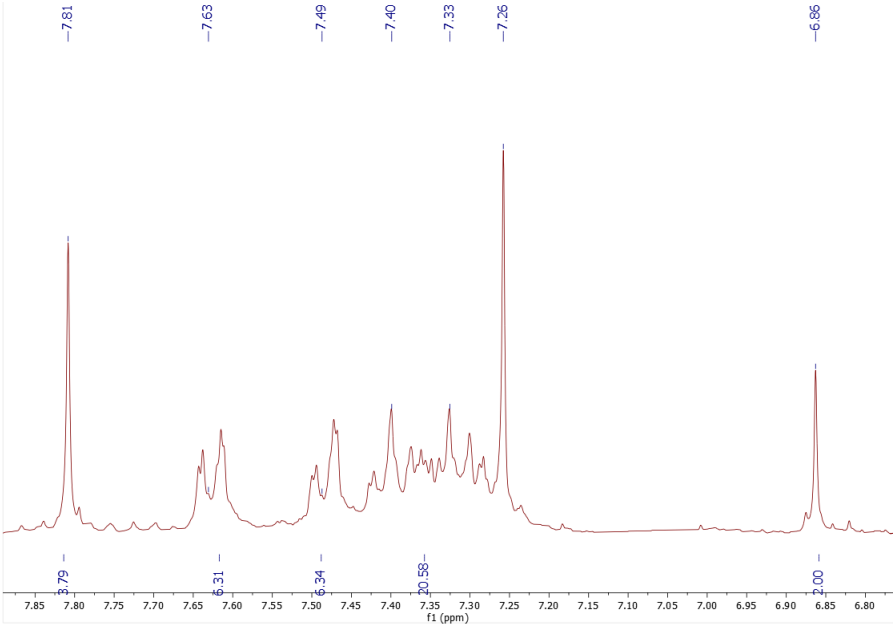

Figure 37. Crude after workup ^{1}H NMR of 2,4,5-arylated-furan (**98**) in $CDCl_3$ (Bruker 300 MHz).

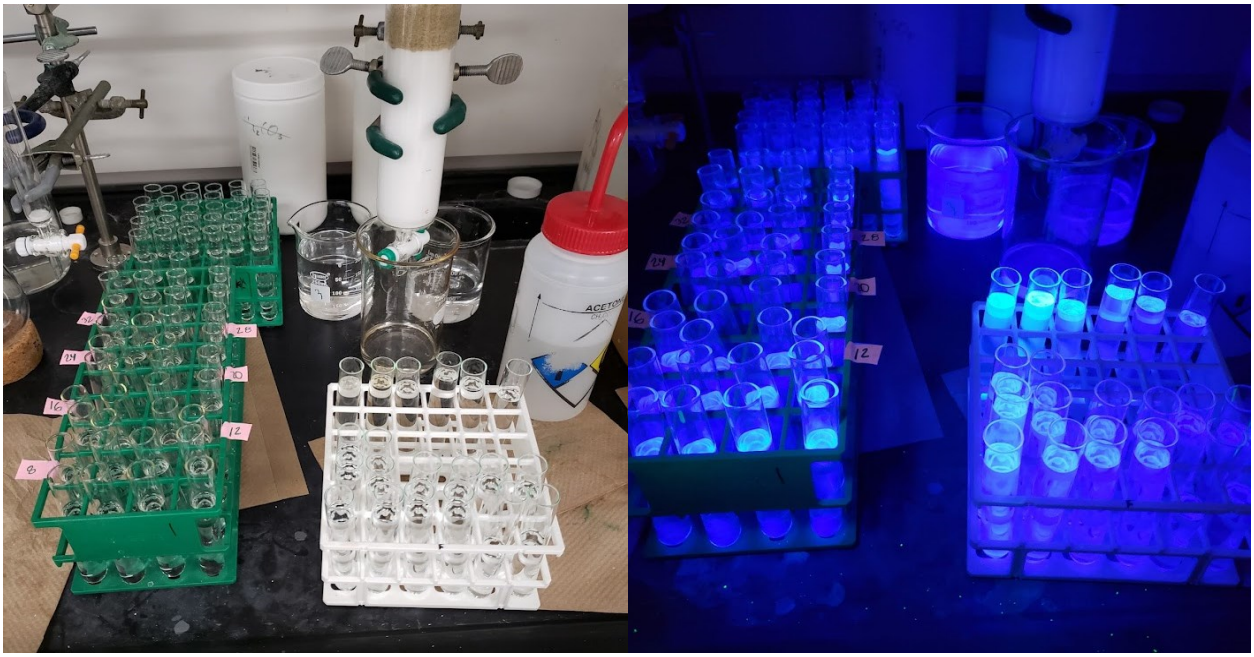

Figure 38. Left: Normal phase column chromatography and fractions of 2,4,5-arylated furan (**98**) using silica gel (mobile phase: 97:1:2 Hexane:Toluene:EtOAc). Right: Fractions under 365nm UV-light.

With the evidence of product (**98**) existing from the crude ^{1}H NMR, it was then time to isolate and purify the desired material. Just like most other organic compounds, column chromatography was first attempted. However, unlike any other column, serious problems isolating the desired product began to arise. Figure 38 represents a column chromatography attempt after collecting close to one hundred test tube fractions. Using standard chromatography conditions, trace amounts of product were detected in over seventy of the collected fractions, indicating chromatographic purification was not an effective approach for isolating this compound. We hypothesize that the desired compound was only slightly soluble towards the mobile phase (97:1:2 Hexane:Toluene:EtOAc) and slowly phases through the silica gel with its closely resembled aromatic by-products co-eluting. Figure 39 validates this theory by stacking ^{1}H NMR of various fractions collected throughout this purification and notices the important peaks at 6.86 and 7.81 ppm integrating at a ratio of 2:4.

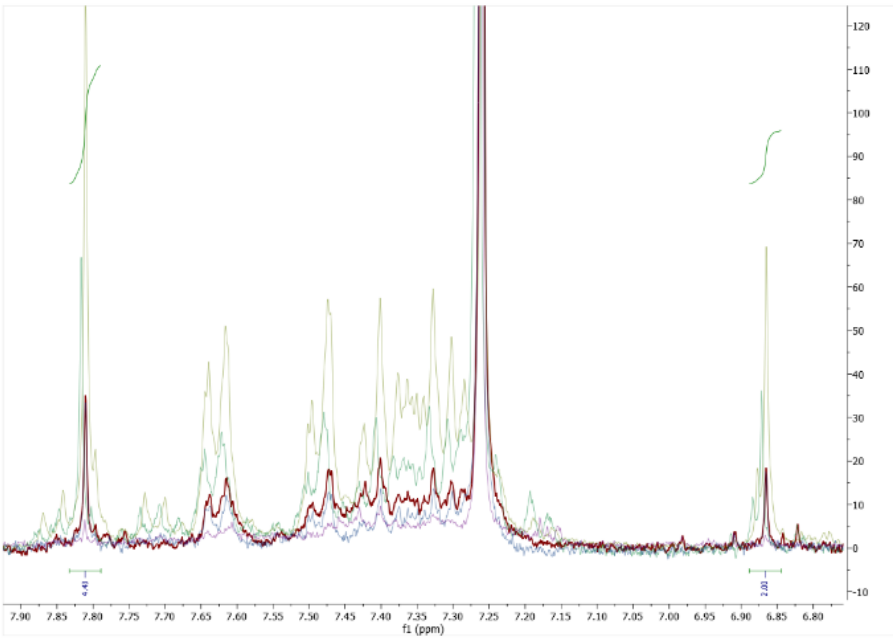

Figure 39. ^{1}H NMR of 2,4,5-arylated-furan (**98**) in $CDCl_3$ (Bruker 300 MHz) where each colour represents a different set of fractions pooled.

At this stage, the chemistry to achieve multi-arylated furans derived from HMF (**1**) felt more validating and possible. However, the last challenge was to overcome purification adversities towards these highly conjugated furan compounds. Once this is solved, future work includes further optimizing the double Pd-catalyzed DCC reaction to produce these materials efficiently and change their electronic characteristics by coupling varied electronic groups at different positions on the furan ring.

2.3 Results and Discussion on Methyl-5-bromofuran-2-carboxylate as a Starting Material

The work presented in this chapter collaborated with Dr. Cynthia Messina (a former Forgione lab member) to develop various multi-arylated furans with thiophene linkers (instead of phenylene) by using methyl-5-bromofuran-2-carboxylate (**99**) as a starting material. Before this work, Messina *et al*. reported the 2,3,4,5-multi-arylated thiophene synthesis using a very similar starting material to furan ester (**99**), however, it was a thiophene derivative with the same functional groups used instead.[62] This work further expands the methodology of the previous work

mentioned, by providing additional conjugation to the overall structures and introducing alternating heterocycles (furan-thiophene-furan core) using a double Pd-catalyzed DCC reaction. All final compounds made were then tested in dilute $CHCl_3$ to observe their absorbance, photoluminescence and PLQY.

The synthesis depicted in Figure 40 begins with furan ester (**99**) as an affordable starting material containing a furan heterocycle. After a Suzuki cross-coupling reaction, the furan is monoarylated to 5-arylated-furan ester (**100**). At this stage, three different paths can branch into a variety of future compounds. Starting with *Path A*; a saponification-producing furan acid (**101**) can then undergo a double Pd-catalyzed DCC reaction with dibrominated-thiophene (**102**) to produce a 2,5-multi-arylated furan compound (**103**). Before saponification *Path B* and *C* differ by selectively halogenating the furan ring at different positions (*Path B* iodinates at C3, whereas *Path C* brominates at C4). Both halogenated products (**100I**, **100Br**) are susceptible to another Suzuki cross-coupling, followed by a saponification and finally a double Pd-catalyzed DCC reaction to produce regioisomers 2,3,5-multi-arylated furan (**104**) *via Path B* or 2,4,5-multi-arylated furan (**105**) *via Path C*.

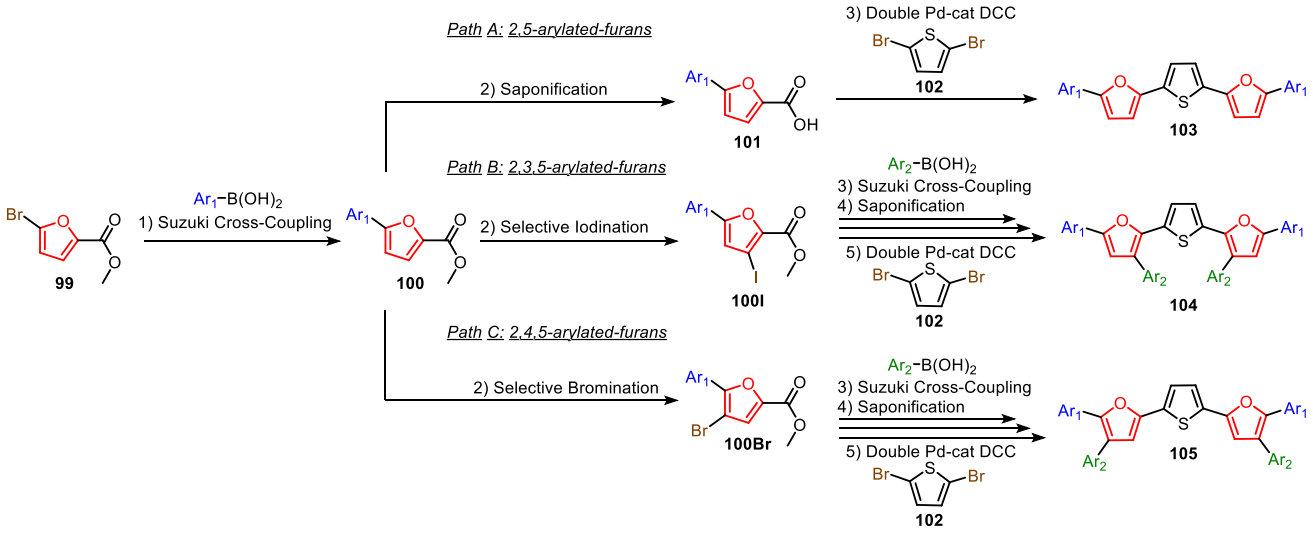

Figure 40. Generalized synthesis starting with methyl-5-bromofuran-2-carboxylate (**99**) to synthesize various multi-arylated furans (**103**, **104**, **105**) in three to five steps.

Beginning with *Path A*, furan ester (**99**) is subjected to a rapid and efficient Suzuki cross-coupling to install a phenyl or *t*-butyl-phenyl partner on the C5 position at quantitative yields (Figure 41). The *t*-butyl-furan ester (**107**) was chosen to be directly saponified by previous hydrolysis

conditions (Figure 42) as seen in Chapter 2.2. Furan acid (**108**) collected is then reacted with dibromo-thiophene (**102**) through DCC conditions from Messina *et al*. (Figure 43).[62] To ensure purification problems using column chromatography did not arise (as seen in the previous chapter), preparative TLC (prepTLC) was attempted instead (Figure 44). PrepTLC separates organic compounds exactly like a TLC would, however, the crude sample is placed on a much larger plate (20×20 cm, backed by glass). The crude sample is dissolved in a minimum amount of volatile organic solvent which is then gently coated onto the silica plate (two inches above the base of the plate). After capillary action is completed, the plate is removed from its chamber where it is allowed to dry. Once dried, the suspected area where the product exists is gently scratched off and collected by vacuum filtration. This method was highly effective for all multi-arylated compounds produced; however, limitations of scale are the main drawback of this approach. While these reactions were performed on an appropriate scale (≈30-60 mg), one should evaluate their final mass before purifying their crude sample, and perform a TLC before performing a prepTLC.

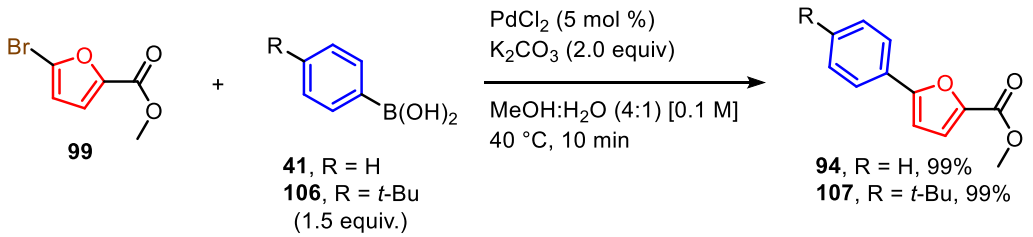

Figure 41. Suzuki cross-coupling reaction of bromo-furan (**99**) with boronic acid (**41**, **106**) to produce diaryl-furan (**94**, **107**).

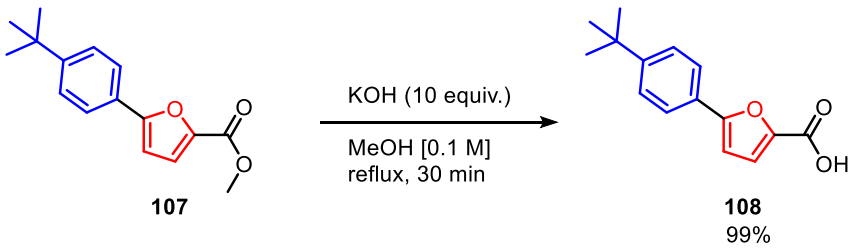

Figure 42. Path A: Hydrolysis of ester (**107**) to carboxylic acid (**108**).

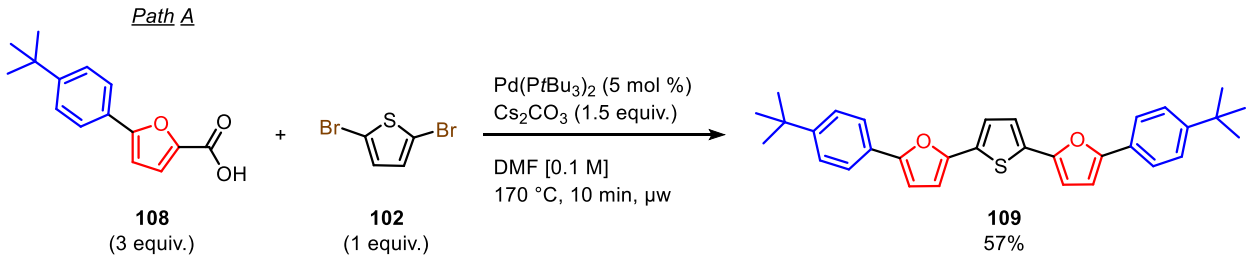

Figure 43. Path A: Double DCC of acid (**108**) and dibromo-thiophene (**102**) to produce 2,5-diarylated-furan (**109**).

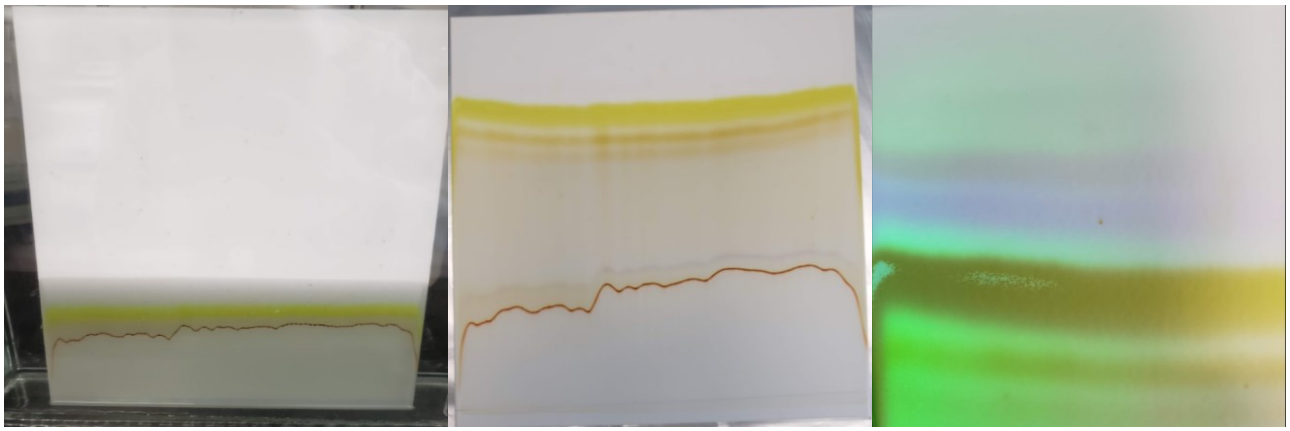

Figure 44. Purification of 2,5-diarylated-furan (**109**) through prepTLC. Left depicting TLC sheet developing through capillary action in 2:1 Hexane:$CHCl_3$ as mobile phase. Middle represents completed prepTLC, where **109** is found as a yellow band. Right showcasing completed prepTLC under 365nm UV-light.

2,5-diarylated-furan compound (**109**) was impressively isolated using the prepTLC method at a yield of 57% (with carbon-carbon bond formation = 75%). This outcome was remarkable, as the isolation of these conjugated materials represented the final challenge to overcome within this methodology. With confirmation that prepTLC purifies 2,5-diarylated furans efficiently, the subsequent step was to synthesize 2,3,5 and 2,4,5-multi arylated furans to ensure the reproducibility of this approach.

After obtaining furan ester (**94**), two different approaches halogenating this compound are possible (Figure 45). *Path B* involves the use of a Hauser-Knochel base TMPMgCl•LiCl to deprotonate the furan at C3 followed by adding freshly grounded iodine pellets to iodinate at this position. TMPMgCl•LiCl is a well-known regioselective magnesium base which deprotonates aromatic protons directly adjacent to ester functional groups.[62,93] This is accomplished by the ester group to

coordinate with the base, and directly deprotonating nearby protons. After allowing the base to react with the furan for an hour, iodine is then transferred into the flask and left to react for an additional two hours while the flask slowly returns to room temperature. With this step, the aim is to produce intermediate C3 iodinated furan (**94I**). Note that no yield is reported for this complex as it is difficult to isolate from the ester starting material through column chromatography. Instead, once the reaction is quenched and worked up, the crude mixture is immediately arylated by a second Suzuki cross-coupling reaction. Affording a 67% yield of diarylated furan ester (**110**) over two steps with *t*-Bu-phenyl boronic acid as the coupling partner (as shown in green).

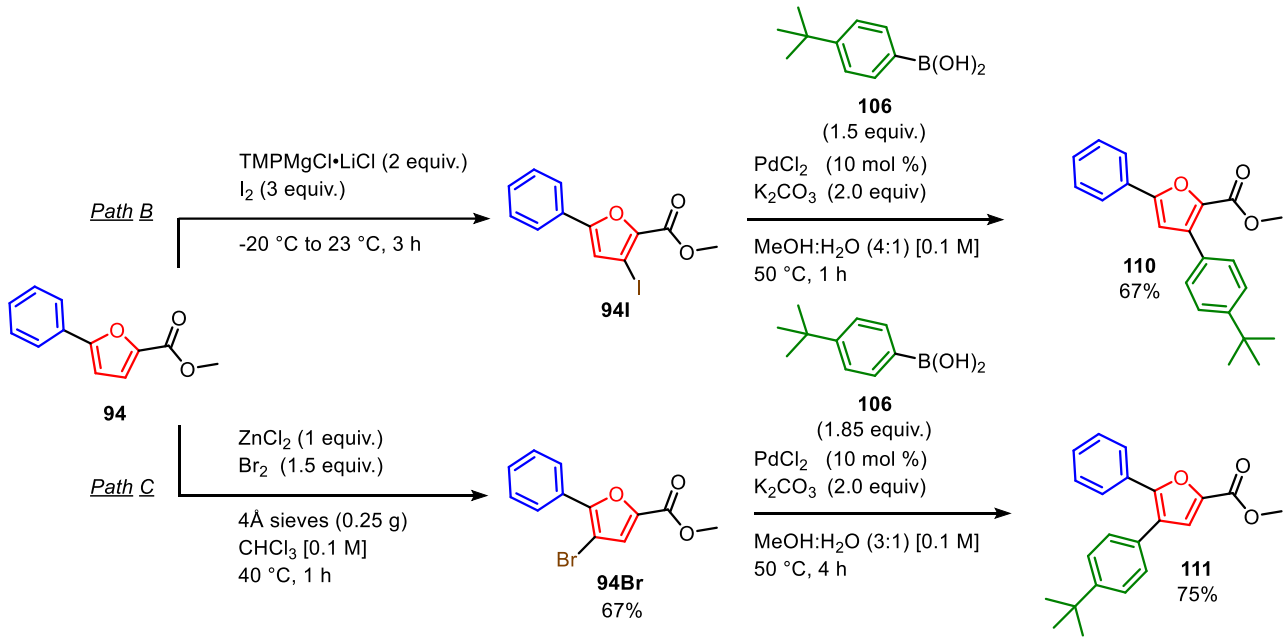

Figure 45. Synthetic pathways *B* and *C* to access 2,3,5-furan esters (**110**) and 2,4,5-furan esters (**111**) respectively.

Path C follows the EAS bromination as described before in Chapter 2.2 where a bromine atom is bonded at the C4 position. Naturally, a second Suzuki cross-coupling is performed like the coupling of *Path B*. However, this cross-coupling took much longer than anticipated (4 hours in *Path C* vs 1 hour in *Path B*). Due to the close proximity of the C5 positioned aryl and the steric hindrance of the bulky *t*-Bu group, we suspect that the rate of the reaction is relatively slower than seen in *Path B*. Overall the reaction performed similarly with an isolated yield of 75%. After the second arylation, newly diarylated esters (**110**, **111**) both underwent hydrolysis followed by a

double Pd-catalyzed DCC reaction to produce 2,3,5-multi-arylated furan (**113**, 47% yield, Figure 46) and 2,4,5-multi-arylated furan (**115**, 46% yield, Figure 47) respectively.

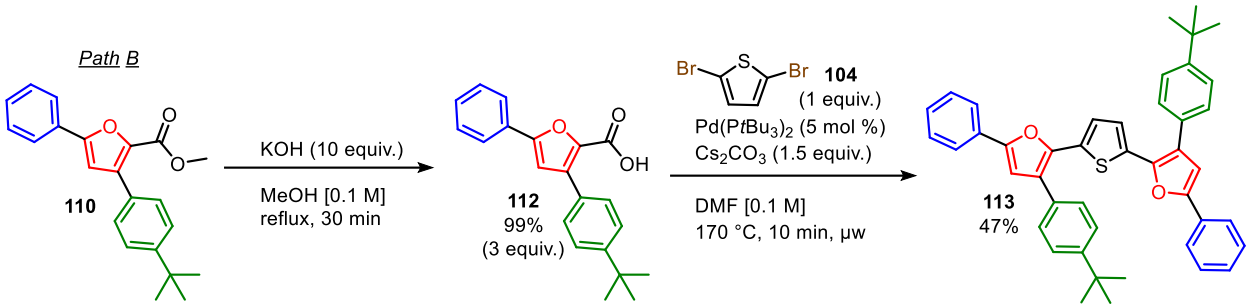

Figure 46. *Path B*: Hydrolysis followed by double Pd DCC to access 2,3,5-multi-arylated furan (**113**).

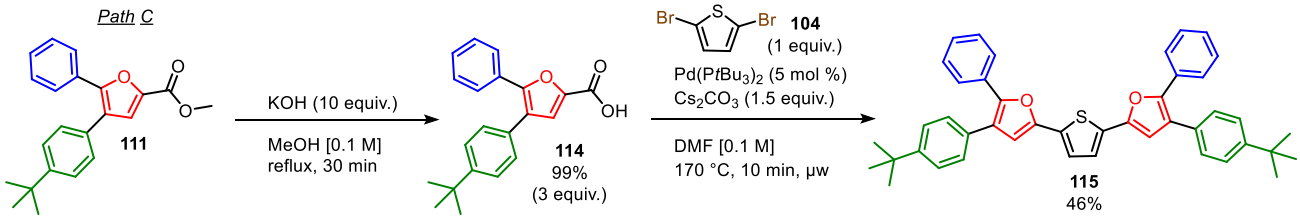

Figure 47. *Path C*: Hydrolysis followed by double Pd DCC to access 2,4,5-multi-arylated furan (**115**).

PrepTLC was once again utilized to effectively isolate both desired multi-arylated furans. Overall, this approach represents a novel synthetic methodology for accessing varied arylated furans starting from furan ester (**99**) without the need for cyclization methods. Instead, it focuses on arylating select furan positions through regioselective brominations followed by Suzuki cross-coupling reactions. Lastly, two arylated furan acids are fused with a dibrominated linker *via* a double Pd-catalyzed DCC reaction, a first for furan species. The following section presents and discusses the spectroscopic data observed of these newly made compounds (**109**, **113**, **115**) in dilute $CHCl_3$ [2×10^{-7} M].

2.4 Spectroscopic Data of Multi-Arylated Furan Compounds

Thanks to the help of Victoria Lapointe from the Majewski group, the optical properties of all three final compounds were studied in $CHCl_3$ solution. Figure 48 represents the absorbance of

each synthesized compound. 2,5-furan (**109**) and 2,4,5-furan (**115**) exhibit very similar absorbances with exceptionally close absorbance maxima (see Table 3). Interestingly, 2,3,5-furan (**113**) is slightly more red-shifted compared to its regioisomer 2,4,5-furan (**115**). Highly π-conjugated regioisomers have been reported to express different photophysical properties, which depend on their molecular structure, orbital overlap, and interactions with the solvent.[94] The large absorption peak expressed by all compounds is most likely the π – π* transition due to the large π-conjugation found within all final structures. The photoluminescence of all three compounds is represented in Figure 49. Like their absorbances, the photoluminescence behaves similarly, where compounds **109** and **115** overlap quite closely and exhibit cyan-green fluorescence. Compound **113** redshifts from the others and fluoresces green light. All samples can be viewed in Figure 50 under 365 nm UV light. Lastly, the photoluminescence of all final compounds relates similarly towards oligofurans[47] (back in Figure 12) demonstrating that these structures retain conjugated furan photoluminescence characteristics even with a thiophene linker. PLQY were also studied; 2,3,5-furan (**113**) expressed the lowest (PLQY = 23%) most likely due to a lack of planarity by arylating the C3 position, whereas 2,5-furan (**109**, PLQY = 41%) and 2,4,5-furan (**115**, PLQY = 43%) almost double the PLQY due to a more planar molecular structure avoiding arylation at C3.

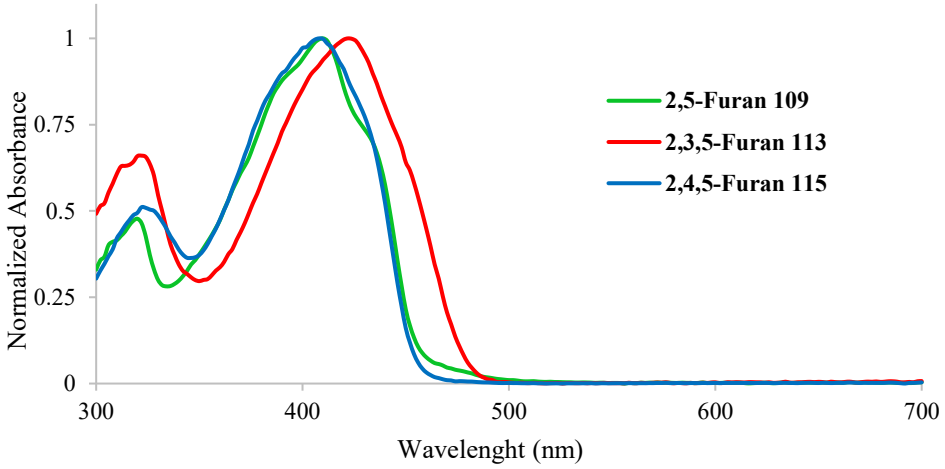

Figure 48. Normalized absorbance spectra of multi-arylated furans **109**, **113** and **115**.

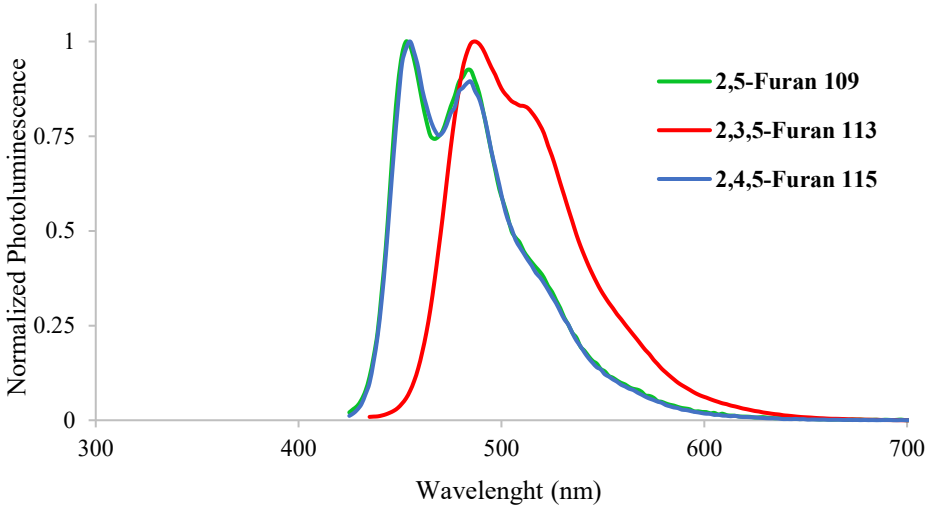

Figure 49. Normalized photoluminescence spectra of multi-arylated furans **109**, **113** and **115**.

Table 3. Optical properties of final multi-arylated furan compounds in dilute $CHCl_3$ solution [2×10^{-7} M]; λ_{abs} and λ_{em} maxima and PLQY spectra.

Final Compound	λ_{abs} (nm)	λ_{em} (nm)	PLQY % (± 5)
2,5-Furan 109	410	453, 483	41
2,3,5-Furan 113	422	487, 513	23
2,4,5-Furan 115	408	455, 485	44

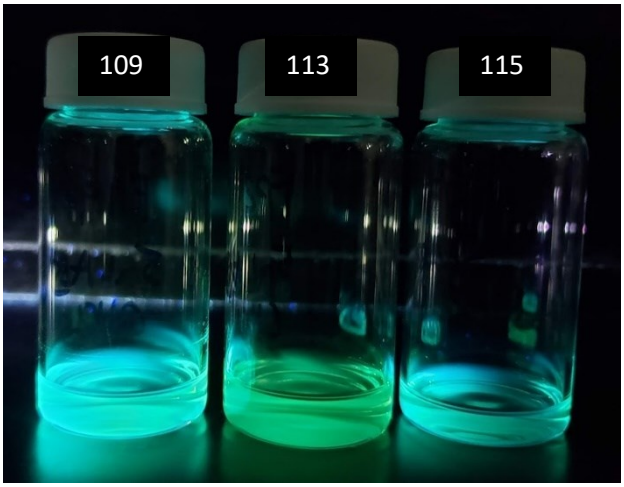

Figure 50. Photoluminescence of multi-arylated furans **109**, **113** and **115** in $CHCl_3$ solution [6×10^{-7} M] under 365 nm UV light.

2.5 Conclusion

In summary, both HMF (**1**) and methyl-5-bromofuran-2-carboxylate (**99**) served as starting materials for accessing multi-arylated furans *via* Pd-catalyzed cross-coupling reactions without the need for any cyclization methods. While HMF did not develop 2,3,5-multi-arylated furans, it did produce a novel and rigid conjugated diol monomer (**82**) at a 40% yield, potentially useful in polyester synthesis. Additionally, a 2,4,5-multi-arylated furan was obtained starting from HMF, however, purification of the desired product was incomplete using column chromatography.

Learning from previous mistakes found in the HMF synthesis, furan ester (**99**) was utilized to synthesize three new multi-arylated furans through cross-coupling methods, which were purified using prepTLC. The directing ester group facilitates various regioselective halogenations onto the furan ring, enabling late-stage functionalization onto the heterocyclic ring. For the synthesis of 2,5-arylated furans, this method is achievable in three steps. However, if 2,3,5 and 2,4,5-multi-arylated furans are preferred, five synthetic steps are required. The double Pd-catalyzed DCC reaction is a first of its kind to fuse two furan carboxylic acids with a dibrominated-thiophene linker, rapidly expanding the material's overall conjugation without generating organometallic waste.

Spectroscopic data (in $CHCl_3$ solution) revealed that regioisomers (**113**, **115**) exhibit different optical properties, where 2,3,5-furan compound **113** red-shifts slightly compared to 2,4,5-furan compound **115**. Impressively, both 2,5 (**109**) and 2,4,5 (**115**) arylated furans nearly doubled the PLQY (= 41 – 44%) of their 2,3,5-multi-arylated furan (**113**) counterpart (PLQY = 23%).

These efforts highlight the late-stage functionalized strategic steps of arylating biomass-derived (or close derivatives) starting material into optoelectronic compounds *via* Suzuki cross-couplings, regioselective halogenations, saponification and a double Pd-catalyzed DCC reaction.

Chapter 3. Synthetic Methodology to Access 2,5-Furan-Based Phenylene/Thiophene Oligomers

3.1 Introduction

Being globally dependent on petroleum-based has consequently promoted severe environmental problems like climate change. Implementing synthetic strategies to convert renewable biomass-derived starting materials into high-valued chemicals or consumer goods offers a promising avenue for reducing dependence on petrochemicals. It is now the responsibility of all modern chemists to design more environmentally conscious synthetic methodologies in the design of final compounds. Incorporating biomass-derived materials or their close derivatives into synthesis is highly appreciated due to the renewable nature of furans. There is a growing interest in producing small 2,5-furan-based phenylene co-oligomers, which have emerged as promising candidates for OFETs due to their impressively planar structure and favourable optoelectronic properties, including high PLQY.[54,71,72,90,95–97]

In this chapter, there is a strong interest in utilizing 5-bromofurfural (5BF, **33**) as the furan source to develop a methodology accessing diverse 2,5-furan-based oligomers. 5BF is a derivative closely related to furfural (**9**), with a bromine atom located at the C5 position of the furan core. This bromine atom, bonded to a sp_2-carbon atom of the furan motif, renders 5BF a promising starting material for Pd-catalyzed cross-coupling reactions aimed at designing π-conjugated organic materials.[51]

The synthesis begins by installing electronically varied aryl groups to arylate 5BF at C5 through the Suzuki cross-coupling reaction. The next step is to oxidize the aldehyde handle present at the C2 position into a carboxylic acid group. The furan acid is then reacted in a double Pd-catalyzed DCC reaction to form the desired furan-based oligomers. Overall, the presented synthesis was able to develop a library of ten small 2,5-furan-based phenylene/thiophene oligomers and one 2,5-furan-based push-pull compound as potential organic optoelectronic candidates in 3 – 4 synthetic steps. Quantitative green chemistry metrics (*E-factor* and *Atom Economy*) were calculated as well to compare the cross-coupling reactions from this methodology to previous methods when producing 2,5-furan-based oligomers. All final materials synthesized through this methodology

were then characterized by ^{1}H NMR and ^{13}C NMR while their optical properties including PLQY were studied in solution.

3.2 Previous Synthesis on Accessing Small Furan-Based Co-Oligomers

Recently, small 2,5-furan-based co-oligomers have been synthesized through classic Pd-catalyzed cross-coupling reactions (Stille and Suzuki couplings)[54,71,72,97,98] or by cyclization practices to produce the furan core.[63] In 2016, Kazantsev *et al.* demonstrated a detailed four-step synthesis to produce 2,5-furan-based phenylene co-oligomer (**42**, seen in Figure 51).[54]

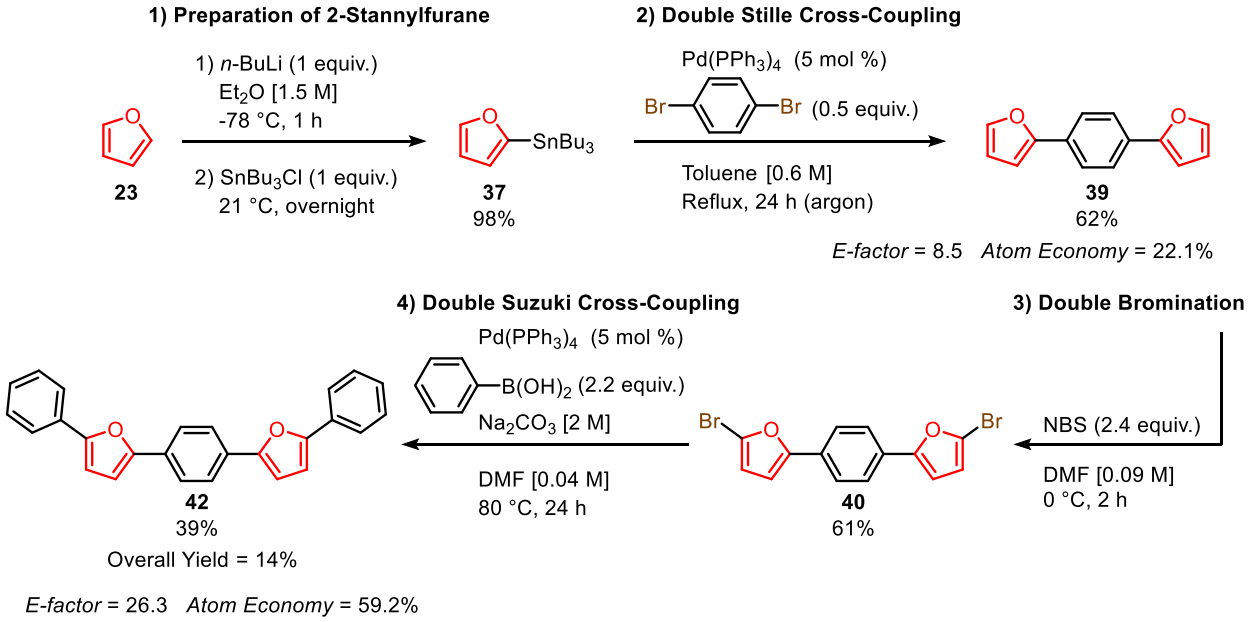

Figure 51. Synthesis of 2,5-furan-based phenylene co-oligomer (**42**) by Kazantsev *et al.*

This methodology begins with the deprotonation of furan (**23**) at -78 °C to prepare the 2-stannylfurane (**37**) reagent for a double Stille cross-coupling reaction coupling to a 1,4-dibromophenyl linker to produce the furan-phenylene-furan core (**39**) after 24 hours. The core is immediately dibrominated using NBS in DMF and succinctly undergoes a double Suzuki cross-coupling reaction with phenylboronic acid twice in DMF to produce the desired co-oligomer (**42**) in an overall yield of 14% over four steps (72+ hours of reaction times). The major limitations of this synthesis stem from the double Stille cross-coupling reaction as it produces two stoichiometric amounts of highly toxic organotin (Chapter 1.3.1) and requires DMF solvent for half of the total

steps. Since this thesis covers Pd-catalyzed cross-coupling reactions extensively, we were curious to also evaluate green chemistry metrics such as *E-factor* and *Atom Economy* for both cross-coupling reactions in this method, where we would then compare it to our synthesis (calculations found in Chapter 5.2).

The double Stille coupling in Figure 51 expresses a poor *Atom Economy* value of 22.1% with a relatively fair *E-factor* of 8.5. The *Atom Economy* is quite poor since two organotin compounds are required to react with a dibromo linker. Both tin and bromine are relatively heavy atoms from a molar mass perspective (118 and 80 g/mol respectively) and are not found in the final product, explaining the low *Atom Economy* observed. As for the double Suzuki coupling, it has a much higher *Atom Economy* value of 59.2%, however, has an incredibly high *E-factor* of 26.3. This means, that for every 1 gram of product made, 26.3 grams of waste is made alongside it. In this chapter, we attempt to produce a new synthetic methodology including a double Pd-catalyzed DCC reaction to produce co-oligomers such as **42** (as well as other electronically different oligomers) while reducing the overall waste made by traditional couplings.

3.3 Results and Discussion

This work begins with a generalized scheme as seen in Figure 52, to identify a synthetic strategy of accessing 2,5-furan-based oligomers starting with 5BF (**33**). 5BF is a synthetically close derivative of biomass-derived platform chemical, furfural (**9**), where it can be produced after a selective bromination.[99] Working with 5BF is advantageous for two reasons in particular; it is a biomass-derived heterocycle which is useful in promoting green chemistry practices into synthesis and has been shown to undergo mild Suzuki cross-coupling reactions to readily install electronically diverse aryl-boronic acids (phenylene or thiophene-boronic acids) onto the C5 position of the furfural ring.[79,100] Forming the newly arylated furan can then lead to an aldehyde oxidation. A necessary step to acquire the nucleophilic carboxylic acid partner (**116**), followed by a double Pd-catalyzed DCC reaction with a dibrominated phenylene/thiophene linker, resulting in

the production of alternating 2,5-furan-based oligomer (**117**) releasing two molecules of CO_2 instead of traditional heavy organometallic waste.[80,82]

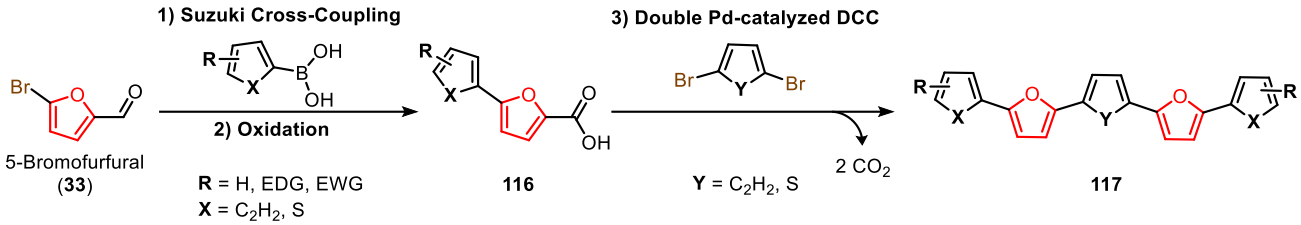

Figure 52. Generalized synthesis starting with 5-bromofurfural (**33**) to produce varied 2,5-furan-based oligomers (**117**) in three steps.

5BF is an excellent electrophilic coupling partner for cross-coupling reactions due to the activating nature of the aldehyde motif on C2 which promotes the oxidative addition of the Pd-catalyst into the aryl-halide bond.[79] Our results begin with the primary Suzuki cross-coupling arylation of 5-bromofurfural (**33**) with thiophene boronic acid (**118**) as the coupling partner (seen in Figure 53). The goal of coupling thiophenes with furans was to produce a synthetic strategy that could access alternating heterocyclic oligomers. Spectroscopic techniques would then follow to evaluate their optical properties and compare them to alternating phenylene-furan oligomers to observe if alternating heterocycles can cause optical shifts in the absorbance and photoluminescent maxima. Table 4 represents a small optimization of the Suzuki cross-coupling reactions performed with reagents **33** and **118**. Ultimately, a reported mild Suzuki cross-coupling procedure in water at room temperature with minimal Pd-catalyst ($Pd(OAc)_2$, 2 mol %) and a full equivalent of TBAB (helpful reagent to solubilize organics into aqueous solvent) after 18 hours produced the thiophene-furan aldehyde (**119**) in an excellent isolated yield of 96 % at relatively large scales (10 mmol, Entry 6).[79,100]

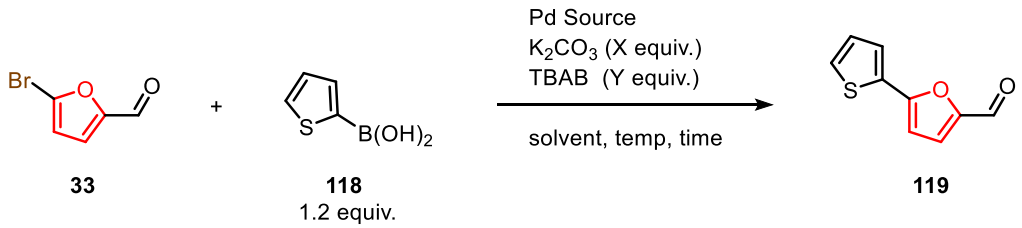

Figure 53. Suzuki cross-coupling of 5-bromofufural (**33**) and thiophene boronic acid (**118**).

Table 4. Optimization Table of Suzuki coupling on alternating heterocycles.

Entry	Pd Source	Pd mol %	K_2CO_3 X equiv.	TBAB Y equiv.	Solvent	Temp (°C)	Time (h)	^1H NMR Yield %
1[a]	$PdCl_2$	5	2	0	MeOH:H_2O	50	18	15
2[b]	$Pd(PPh_3)_4$	2	2	0	EtOH: Dioxane	80	0.25	0
3[b]	$Pd(OAc)_2$	2	2	0.1	H_2O	80	0.25	50
4	$Pd(OAc)_2$	2	2.5	0.1	H_2O	50	18	32
5	$Pd(OAc)_2$	2	2.5	1	H_2O	23	2	46
6[c]	$Pd(OAc)_2$	2	2.5	1	H_2O	23	18	96

[a] Conditions inspired by previous cross-coupling work.[62] [b] Reaction performed in the microwave. [c] Isolated yields, 10 mmol scale.

These conditions were repeated on a diverse selection of phenylboronic acid substrates (**120**) to access sterically different and electronically varied phenylene-furan aldehyde compounds (**121**) as seen in Figure 54. Neutral phenylene (**122**), dimethyl *meta*-functionalized (**123**), bulky (**124**), *para*-functionalized electron-donating (**125** and **126**) and *para*-functionalized electron-withdrawing (**127** and **128**) groups were all produced following the previous conditions (Table 5). The majority of these substrates resulted in high to excellent yields (compounds **122** to **127**, 72 – 99%), and a moderately low yield was observed with *para*-functionalized nitro compound (**128**). We suspect that strong electron-withdrawing groups render a more sluggish reaction, especially at room temperature (**128** yield = 11%) since the boronic acid is the nucleophilic partner of this reaction. Increasing the temperature overcame some of the activation energy requirements, increasing the yield by a factor of four after one hour (**128** yield = 45%).

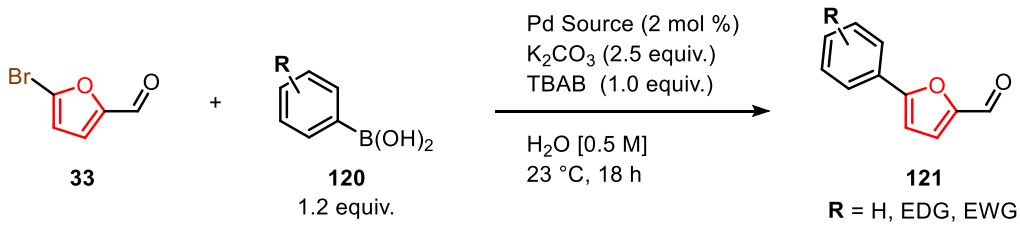

Figure 54. Suzuki cross-coupling of 5-bromofufural (**33**) and phenylene boronic acids (**120**).

Table 5. Scope on Suzuki cross-couplings with diverse phenyl substrates.

Product	C5-Aromatic Partner	Scale	Yield, %
122	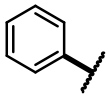	8 mmol	93
123	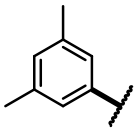	2 mmol	92
124	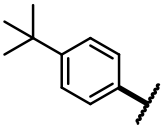	4 mmol	92
125	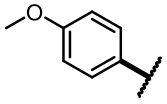	3 mmol	99
126	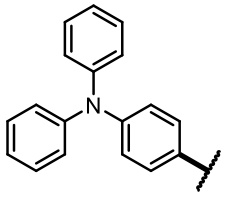	2 mmol	76
127	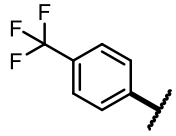	5.8 mmol	72
128	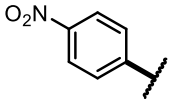	4 mmol 1 mmol	11 45[a]

[a] Reaction performed at 95 °C for 1 hour instead in [0.25 M] of H_2O.

Reducing overall waste throughout a synthesis is generally favoured and a highly encouraged practice that follows green chemistry principles. Attempts to reduce the overall waste of the Suzuki cross-coupling reaction of 5-bromofurfural (**33**) and phenylboronic acid (**41**) began by reducing the total equivalent of TBAB. We hypothesize that the reaction can still be completed with catalytic amounts of TBAB (one-tenth of reported TBAB, 0.1 equiv.), to justify TBAB's role as a phase transfer catalyst. Data reporting ^{1}H NMR yields and *E-factor* (calculations Chapter 5.2) results are detailed in Table 6 alongside the amount of TBAB used. As hypothesized, TBAB can be added catalytically (0.1 equiv.) instead of requiring stoichiometric amounts to perform the reaction. This entry provides the smallest *E-factor* of all the Suzuki attempts (1.5); however, the reaction did not

go to completion after 18 hours. At 0.5 equiv. the reaction was complete and provided slightly more waste than the previous result (1.8). These results indicate that the TBAB reagent can be reduced and allow the desired reaction to proceed, overall minimizing the total waste made by this transformation.

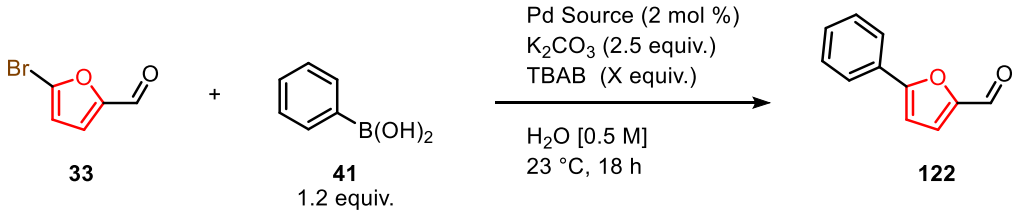

Figure 55. TBAB test on the synthesis of 5-phenylfuran-2-carbaldehyde (**122**).

Table 6. TBAB equivalent test results including ^{1}H NMR yields and *E-factor*.

Entry	TBAB X equiv.	^{1}H NMR Yield %	*E-factor*
1	0.1	83	1.5
2	0.5	99	1.8
3	1	99	2.7

The next step of this synthesis was to take the recently produced aldehyde and convert it to a carboxylic acid group (Figure 56) preparing the necessary reagent for the double Pd-catalyzed DCC reaction. Naturally, a one-step oxidation of aldehyde to carboxylic acid would be ideal from a green chemistry perspective. Table 7 depicts the efforts made to achieve a one-step oxidation through $KMnO_4$ and the Pinnick oxidation (as seen in Chapter 2). Entries 1 and 2 relate to the $KMnO_4$ oxidation, no yield was observed after 10 minutes by ^{1}H NMR, instead newly proton-found peaks between 2 – 4 ppm were observed, insinuating that the furan ring possibly decomposed. Entries 3 to 7 express a Pinnick oxidation method, where solvents and sacrificial scavengers (H_2O_2, Sulfamic acid and 2-methyl-2-butene) were tested. Overall, most results were low-yielding or poorly reproducible to access the desired acid compound. For this methodology to succeed, consistent oxidation results are necessary, which is why additional oxidation transformations were tested alongside to ensure that the desired carboxylic acid was simple to produce and isolate.

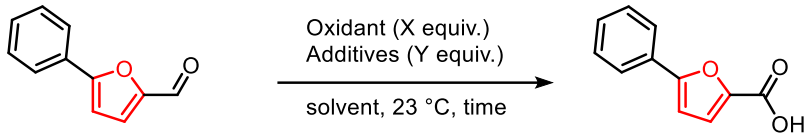

122 140

Figure 56. Oxidation of aldehyde (**122**) to carboxylic acid (**140**) in one step.

Table 7. One-step oxidation of aldehyde to carboxylic acid results.

Entry	Oxidant	X	Additives	Y	Solvent	Time	^{1}H NMR Yield %
1	$KMnO_4$	0.4	NaOH	20	H_2O	10 min	0
2	$KMnO_4$	0.6	NaH_2PO_4 NaOH	0.5 20	*t*-BuOH:H_2O (1:1)	10 min	0
3	$NaClO_2$	1.5	NaH_2PO_4 Sulfamic Acid H_2O_2	0.5 1.05 1	MeCN:H_2O (3:1)	18 h	< 5
4	$NaClO_2$	1.5	NaH_2PO_4 H_2O_2	1 1	MeCN:H_2O (3:1)	18 h	< 5
5	$NaClO_2$	2.5	NaH_2PO_4 2-methyl-2-butene	1.5 7.5	*t*-BuOH:H_2O (3:2)	20 h	14
6	$NaClO_2$	1.5	Sulfamic Acid	1.5	DMSO:H_2O (1:1)	18 h	32
7	$NaClO_2$	2	NaH_2PO_4 Sulfamic Acid	1 1.05	DMSO:H_2O (1:1)	18 h	60

Converting the aldehyde into a nitrile group, followed by a basic hydrolysis, producing the needed carboxylic acid was the next synthetic pathway to test. Select aromatic aldehydes have been reported to convert into a nitrile using ammonia in water and iodine at room temperature (Figure 57).[101] The reaction proceeds by ammonia attacking the carbonyl forming an aldimine species, once formed, the aldimine can oxidize with iodine to give an N-iodo aldimine intermediate which eliminates HI as a by-product forming the desired nitrile.[101] The reaction is tracked by TLC and once complete, the reaction should be immediately quenched with sodium thiosulfate solution to ensure no nitrogen triiodide monoamine[101] (a black explosive powder when dried, however, it was never observed during reaction trials) is produced as a hazardous by-product.

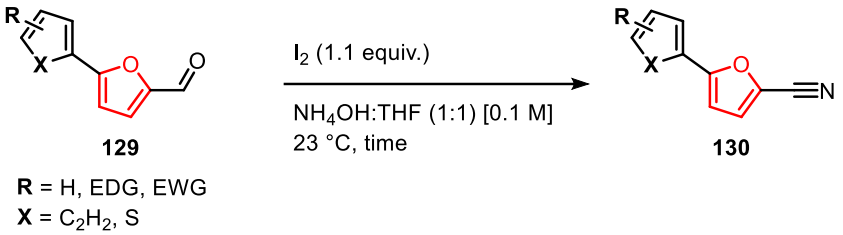

Figure 57. Generalize scheme of furan aldehydes (**129**) to furan nitriles (**130**).

Table 8. Scope of aldehyde to nitrile synthesis with diverse substrates.

Aldehyde	Product	C5-Aromatic	Scale	Time (h)	Yield %
119	**131**	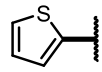	2 mmol	3	94
122	**132**	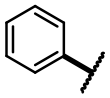	2 mmol	4.5	96
123	**133**	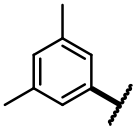	2 mmol	4.5	86
124	**134**	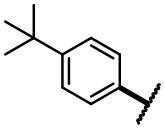	2 mmol	4.5	95
125	**135**	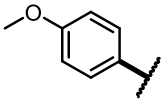	2 mmol	9	93
126	**136**	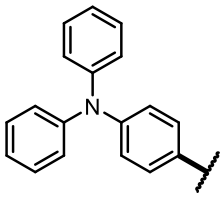	1.5 mmol	24	84
127	**137**	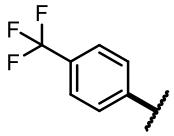	2 mmol	4	94
128	**138**	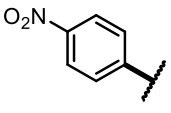	0.23 mmol	4	99

Impressively, this method easily prepared all furan-nitriles (**131** to **138**) in high yields (84-99%), regardless of the electronic groups existing within the phenyl substituent (see Table 8). The electronic groups at C5 however, did play a role regarding the overall reaction times. Neutral aldehydes (**119**, **122** – **124**) as well as electron-withdrawing groups (**127** and **128**) had converted fully to the corresponding nitrile within 3 – 4.5 hours. Whereas stronger electron-donating groups (**125** and **126**) have substantially longer reaction times at 9 and 24 hours respectively. This is most likely due to a less electrophilic carbonyl contributed by the electron-donating groups present. Figure 58 represents the immediate scheme to hydrolyze the newly formed nitrile to a carboxylic acid under basic conditions. After the reaction is complete, the desired carboxylic acid (**116**) is easily obtainable by a simple acidic workup. Table 9 presents the excellent yields obtained (88-99%) *via* basic hydrolysis.

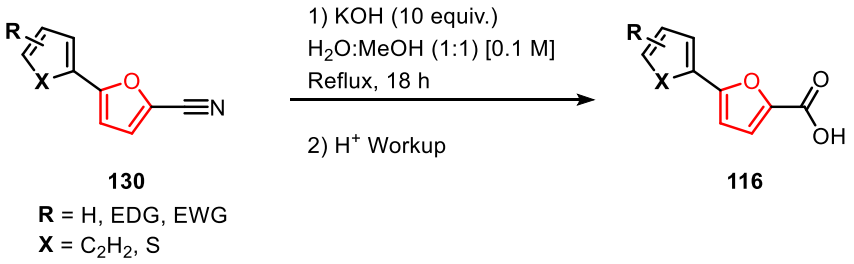

Figure 58. Basic hydrolysis of nitrile (**130**) towards acid (**116**).

Table 9. Scope of hydrolysis of nitriles towards carboxylic acids.

Product	C5-Aromatic	Scale	Yield %
139	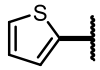	1 mmol	91
140	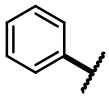	1 mmol	92
141	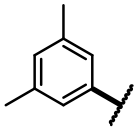	1 mmol	90
142	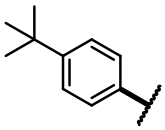	1 mmol	88
143	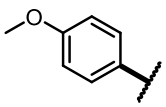	1 mmol	99

144[a]	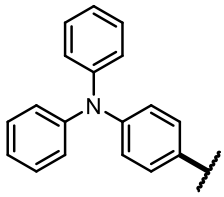	0.48 mmol	94
145	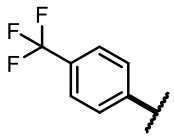	1 mmol	96
146	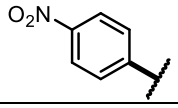	0.23 mmol	99

[a] 1 mL of THF was added for solubility purposes.

Formation of the nitrile species is an effective method to obtain the required acid at high yields (79 – 98% over two-steps) but at a cost of time (21 – 42 hours given the substrate). To achieve a faster oxidation, a one-step solvent-free mechanochemical Cannizzaro disproportionation was attempted using a planetary ball miller (as seen in Figure 59). Mechanochemistry enables solid-state chemical transformations to proceed through mechanical force while excluding the need for large volumes of solvents as performed by traditional reaction methods.[102] Ultimately, mechanochemistry provides an additional tool for chemists to design reactions while also practicing green chemistry principles by minimizing solvent waste. Previous work from Chacón *et al.* reports a highly green, solvent-free Cannizzaro disproportionation on HMF (**1**) using KOH exclusively to yield both acid and alcohol at 50% respectively.[103] *E-factor* comparisons show that this approach (*E-factor* = 0.55) is 6.5 times less wasteful than a solution-based Cannizzaro disproportionation (*E-factor* = 3.61).[103] Not only is this reaction more environmentally benign than other methods, it is exceptionally fast requiring only 5 minutes of reaction time. The only drawback of this disproportionation is the unwanted alcohol by-product, which is made alongside the acid, limiting the total yield of acid to 50%. However, the obtained alcohol could then be recycled back into the aldehyde after oxidation and later reintroduced into the planetary ball miller to further derive the wanted carboxylic acid, if necessary.

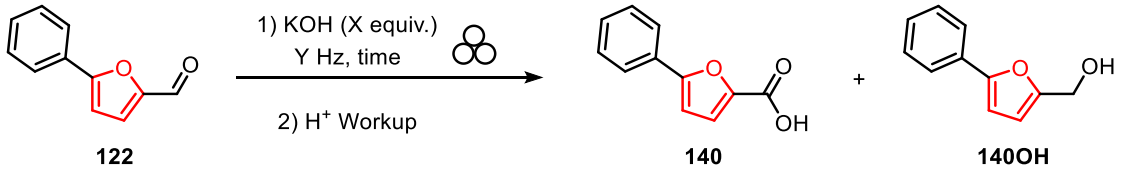

Figure 59. Generalized solvent-free Cannizzaro disproportionation of aldehyde (**122**) towards acid (**140**) and alcohol by-product (**140OH**).

Preliminary testing began with aldehyde (**122**) with reported conditions (2 equiv. KOH, 60 Hz and 5 minutes total) to yield the desired acid at 32% (Table 10). Noticeable amounts of the remaining starting aldehyde were leftover, theorizing that more time is required for the reaction to complete. An additional 5 minutes increased the yield by 10% and was later repeated on a larger scale (1 gram, Figure 60), achieving the same result. Figure 60 represents the planetary ball miller used, alongside the 1-gram scale reaction before and after mixing.

Ultimately, reducing the high frequency of the miller by half (60 to 30 Hz), providing an additional equivalent of KOH and 15 minutes total achieved the highest acid yield of 48%. Separating both acid and alcohol is simple due to the solubility of the carboxylate ion in water, whereas the alcohol is more soluble in the organic layer.[103] Once separated, the carboxylate is converted to the carboxylic acid by acid workup.

Figure 60. From left to right: Planetary ball miller. Stainless steel jar with starting reagents and 8mm steel balls with 1 gram reactants. Stainless steel jar after mixing at 60 Hz for 10 minutes.

Table 10. Optimization of solid-state Cannizaro disproportionation.

Entry	KOH X equiv.	Y Hz	Scale (mg)	Time (min)	Yield %
1[a]	2	60	100	5	32
2[a]	2	60	100	10	42
3[a]	2	60	1000	10	43
4[b]	3	30	100	15	48

[a] Mechanochemical reaction was performed in a stainless-steel jar with a ball miller and 7 stainless steel balls (8 mm diameter). EtOAc was added after opening jar. Yield of **140OH** was observed to be over 50 % due to the addition of EtOAc before H_2O, producing unwanted ester product (**140Ester**, Figure 61).[103] [b] Mechanochemical reaction was performed in a stainless-steel jar with a ball miller and 6 stainless steel balls (8 mm diameter). H_2O was added after opening the jar and the aqueous layer was washed with DCM.

After the reaction was complete, it was noticed that if EtOAc was added to the jar first, an ester by-product (**140Ester**) would be noticed on TLC and by ^{1}H NMR. We suspect that any alkoxide formed after the reaction can react with EtOAc solvent to produce the ester by-product (seen in Figure 61). **140Ester** was later confirmed by GCMS, however, to avoid the formation of ester, water should be added first to quench any potential alkoxide and then an organic solvent should be added to collect the remaining alcohol where it is separated by liquid-liquid extraction.

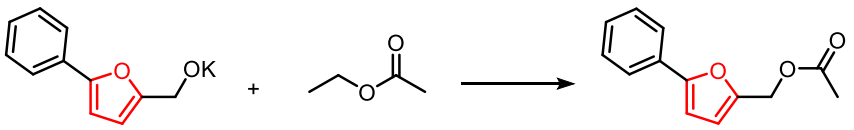

140OK **EtOAc** **140Ester**

Figure 61. Ester by-product (**140Ester**) after treating alkoxide (**140OK**) with EtOAc immediately.

Continuing with the optimized conditions (Figure 62) led to a majority of aldehyde being converted into a carboxylic acid (and the respected alcohol) at close to maximum yields (50%) as seen in Table 11. Bulky aldehyde (**124**) required 60 Hz and a full 30 minutes to fully convert into the desired materials. The formation of triphenylamine acid (**144**) and triphenylamine alcohol (**144OH**) had a considerably low conversion with the optimized conditions. A viscous oil was noticed after mixing, suggesting that the triphenylamine substrate and the KOH had poor overall

mixing and could not go to completion. Triphenylamine acid (**144**) had already been synthesized in great yields (60% over three steps using the solution-based oxidation) and was not further investigated in the solid state.

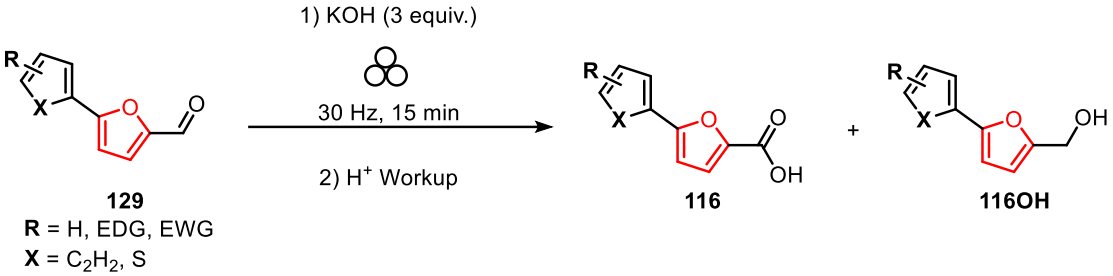

Figure 62. Cannizzaro disproportionation of aldehyde (**129**) to acid (**116**) and alcohol (**116OH**).

Table 11. Scope of Cannizzaro disproportionation with diverse substrates.

Aldehyde	Product	C5-Aromatic	Scale (mg)	Acid Yield %	OH Yield %
119	**139** & **139OH**		100	48	42
122	**140** & **140OH**	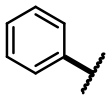	100	49	49
123	**141** & **141OH**	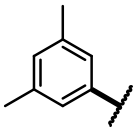	100	47	49
124	**142** & **142OH**	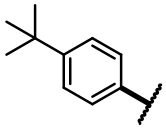	100 100	13 44[a]	8 40[a]
125	**143** & **143OH**	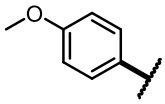	100	46	45
126	**144** & **144OH**	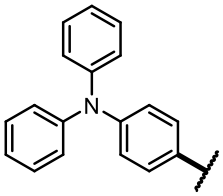	66	18[b]	15
127	**145** & **145OH**	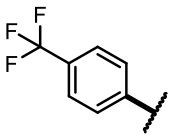	30	48	46
128	**146** & **146OH**	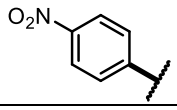	30	42	39

[a] Frequency changed to 60 Hz for 30 minutes. [b] Yields estimated by ^{1}H NMR.

The previous two oxidations discussed represent a versatile methodology to obtain the needed carboxylic acid (as a DCC nucleophilic partner) either through a high-yielding two-step solution-based oxidation (aldehyde → nitrile → carboxylic acid, 21 – 42 hours, 79 – 98% over two-steps) or *via* a quick (15 minute) solvent-free Cannizzaro disproportionation to access the acid immediately from the aldehyde at a cost of yield (50% maximum).

At last, the final reaction to formally optimize is the final double Pd-catalyzed DCC reaction as seen in Figure 63. Optimizing this reaction began by coupling a neutral acid partner (**140**) with a 2,5-dibromothiophene (**104**) linker using the same conditions as seen in Chapter 2 (Entry 1, Table 12).[62] A fair yield of 49% (70% C-C bond formation) was observed using ^{1}H NMR. Entry 2 was prepared the same way as the first, however, before the addition of the palladium catalyst ($Pd(PtBu_3)_2$, cone angle = 182°), the solution was left on a sonicator under a stream of argon gas (10 minutes), to deoxygenate the amide solvent and provide a more inert atmosphere for the reaction to take place. Impressively, degassing the solvent increased the potential yield of the reaction by 9%. Henceforth, this change was then applied to all future reactions due to the benefit observed by degassing.

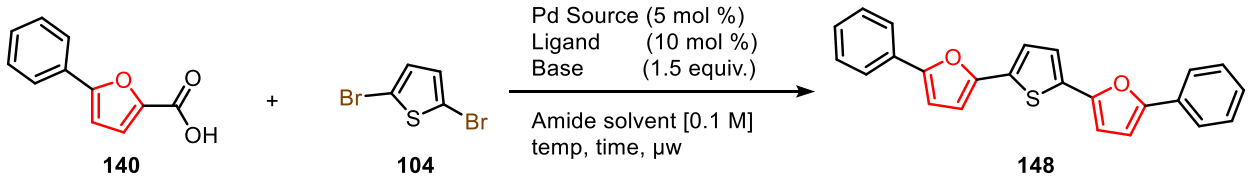

140 **104** **148**

Figure 63. Double Pd-catalyzed DCC reaction of phenyl-furan acid (**140**) and dibromo-thiophene (**104**) to obtain alternating 2,5-furan-based oligomer (**148**).

Table 12. Optimization of double Pd-catalyzed DCC reaction.

Entry	Acid X equiv.	Pd Source	Ligand	Base	Amide solvent	Temp (°C)	Time (min)	^{1}H NMR Yield %
1[a]	3	$Pd(PtBu_3)_2$	-	Cs_2CO_3	DMF	170	10	49
2	3	$Pd(PtBu_3)_2$	-	Cs_2CO_3	DMF	170	10	58
3	3	$Pd(PtBu_3)_2$	-	Cs_2CO_3	DMA	170	10	61
4	3	$Pd(PtBu_3)_2$	-	Cs_2CO_3	DMA	200	10	61
5[b]	3	$PdCl_2$	P(*o*-tolyl)$_3$	Cs_2CO_3	DMA	170	15	74
6[b]	2.2	$PdCl_2$	P(*o*-tolyl)$_3$	Cs_2CO_3	DMA	170	15	71
7[b]	2.2	$PdCl_2$	P(*o*-tolyl)$_3$	Na_2CO_3	DMA	190	8	29
8[b]	2.2	$PdCl_2$	P(*o*-tolyl)$_3$	K_2CO_3	DMA	190	8	67
9[b]	2.2	$PdCl_2$	P(*o*-tolyl)$_3$	Cs_2CO_3	DMA	190	8	85
10[b]	2.2	$PdCl_2$	P(*o*-tolyl)$_3$	Cs_2CO_3	DMA	190	15	85

[a] Same procedure described, not degassed with argon gas. [b] Conditions inspired by previous double decarboxylative cross-coupling work on oligothiophenes.[82]

Entries 3 and 4 changed solvents from DMF to DMA and also tested to see if more product would be observed at higher temperatures (170 vs 200°C). These results indicated that DMA might be a better solvent choice (by a 3% increase), however, additional heat did not favour a higher yield given these conditions. Entry 5 took conditions directly from Liu *et al.* (who reported on the first double Pd-catalyzed DCC reaction on oligothiophenes) with a more commercially available Pd(II) catalyst ($PdCl_2$) included with a bulky steric hindered phosphine ligand (P(*o*-tolyl)$_3$, cone angle = 194°).[82] This entry provided a significant increase in yield (13% increase) suggesting that the change from a moderately steric ligand to a more bulk ligand (P*t*Bu$_3$ vs P(*o*-tolyl)$_3$) is preferred to effectively couple heterocyclic acid partners in double DCC reactions. Entries 7 to 9 compared carbonate bases (at 190°C) and found a staggering difference in yields depending on the countercation of each base. A trend of yields increased with larger alkali metal cations (Na < K < Cs, 29% < 67% < 85 % respectively) suggesting that the counter cation may play a key role in the mechanism due to its larger atomic radius which may help in stabilizing anionic intermediates. Entry 10 tested if additional time is necessary given the extraordinary results seen in Entry 9, however, no significant change was observed (85% yield, 92% C-C bond formation).

After optimizing the double Pd-catalyzed DCC conditions to achieve 85% ^{1}H NMR yields, it was then time to produce a scope and decide what linkers could couple to the selection of arylated furan acids (**139** – **146**) previously synthesized. Figure 64 depicts the generalized double Pd-catalyzed DCC reaction of arylated furan acid (**116**) to react with a dibromo aromatic linker producing the desired 2,5-furan-based oligomers (**117**) using the optimized conditions.

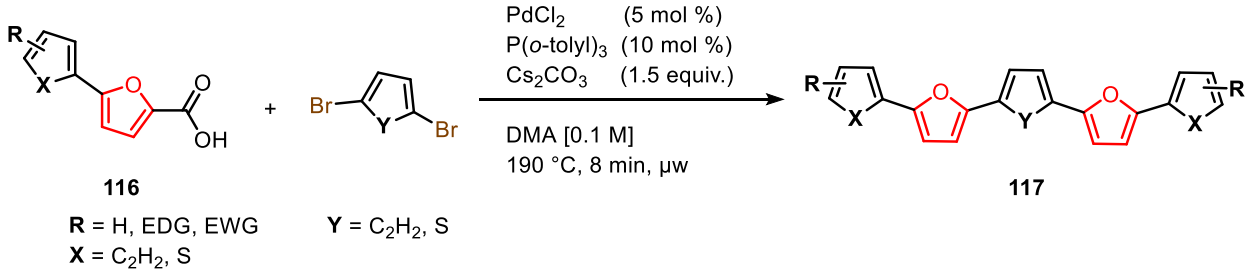

Figure 64. Final double Pd-catalyzed DCC of acid (116) and dibromoaryl linker to access 2,5-furan-based oligomers.

Thiophene-furan acid (**139**) showed excellent reactivity when coupled to either a thiophene or phenylene linker, producing products **44** (**TFT**) and **147** (**TFP**) at great yields of 71% and 65% respectively as seen in Table 13. Recall that product **44** (**TFT**) is a fully alternating heterocyclic oligomer (Figure 16) previously synthesized by cyclization methods.[63] This methodology is the first to access oligomer **TFT** *via* a cross-coupling strategy, excluding the need for cyclization methods while incorporating biomass-derived starting materials. Product **147** (**TFP**), however, is a novel alternating oligomer following a thiophene-furan-phenylene-furan-thiophene structure, we suspect this compound could exhibit favorable optoelectronic properties associated with highly planar furan-phenylene-furan cored molecules.[54,72,98] While also shifting the absorbance and photoluminescence maxima due to the thiophene groups directly bonded to the C5 position of the furan ring, the spectroscopic observations are found and further discussed in the following chapter.

Neutral phenylene furan acid (**140**) also demonstrated great yields as a coupling partner to both dihalogenated aromatic linkers. With a thiophene linker, an isolated 62% yield was obtained producing a novel alternating phenyl-furan-thiophene oligomer **148** (**PFT**), whereas a phenylene linker obtained similar yields of 66% of phenyl-furan-phenyl co-oligomer **42** (**PFP**). To quantitively compare this final DCC cross-coupling to reported synthetic Kazantsev *et al.*[54] a 1.0 mmol scale reaction was also attempted in the microwave. A slight decrease in yield was observed with this scale-up reaction, yielding an overall good yield of 55% (74% C-C bond formation). Using the scaled-up reaction as a benchmark, the ability to fully compare all synthetic statistics (overall yield, total reaction times) as well as green metrics (*E-factor* and *Atom Economy*) was now possible.

From a retrosynthetic point of view (as represented in Figure 65), the methodology discussed in this thesis can be viewed as a difference in the order of operations compared to previous work.[54,72] Recall, that previous work produced co-oligomer **42** (**PFP**) after a double Suzuki cross-coupling reaction (*E-factor* = 26.3, *Atom Economy* = 59.2%) which installed the phenyl groups (**41**) at the extremities of furan-phenylene-furan core (**40**) that were made available after a double Stille cross-coupling (*E-factor* = 8.5, *Atom Economy* = 22.1%) between a dibromophenylene linker (**38**) and organotin compounds (**37**) derived from furan (**23**). Their approach provides the **PFP** co-oligomer at an overall yield of 14% over four steps, requiring over 72 hours of reaction time. The method presented here decided to cut the **PFP** co-oligomer bonds between the linker and furan ring to fuse

the central phenylene core last. In doing so, a double DCC reaction has taken place with two acid partners (**140**) and the same dibromophenylene linker (**38**), reporting a low cross-coupling *E-factor* of 7.0 with an *Atom Economy* of 59.2%. This step was made possible after a versatile method to produce the acid after a solution-based or solid-state oxidation step (not shown in Figure 65).

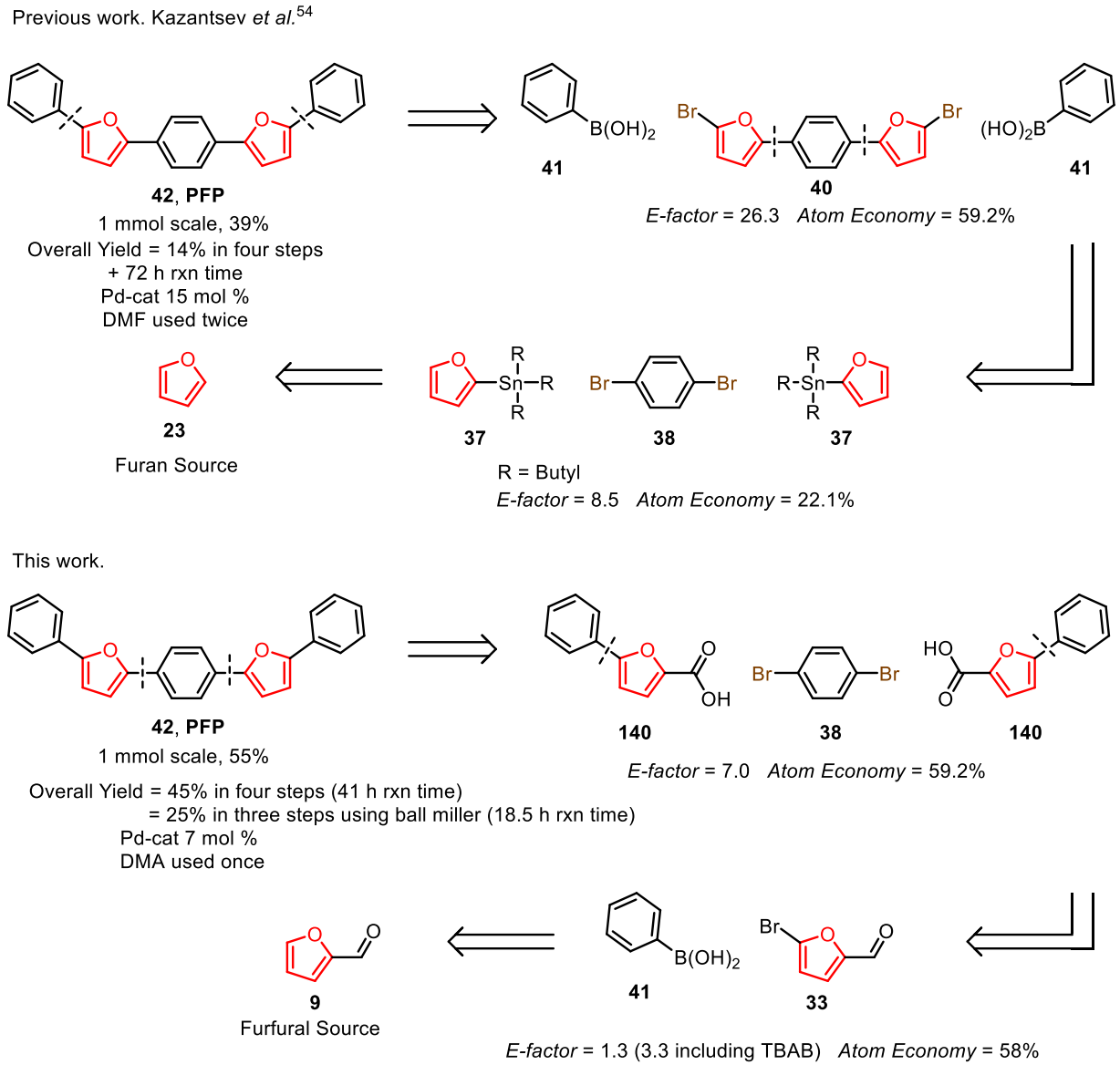

Figure 65. Retrosynthetic comparison of **PFP** co-oligomer **42** from previous work[54] to this reported methodology starting with 5BF (**33**).

Using 5BF (**33**) was an optimal choice of starting material as the phenyl extremities could be mildly bonded by a Suzuki cross-coupling in water at room temperature, this step reports a very

low *E-factor* of 1.3 (or 3.3 including TBAB) with an *Atom Economy* of 58.0%. 5BF is also derived from furfural, indicating that this co-oligomer **PFP** can be accessed by biomass-derived platform chemicals. Ultimately, depending on the synthetic route of choice, this methodology has produced **PFP** at an overall yield of 45% after four-steps, requiring 41 hours of reaction time, or if the solid-state Cannizzaro disproportion is attempted, the overall yield is found at 25% after three-steps with 18 and a half hour worth of reaction time.

By altering the sequence of operations, another notable observation pertains to the use of amide solvents. Due to the high conjugation found in this **PFP** core, we speculate that a highly planar **PFP** core requires polar amide solvents for dissolution and processibility purposes. This could explain why previous work reports the use of DMF solvent twice throughout their synthesis.[54] The decision to produce the central core last in our approach, stands with previous goals of reducing the need of amide solvents throughout a synthesis. This synthetic approach instead requires the use of DMA solvent once, halving the use of amide solvents overall. When these syntheses are further compared, this work also reduces the total amount of Pd-catalyst needed (7 mol % total, a reduction of 50% in comparison). In summary, the synthesis presented demonstrates the ability to design co-oligomer **42** (**PFP**) at an improved overall yield (25 – 45%) with shorter reaction times (18.5 – 41 h) while reducing the total amount of reaction steps (from four to three) and generating less waste produced from traditional coupling methods. This approach highlights the goals of developing more environmentally benign yet effective synthetic strategies to produce optoelectronic candidates through biomass-derived starting materials.

Further applying this synthetic methodology to expand the chemical library of 2,5-furan-based oligomers. *Meta*-functionalized phenylene furan acids (**141**) provided great isolated yields of 74% (86% C-C bond formation) with a phenylene linker to produce previously reported co-oligomer **149** (3,5-diMe**PFP)**.[72] *Para*-functionalized bulky (**142**) and electron-donating acid groups (**143** and **144**) provided fair yields of sterically hindered electron-rich co-oligomers **150** (4-*t*-Bu**PFP**), **151** (4-MeO**PFP**) and **152** (4-TPA**PFP**) at 58%, 50% and 32 % respectively. To our knowledge, no reports of these three **PFP** cored furan-oligomers have been made. *Para*-functionalized electron-withdrawing groups were tested as acid nucleophilic coupling partners (**145** and **146**) and produced the desired electron-poor co-oligomers **153** (4-CF_3**PFP**) and **154** (4-Nitro**PFP**) with phenylene linkers at poor isolated yields (21% and 18% respectively). In 2018, Sonina *et al*.[97] repeated the

previous method reported by Kazantsev *et al.*[54] where they reported the overall yield of electron-withdrawing co-oligomer 4-CF_3**PFP** at 21% over four steps. Whereas this methodology calculates an overall yield of 13% producing 4-CF_3**PFP** over four steps. While this strategy to access 2,5-furan-based oligomers is more environmentally benign than the previous, from an overall yield perspective regarding electron-withdrawing substituents, it is slightly less effective than previous reports (8%).[97] Given the weaker nucleophilic nature of these acids for this given reaction, it is not surprising a decrease in yield is observed, additionally two nucleophilic partners must react with the dibrominated phenylene partner, which may be more difficult for less activated carboxylic acids to undergo twice.

Table 13. Scope of alternating 2,5-furan-based oligomers *via* double Pd-catalyzed DCC reaction.

Acid	Product	Short Name	C5-Aromatic	Y	Scale	Yield %
139	**44**	**TFT**	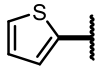	S	0.1 mmol	71
	147	**TFP**		C_2H_2	0.1 mmol	65
140	**148**	**PFT**	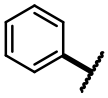	S	0.2 mmol	62
	42	**PFP**		C_2H_2	0.2 mmol	66
					1.0 mmol	55
141	**149**	3,5-diMe**PFP**	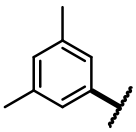	C_2H_2	0.1 mmol	74
142	**150**	4-*t*-Bu**PFP**	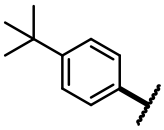	C_2H_2	0.1 mmol	58
143	**151**	4-MeO**PFP**	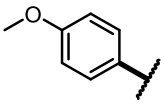	C_2H_2	0.1 mmol	50
144	**152**	4-TPA**PFP**	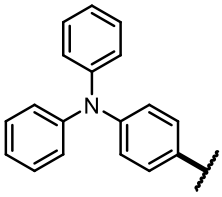	C_2H_2	0.1 mmol	32
145	**153**	4-CF_3**PFP**	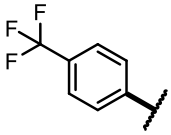	C_2H_2	0.1 mmol	21
146	**154**	4-Nitro**PFP**	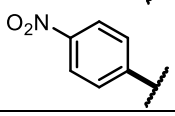	C_2H_2	0.1 mmol	18

Finally, given the interest in push-pull compounds and their possession of unique optical properties arising from electron movements from donor to acceptor.[51,60] This study aimed to synthesize a small asymmetric push-pull compound to compare with the 2,5-furan-based oligomers and see how optically different they are. Figure 66 illustrates the coupling of *para*-nitro-phenylene furan acid (**146**) with bromo-thiophene (**155**) in a Pd-catalyzed DCC reaction, yielding the desired small push-pull compound **156** (4-Nitro**PFT**) at 52%. Despite the limited nucleophilic activity of the nitro acid observed for double Pd-catalyzed DCC reactions, in this single reaction, a decent isolated yield is obtained. In this push-pull system, the nitro group acts as the electron acceptor, with furan serving as the π-spacer, and the thiophene behaves as the electron donor.

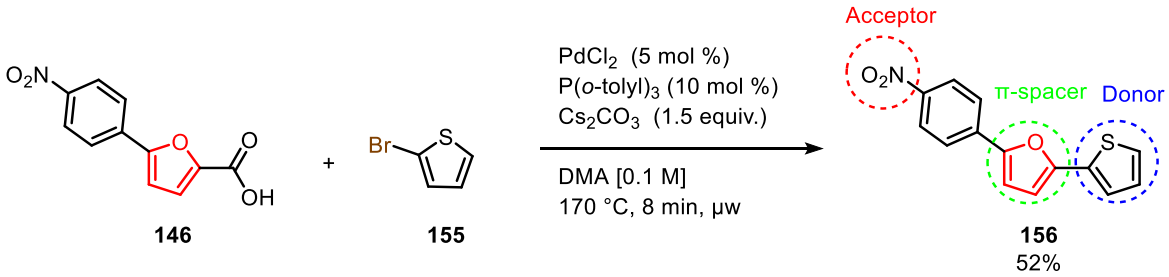

Figure 66. Producing push-pull compound **156** by single DCC of furan acid (**146**) and bromo-thiophene (**155**).

The following chapter discusses and compares the optical properties of these synthesized co-oligomers as well as the single push-pull chromophore derived. For the sake of simplicity, absorbances have not been compared throughout the discussion and instead are all shown within Table 14 of Chapter 3.4. Photoluminescence and PLQY are instead the focus of discussion.

3.4 Spectroscopic Data of 2,5-Furan-Based Phenylene/Thiophene Oligomers

Another big thank you to Victoria Lapointe of the Majewski group for obtaining the following optical properties of all final compounds produced in Chapter 3. Table 14 organizes all the spectroscopic data in dilute $CHCl_3$ solution: including absorbance (λ_{abs}), photoluminescence (λ_{em}) and PLQY of 2,5-furan-based co-oligomers (**42**, **44**, **147-154**) and 2,5-furan push-pull compound (**156**). Whenever possible, spectroscopic literature values of certain co-oligomers are presented in the "Literature Values" column of Table 14.

Table 14. Complete spectroscopic data for all final 2,5-furan-based oligomers and push-pull compound.

Product	Final Compound Structure	Absorbance (λ_{abs})	Photoluminescence (λ_{em})	PLQY % (± 5)	Literature Values
42 **PFP**	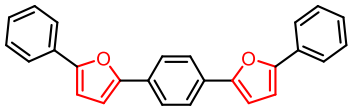	378 nm	412, 438 nm	92	λ_{abs}: 372 nm[54] λ_{em}: 407, 431 nm[54] PLQY: 91 ± 3[54] Solvent: ACN
148 **PFT**	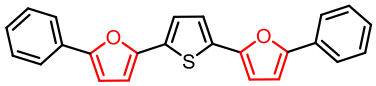	404 nm	448, 478 nm	37	N/A
147 **TFP**	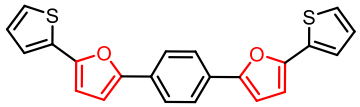	389 nm	428, 454 nm	92	N/A
44 **TFT**	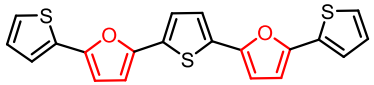	416 nm	464, 496 nm	61	λ_{abs}: 414 nm ($CHCl_3$)[63] 409 nm (ACN), 415 nm (benzene)[104] λ_{em}: 486 nm (ACN), 488 nm (benzene)[104] PLQY: 35 (ACN), 30 (benzene)[104]

149 3,5-diMe**PFP**	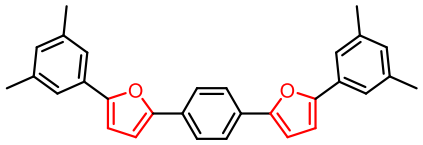	380 nm	416, 442 nm	97	λ_{abs}: 379 nm[72] λ_{em}: 413, 438 nm[72] PLQY: 89[72] Solvent: THF
150 4-*t*-Bu**PFP**	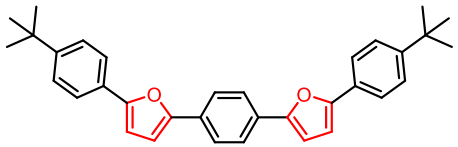	381 nm	418, 442 nm	83	N/A
151 4-MeO**PFP**	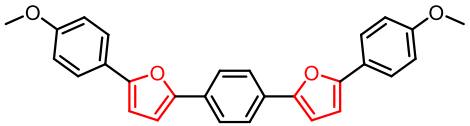	383 nm	422, 448 nm	85	N/A
152 4-TPA**PFP**	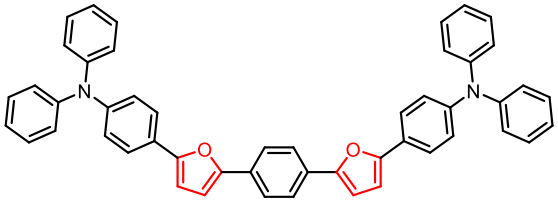	406 nm	456, 482 nm	92	N/A
153 4-CF_3**PFP**	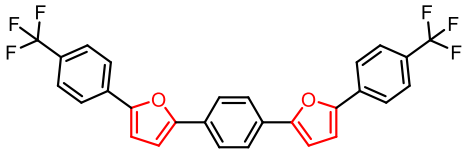	382 nm	418, 444 nm	98	λ_{abs}: ~380 nm[97] λ_{em}: ~415, 433 nm[97] PLQY: 86[97] Solvent: THF
154 4-Nitro**PFP**	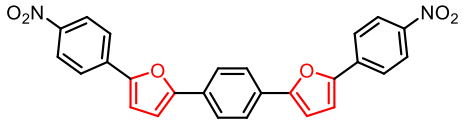	433 nm	606 nm	14	N/A
156 4-Nitro**PFT**	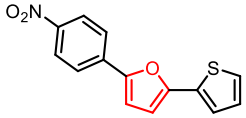	404 nm	590 nm	44	N/A

All compounds were tested in $CHCl_3$ at a concentration of [2 x 10^{-7} M] to ensure absorption was at or below 0.1 absorbing units.

PLQY testing done at maximum absorption for each compound respectively using an integrating sphere.

Comparing spectroscopic properties in this chapter will focus on the photoluminescence and PLQY data presented from Table 14. Firstly, there is an interest to observe the optical property differences among 2,5-furan-based phenylene/thiophene containing co-oligomers **42** (**PFP**), **44** (**TFT**), **147** (**TFP**) and **148** (**PFT**). Evaluating the increasing number of heterocycles within the furan system as well as the location of each aromatic group (phenylene vs thiophene, C5 vs C2 positions) bonded to the furan ring is suspected to affect the photoluminescence and PLQY respectively. Previous reports have synthesized and optically tested 2,5-furan-based co-oligomers **42** (**PFP**)[54] and **44** (**TFT**),[63,104] however, none have synthesized symmetrically alternating co-oligomers to include phenylene and thiophene groups simultaneously such as **147** (**TFP**) and **148** (**PFT**). After graphing the photoluminescence of the materials discussed, illustrated in Figure 67, unsurprisingly 2,5-furan-based phenylene co-oligomer **42** (**PFP**) is mostly found to fluoresce blue light (λ_{em} = 412, 428 nm), whereas 2,5-furan-based thiophene co-oligomer **44** (**TFT**) red-shifts to fluoresce cyan-green light (λ_{em} = 464, 496 nm). Photoluminescent data points of these co-oligomers relate well to literature values seen in Table 14. Although slight deviations are noticed, this is quite normal given that different solvents were used in testing these materials.[54,104]

What is surprising to observe, is that increasing the total amount of thiophenes in the furan system does not fully relate to consistent red shifts in the photoluminescence spectra. Co-oligomer **147** (**TFP**) differs from co-oligomer **148** (**PFT**) by having an extra thiophene unit. In compound **147** (**TFP**), both thiophenes are located at the C5 position, whereas in compound **148** (**PFT**), there is only one thiophene unit linked between two phenylene-furan species at C2. It was hypothesized that due to an increase in delocalized electrons contributed by additional thiophene units, co-oligomer **147** (**TFP**) would slightly red shift its photoluminescence in comparison to the single linked thiophene co-oligomer **148** (**PFT**). Figure 67 represents that this is not the case and instead the opposite is seen, where thiophene linked co-oligomer **148** (**PFT**) fluoresces cyan-green light at 448 and 478 nm, resulting in a slight red shift compared to the cyan light fluoresced by phenylene linked co-oligomer **147** (**TFP**) at 428 and 454 nm (λ_{em}). PLQY studies were also conducted to better understand what is potentially happening with these given oligomers.

These four co-oligomers were further investigated by their PLQY to evaluate how efficient these molecules emit light in solution after excitation. Literature does discuss that the highly planar and rigid furan-phenylene-furan core containing materials, possess impressively high PLQY (**42**, **PFP**,

= 91% in ACN solution).[54,71,89,90] The furan quinoidal resonance (discussed in Chapter 1.2) could be the cause as to why this furan-phenylene-furan core is exceptionally rigid.[42] This specific core is found in half the materials discussed in this section and when PLQY are compared, a trend is observed; the PLQY of thiophene linked co-oligomers increase with the addition of thiophene units **148** (**PFT**) PLQY = 37%, where **44** (**TFT**) PLQY = 61%. This observed trend agrees with previous literature depicting an increase in PLQY when additional thiophene units are conjugated in α-oligothiophenes.[105] Furan-phenylene-furan core derivatives **42** (**PFP**) and **147** (**TFP**) attain the exact same high PLQY observed at 92%, agreeing with previous literature on how brightly luminescent these types of oligomers really are.[54,71,89,90] Given the high PLQY relating to the strong rigidity found in furan-phenylene-furan cored materials. We speculate, when the phenylene linker is swapped with thiophene, the degrees of freedom are increased resulting in more rotatable bonds between furan and the thiophene linker. Overall, this reduces the materials planarity allowing for more non-radiative decay processes (lost as heat) to occur, resulting in a decrease in PLQY. Recall in Chapter 2.4, where the PLQY of multi-arylated furan linked with thiophenes were studied and had similar values (2,5-Furan **109**, PLQY = 41%, 2,3,5-Furan **113**, PLQY = 23%, 2,4,5-Furan **115**, PLQY = 43%).

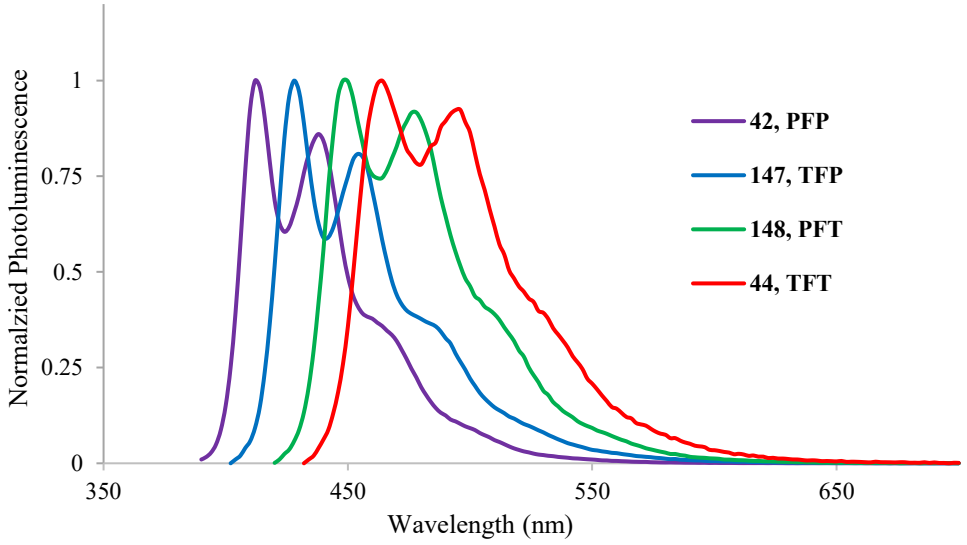

Figure 67. Normalized photoluminescence spectra of 2,5-furan-based phenylene/thiophene oligomers: **42** (**PFP**), **147** (**TFP**), **148** (**PFT**), and **44** (**TFT**).

For these reasons, we suspect that an increase in the degrees of freedom with thiophene linkers relates to an intrinsic photoluminescent red shift observed between planar co-oligomer **147** (**TFP**) and thiophene linked co-oligomer **148** (**PFT**). The central linker chosen plays an important role tuning the optical properties observed. To further prove this hypothesis, computational chemistry would be a viable method to view and evaluate the molecular orbitals of these structures.

The remaining furan-phenylene-furan cored co-oligomers (**149** – **154**) including the 2,5-furan push-pull chromophore (**156**) was studied for their optical properties (see Figure 68). Co-oligomers **149** (3,5-diMe**PFP**), **150** (4-*t*-Bu**PFP**), **153** (4-CF_3**PFP**) all fluoresced similar blue-light emissions (see Table 14). Suggesting that these relatively steric groups behave similarly from a luminescent perspective. A small red shift is observed when compared to co-oligomer **151** (4-MeO**PFP**) which contains a methoxy functional group (MeO) known to have electron-donating characteristics, fluorescing cyan light at 422 and 448 nm (λ_{em}). Impressively, strong electron-donating triphenylamine (TPA) 2,5-furan-based co-oligomer **152** (4-TPA**PFP**), provided a significant red shift, fluorescing cyan-green light at 456 and 482 nm (λ_{em}). This co-oligomer differs from most oligomers produced, as it contains the most aromatic species of all compounds in this thesis, totaling nine aromatic rings, supported with two nitrogen heteroatoms. The final furan-phenylene-furan cored co-oligomer **154** (4-Nitro**PFP**) represented the most drastic red shift observed throughout this work. Having access to two strong electron-withdrawing nitro groups exhibits one orange photoluminescence peak at 606 nm (λ_{em}). Additionally, the classical two peaks found in the emission of furan-based oligomers no longer appear, suggesting that this species does not retain the conjugated furan characteristics seen with every other furan-based compound before it. Given this peculiar result, there was interest in developing a nitro containing furan-based push-pull chromophore and comparing it to co-oligomer **154** (4-Nitro**PFP**). Hence, a small three-ringed push-pull like compound with thiophene as the donor was synthesized, **156** (4-Nitro**PFT**). Even with a single nitro group present, this compound emitted one large orange peak (λ_{em} = 590 nm) like **154** (4-Nitro**PFP**), suggesting that the incorporation of a nitro group could drastically red shift these types of compounds while also removing the furan photoluminescent characteristic peaks seen. However, this compound does have push-pull like behavior and will possess different optical properties than the symmetrical co-oligomers present. This section further highlights that the peripheral aromatic groups chosen at C5 can tune the photoluminescent maxima with either strong electron-donating (MeO, TPA) or strong electron-withdrawing groups (nitro).

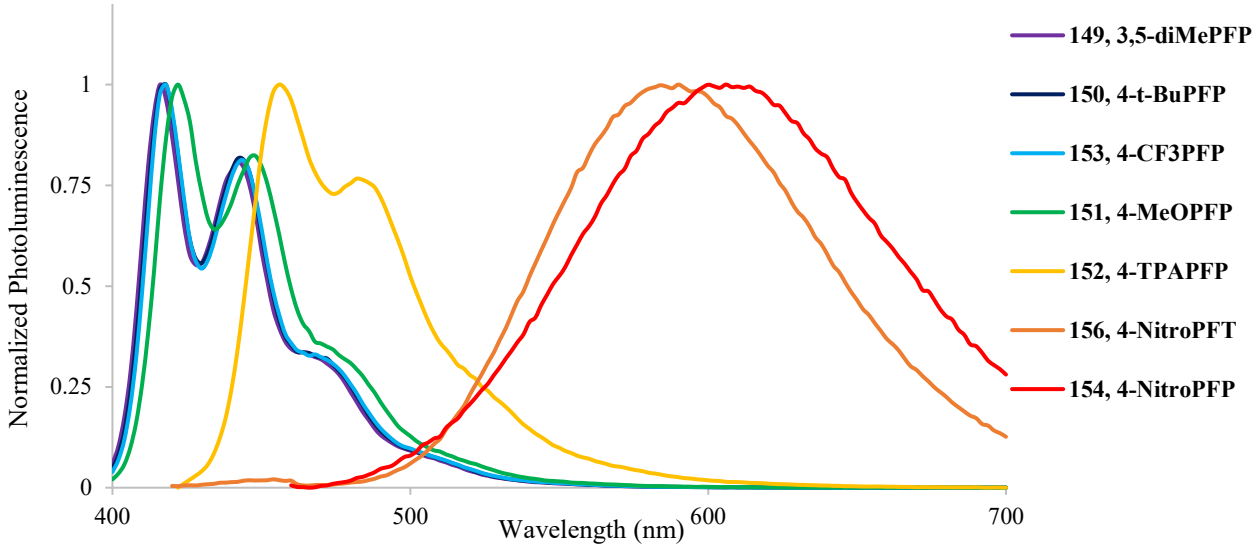

Figure 68. Normalized photoluminescence spectra of 2,5-furan-based phenylene oligomers: **149** (3,5-diMe**PFP**), **150** (4-*t*-Bu**PFP**), **153** (4-CF_3**PFP**), **151** (4-MeO**PFP**), **152** (4-TPA**PFP**), **154** (4-Nitro**PFP**) and 2,5-furan-based push-pull compound **156** (4-Nitro**PFT**).

Lastly, the PLQY of the following furan-phenylene-furan co-oligomers were studied. All co-oligomers were found to have exceptionally high PLQY (**149** – **153**, PLQY = 83 – 98%), except for co-oligomer **154** (4-Nitro**PFP**), exhibiting a very low PLQY = 14% due to the nitro species present which are known to quench photoluminescence.[106] The small three ring push-pull compound **156** (4-Nitro**PFT**) was substantially brighter, possessing a PLQY = 44% (Figure 69).

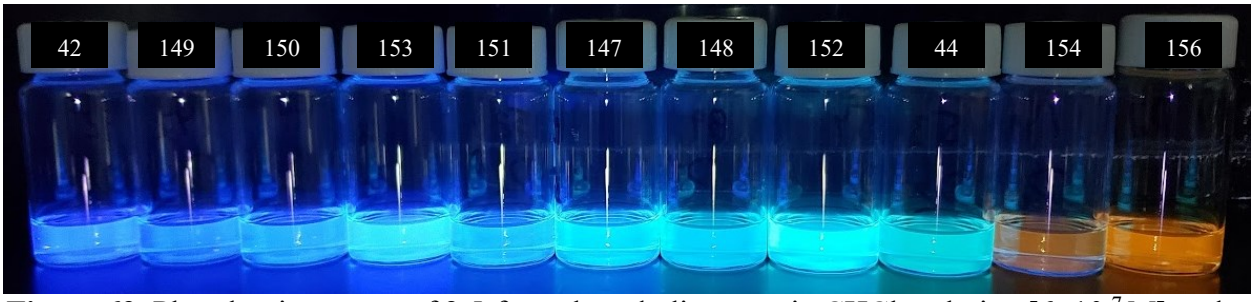

Figure 69. Photoluminescence of 2,5-furan-based oligomers in $CHCl_3$ solution [6×10^{-7} M] under 365 nm UV light. In order from most blue to most red emitting fluorescence for oligomers: **42** (**PFP**), **149** (3,5-diMe**PFP**), **150** (4-*t*-Bu**PFP**), **153** (4-CF_3**PFP**), **151** (4-MeO**PFP**), **147** (**TFP**), **148** (**PFT**), **152** (4-TPA**PFP**), **44** (**TFT**), **154** (4-Nitro**PFP**) and 2,5-furan-based push-pull compound **156** (4-Nitro**PFT**).

3.5 Conclusion

In summary, 5BF (**33**) is a close derivative of biomass-derived starting material, furfural (**9**), which proved to be an excellent starting point for designing a library of ten 2,5-furan-based co-oligomers, as well as a push-pull 2,5-furan-based compound, **156** (4-Nitro**PFT**), as potential optoelectronic candidates. The advantage of this methodology lies in its production of significantly less waste compared to traditional Pd-catalyzed coupling methods (CO_2 gas being expelled, compared to toxic organotin waste). Additionally, it involves a solvent-free mechanochemical Cannizzaro disproportionation that quickly derives the necessary carboxylic acid (in 15 minutes), further minimizing waste. This method also requires only half the Pd-catalyst loading compared to previous methods (from 15 mol % to 7 mol %) and utilizes biomass-derived starting materials into synthesis, further promoting sustainable practices in the development of highly conjugated organic furan materials.

Furthermore, this method achieves 2,5-furan phenylene co-oligomer **42** (**PFP**) in higher overall yields than previously reported (previous method: 14% over four steps, taking 72+ hours of reaction time). In contrast, this method demonstrated 25 – 45% overall yields over three to four steps, respectively, with shorter total reaction times of 18.5 – 41 hours. The key to this synthesis once more relies on the one-pot double Pd-catalyzed DCC strategy, which was further optimized during this synthesis through changes in the choice of DMA solvent, degassing the solution with argon, and using a more commercially available $PdCl_2$ catalyst with P(*o*-tolyl)$_3$ as the ligand of choice.

Spectroscopic data demonstrated the tunability of these functionalized materials, depending on the choice of linker as well as the electron-donating or withdrawing groups present (thiophenes, MeO, TPA and nitro). Seven final co-oligomers containing the highly planar furan-phenylene-furan core exhibited remarkably high PLQY (83 – 98%) in dilute $CHCl_3$ solution at room temperature, an important characteristic for optoelectronic devices. The small push-pull **156** (4-Nitro**PFT**) also exhibited impressive fluorescence for a three-ringed aromatic species, emitting orange light (λ_{em} = 590 nm) with a surprisingly high PLQY (44%), surpassing all multi-arylated furan compounds from Chapter 2.

Chapter 4. General Conclusions and Future Work

The goals of this thesis were twofold: to integrate biomass-derived starting materials into multi-arylated furan species, circumventing the need for petroleum-based cyclization methods, and to devise a synthetic methodology for accessing 2,5-furan-based co-oligomers while minimizing waste generation found from traditional Pd-catalyzed cross-coupling approaches. These highly arylated furan species possess favorable optoelectronic properties, making them interesting targets to produce from biomass-derived sources. The methodologies presented in this thesis achieve both objectives by producing a small library of three novel multi-arylated furans containing thiophene as a linker, along with ten 2,5-furan-based co-oligomers. Furthermore, the synthetic decisions to access 2,5-furan-based co-oligomers are more environmentally benign (including an improved *E-factor*), offers a higher *Atom Economy*, requires shorter overall reaction times, employing a solvent-free transformation, requires half the total amount of Pd-catalyst loading and enables the design of diverse alternating 2,5-furan-based oligomers. In doing so, six newly made furan co-oligomers were developed alongside a novel furan push-pull compound containing nitro and thiophene groups. Spectroscopic data revealed that most furan-phenylene-furan cores exhibit impressively high PLQY, while also demonstrating the ability to tune the absorbance and photoluminescence maxima through changes in the peripheral functional groups at C5 as well as the choice of the center linker fused onto the furan backbone.

Future work involving this project can branch out into several directions. Firstly, the furan-phenylene-furan diol synthesized in Chapter 2 could be further optimized and subsequently tested as a monomer for polymer synthesis. Additionally, by establishing pathways for accessing multi-arylated-furans, this synthesis could explore the functionalization of push-pull-like compounds by determining which electron groups (donor or acceptor) could be incorporated at specific positions on the furan ring. Chapter 3 could be expanded by exploring various dihalogenated aromatic linkers to investigate their role based on the optical properties observed. From a device standpoint, the isolated co-oligomers synthesized in this thesis could be optically studied in the solid state and later tested as a "top-gate top-contact" device, as constructed by Kazantsev *et al*.[54] to evaluate their suitability as potential OFET candidates.

Chapter 5. Experimental Information

5.1 General Conditions and Instrumentations

Reactions were carried out in regular glassware exposed to air unless otherwise noted. Due to the reactive nature of furan compounds when exposed to light or air for prolonged exposure. All final products (excluding carboxylic acids) were stored under argon gas, wrapped in aluminum foil, and stored in a -20 °C freezer for long-time storage. 5-bromofurfural (**33**) was purchased from Oakwood Chemical and AK Scientific and used after recrystallization in 9:1 (v/v%) Diethyl ether:EtOAc. Commercially available starting materials (all boronic acids, 1,4-dibromobenzene and 2,5-dibromothiophene) and reagents (KOH, K_2CO_3, Cs_2CO_3, NH_4OH, I_2 and TBAB) were purchased from Sigma-Aldrich and AK Scientific and used without further purification. Palladium catalysts: $Pd(OAc)_2$ (purchased from STREM) and $PdCl_2$ (purchased from AK Scientific) were stored under argon gas in a desiccator at room temperature. All solvents purchased from Fisher ACP chemicals and Sigma-Aldrich as ACS grade. Dimethylacetamide (DMA) was dried using activated 3 Å molecular sieves and stored in an oven-dried Schlenk flask under argon gas. Distilled water was obtained from an in-house distillery. Compounds were purified using column chromatography on silica gel (SiliCycle® SiliaFlash® F60, 40 – 63 μm, 60Å) and/or preparative thin-layer chromatography (PTLC) when noted (SiliCycle® TLC Plates, Glass-Backed, Silica, Hard Layer, 250 μm, 20 x 20 cm). Microwave-assisted reactions were carried out using the Biotage Initiator^{TM} + (400 W magnetron) with oven-dried 0.5 – 2.0 mL and 10 – 20 mL microwave vials respectively. ^1H and ^{13}C NMR data were measured on a Varian VNMRS-500. High resolution mass spectrometry (HRMS) data was collected using a LC-TOF ESI mass spectrometer operated in positive ion mode. ^1H NMR yields were taken with trimethoxybenzene (TMB) as an internal standard. Absorbance data was collected using an Agilent Cary 5000 Series UV-Vis-NIR Spectrophotometer and baseline was corrected for absorbance data; samples were measured with $CHCl_3$ as the solvent and as the blank/baseline correction in quartz cuvettes. Photoluminescent data was collected using a Horiba PTI QuantaMaster 8075 Spectrofluorometer. Photoluminescence measurements were done by exciting the diluted analytes according to their maximum absorbance wavelengths collected from the absorbance measurements with an integration time of 0.5 s, step size of 2 nm, slits of 1 nm, with an automatic 5 second dark background collection. All samples were diluted to [2 x 10^{-7} M] in $CHCl_3$. Photoluminescent

quantum yield (PLQY) measurements were taken with an integrating sphere (Horiba K-Sphere Petit) and all measurements were done with a pair of matching quartz cuvettes, the blank was measured with $CHCl_3$ and the samples were diluted in $CHCl_3$ as indicated previously.

5.2 Atom Economy and E-factor Calculations

Simple *Atom Economy* and *E-factor* values were calculated following guidelines from literature.[107]

Calculation of *Atom Economy* only considered the molecular weight of starting reagents and product. Solvents, additional reagents, catalysts, and ligands were not considered in calculations. All calculated reactions (aside from the Suzuki cross-coupling of 5-bromofurfural in this thesis) are treated like a double reaction. Where 2A + B → C. Equation 1 is used to calculate each value.

$$\boldsymbol{Atom\ Economy = \frac{molecular\ mass\ of\ desired\ product}{molecular\ mass\ of\ starting\ reactants}\ x\ 100\%} \qquad \textbf{(1)}$$

Equation 2 is used to calculate *E-factor*, where mass of reagents, 10% of reaction solvent and product are considered for the value.

$$\boldsymbol{E - Factor = \frac{\Sigma mass\ of\ (starting\ materials) + \Sigma mass(0.1(solvent)) - \Sigma mass(product)}{\Sigma mass\ of\ product}} \qquad \textbf{(2)}$$

Double Stille Cross-Coupling Calculations from Kazantsev *et al.* (11.7 mmol scale**)**[54]

Reagents: 2-tri(butyl)stannylfurane (**37**) = 357.1 g/mol (10.0 g)

1,4-dibromobenzene (**38**) = 235.9 g/mol (2.87 g)

Solvent: 20 mL of Toluene (Density = 0.867 g/mL)

Product: Furan-phenylene-furan core (**39**) = 210.2 g/mol (1.53 g, 62% yield)

$$\boldsymbol{Atom\ Economy = \frac{210.2}{2(357.1) + 235.91}\ x\ 100\%}$$

$$\boldsymbol{Atom\ Economy = 22.1\ \%}$$

$$\boldsymbol{E - Factor = \frac{(10.0g + 2.87g) + \left(0.1x20mLx\frac{0.867g}{mL}\right) - 1.53g}{1.53\ g}}$$

$$\boldsymbol{E - Factor = 8.5}$$

Double Suzuki Cross-Coupling Calculations from Kazantsev *et al.* (1.0 mmol scale**)**[54]

Reagents: 1,4-bis(5-bromofuran-2-yl)benzene (**40**) = 368 g/mol (0.368 g)

Phenylboronic acid (**41**) = 121.9 g/mol (0.299 g)

Solvent: 25 mL of DMF (Density = 0.944 g/mL)

Product: 1,4-bis(5-phenylfuran-2-yl)benzene (**42**) = 362.4 g/mol (0.115 g, 39% yield)

$$\boldsymbol{Atom\ Economy = \frac{362.4}{2(121.9) + 368}\ x\ 100\%}$$

$$\boldsymbol{Atom\ Economy = \ 59.2\ \%}$$

$$\boldsymbol{E - Factor = \frac{(0.368\ g + 0.299\ g) + \left(0.1 x 25 mL x \frac{0.944 g}{mL}\right) - 0.115 g}{0.115\ g}}$$

$$\boldsymbol{E - Factor = 26.3}$$

Double Decarboxylative Cross-Coupling Calculations from this work (1.0 mmol scale**)**

Reagents: 5-phenylfuran-2-carboxylic acid (**140**) = 188.1 g/mol (0.413 g)

1,4-dibromobenzene (**38**) = 235.9 g/mol (0.236 g)

Solvent: 10 mL of DMA (Density = 0.940 g/mL)

Product: 1,4-bis(5-phenylfuran-2-yl)benzene (**42**) = 362.4 g/mol (0.199 g, 55% yield)

$$\boldsymbol{Atom\ Economy = \frac{362.4}{2(188.1) + 235.9}\ x\ 100\%}$$

$$\boldsymbol{Atom\ Economy = 59.2\ \%}$$

$$\boldsymbol{E - Factor = \frac{(0.413\ g + 0.236\ g) + \left(0.1 x 10 mL x \frac{0.940 g}{mL}\right) - 0.199 g}{0.199\ g}}$$

$$\boldsymbol{E - Factor = 7.0}$$

Suzuki Cross-Coupling Calculations from this work. (8.0 mmol scale**)**

Reagents: 5-bromofurfural (**33**) = 175 g/mol (1.40 g)

Phenylboronic acid (**41**) = 121.9 g/mol (1.17 g)

Solvent: 4 mL of H_2O (Density = 1.0 g/mL)

Product: 5-phenylfuran-2-carbaldehyde (**122**) = 172.2 g/mol (1.28 g, 93% yield)

$$\boldsymbol{Atom\ Economy = \frac{172.2}{175 + 121.9}\ x\ 100\%}$$

$$\boldsymbol{Atom\ Economy = \ 58.0\ \%}$$

$$\boldsymbol{E - Factor = \frac{(1.40\ g + 1.17\ g) + \left(0.1x4mLx\frac{1.0g}{mL}\right) - 1.28\ g}{1.28\ g}}$$

$$\boldsymbol{E - Factor = 1.3}$$

Note! This last *E-factor* calculation did not take TBAB into account. If TBAB is taken into consideration the following calculation is shown as followed:

Additional Reagents*:* TBAB = 322.4 g/mol (2.58 g, 8 mmol)

$$\boldsymbol{E - Factor = \frac{(1.40\ g + 1.17\ g + 2.58) + \left(0.1x4mLx\frac{1.0g}{mL}\right) - 1.28\ g}{1.28\ g}}$$

$$\boldsymbol{E - Factor = 3.3}$$

TBAB Suzuki Cross-Coupling Calculations from this work. (0.2 mmol scale, *ignoring water***)**

At 0.1 equiv. TBAB (0.02 mmol scale**):**

Reagents: 5-bromofurfural (**33**) = 175 g/mol (34.99 mg)

Phenylboronic acid (**41**) = 121.9 g/mol (29.26 mg)

TBAB at **0.1 equiv**. = 322.37 g/mol (6.45 mg)

Product: 5-phenylfuran-2-carbaldehyde (**122**) = 172.2 g/mol (28.58 mg, 83% yield)

$$\boldsymbol{E - Factor = \frac{(34.99\ mg + 29.26\ mg + 6.45\ mg) - 28.58\ mg}{28.58\ mg}}$$

$$\boldsymbol{E - Factor = 1.5}$$

At 0.5 equiv. TBAB (0.1 mmol scale**):**

Reagents: 5-bromofurfural (**33**) = 175 g/mol (34.99 mg)

Phenylboronic acid (**41**) = 121.9 g/mol (29.26 mg)

TBAB at **0.5 equiv**. = 322.37 g/mol (32.24 mg)

Product: 5-phenylfuran-2-carbaldehyde (**122**) = 172.2 g/mol (34.44 mg, 99% yield)

$$\boldsymbol{E - Factor = \frac{(34.99\,mg + 29.26\,mg + 32.24\,mg) - 34.44\,mg}{34.44\,mg}}$$

$$\boldsymbol{E - Factor = 1.8}$$

At 1.0 equiv. TBAB (0.2 mmol scale**):**

Reagents: 5-bromofurfural (**33**) = 175 g/mol (34.99 mg)

Phenylboronic acid (**41**) = 121.9 g/mol (29.26 mg)

TBAB at **1.0 equiv**. = 322.37 g/mol (64.47 mg)

Product: 5-phenylfuran-2-carbaldehyde (**122**) = 172.2 g/mol (34.44 mg, 99% yield)

$$\boldsymbol{E - Factor = \frac{(34.99\,mg + 29.26\,mg + 64.47\,mg) - 34.44\,mg}{34.44\,mg}}$$

$$\boldsymbol{E - Factor = 2.7}$$

5.3 Experimental Procedures and Characterization of Compounds

Experimental Procedures:

Procedure 1: Suzuki cross-coupling with methyl 5-bromofuran-2-carboxylate (99) as a starting material.

To a 50 mL round bottom flask that is open to air, methyl 5-bromofuran-2-carboxylate (**99**) (1 equiv.), aryl boronic acid (1.5 equiv.), potassium carbonate (2 equiv.) was added. A 4:1 MeOH:H_2O [0.1 M] solution was then added to the reaction flask, the reaction was stirred and heated to 40 °C on a silicon oil bath. $PdCl_2$ (5 mol%) was added to the reaction vessel. After 10 minutes, the reaction is complete. To ensure completion the reaction was tracked by TLC. Once complete, the reaction was left to cool to room temperature and transferred to a separatory funnel. To the separatory funnel, 30 mL of H_2O and 30 mL of EtOAc are added. The aqueous layer was extracted two more times with 20 mL EtOAc. The combined organic layer was washed with brine

three times, dried with sodium sulphate and the solvent was evaporated under reduced pressure. The crude compound is purified by gravity column chromatography (95:5 hexanes/EtOAc).

Procedure 2: Selective 4-position bromination of 5-mono-arylated-2-methylester-furan.

To a flame-dried 25 mL round bottom flask that is closed to air, mono-arylated furan (1 equiv.), $ZnCl_2$ (1 equiv.), activated 4Å sieves (0.2 – 0.3 g) and $CHCl_3$ [0.1 M] was added. The reaction is stirred and heated to 40 °C on a silicon oil bath. Br_2 (1.5 equiv.) was then added to the solution. The reaction was tracked by TLC until completion. Once complete, the reaction was left to cool to room temperature, quenched with sodium thiosulfate solution and transferred to a separatory funnel. To the separatory funnel, 30 mL of H_2O and 30 mL of EtOAc are added. The aqueous layer was extracted two more times with 20 mL EtOAc. The combined organic layer was washed with brine three times, dried with sodium sulphate and the solvent was evaporated under reduced pressure. The crude compound is purified by gravity column chromatography (95:5 hexanes/EtOAc).

Procedure 3: Selective 3-position iodination of 5-mono-arylated-2-methylester-furan.

To a flame-dried 25 mL round bottom flask under argon, mono-arylated furan (1 equiv.) was added. The flask was then placed in an ethylene glycol bath with dry ice (-20 °C). A solution of 1M TMPMgCl•LiCl (2 equiv.) is added dropwise. The solution is left to stir for 30 minutes. Afterwards, crushed I_2 pellets (3 equiv.) were quickly added to the flask (the flask is resealed under argon) and left to stir for an additional 1.5 hours. The reaction was then removed from the bath and allowed to warm up back to room temperature. Once complete, the reaction was quenched with MeOH, then sodium thiosulfate solution and transferred to a separatory funnel. To the separatory funnel, 30 mL of H_2O and 30 mL of EtOAc are added. The aqueous layer was extracted two more times with 20 mL EtOAc. The combined organic layer was washed with brine three times, dried with sodium sulphate and the solvent was evaporated under reduced pressure. The crude mixture contains both starting material and iodinated product. Efforts have been made to separate both compounds through gravity column chromatography, however, attempts were never successful. Instead, crude mixture was used in next Suzuki-Miyaura cross coupling step immediately.

Procedure 4: Second Suzuki cross-coupling on newly halogenated furans.

To a 50 mL round bottom flask that is open to air, newly made halogenated furan (1 equiv.), aryl boronic acid (1.5 – 1.85 equiv.), potassium carbonate (2 equiv.) was added. A 3:1 or 4:1 MeOH:H_2O [0.05 M] solution was then added to the reaction flask, the reaction was stirred and heated to 50 °C in a silicon oil bath. $PdCl_2$ (10 mol%) was added to the reaction vessel. To ensure completion the reaction was tracked by TLC. Once complete, the reaction was left to cool to room temperature and transferred to a separatory funnel. To the separatory funnel, 30 mL of H_2O and 30 mL of EtOAc are added. The aqueous layer was extracted two more times with 20 mL EtOAc. The combined organic layer was washed with brine three times, dried with sodium sulphate and the solvent was evaporated under reduced pressure. The crude compound is purified by gravity column chromatography (95:5 hexanes/EtOAc).

Procedure 5: Hydrolysis followed by double decarboxylative cross-coupling of multi-arylated furans.

To a 10 mL round bottom flask, arylated furan ester (1 equiv.), potassium hydroxide (10 equiv.) and MeOH [0.1 M] were added. The reaction was heated in a silicon oil bath under reflux for 30 minutes (confirmed by TLC). The reaction was then cooled to room temperature and acidified with concentrated HCl (in an ice bath) until a pH of 2. The newly acidic solution was transferred to a separatory funnel. To the separatory funnel, 30 mL of H_2O and 30 mL of EtOAc are added. The aqueous layer was extracted two more times with 20 mL EtOAc. The combined organic layer was washed with brine three times, dried with sodium sulphate and the solvent was evaporated under reduced pressure to produce the carboxylic acid (white solid).

The white solid is then directly used in the following reaction. To an oven-dried 0.5–2 mL conical microwave vial, newly made carboxylic acid (3 equiv.), 2,5-dibromothiophene (1 equiv.), Cs_2CO_3 (1.5 equiv.) and $Pd(P\mathit{t}Bu_3)_2$ (5 mol%) was added. Anhydrous DMF ([0.1 M] of the dibromothiophene) was added to the vial. The vial is sealed with a rubber septum and aluminum cap, pre-stirred for 45 seconds at room temperature and reacted in a Biotage® Initiator+ microwave at 170 °C for 10 minutes on the high absorption setting. The crude mixture was cooled to room temperature and passed through a small silica plug and washed with EtOAc. The filtrate was evaporated under reduced pressure and purified by preparative TLC.

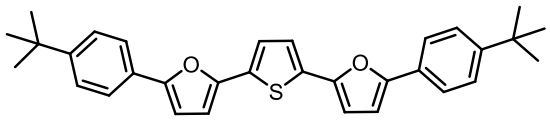

109

(109) - **2,5-bis(5-(4-(tert-butyl)phenyl)furan-2-yl)thiophene:** 0.1 mmol scale, yellow solid (27.3 mg, 57 % yield); purified by preparative TLC (silica gel) in 2:1 hexanes/chloroform; ^{1}H NMR (500 MHz, Chloroform-d): δ 7.67 (d, *J* = 8.3 Hz, 4H), 7.44 (d, *J* = 8.5 Hz, 4H), 7.24 (s, 2H), 6.67 (d, *J* = 3.4 Hz, 2H), 6.60 (d, *J* = 3.4 Hz, 2H), 1.35 (s, 18H); ^{13}C NMR (500 MHz, Chloroform-d): δ 153.36, 150.64, 148.41, 132.16, 127.75, 125.68, 123.59, 122.92, 107.46, 106.79, 34.70, 31.30; HRMS (ESI) m/z: $[M]^+$ cacld for $C_{32}H_{32}O_2S$: 480.2118; Found 480.2116.

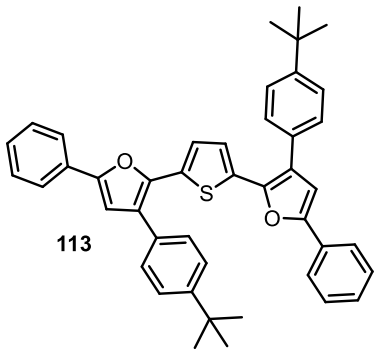

113

(113) - **2,5-bis(3-(4-(tert-butyl)phenyl)-5-phenylfuran-2-yl)thiophene:** 0.1 mmol scale, bright yellow solid (29.2 mg, 47 % yield); purified by preparative TLC (silica gel) in 92:8 hexanes/chloroform, after isolation, solid is washed with cold methanol to afford bright yellow solid; ^{1}H NMR (500 MHz, Chloroform-d): δ 7.73 (m, 4H), 7.48 – 7.44 (m, 8H), 7.40 (t, *J* = 7.7 Hz, 4H), 7.28 (t, *J* = 7.4 Hz, 2H), 7.09 (s, 2H), 6.78 (s, 2H), 1.38 (s, 18H); ^{13}C NMR (500 MHz, Chloroform-d): δ 152.28, 150.76, 143.78, 130.50, 128.76, 128.47, 127.59, 125.63, 123.89, 123.80, 109.65, 34.72, 31.41; HRMS (ESI) m/z: $[M]^+$ cacld for $C_{44}H_{40}O_2S$: 632.2744; Found 632.2741.

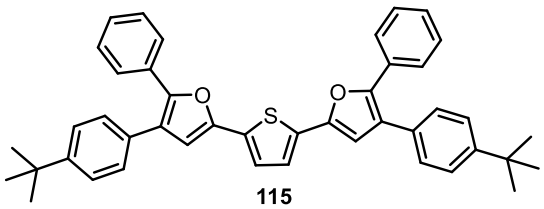

115

(115) - **2,5-bis(3-(4-(tert-butyl)phenyl)-5-phenylfuran-2-yl)thiophene:** 0.1 mmol scale, bright yellow solid (29.1 mg, 46 % yield); purified by preparative TLC (silica gel) in 92:8

hexanes/chloroform, after isolation, solid is washed with cold methanol to afford bright yellow solid; ^{1}H NMR (500 MHz, Chloroform-d): δ 7.64 (dd, *J* = 8.4, 1.2 Hz, 4H), 7.41 (s, 8H), 7.33 (t, *J* = 7.5 Hz, 4H), 7.28 – 7.25 (m, 4H), 6.70 (s, 2H), 1.38 (s, 18H); ^{13}C NMR (500 MHz, Chloroform-d): δ 150.42, 147.83, 147.53, 132.11, 130.93, 130.84, 128.40, 128.24, 127.51, 126.13, 125.60, 124.55, 123.31, 109.78, 34.63, 31.37; HRMS (ESI) m/z: $[M]^+$ cacld for $C_{44}H_{40}O_2S$: 632.2744; Found 632.2740.

Procedure 6: Suzuki cross-coupling with 5-bromofurfural (33) as a starting material.

To a 25 mL round bottom flask equipped with a stir bar; 5-bromofurfural (**33**) (2 mmol, 350 mg) corresponding aryl boronic acid (2.4 mmol, 1.2 equiv.), K_2CO_3 (5 mmol, 695 mg), TBAB (2 mmol, 690 mg) and $Pd(OAc)_2$ (0.04 mmol, 8.96 mg) are added. Water [0.5 M] is then added and the solution is stirred vigorously for 18 hours open to atmosphere. Additional water (1 – 2 mL) can be added if reagents get stuck on sides of glassware (with no ill effect towards the reaction). Completion of reaction was determined by TLC (add 0.5 mL of EtOAc into reaction, use this to spot for TLC), product spot is often seen below 5-bromofurfural starting material. Once complete, the solution is transferred to a separatory funnel. 15 mL of water and 20 mL of EtOAc are added. The aqueous layer is extracted twice more with 20 mL EtOAc, all organics are pooled, washed with brine (three times, 20 mL each), dried with sodium sulfate and the solvent is evaporated under reduced pressure. The crude is then purified by gravity column chromatography (silica gel in its respected mobile solvent) to produce the corresponding aldehydes. Each product was sealed with aluminum foil and stored in a freezer under argon gas for long term storage.

*Keep note! Before transferring the reaction into a separatory funnel. The crude solution can be passed through a celite plug to remove insoluble by-products and be washed with EtOAc before liquid-liquid extraction. This is especially favoured for larger-scale reactions.

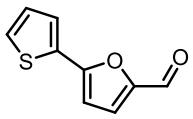

119

(119) - 5-(thiophen-2-yl)furan-2-carbaldehyde: 10 mmol scale, orange oil (1708.8 mg, 96 % yield); purified by gravity column chromatography (silica gel) in 9:1 hexanes/ethyl acetate; R_f =

0.12; ^{1}H NMR (500 MHz, Chloroform-d): δ 9.59 (s, 1H), 7.51 (d, *J* = 3.7 Hz, 1H), 7.39 (d, *J* = 5.0 Hz, 1H), 7.27 (d, *J* = 3.7 Hz, 1H), 7.09 (dd, *J* = 4.9, 3.7 Hz 1H), 6.66 (d, *J* = 3.8 Hz, 1H); ^{13}C NMR (500 MHz, Chloroform-d): δ 176.88, 154.88, 151.49, 131.66, 128.18, 127.52, 126.26, 107.51; HRMS (ESI) m/z: $[M+H]^+$ cacld for $C_9H_6O_2S$: 179.0161; Found 179.0161.

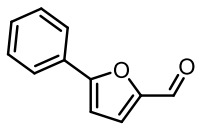

122

(122) - 5-phenylfuran-2-carbaldehyde: 8 mmol scale, yellow oil (1285.4 mg, 93 % yield); solidifies as a light orange solid after leaving in freezer overnight; purified by gravity column chromatography (silica gel) in 9:1 hexanes/ethyl acetate; R_f = 0.13; ^{1}H NMR (500 MHz, Chloroform-d): δ 9.65 (s, 1H), 7.83 (m, 2H), 7.44 (m, 2H), 7.39 (m, 1H), 7.32 (d, *J* = 3.7 Hz, 1H), 6.85 (d, *J* = 3.7 Hz, 1H); ^{13}C NMR (500 MHz, Chloroform-d): δ 177.24, 159.43, 152.05, 129.70, 128.98, 128.96, 125.30, 107.68; HRMS (ESI) m/z: $[M+H]^+$ cacld for $C_{11}H_8O_2$: 173.0597; Found 173.0598.

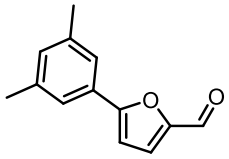

123

(123) - 5-(3,5-dimethylphenyl)furan-2-carbaldehyde: 2 mmol scale, light orange solid (368 mg, 92 % yield); purified by gravity column chromatography (silica gel) in 9:1 hexanes/ethyl acetate; R_f = 0.15; ^{1}H NMR (500 MHz, Chloroform-d): δ 9.63 (s, 1H), 7.45 (s, 2H), 7.31 (d, *J* = 3.7 Hz, 1H), 7.03 (s, 1H), 6.81 (d, *J* = 3.7 Hz, 1H), 2.36 (s, 6H); ^{13}C NMR (500 MHz, Chloroform-d): δ 177.11, 159.95, 151.86, 138.60, 131.53, 128.78, 123.14, 107.48, 21.25; HRMS (ESI) m/z: $[M+H]^+$ cacld for $C_{13}H_{12}O_2$: 201.0910; Found 201.0909.

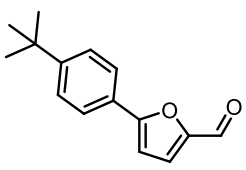

124

(124) - 5-(4-(*tert*-butyl)phenyl)furan-2-carbaldehyde: 4 mmol scale, yellow/orange oil (843.3 mg, 92 % yield); solidifies as a yellow solid after leaving in freezer overnight; purified by gravity column chromatography (silica gel) in 9:1 hexanes/ethyl acetate; R_f = 0.13; ^{1}H NMR (500 MHz,

Chloroform-d): δ 9.63 (s, 1H), 7.76 (m, 2H), 7.47 (m, 2H), 7.31 (d, *J* = 3.7 Hz, 1H), 6.80 (d, *J* = 3.7 Hz, 1H), 1.34 (s, 9H); ^{13}C NMR (500 MHz, Chloroform-d): δ 177.11, 159.78, 153.18, 151.87, 126.23, 125.91, 125.15, 107.20, 34.87, 31.15; HRMS (ESI) m/z: $[M+H]^+$ cacld for $C_{15}H_{16}O_2$: 229.1223; Found 229.1221.

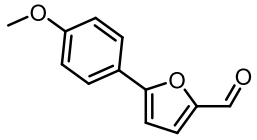

125

(125) - 5-(4-methoxyphenyl)furan-2-carbaldehyde: 3 mmol scale, yellow oil (606 mg, 99 % yield); solidifies as a yellow solid after leaving in freezer overnight; purified by gravity column chromatography (silica gel) in 4:1 hexanes/ethyl acetate; R_f = 0.10; ^{1}H NMR (500 MHz, Chloroform-d): δ 9.56 (s, 1H), 7.73 (d, *J* = 8.9 Hz, 2H), 7.27 (d, *J* = 3.7 Hz, 1H), 6.93 (d, *J* = 9.0 Hz, 2H), 6.68 (d, *J* = 3.7 Hz, 1H), 3.82 (s, 3H); ^{13}C NMR (500 MHz, Chloroform-d): δ 176.80, 160.86, 159.79, 151.58, 126.95, 121.75, 114.40, 106.31, 55.37; HRMS (ESI) m/z: $[M+H]^+$ cacld for $C_{12}H_{10}O_3$: 203.0703; Found 203.0702.

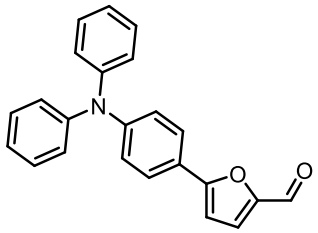

126

(126) - 5-(4-(diphenylamino)phenyl)furan-2-carbaldehyde: 1.5 mmol scale, orange oil (532.1 mg, 76 % yield); purified by gravity column chromatography (silica gel) in 1:1 hexanes/dichloromethane; R_f = 0.09; ^{1}H NMR (500 MHz, Chloroform-d): δ 9.58 (s, 1H), 7.67 (m, 2H), 7.31 – 7.28 (m, 5H), 7.14 – 7.07 (m, 8H), 6.71 (d, *J* = 3.8 Hz, 1H); ^{13}C NMR (500 MHz, Chloroform-d): δ 176.72, 159.82, 151.61, 149.28, 146.95, 129.53, 126.42, 125.26, 123.96, 122.08, 122.05, 106.49; HRMS (ESI) m/z: $[M+H]^+$ cacld for $C_{23}H_{17}NO_2$: 340.1332; Found 340.1329.

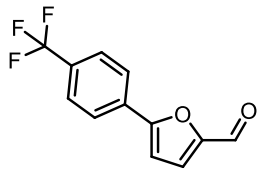

127

(127) - 5-(4-(trifluoromethyl)phenyl)furan-2-carbaldehyde: 5.78 mmol scale, white solid (996.9 mg, 72 % yield); purified by gravity column chromatography (silica gel) in 9:1 hexanes/ethyl acetate; R_f = 0.06; ^{1}H NMR (500 MHz, Chloroform-d): δ 9.70 (s, 1H), 7.93 (d, *J* = 8.2 Hz, 2H), 7.70 (d, *J* = 8.2 Hz, 2H), 7.35 (d, *J* = 3.7 Hz, 1H), 6.95 (d, *J* = 3.7 Hz, 1H); ^{13}C NMR (500 MHz, Chloroform-d): δ 177.44, 157.40, 152.58, 132.14, 131.31, 131.05, 126.03 – 125.93 (q, J_{CF} = 3.8 Hz), 125.40, 124.88, 122.71, 109.22; HRMS (ESI) m/z: $[M+H]^+$ cacld for $C_{12}H_7F_3O_2$: 241.0471; Found 241.0472.

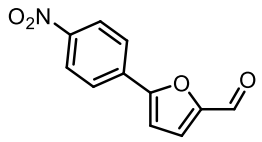

128

(128) - 5-(4-nitrophenyl)furan-2-carbaldehyde: Reaction performed at 95 °C for 1 hour in H_2O [0.25 M]: 1 mmol scale, light yellow solid (97.7 mg, 45 % yield); purified by gravity column chromatography (silica gel) in chloroform; R_f = 0.39; ^{1}H NMR (500 MHz, Chloroform-d): δ 9.73 (s, 1H), 8.32 (m, 2H), 7.99 (m, 2H), 7.37 (d, *J* = 3.8 Hz, 1H), 7.05 (d, *J* = 3.8 Hz, 1H); ^{13}C NMR (500 MHz, Chloroform-d): δ 177.54, 156.28, 153.06, 147.95, 134.56, 125.76, 124.42, 122.72, 110.63; HRMS (ESI) m/z: $[M+H]^+$ cacld for $C_{11}H_7NO_4$: 218.0448; Found 218.0448.

Procedure 7: **Aldehyde to nitrile conversion of mono-arylated furans.**

To a 50 mL round bottom flask equipped with a stir bar; corresponding furan aldehyde (2 mmol) is dissolved in 1-part ammonia water and 1-part THF, producing a 1:1 NH_4OH:THF [0.1 M] solution. The solution is left to stir for 5 minutes and is followed by the addition of freshly crushed iodine (2.2 mmol). The dark solution is left to stir vigorously (closed to the atmosphere) for 2 hours and is tracked by TLC. With time, the dark solution becomes lighter to indicate the reaction is close to completion. If starting aldehyde is still observed by TLC, additional ammonia water solution (1 – 3 mL) and iodine (0.2 – 0.3 mmol) can be added until the reaction is complete. Completion of the reaction was determined by TLC. The product spot is seen above starting

aldehyde. Once complete, reaction is quenched with aqueous sodium thiosulfate (5 – 10 mL) and transferred to a separatory funnel. 15 mL of water and 20 mL of EtOAc are added. The aqueous layer is extracted twice more with 20 mL EtOAc, all organics are pooled, washed with brine (three times, 20 mL each), dried with sodium sulfate and the solvent is evaporated under reduced pressure. The crude is then purified by gravity column chromatography (silica gel in its respected mobile solvent) to produce the desired nitrile. Each product was sealed with aluminum foil and stored in a freezer under argon gas for long term storage.

CAUTION: Iodine is known to react with ammonia to potentially produce nitrogen triiodide monoamine an explosive black powder. However, this was not observed during these experiments. It is crucial to quench the reaction with aqueous sodium thiosulfate when complete and one should avoid a heavy excess in reagents.[101]

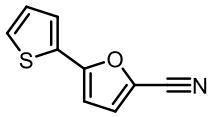

131

(131) - 5-(thiophen-2-yl)furan-2-carbonitrile: Reaction for 3 hours, 2 mmol scale, yellow crystal (308.3 mg, 94 % yield); purified by gravity column chromatography (silica gel) in 6:1 hexanes/ethyl acetate; R_f = 0.46; ^{1}H NMR (500 MHz, Chloroform-d): δ 7.42 (dd, *J* = 3.7, 1.2 Hz, 1H), 7.38 (dd, *J* = 5.1, 1.1 Hz, 1H), 7.14 (d, *J* = 3.7 Hz, 1H), 7.10 (dd, *J* = 5.0, 3.7 Hz**,** 1H), 6.56 (d, *J* = 3.7 Hz, 1H); ^{13}C NMR (500 MHz, Chloroform-d): δ 154.01, 131.24, 128.08, 127.06, 125.69, 124.58, 124.01, 111.75, 105.74; HRMS (ESI) m/z: $[M]^+$ cacld for C_9H_5NOS: 175.0086; Found 175.0085.

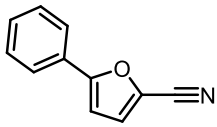

132

(132) - 5-phenylfuran-2-carbonitrile: Reaction for 4.5 hours, 2 mmol scale, white solid (326 mg, 96 % yield); purified by gravity column chromatography (silica gel) in 6:1 hexanes/ethyl acetate; R_f = 0.47; ^{1}H NMR (500 MHz, Chloroform-d): δ 7.72 (m, 2H), 7.44 (m, 2H), 7.39 (m, 1H), 7.17 (d, *J* = 3.7 Hz, 1H), 6.73 (d, *J* = 3.6 Hz, 1H); ^{13}C NMR (500 MHz, Chloroform-d): δ 158.65, 129.54, 129.01, 128.68, 125.09, 124.84, 123.98, 111.94, 106.03; HRMS (ESI) m/z: $[M]^+$ cacld for $C_{11}H_7NO$: 169.0522; Found 169.0524.

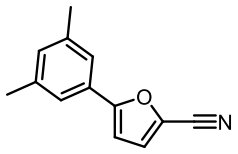

133

(133) - 5-(3,5-dimethylphenyl)furan-2-carbonitrile: Reaction for 4.5 hours, 2 mmol scale, pale orange solid (338.4 mg, 86 % yield); purified by gravity column chromatography (silica gel) in 6:1 hexanes/ethyl acetate; $R_f = 0.50$; ^{1}H NMR (500 MHz, Chloroform-d): δ 7.34 (s, 2H), 7.15 (d, J = 3.7 Hz, 1H), 7.03 (s, 1H), 6.68 (d, J = 3.7 Hz, 1H), 2.37 (s, 6H); ^{13}C NMR (500 MHz, Chloroform-d): δ 159.07, 138.65, 131.30, 128.54, 124.83, 123.92, 122.67, 112.03, 105.76, 21.28; HRMS (ESI) m/z: $[M]^+$ cacld for $C_{13}H_{11}NO$: 197.0835; Found 197.0834.

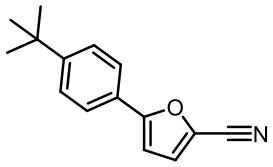

134

(134) - 5-(4-(*tert*-butyl)phenyl)furan-2-carbonitrile: Reaction for 4.5 hours, 2 mmol scale, white/light orange solid (427 mg, 95 % yield); purified by gravity column chromatography (silica gel) in 6:1 hexanes/ethyl acetate; $R_f = 0.49$; ^{1}H NMR (500 MHz, Chloroform-d): δ 7.66 (m, 2H), 7.47 (m, 2H), 7.16 (d, J = 3.7 Hz, 1H), 6.68 (d, J = 3.7 Hz, 1H), 1.35 (s, 9H); ^{13}C NMR (500 MHz, Chloroform-d): δ 158.92, 152.96, 126.00, 125.95, 124.78, 124.68, 124.00, 112.09, 105.43, 34.85, 31.15; HRMS (ESI) m/z: $[M]^+$ cacld for $C_{15}H_{15}NO$: 225.1148; Found 225.1147.

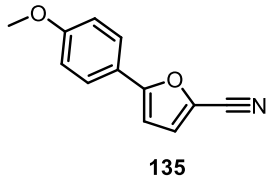

135

(135) - 5-(4-methoxyphenyl)furan-2-carbonitrile: Reaction for 9 hours, 2 mmol scale, light pink solid (357.6 mg, 93 % yield); purified by gravity column chromatography (silica gel) in 4:1 hexanes/ethyl acetate; $R_f = 0.25$; ^{1}H NMR (500 MHz, Chloroform-d): δ 7.66 (m, 2H), 7.14 (d, J = 3.7 Hz, 1H), 6.96 (m, 2H), 6.58 (d, J = 3.7 Hz, 1H), 3.85 (s, 3H); ^{13}C NMR (500 MHz, Chloroform-

d): δ 160.64, 158.83, 126.45, 124.41, 124.12, 121.65, 114.43, 112.18, 104.47, 55.40; HRMS (ESI) m/z: $[M]^+$ cacld for $C_{12}H_9NO_2$: 199.0628; Found 199.0623.

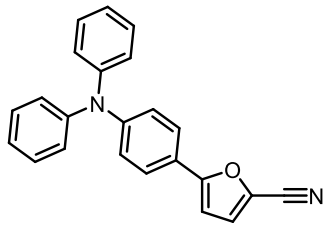

136

(136) - 5-(4-(diphenylamino)phenyl)furan-2-carbonitrile: Reaction for 24 hours, 1.5 mmol scale, dark oil (301.4 mg, 84 % yield); purified by gravity column chromatography (silica gel) in 6:2:1 hexanes/dichloromethane/ethyl acetate; R_f = 0.47; ^{1}H NMR (500 MHz, Chloroform-d): δ 7.56 (m, 2H), 7.30 (m, 4H), 7.14 – 7.07 (m, 9H), 6.58 (d, *J* = 3.8 Hz, 1H); ^{13}C NMR (500 MHz, Chloroform-d): δ 158.87, 149.07, 146.98, 129.49, 125.87, 125.18, 124.36, 124.16, 123.88, 122.21, 121.94, 112.25, 104.56; HRMS (ESI) m/z: $[M]^+$ cacld for $C_{23}H_{16}N_2O$: 336.1257; Found 336.1255.

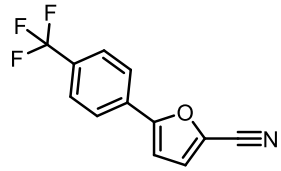

137

(137) - 5-(4-(trifluoromethyl)phenyl)furan-2-carbonitrile: Reaction for 4 hours, 2 mmol scale, pale beige solid (443.1 mg, 94 % yield); purified by gravity column chromatography (silica gel) in 6:1 hexanes/ethyl acetate; R_f = 0.36; ^{1}H NMR (500 MHz, Chloroform-d): δ 7.84 (d, *J* = 8.0 Hz, 2H), 7.71 (d, *J* = 8.2 Hz, 2H), 7.21 (d, *J* = 3.7 Hz, 1H), 6.86 (d, *J* = 3.7 Hz, 1H); ^{13}C NMR (500 MHz, Chloroform-d): δ 156.85, 131.70, 131.28, 131.02, 126.10 – 126.02 (q, J_{CF} = 3.8 Hz), 125.01, 124.83, 123.87, 122.67, 111.45, 107.75; HRMS (ESI) m/z: $[M]^+$ cacld for $C_{12}H_6F_3NO$: 237.0396; Found 237.0396.

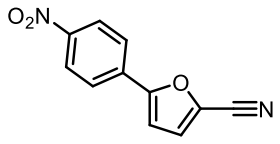

138

(138) - 5-(4-nitrophenyl)furan-2-carbonitrile: Reaction for 4 hours, 0.23 mmol scale, white solid (49.3 mg, 99 % yield); purified by gravity column chromatography (silica gel) in 4:1

hexanes/ethyl acetate; R_f = 0.14; ^{1}H NMR (500 MHz, Chloroform-d): δ 8.32 (m, 2H), 7.89 (m, 2H), 7.24 (d, *J* = 3.7 Hz, 1H), 6.96 (d, *J* = 3.7 Hz, 1H); ^{13}C NMR (500 MHz, Chloroform-d): δ 155.87, 147.90, 134.00, 126.90, 125.40, 124.50, 123.93, 111.15, 109.25; HRMS (ESI) m/z: $[M]^+$ cacld for $C_{11}H_6N_2O_3$: 214.0373; Found 214.0371.

Procedure 8: **Nitrile hydrolysis to carboxylic acids of mono-arylated furans.**

To a 25 mL round bottom flask equipped with a stir bar; corresponding furan nitrile (1 mmol), KOH pellets (10 mmol, 560 mg) and 1:1 solution of H_2O:MeOH [0.1 M] are added. A reflux condenser is attached, and the reaction is gently refluxed in a silicon oil bath for 18 hours. The reaction is then cooled to room temperature and MeOH is evaporated under reduced pressure. The remaining aqueous solution is acidified with concentrated HCl slowly until pH of 2 is observed. The acidic solution is transferred to a separatory funnel. Where 10 mL of water and 20 mL of DCM are added. The aqueous layer is extracted twice more with 20 mL DCM, all organics are pooled, washed with brine (three times, 20 mL each), dried with sodium sulfate and the solvent is evaporated under reduced pressure. The resulting solid requires no further purification and is dried in a high vacuum chamber away from light.

Note: EtOAc could be used as organic solvent in workup, however, formation of acetic acid is possible to exist in sample, as seen with product **145**.

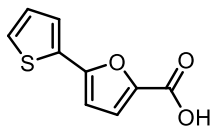

139

(139) - 5-(thiophen-2-yl)furan-2-carboxylic acid: 1 mmol scale, white solid (131.8 mg, 91 % yield); ^{1}H NMR (500 MHz, Dimethyl sulfoxide-d): δ 7.67 (d, *J* = 5.0 Hz, 1H), 7.56 (d, *J* = 4.9 Hz, 1H), 7.30 (d, *J* = 3.6 Hz, 1H), 7.17 (m, 1H), 6.94 (d, *J* = 3.6 Hz, 1H); ^{13}C NMR (500 MHz, Dimethyl sulfoxide -d): δ 159.56, 152.45, 144.01, 131.94, 128.89, 127.82, 125.94, 120.43, 107.78; HRMS (ESI) m/z: $[M+H]^+$ cacld for $C_9H_6O_3S$: 195.0110; Found 195.0109.

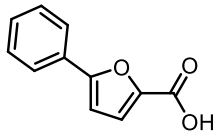

140

(140) - 5-phenylfuran-2-carboxylic acid: 1 mmol scale, white solid (172.5 mg, 92 % yield); ^{1}H NMR (500 MHz, Dimethyl sulfoxide-d): δ 13.14 (br. s, 1H), 7.82 (m, 2H), 7.48 (m, 2H), 7.40 (t, *J* = 7.4 Hz, 1H), 7.32 (d, *J* = 3.6 Hz, 1H), 7.15 (d, *J* = 3.6 Hz, 1H); ^{13}C NMR (500 MHz, Dimethyl sulfoxide -d): δ 159.74, 156.66, 144.65, 129.62, 129.53, 129.39, 124.82, 120.26, 108.35; HRMS (ESI) m/z: $[M+H]^+$ cacld for $C_{11}H_8O_3$: 189.0546; Found 189.0547.

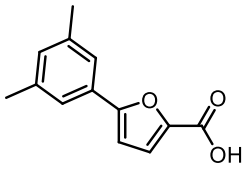

141

(141) - 5-(3,5-dimethylphenyl)furan-2-carboxylic acid: 1 mmol scale, white solid (177.3 mg, 90 % yield); ^{1}H NMR (500 MHz, Dimethyl sulfoxide-d): δ 13.08 (br. s, 1H), 7.43 (br. s, 2H), 7.30 (d, *J* = 3.6 Hz, 1H), 7.08 (d, *J* = 3.5 Hz, 1H), 7.03 (br. s, 1H), 2.32 (s, 6H); ^{13}C NMR (500 MHz, Dimethyl sulfoxide -d): δ 159.74, 157.00, 144.36, 138.67, 130.92, 129.50, 122.54, 120.28, 108.09, 21.30; HRMS (ESI) m/z: $[M+H]^+$ cacld for $C_{13}H_{12}O_3$: 217.0859; Found 217.0859.

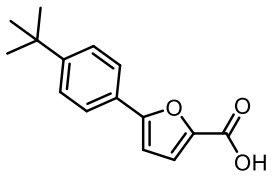

142

(142) - 5-(4-(*tert*-butyl)phenyl)furan-2-carboxylic acid: 1 mmol scale, white solid (214.2 mg, 88 % yield); ^{1}H NMR (500 MHz, Dimethyl sulfoxide-d): δ 7.73 (d, *J* = 8.2 Hz, 2H), 7.49 (d, *J* = 8.2 Hz, 2H), 7.23 (d, *J* = 3.6 Hz, 1H), 7.04 (d, *J* = 3.6 Hz, 1H), 1.29 (s, 9 H); ^{13}C NMR (500 MHz, Dimethyl sulfoxide -d): δ 160.18, 156.33, 151.85, 145.57, 127.18, 126.26, 124.56, 119.42, 107.60, 34.93, 31.39; HRMS (ESI) m/z: $[M+H]^+$ cacld for $C_{15}H_{16}O_3$: 245.1171; Found 245.1172.

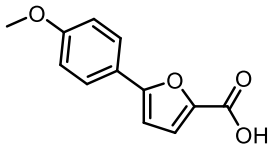

143

(143) - 5-(4-methoxyphenyl)furan-2-carboxylic acid: 1 mmol scale, white solid (199 mg, 99 % yield); ^{1}H NMR (500 MHz, Dimethyl sulfoxide-d): δ 12.99 (br. s, 1H), 7.75 (d, *J* = 8.8 Hz, 2H), 7.29 (d, *J* = 3.6 Hz, 1H), 7.05 (d, *J* = 8.8 Hz, 2H), 6.98 (d, *J* = 3.6 Hz, 1H), 3.80 (s, 3H); ^{13}C NMR (500 MHz, Dimethyl sulfoxide -d): δ 160.29, 159.76, 156.99, 143.91, 126.48, 122.41, 120.45, 114.98, 106.68, 55.73; HRMS (ESI) m/z: $[M+H]^+$ cacld for $C_{12}H_{10}O_4$: 219.0652; Found 219.0648.

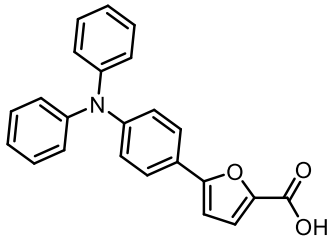

144

(144) - 5-(4-(diphenylamino)phenyl)furan-2-carboxylic acid: Added 1 mL of THF to help solubilize nitrile, 0.48 mmol scale, golden solid (157.5 mg, 94 % yield); ^{1}H NMR (500 MHz, Dimethyl sulfoxide-d): δ 7.87 (br. s, 0.5H), 7.77 (m, 1H), 7.67 (m, 1H), 7.40 (br. s, 0.5H) 7.33 (ddd, *J* = 8.9, 7.4, 2.0 Hz, 4H), 7.17 (dd, *J* = 30.8, 3.5 Hz, 1H), 7.12 – 7.04 (m, 6H), 6.99 (d, *J* = 8.4 Hz, 2H), 6.92 (dd, *J* = 10.5, 3.5 Hz, 1H); ^{13}C NMR (500 MHz, Dimethyl sulfoxide -d): δ 160.10, 159.79, 155.02, 148.11, 147.89, 147.17, 147.11, 130.16, 130.12, 126.06, 126.04, 125.08, 124.90, 124.20, 124.07, 123.81, 123.48, 122.90, 122.69, 116.29, 106.89, 106.71; HRMS (ESI) m/z: $[M]^+$ cacld for $C_{23}H_{17}NO_3$: 355.1203; Found 355.1203.

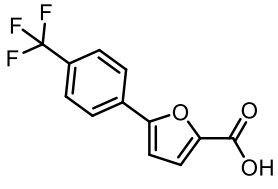

145

(145) - 5-(4-(trifluoromethyl)phenyl)furan-2-carboxylic acid: 1 mmol scale, white solid (245.2 mg, 96 % yield); ^{1}H NMR (500 MHz, Dimethyl sulfoxide-d): δ 12.89 (br. s, 1H), 8.01 (d, J = 8.2 Hz, 2H), 7.83 (d, J = 8.3 Hz, H), 7.35 (m, 2H); ^{13}C NMR (500 MHz, Dimethyl sulfoxide -d): δ 159.62, 154.86, 145.58, 133.20, 129.21, 128.95, 126.53 – 126.43 (q, J_{CF} = 3.8 Hz), 125.59, 125.35, 123.43, 120.19, 110.55; HRMS (ESI) m/z: $[M+H]^+$ cacld for $C_{12}H_7F_3O_3$: 257.0420; Found 257.0417.

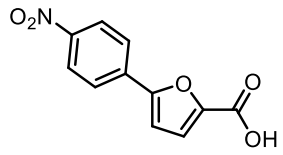

146

(146) - 5-(4-nitrophenyl)furan-2-carboxylic acid: 0.23 mmol scale, pale yellow solid (49.4 mg, 99 % yield); ^{1}H NMR (500 MHz, Dimethyl sulfoxide-d): δ 13.39 (d, 1H), 8.32 (d, J = 8.9 Hz, 2H), 8.06 (d, J = 8.9 Hz, 2H), 7.46 (d, J = 3.7 Hz, 1H), 7.39 (d, J = 3.6 Hz, 1H); ^{13}C NMR (500 MHz, Dimethyl sulfoxide -d): δ 159.54, 154.24, 147.35, 146.22, 135.27, 125.69, 124.96, 120.33, 112.11; HRMS (ESI) m/z: $[M]^+$ cacld for $C_{11}H_7NO_5$: 233.0319; Found 233.0318.

Procedure 9: **Solid state Cannizzaro disproportionation of mono-arylated furans.**

To a 50 mL capacity stainless steel planetary milling jar with 6 stainless steel balls (8 mm in diameter); corresponding furan aldehyde (1 equiv.) and oven-dried finely ground KOH (3 equiv.) are added. The jar is closed, and the reaction is spun at 30 Hz frequency for 15 minutes. The mixture is washed with H_2O (3 x 5 mL) and added to a separatory funnel. DCM or diethyl ether (3 x 5 mL) is added to wash the jar and is also added to the separatory funnel. It is important to collect and keep the washed aqueous layer to obtain the carboxylic acid product after washing with organics. The aqueous layer is extracted twice more with 20 mL DCM or diethyl ether, all organics are pooled, washed with brine (three times, 20 mL each), dried with sodium sulfate and the solvent is evaporated under reduced pressure to provide the corresponding furan alcohol. The primary alcohol can then be purified by gravity column chromatography if necessary (silica gel in its respected mobile solvent) to produce primary alcohol.

The washed aqueous solution remaining is acidified with concentrated HCl slowly until pH of 2 is observed. The acidic solution is transferred to a clean separatory funnel. Where 10 mL of water and 20 mL of DCM are added. The aqueous layer is extracted twice more with 20 mL DCM, all organics are pooled, washed with brine (three times, 20 mL each), dried with sodium sulfate and the solvent is evaporated under reduced pressure to afford the corresponding furan carboxylic acid.

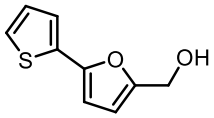

139OH

(139OH) - (5-(thiophen-2-yl)furan-2-yl)methanol: 100 mg scale, expected 50.5 mg, orange solid (42.4 mg, 84 % yield or 42 % yield out of 50 %); R_f = 0.11 (4:1 hexanes/ethyl acetate); ^{1}H NMR (500 MHz, Chloroform-d): δ 7.26 (m, 1H), 7.22 (d, *J* = 5.0 Hz, 1H), 7.03 (dd, *J* = 5.0, 3.6 Hz, 1H), 6.44 (d, *J* = 3.3 Hz, 1H), 6.34 (d, *J* = 3.3 Hz, 1H), 4.63 (s, 2H), 2.10 (br. s, 1H); ^{13}C NMR (500 MHz, Chloroform-d): δ 153.18, 149.49, 133.54, 127.62, 124.26, 122.75, 109.96, 105.73, 57.47; HRMS (ESI) m/z: $[M]^+$ cacld for $C_9H_8O_2S$: 180.0240; Found 180.0238.

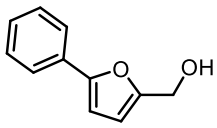

140OH

(140OH) - (5-phenylfuran-2-yl)methanol: 100 mg scale, expected 50.4 mg, orange oil (49.8 mg, 99 % yield or 49 % yield out of 50 %); R_f = 0.11 (4:1 hexanes/ethyl acetate); ^{1}H NMR (500 MHz, Chloroform-d): δ 7.68 (m, 2H), 7.38 (dd, *J* = 8.5, 7.0 Hz, 2H), 7.28 (m, 1H), 6.60 (d, *J* = 3.3 Hz, 1H), 6.38 (d, *J* = 3.6 Hz, 1H), 4.66 (s, 2H), 2.02 (br. s, 1H); ^{13}C NMR (500 MHz, Chloroform-d): δ 154.01, 153.56, 130.66, 128.66, 127.46, 123.79, 109.98, 105.69, 57.64; HRMS (ESI) m/z: $[M]^+$ cacld for $C_{11}H_{10}O_2$: 174.0675; Found 174.0676.

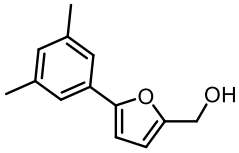

141OH

(141OH) - (5-(3,5-dimethylphenyl)furan-2-yl)methanol: 100 mg scale, expected 49.6 mg, orange oil (49.3 mg, 99 % yield or 49 % yield out of 50 %); R_f = 0.12 (4:1 hexanes/ethyl acetate); ^{1}H NMR (500 MHz, Chloroform-d): δ 7.31 (s, 2H), 6.91 (s, 1H), 6.56 (d, *J* = 3.3 Hz, 1H), 6.36 (d,

J = 3.3 Hz, 1H), 4.66 (s, 2H), 2.34 (s, 6H), 1.82 (br. s, 1H); ^{13}C NMR (500 MHz, Chloroform-d): δ 154.37, 153.24, 138.18, 130.49, 129.26, 121.65, 109.93, 105.42, 57.71, 21.33; HRMS (ESI) m/z: $[M]^+$ cacld for $C_{13}H_{14}O_2$: 202.0988; Found 202.0985.

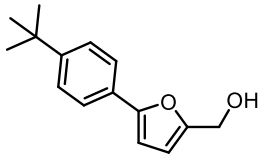

142OH

(142OH) - (5-(4-(*tert*-butyl)phenyl)furan-2-yl)methanol: Reaction for 30 minutes at 60 Hz frequency, 100 mg scale, expected 52.0 mg, orange oil (41.6 mg, 80 % yield or 40 % yield out of 50 %); purified by gravity column chromatography (silica gel) in 4:1 hexanes/ethyl acetate; R_f = 0.13 (4:1 hexanes/ethyl acetate); ^{1}H NMR (500 MHz, Chloroform-d): δ 7.61 (m, 2H), 7.41 (m, 2H), 6.55 (d, *J* = 3.3 Hz, 1H), 6.37 (d, *J* = 3.2 Hz, 1H), 1.92 (br. s, 1H), 1.34 (s, 9H); ^{13}C NMR (500 MHz, Chloroform-d): δ 154.24, 153.22, 150.58, 127.98, 125.57, 123.61, 109.93, 105.08, 57.69, 34.62, 31.25; HRMS (ESI) m/z: $[M]^+$ cacld for $C_{15}H_{18}O_2$: 230.1301; Found 230.1298.

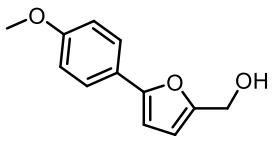

143OH

(143OH) - (5-(4-methoxyphenyl)furan-2-yl)methanol: 100 mg scale, expected 50.5 mg, orange solid (45.5 mg, 90 % yield or 45 % yield out of 50 %); R_f = 0.08 (4:1 hexanes/ethyl acetate); ^{1}H NMR (500 MHz, Chloroform-d): δ 7.62 (m, 2H), 6.93 (m, 2H), 6.45 (d, *J* = 3.3 Hz, 1H), 6.35 (d, *J* = 3.3 Hz, 1H), 4.65 (s, 2H), 3.83 (s, 3H), 1.92 (br. s, 1H); ^{13}C NMR (500 MHz, Chloroform-d): δ 159.10, 154.11, 152.84, 125.25, 123.75, 114.09, 109.96, 104.07, 57.63, 55.29; HRMS (ESI) m/z: $[M]^+$ cacld for $C_{12}H_{12}O_3$: 204.0781; Found 204.0778.

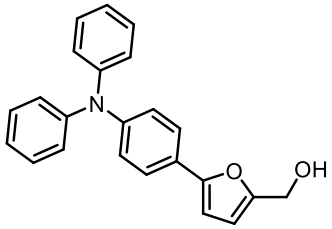

144OH

(144OH) - (5-(4-(diphenylamino)phenyl)furan-2-yl)methanol: 66 mg scale, expected 33.3 mg, amber oil (9.7 mg, 30 % yield or 15 % yield out of 50 %); purified by gravity column chromatography (silica gel) in 9:1 hexanes/ethyl acetate, followed by 4:1 hexanes/ethyl acetate after aldehyde eluted out; R_f = 0.12 (4:1 hexane/ethyl acetate); ^{1}H NMR (500 MHz, Chloroform-d): δ 7.54 (d, *J* = 8.8 Hz, 2H), 7.28 – 7.25 (m, 3H), 7.11 (m, 4H), 7.08 (m, 2H), 7.03 (m, 3H), 6.49 (d, *J* = 3.3 Hz, 1H), 6.36 (d, *J* = 3.3 Hz, 1H), 4.65 (s, 2H), 1.58 (br. s, 1H); ^{13}C NMR (500 MHz, Chloroform-d): δ 154.09, 153.02, 147.48, 147.19, 129.28, 124.89, 124.78, 124.45, 123.59, 123.04, 110.06, 104.58, 57.69; HRMS (ESI) m/z: $[M]^+$ cacld for $C_{23}H_{19}NO_2$: 341.1410; Found 341.1408.

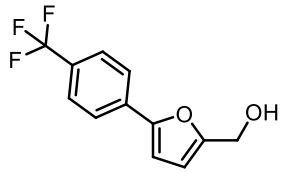

145OH

(145OH) - (5-(4-(trifluoromethyl)phenyl)furan-2-yl)methanol: 30 mg scale, expected 15.1 mg, yellow solid (13.9 mg, 92 % yield or 46 % yield out of 50 %); purified by gravity column chromatography (silica gel) in 2:1 hexanes/ethyl acetate; R_f = 0.19 (2:1 hexanes/ethyl acetate); ^{1}H NMR (500 MHz, Chloroform-d): δ 7.76 (d, *J* = 9.0 Hz, 2H), 7.62 (d, *J* = 9.0 Hz, 2H), 6.72 (d, *J* = 3.3 Hz, 1H), 6.42 (d, *J* = 3.3 Hz, 1H), 4.69 (s, 2H), 1.87 (br. s, 1H); ^{13}C NMR (500 MHz, Chloroform-d): δ 154.62, 152.48, 133.72, 129.18, 128.92, 125.74 – 125.65 (q, J_{CF} = 3.8 Hz), 125.20, 123.75, 123.04, 110.22, 107.70, 57.61; HRMS (ESI) m/z: $[M]^+$ cacld for $C_{12}H_9F_3O_2$: 242.0549; Found 242.0550.

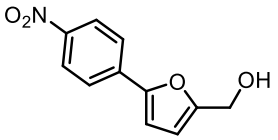

146OH

(146OH) - (5-(4-nitrophenyl)furan-2-yl)methanol: 30 mg scale, expected 15.1 mg, orange solid (11.7 mg, 78 % yield or 39 % yield out of 50 %); purified by gravity column chromatography (silica gel) in 3:3:1 hexanes/dichloromethane/ethyl acetate; R_f = 0.17 (3:3:1 hexanes/dichloromethane/ethyl acetate); ^{1}H NMR (500 MHz, Chloroform-d): δ 8.24 (d, *J* = 8.9 Hz, 2H), 7.79 (d, *J* = 8.9 Hz, 2H), 6.83 (d, *J* = 3.4 Hz, 1H), 6.46 (d, *J* = 3.4 Hz, 1H), 4.71 (s, 2H), 1.85 (br. s, 1H); ^{13}C NMR (500 MHz, Chloroform-d): δ 155.78, 151.65, 146.46, 136.22, 124.33,

123.92, 110.58, 109.73, 57.60; HRMS (ESI) m/z: $[M]^+$ cacld for $C_{11}H_9NO_4$: 219.0526; Found 219.0524.

Procedure 10: **Double decarboxylative cross-coupling towards di-arylated furan oligomers.**

To an oven-dried 0.5 - 2 mL conical microwave vial equipped with a stir bar; corresponding furan carboxylic acid (0.22 mmol, 2.2 equiv.), dibromo-aryl compound (0.1 mmol, 1.0 equiv.), Cs_2CO_3 (0.15 mmol, 1.5 equiv.) and 1 mL of anhydrous DMA [0.1 M] are added. The vial is then closed with a removable rubber septum and the solution is degassed with argon in a sonicator bath for 10 minutes (to degas solution: insert a flame dried needle through septum and ensure needle tip is in solution, attach a balloon with argon to needle, clamp vial into sonicator bath and then slowly insert a smaller needle through septum to allow air to escape). After sonication, $PdCl_2$ (0.89 mg, 5 mol %) and P(*o*-Tolyl)$_3$ (3.04 mg, 10 mol %) are added to solution. Vial is capped with a rubber septum and an aluminum cap. DMA is carefully rotated alongside the glass to ensure catalyst and ligand are submerged into the solution and the solution is pre-stirred at 23 °C to ensure stirring is effective. Reaction vial is then placed to react in Biotage Initiator^{TM} + (400 W magneton) at 190 °C for 8 minutes with stirring on the high absorption setting. The reaction is then cooled to room temperature and each product is purified distinctly. After purification, products are dried in a high vacuum chamber away from light and are then wrapped in aluminum foil and stored in a -20 °C freezer.

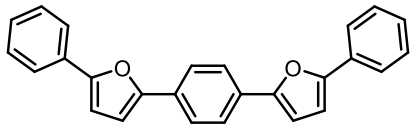

42

(42) - 1,4-bis(5-phenylfuran-2-yl)benzene: Purification of **42**: After cooling reaction to room temperature, H_2O was added to the conical vial. A yellow precipitation is then seen and is collected by vacuum filtration. The precipitation is then washed with H_2O, followed by ethanol, hexanes and lastly acetone. To remove palladium, the precipitate was past through a small celite/silica plug with DCM. DCM was evaporated under reduced pressure producing a shiny yellow solid.

0.2 mmol scale, shiny yellow solid (47.7 mg, 66 %); 1.0 mmol scale (10 – 20 mL microwave vial used), shiny yellow solid (199.1 mg, 55 %); R_f = 0.62 (3:2:1 hexanes/DCM/ethyl acetate); ^{1}H NMR (500 MHz, Chloroform-d): δ 7.78 (s, 4H), 7.76 (d, *J* = 7.1 Hz, 4H), 7.43 (t, *J* = 7.8 Hz, 4H),

7.29 (t, J = 7.4 Hz, 2H), 6.78 (q, J = 3.4 Hz, 4H); ^{13}C NMR (500 MHz, Chloroform-d): δ 153.51, 153.12, 130.71, 129.52, 128.72, 127.40, 123.98, 123.75, 107.50, 107.40; HRMS (ESI) m/z: $[M]^+$ cacld for $C_{26}H_{18}O_2$: 362.1301; Found 362.1301.

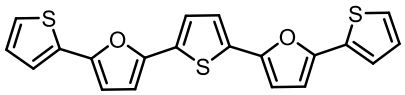

44

(44) - 2,5-bis(5-(thiophen-2-yl)furan-2-yl)thiophene: Purification of **44**: After cooling reaction to room temperature, crude solution was added to a separatory funnel. To funnel, ethyl acetate (20 mL) and 20 mL of water were added. Aqueous layer was washed with ethyl acetate twice more (2x 20 mL). Organic layer was then washed with brine (3x 20 mL), organic was recollected, dried with sodium sulfate, and evaporated under reduced pressure. The crude sample was then purified by gravity column chromatography (neutralized silica gel) in 5:1 hexanes/toluene. Silica gel was neutralized by passing a solution of 2% (v/v) triethylamine in hexanes. After pooling the fractions and evaporating the solvent under reduced pressure, a golden yellow solid was observed.

0.1 mmol scale, golden yellow solid (26.9 mg, 71 %); R_f = 0.38 (9:1 hexanes/ethyl acetate); ^{1}H NMR (500 MHz, Chloroform-d): δ 7.33 (dd, J = 3.7, 1.2 Hz, 2H), 7.26 (dd, J = 5.2, 1.4 Hz, 2H), 7.23 (s, 2H), 7.06 (2d, J = 5.0, 3.6 Hz, 2H), 6.57 (s, 4H),; ^{13}C NMR (500 MHz, Chloroform-d): δ 148.75, 148.18, 133.31, 131.87, 127.76, 124.35, 123.23, 122.80, 107.49, 107.38; HRMS (ESI) m/z: $[M]^+$ cacld for $C_{20}H_{12}O_2S_2$: 379.9994; Found 379.9994.

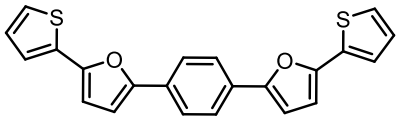

147

(147) - 1,4-bis(5-(thiophen-2-yl)furan-2-yl)benzene: Purification of **147**: After cooling reaction to room temperature, H_2O was added to the conical vial. A yellow precipitation is then seen and is collected by vacuum filtration. The precipitation is then washed with H_2O, followed by ethanol (2 mL) and hexanes (2 mL). Precipitate was then collected by dissolving it in acetone. Acetone was evaporated under reduced pressure leaving a crude solution. The crude sample was then dissolved in minimum DCM and the concentrated solution was carefully dripped onto a preparative TLC sheet. PTLC was performed in 27:2:1 hexanes/ethyl acetate/dichloromethane. Yellow band was

scratched off and washed with acetone. The solvent was then evaporated under reduced pressure leaving a golden yellow solid.

0.1 mmol scale, golden yellow solid (24.3 mg, 65 %); R_f = 0.65 (3:2:1 hexanes/DCM/ethyl acetate); ^{1}H NMR (500 MHz, Chloroform-d): δ 7.73 (s, 4H), 7.34 (d, *J* = 2.1 Hz, 2H), 7.25 (d, *J* = 4.6 Hz, 2H), 7.07 (dd, *J* = 5.0, 3.1 Hz, 2H), 6.73 (d, *J* = 2.9 Hz, 2H), 6.60 (d, *J* = 2.7 Hz, 2H); ^{13}C NMR (500 MHz, Chloroform-d): δ 152.66, 149.12, 133.68, 129.26, 127.73, 124.24, 123.95, 122.63, 107.44, 107.40; HRMS (ESI) m/z: $[M]^+$ cacld for $C_{22}H_{14}O_2S_2$: 374.0430; Found 374.0429.

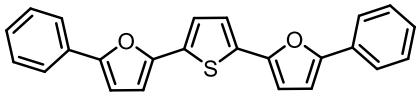

148

(148) - 2,5-bis(5-phenylfuran-2-yl)thiophene: Purification of **148**: After cooling reaction to room temperature, H_2O was added to the conical vial. A yellow precipitation is then seen and is collected by vacuum filtration. The precipitation is then washed with H_2O, followed by methanol (5 mL), ethanol (2 mL) and hexanes (2 mL). Precipitate was then collected by dissolving it in chloroform. Chloroform was evaporated under reduced pressure leaving a crude orange crystal. Crude orange crystal was then dissolved in minimum DCM and the concentrated solution was carefully dripped onto a preparative TLC sheet. PTLC was performed in 8:1:1 hexanes/chloroform/ethyl acetate. Yellow band was scratched off and passed though small silica plug. Plug was washed with 3x 5 mL hexanes and 8x 10 mL 19:1 hexanes/ethyl acetate, solvent was evaporated under reduced pressure leaving a bright yellow solid.

0.2 mmol scale, bright yellow solid (45.4 mg, 62 %); R_f = 0.63 (3:2:1 hexanes/DCM/ethyl acetate); ^{1}H NMR (500 MHz, Chloroform-d): δ 7.75 (dd, *J* = 8.3, 1.3 Hz, 4H), 7.42 (m,4H), 7.29 (m, 2H), 7.27 (s, 2H), 6.74 (d, *J* = 3.5 Hz, 2H), 6.62 (d, *J* = 3.5 Hz, 2H); ^{13}C NMR (500 MHz, Chloroform-d): δ 153.15, 148.67, 132.17, 130.40, 128.73, 127.47, 123.73, 123.09, 107.50, 107.37; HRMS (ESI) m/z: $[M]^+$ cacld for $C_{24}H_{16}O_2S$: 368.0866; Found 368.0864.

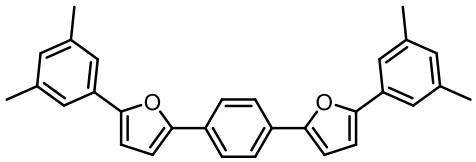

149

(149) - 1,4-bis(5-(3,5-dimethylphenyl)furan-2-yl)benzene: Purification of **149**: After cooling reaction to room temperature, **149** was noticed to have crashed out of the DMA solution. With a pipette, DMA was slowly and carefully removed, and the precipitated solid was washed with ethanol. Precipitation was collected by vacuum filtration and additional ethanol was used to wash. To remove palladium, the precipitate was then dissolved in chloroform (20 mL) and added to a separatory funnel. 20 mL of brine was added, and the aqueous layer was washed with chloroform twice more (2x 20 mL), dried with sodium sulfate and evaporated under reduced pressure to produce a sparkly yellow solid.

0.1 mmol scale, sparkly yellow solid (30.9 mg, 74 %); R_f = 0.00 (9:1 hexanes/ethyl acetate); ^{1}H NMR (500 MHz, Chloroform-d): δ 7.78 (s, 4H), 7.39 (s, 4H), 6.93 (s, 2H), 6.76 (d, *J* = 3.4 Hz, 2H), 6.73 (d, *J* = 3.4 Hz, 2H), 2.38 (s, 12H); Compound **149** is too insoluble to record a ^{13}C NMR. HRMS (ESI) m/z: $[M]^+$ cacld for $C_{30}H_{26}O_2$: 418.1927; Found 418.1927.

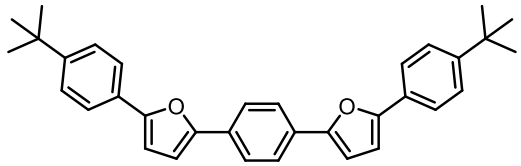

150

(150) - 1,4-bis(5-(4-(tert-butyl)phenyl)furan-2-yl)benzene: Purification of **150**: After cooling reaction to room temperature, H_2O was added to the conical vial. A yellow precipitation is then seen and is collected by vacuum filtration. The precipitation is then washed with H_2O, followed by ethanol (2 - 4 mL) and hexanes (2 - 4 mL). To remove palladium, the precipitate was then dissolved in chloroform (20 mL) and added to a separatory funnel. 20 mL of brine was added, and the aqueous layer was washed with chloroform twice more (2x 20 mL), dried with sodium sulfate and evaporated under reduced pressure to produce a crude yellow solid. Crude solid was then dissolved in minimum DCM and the concentrated solution was carefully dripped onto a preparative TLC sheet. PTLC was performed in 25:1:1 hexanes/dichloromethane/ethyl acetate. Yellow band at baseline was scratched off, producing a bright yellow solid.

0.1 mmol scale, bright yellow solid (45.4 mg, 62 %); R_f = 0.00 (25:1:1 hexanes/DCM/ethyl acetate); ^{1}H NMR (500 MHz, Chloroform-d): δ 7.77 (s, 4H), 7.70 (d, *J* = 8.4 Hz, 4H), 7.45 (d, *J* = 8.5 Hz, 4H), 6.76 (d, *J* = 3.4 Hz, 2H), 6.72 (d, *J* = 3.5 Hz, 2H), 1.36 (s, 18H); ^{13}C NMR (500 MHz,

Chloroform-d): δ 153.70, 152.83, 150.55, 129.50, 128.04, 125.66, 123.89, 123.58, 107.42, 106.83, 34.68, 31.28; HRMS (ESI) m/z: $[M]^+$ cacld for $C_{34}H_{34}O_2$: 474.2553; Found 474.2552.

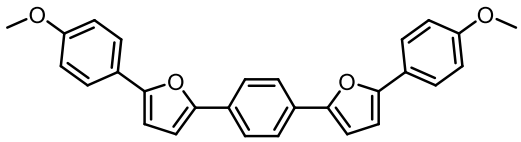

151

(151) - 1,4-bis(5-(4-methoxyphenyl)furan-2-yl)benzene: Purification of **151**: After cooling reaction to room temperature, **151** was noticed to have crashed out of the DMA solution. With a pipette, DMA was slowly and carefully removed, and the precipitated solid was washed with ethanol. Precipitation was collected by vacuum filtration and additional ethanol was used to wash. To remove palladium, the precipitate was then dissolved in chloroform (20 mL) and added to a separatory funnel. 20 mL of brine was added, and the aqueous layer was washed with chloroform twice more (2x 20 mL), dried with sodium sulfate and evaporated under reduced pressure to produce a yellow solid.

0.1 mmol scale, bright yellow solid (21.1 mg, 50 %); R_f = 0.00 (9:1 hexanes/ethyl acetate); ^{1}H NMR (500 MHz, Chloroform-d): δ 7.75 (s, 4H), 7.70 (d, *J* = 8.6 Hz, 4H), 6.96 (d, *J* = 8.7 Hz, 4H), 6.75 (d, *J* = 3.4, 2H), 6.63 (d, *J* = 3.5, 2H), 3.86 (s, 6H); Compound **151** is too insoluble to record a ^{13}C NMR. HRMS (ESI) m/z: $[M]^+$ cacld for $C_{28}H_{22}O_4$: 422.1513; Found 422.1511.

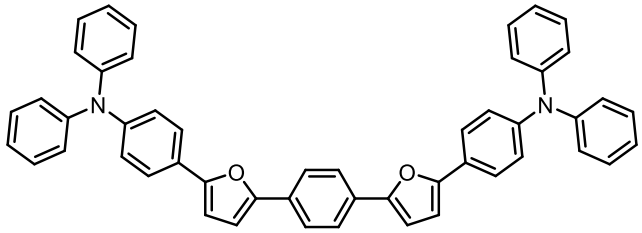

152

(152) - 4,4'-(1,4-phenylenebis(furan-5,2-diyl))bis(N,N-diphenylaniline): Purification of **152**: After cooling reaction to room temperature, solution was added to a separatory funnel. To funnel, EtOAc (20 mL) and 20 mL of water were added. Aqueous layer was washed with EtOAc twice more (2x 20 mL). Organic layer was then washed with brine (3x 20 ml), organic was recollected, dried with sodium sulfate, and evaporated under reduced pressure to obtain a crude oil. Crude oil was dissolved in minimum amount of DCM and carefully dripped onto a preparative TLC sheet.

PTLC was performed in 9:1 hexanes/ethyl acetate. The entire yellow/orange band (including baseline) was collected and further purified by gravity column chromatography (silica gel was neutralized prior with a 2 % (v/v) triethylamine in hexane solution) in 20:4:1 hexanes/toluene/ethyl acetate, producing a bright yellow solid.

0.1 mmol scale, bright yellow solid (22.1 mg, 32 %); R_f = 0.36 (9:1 hexanes/ethyl acetate); ^{1}H NMR (500 MHz, Chloroform-d): δ 7.74 (s, 4H), 7.63 (d, *J* = 8.7 Hz, 4H), 7.28 (m, 8H), 7.13 (m, 12H), 7.05 (t, *J* = 7.3 Hz, 4H), 6.75 (d, *J* = 3.5 Hz, 2H), 6.65 (d, *J* = 3.5 Hz, 2H); ^{13}C NMR (500 MHz, Chloroform-d): δ 153.51, 152.66, 147.49, 147.12, 129.39, 129.31, 124.93, 124.72, 124.49, 123.81, 123.65, 123.07, 107.52, 106.37; HRMS (ESI) m/z: $[M]^+$ cacld for $C_{50}H_{36}N_2O_2$: 696.2771; Found 696.2767.

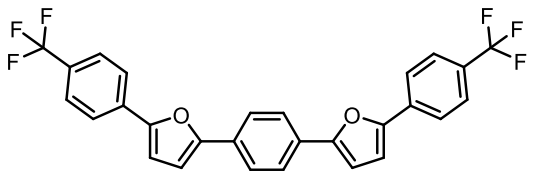

153

(153) - 1,4-bis(5-(4-(trifluoromethyl)phenyl)furan-2-yl)benzene: Purification of **153**: After cooling reaction to room temperature, H_2O was added to the conical vial. A yellow precipitation is then seen and is collected by vacuum filtration. The precipitation is then washed with additional H_2O. Precipitate was then collected by dissolving it in chloroform. Chloroform was evaporated under reduced pressure. The crude sample was then dissolved in minimum DCM and the concentrated solution was carefully dripped onto a preparative TLC sheet. PTLC was performed in 9:1 hexanes/ethyl acetate. Yellow band at baseline was scratched off and washed off with chloroform. Solvent was evaporated under reduced pressure leaving a yellow solid.

0.1 mmol scale, yellow solid (10.2 mg, 21 %); R_f = 0.00 (9:1 hexanes/ethyl acetate); ^{1}H NMR (500 MHz, Chloroform-d): δ 7.85 (d, *J* = 8.1 Hz, 4H), 7.81 (s, 4H), 7.67 (d, *J* = 8.1 Hz, 4H), 6.89 (d, *J* = 3.4 Hz, 2H), 6.83 (d, *J* = 3.6 Hz, 2H); Compound **153** is too insoluble to record a ^{13}C NMR. HRMS (ESI) m/z: $[M]^+$ cacld for $C_{28}H_{16}F_6O_2$: 498.1049; Found 498.1047.

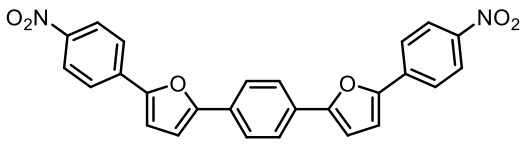

154

(154) - 1,4-bis(5-(4-nitrophenyl)furan-2-yl)benzene: Purification of **154**: After cooling reaction to room temperature, crude solution was added to a separatory funnel. To funnel, chloroform (20 mL) and 20 mL of water were added. Aqueous layer was washed with chloroform twice more (2x 20 mL). Organic layer was then washed with brine (3x 20 mL), organic was recollected, dried with sodium sulfate, and evaporated under reduced pressure. The crude sample was then dissolved in minimum DCM and the concentrated solution was carefully dripped onto a preparative TLC sheet. PTLC was performed in 9:1 hexanes/ethyl acetate. Red band at baseline was scratched off and washed off with chloroform. Solvent was evaporated under reduced pressure leaving a red solid.

0.1 mmol scale, red solid (7.9 mg, 18 %); R_f = 0.00 (9:1 hexanes/ethyl acetate); ^{1}H NMR (500 MHz, Chloroform-d): δ 8.29 (d, *J* = 8.9 Hz, 4H), 7.88 (d, *J* = 8.9, 4H), 7.84 (s, 4H), 7.02 (d, *J* = 3.5 Hz, 2H), 6.88 (d, *J* = 3.5 Hz, 2H); Compound **154** is too insoluble to record a ^{13}C NMR. HRMS (ESI) m/z: $[M]^+$ cacld for $C_{26}H_{16}N_2O_6$: 452.1003; Found 452.1002.

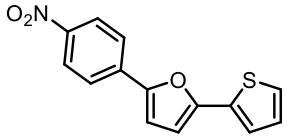

156

(**156**) – **2-(4-nitrophenyl)-5-(thiophen-2-yl)furan:** Purification of **156**: Crude reaction is transferred to a separatory funnel where 15 mL of water and 20 mL of EtOAc are added. The aqueous layer is extracted twice more with 20 mL EtOAc, all organics are pooled, washed with brine (three times, 20 mL each), dried with sodium sulfate and the solvent is evaporated under reduced pressure. The crude is then purified by gravity column chromatography (2:1 hexanes/DCM) to produce the desired light orange solid.

0.2 mmol scale, light orange solid (28 mg, 52 %); R_f = 0.17 (2:1 hexanes/DCM); ^{1}H NMR (500 MHz, Chloroform-d): δ 8.27 (d, *J* = 9.0 Hz, 2H), 7.82 (d, *J* = 8.9 Hz, 2H), 7.39 (dd, *J* = 3.6, 1.1 Hz, 1H), 7.32 (dd, *J* = 5.1, 1.1 Hz, 1H), 7.10 (dd, *J* = 5.1, 3.6, 1.1 Hz), 6.93 (d, *J* = 3.6 Hz, 1H), 6.66 (d, *J* = 3.5 Hz, 1H); ^{13}C NMR (500 MHz, Chloroform-d): δ 151.17, 150.51, 146.25, 136.02, 132.82, 127.93, 125.38, 124.41, 123.74, 123.67, 111.32, 107.77; HRMS (ESI) m/z: $[M]^+$ cacld for $C_{14}H_9NO_3S$: 271.0298; Found 271.0298.

5.4 ^{1}H NMR and ^{13}C NMR Spectra

109, 2,5-bis(5-(4-(tert-butyl)phenyl)furan-2-yl)thiophene

^{1}H NMR (500 MHz, $CDCl_3$)

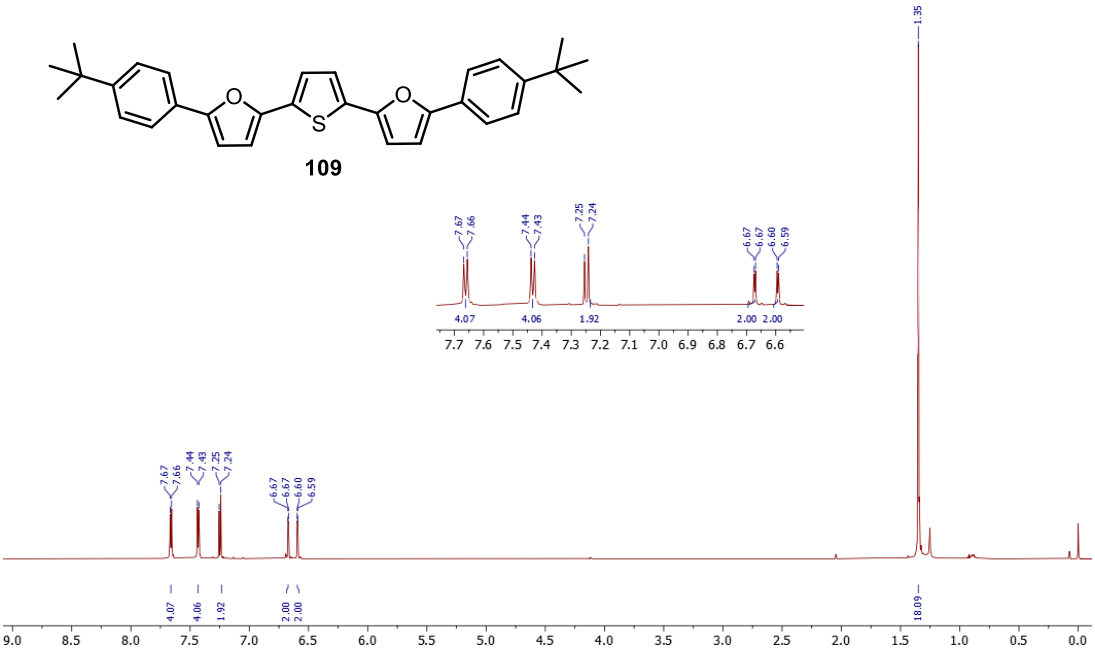

^{13}C NMR (700 MHz, $CDCl_3$)

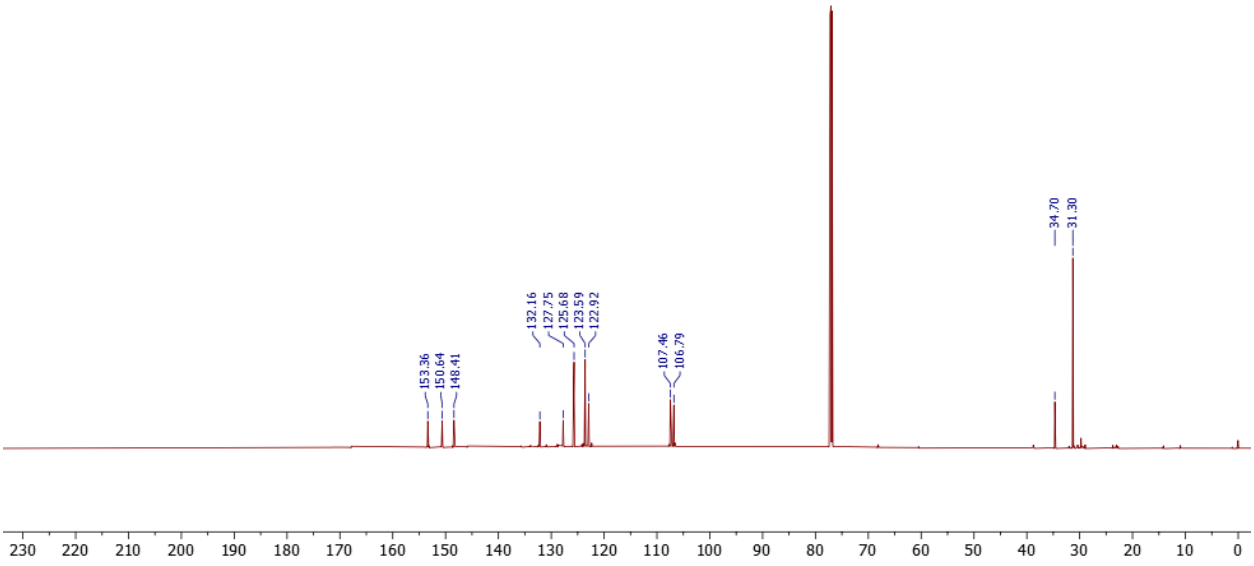

113, 2,5-bis(3-(4-(tert-butyl)phenyl)-5-phenylfuran-2-yl)thiophene

^{1}H NMR (500 MHz, $CDCl_3$)

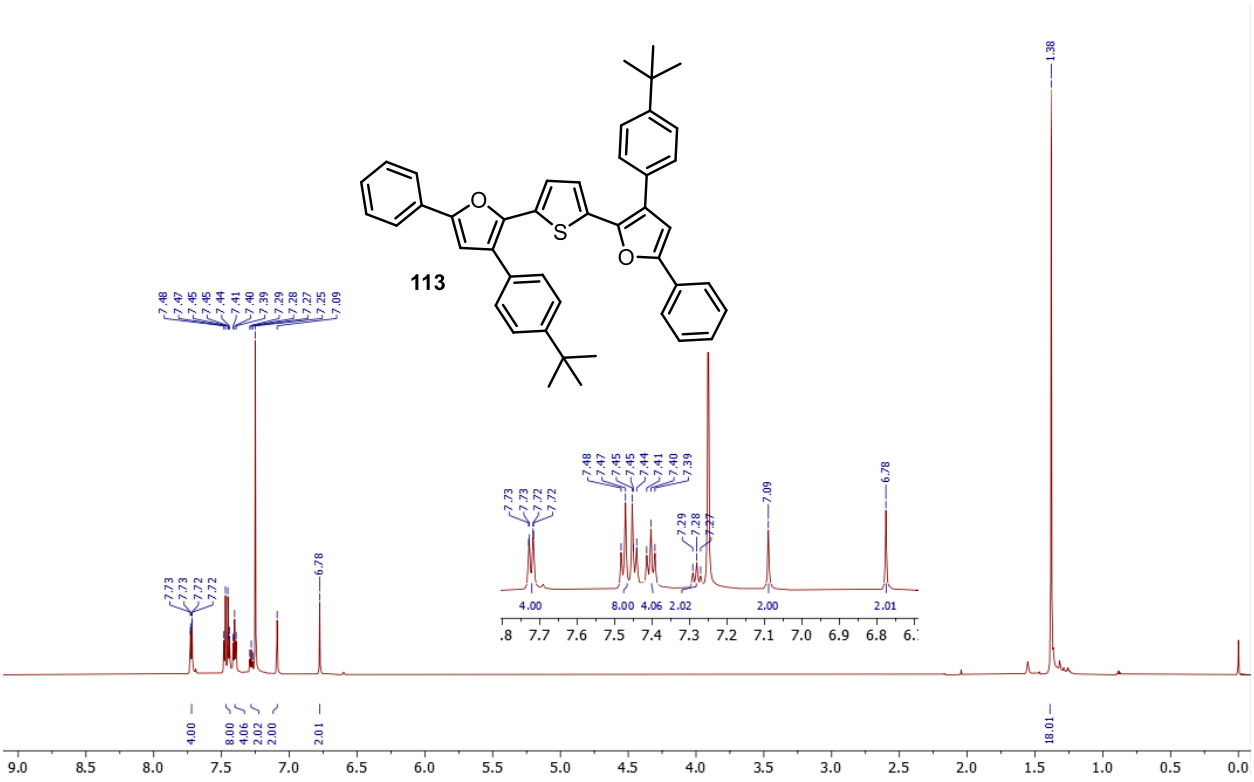

^{13}C NMR (700 MHz, $CDCl_3$)

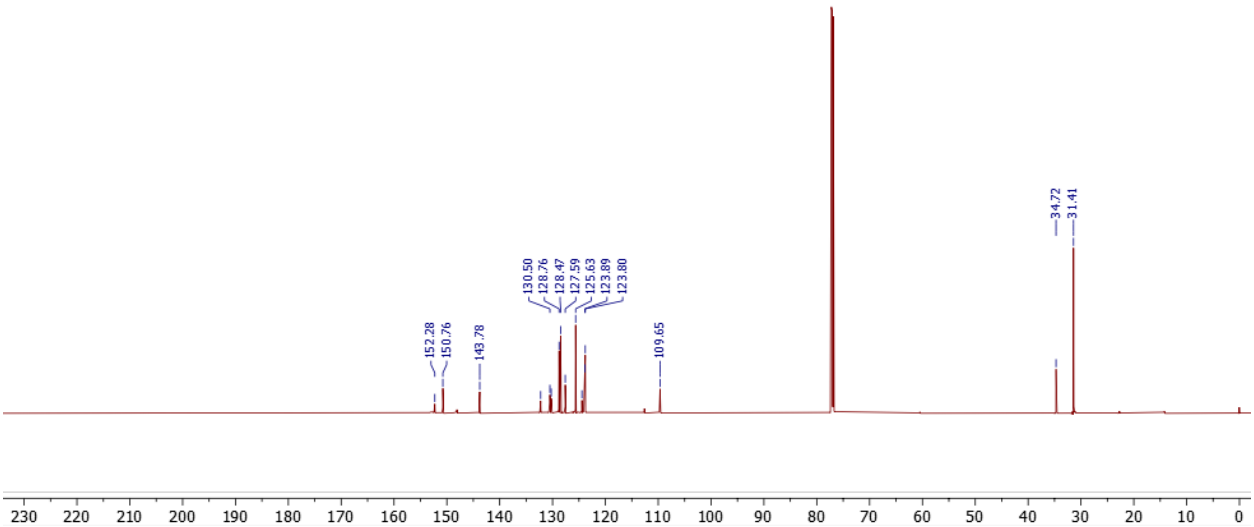

115, 2,5-bis(4-(4-(tert-butyl)phenyl)-5-phenylfuran-2-yl)thiophene

^{1}H NMR (500 MHz, $CDCl_3$)

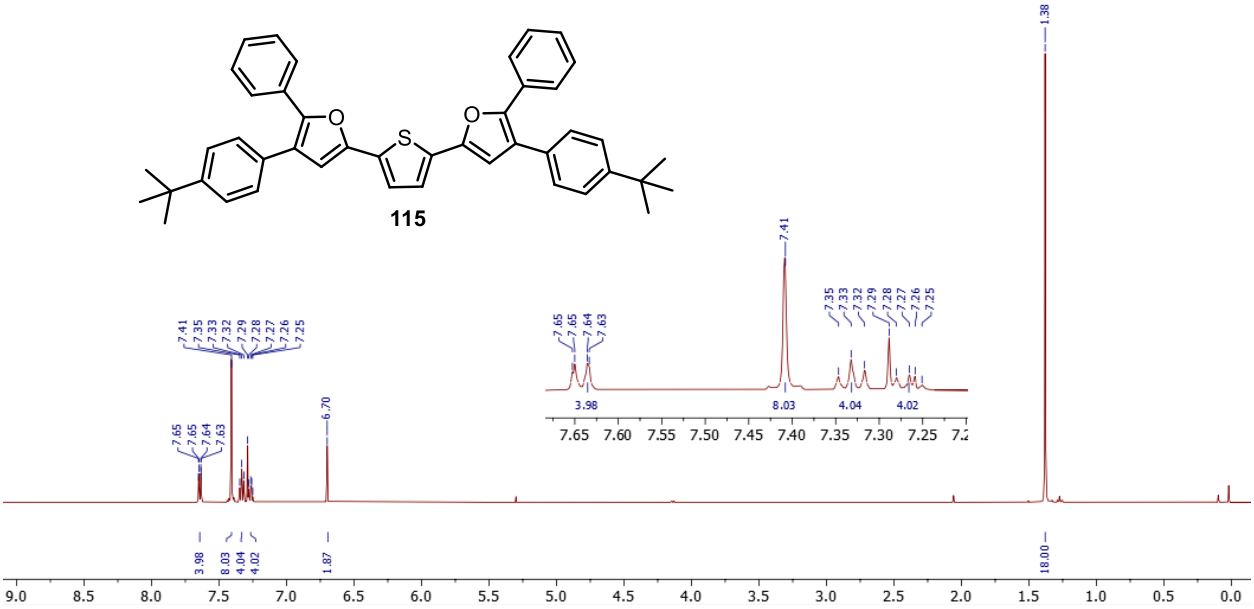

^{13}C NMR (700 MHz, $CDCl_3$)

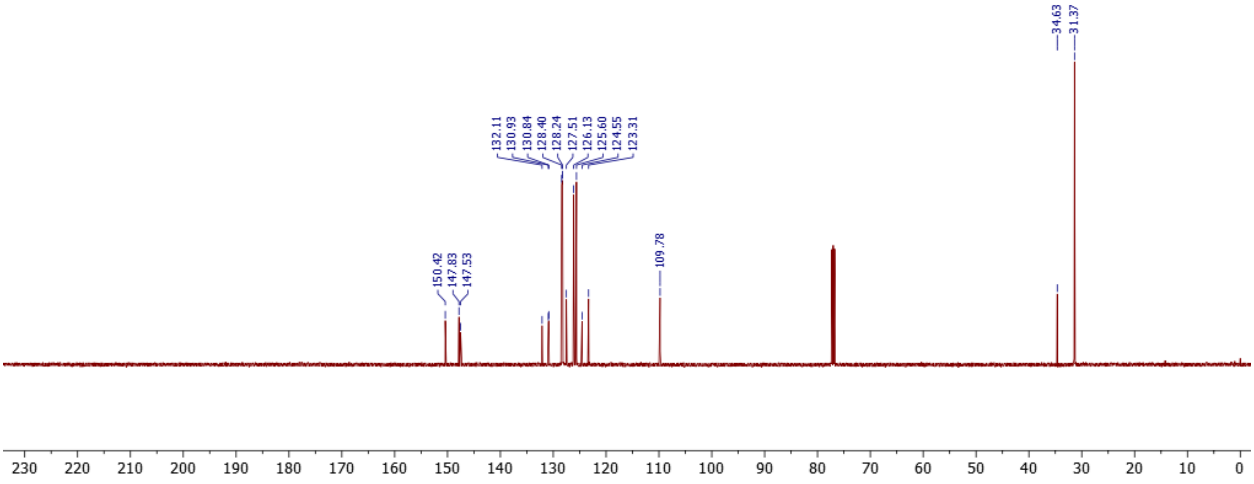

119, 5-(thiophen-2-yl)furan-2-carbaldehyde

^{1}H NMR (500 MHz, $CDCl_3$)

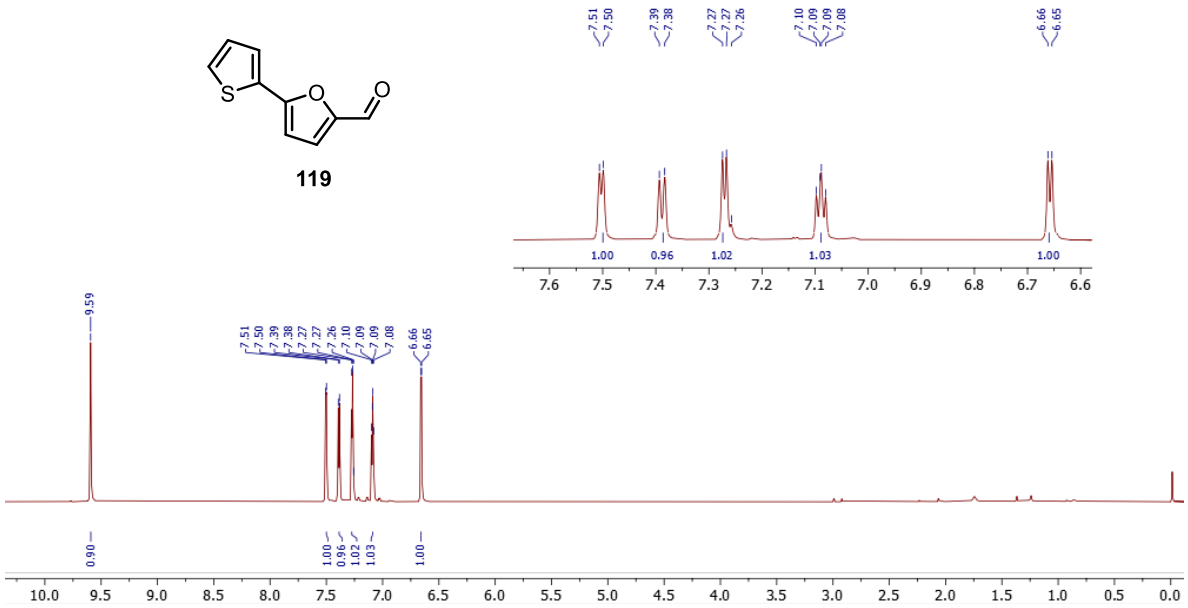

^{13}C NMR (500 MHz, $CDCl_3$)

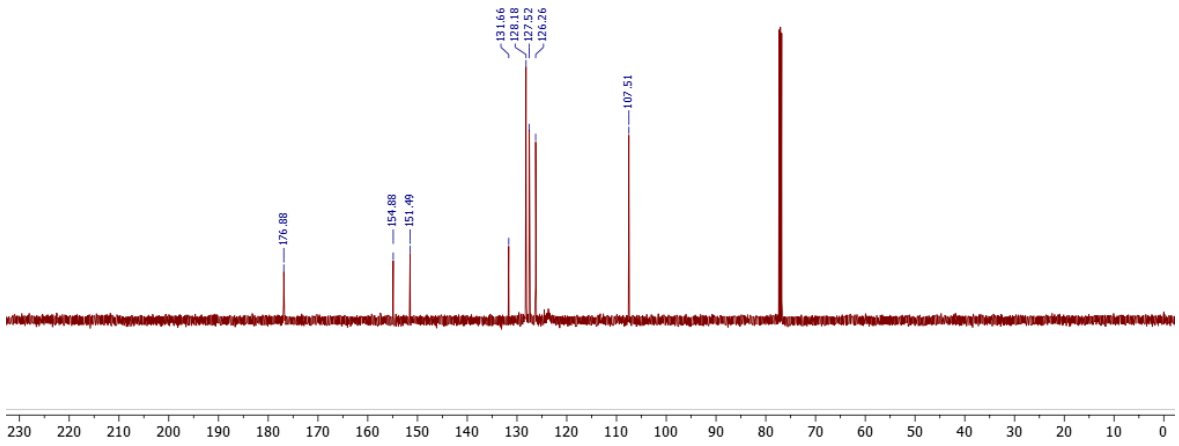

122, 5-phenylfuran-2-carbaldehyde

^{1}H NMR (500 MHz, $CDCl_3$)

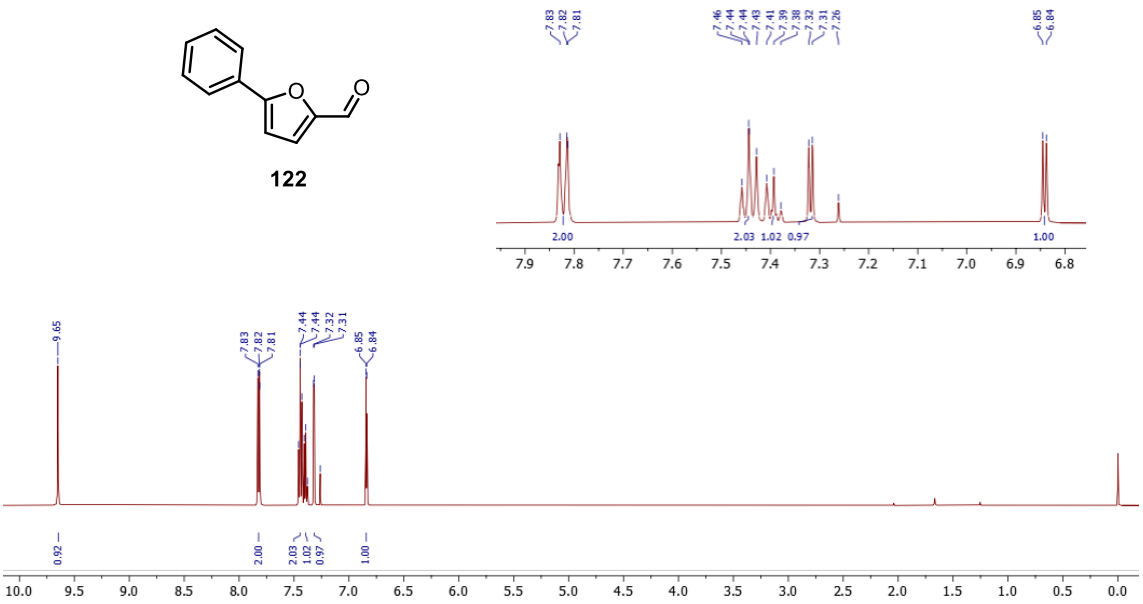

^{13}C NMR (500 MHz, $CDCl_3$)

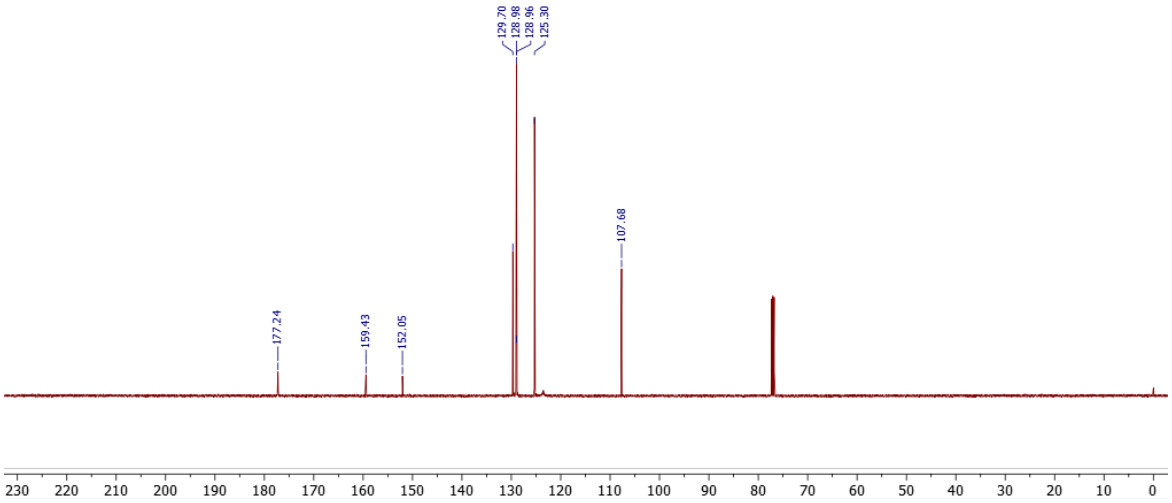

123, 5-(3,5-dimethylphenyl)furan-2-carbaldehyde

^{1}H NMR (500 MHz, $CDCl_3$)

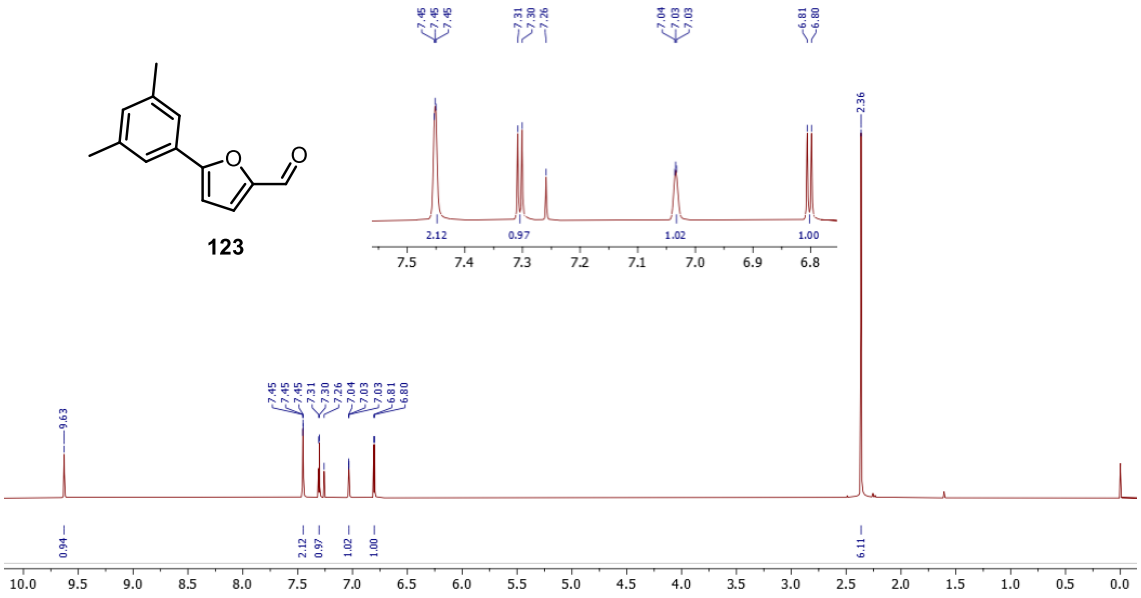

^{13}C NMR (500 MHz, $CDCl_3$)

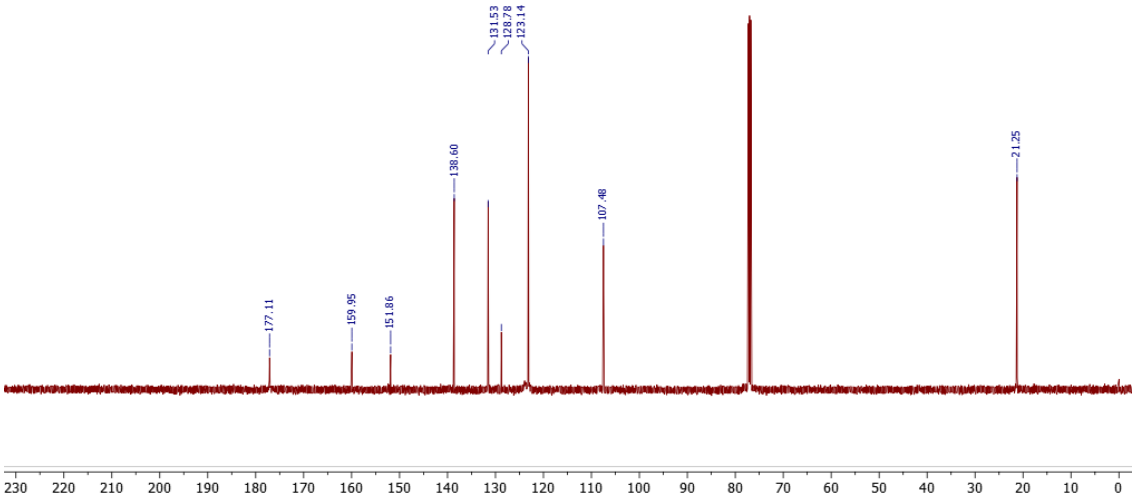

124, 5-(4-(*tert*-butyl)phenyl)furan-2-carbaldehyde

^{1}H NMR (500 MHz, $CDCl_3$)

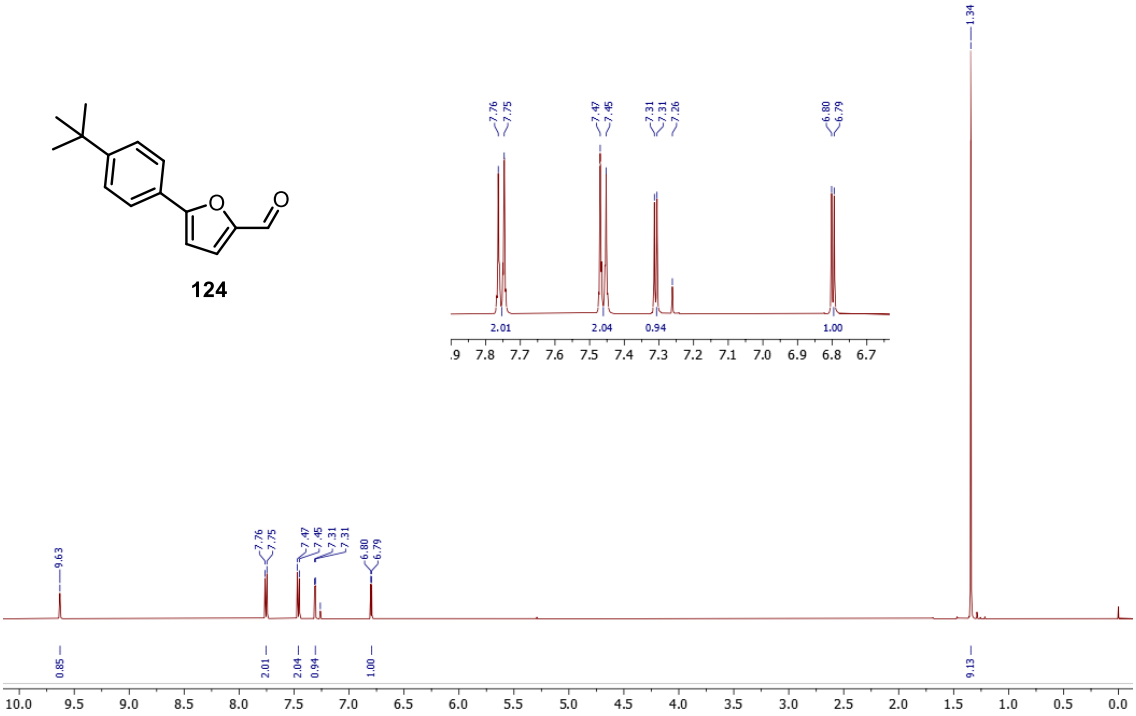

^{13}C NMR (500 MHz, $CDCl_3$)

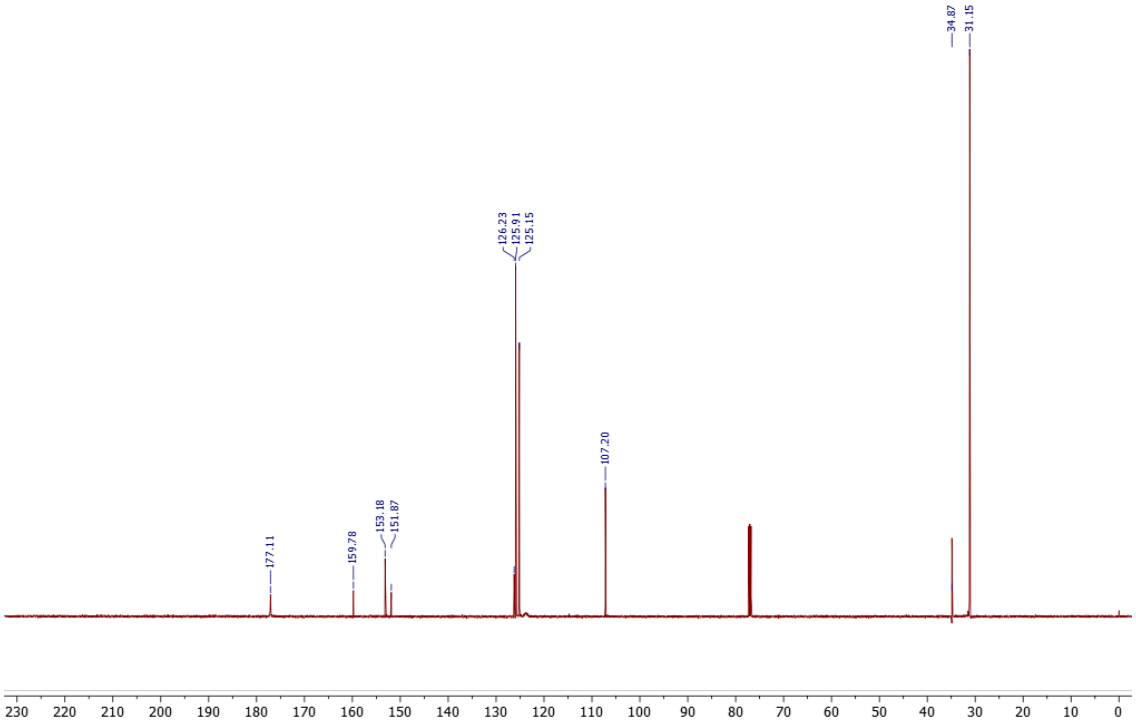

125, 5-(4-methoxyphenyl)furan-2-carbaldehyde

^{1}H NMR (500 MHz, $CDCl_3$)

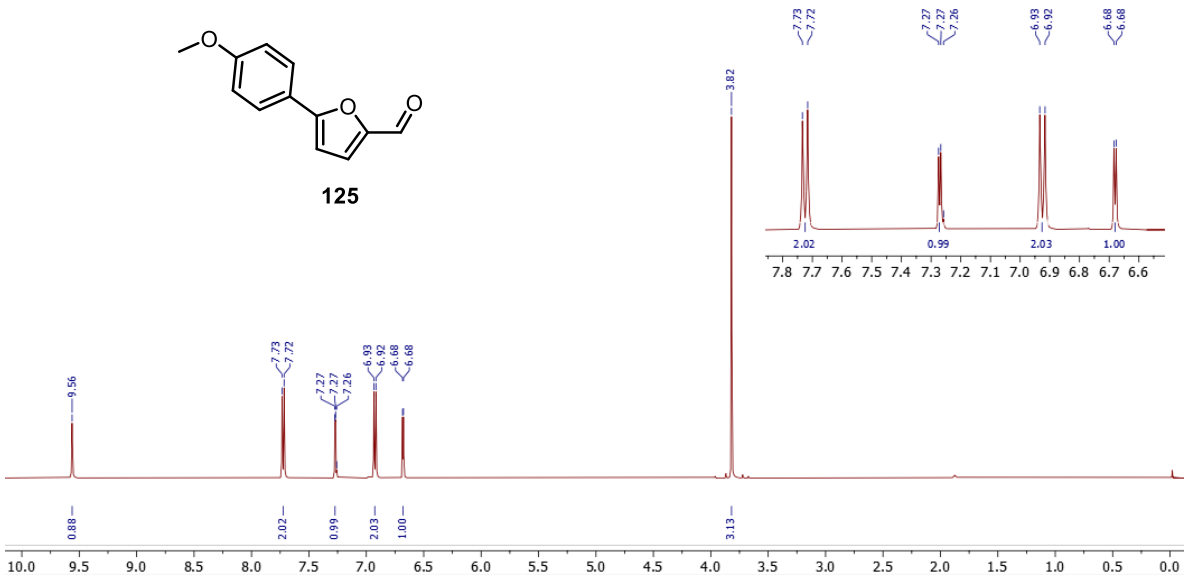

^{13}C NMR (500 MHz, $CDCl_3$)

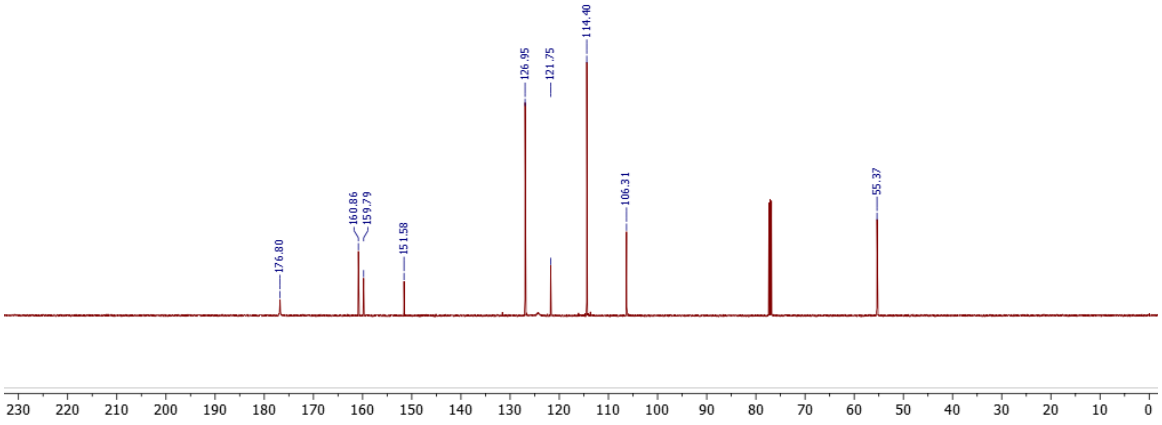

126, 5-(4-(diphenylamino)phenyl)furan-2-carbaldehyde

^{1}H NMR (500 MHz, $CDCl_3$)

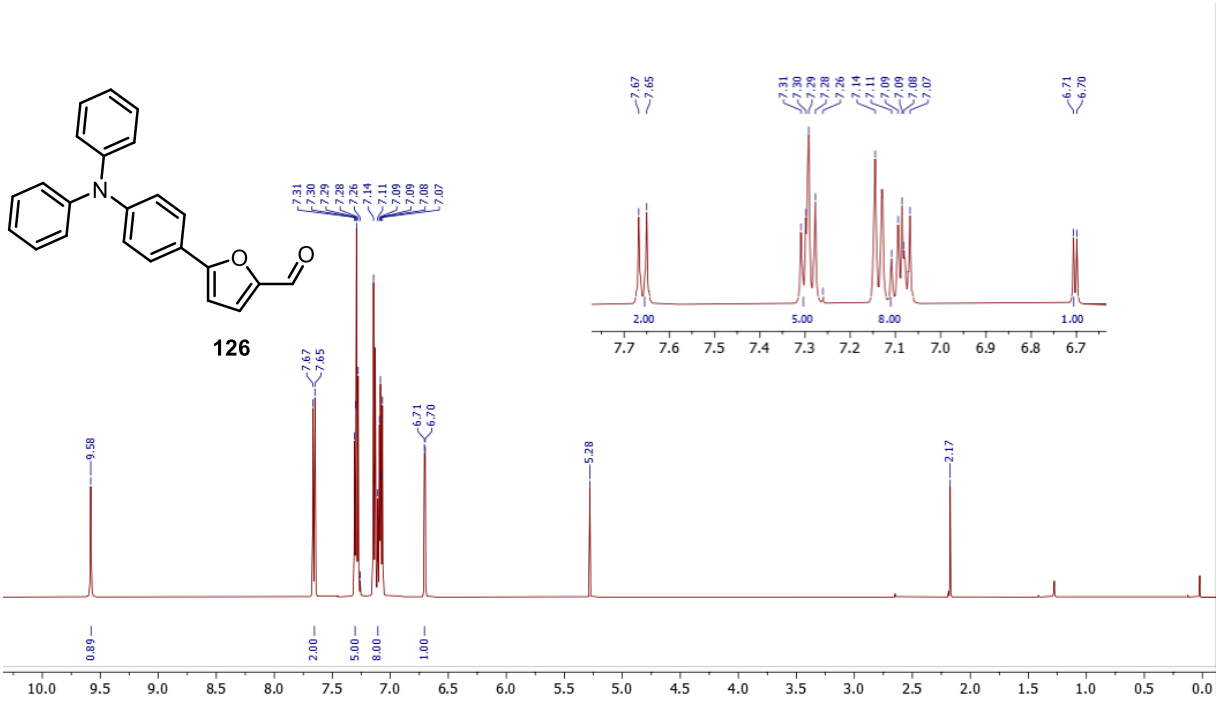

^{13}C NMR (500 MHz, $CDCl_3$)

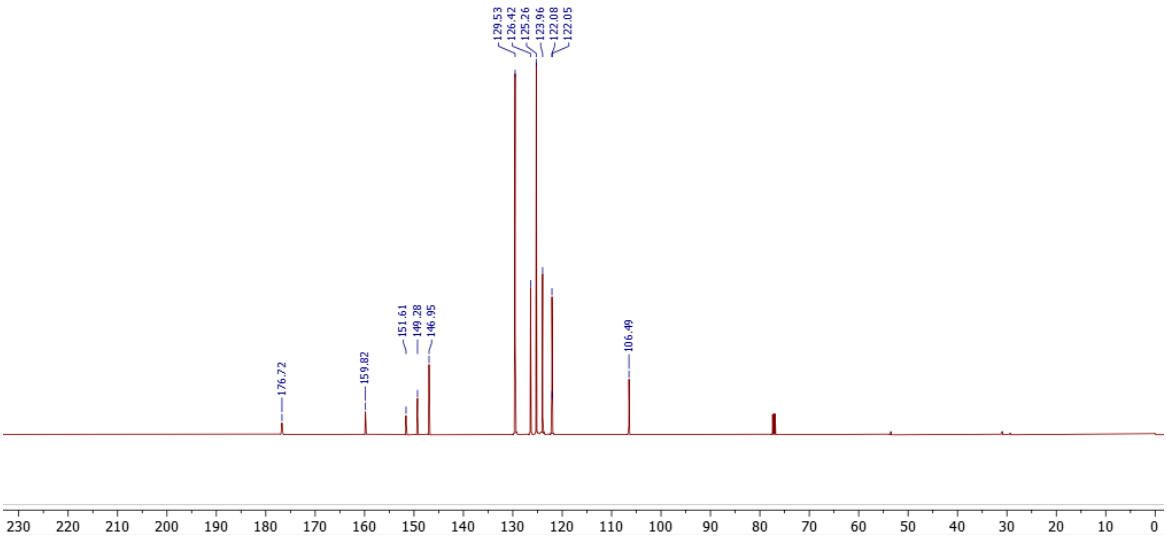

127, 5-(4-(trifluoromethyl)phenyl)furan-2-carbaldehyde

^{1}H NMR (500 MHz, $CDCl_3$)

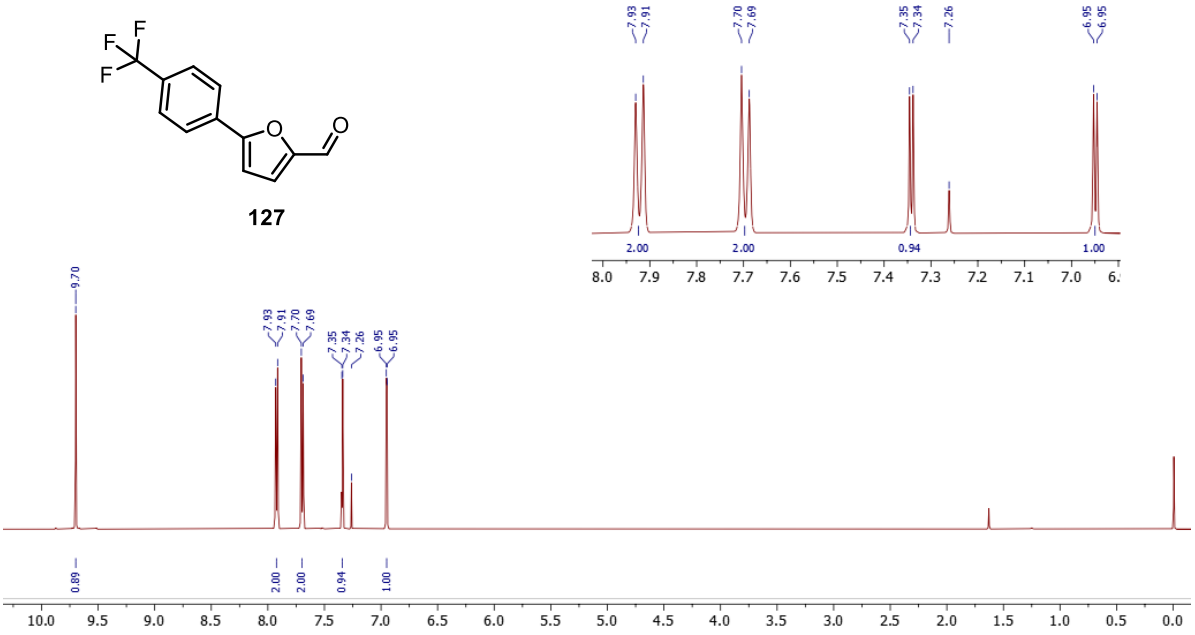

^{13}C NMR (500 MHz, $CDCl_3$)

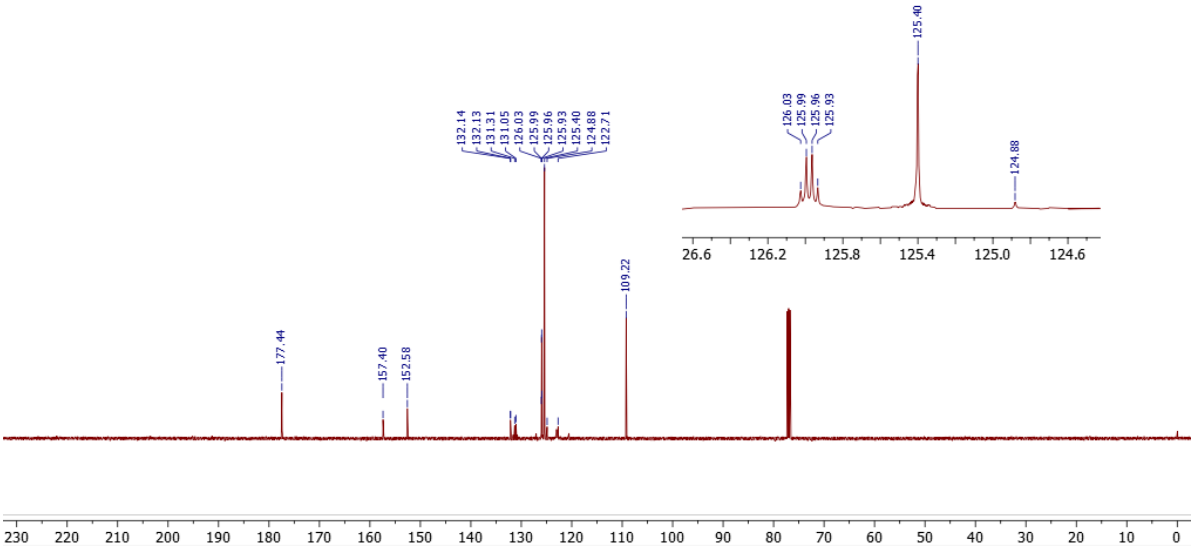

128, 5-(4-nitrophenyl)furan-2-carbaldehyde

^{1}H NMR (500 MHz, $CDCl_3$)

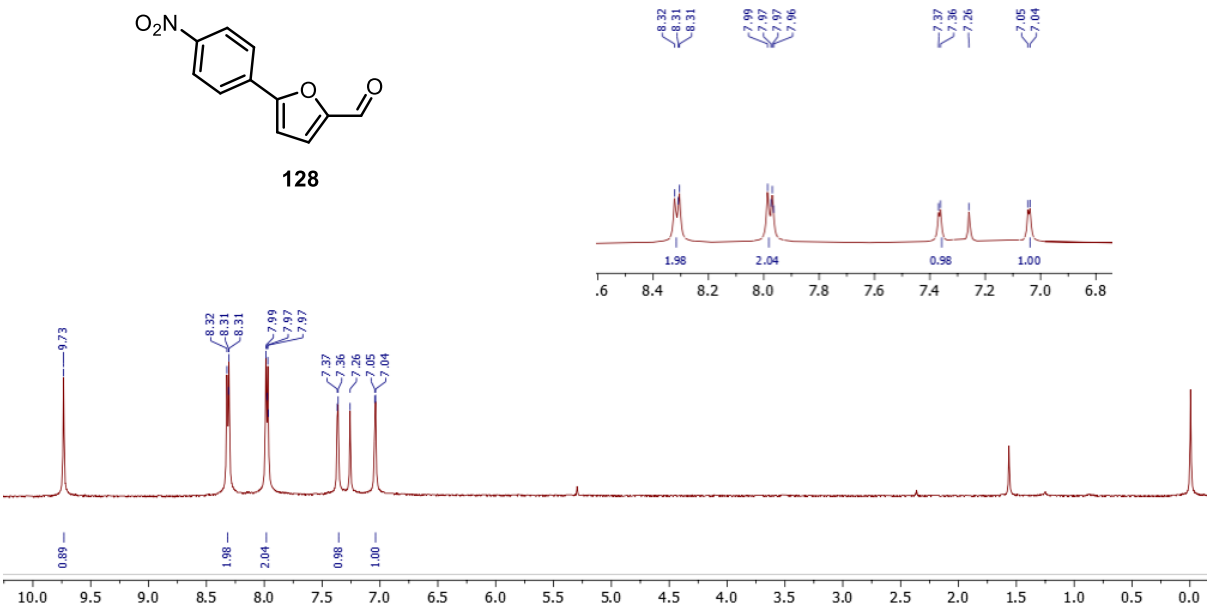

^{13}C NMR (500 MHz, $CDCl_3$)

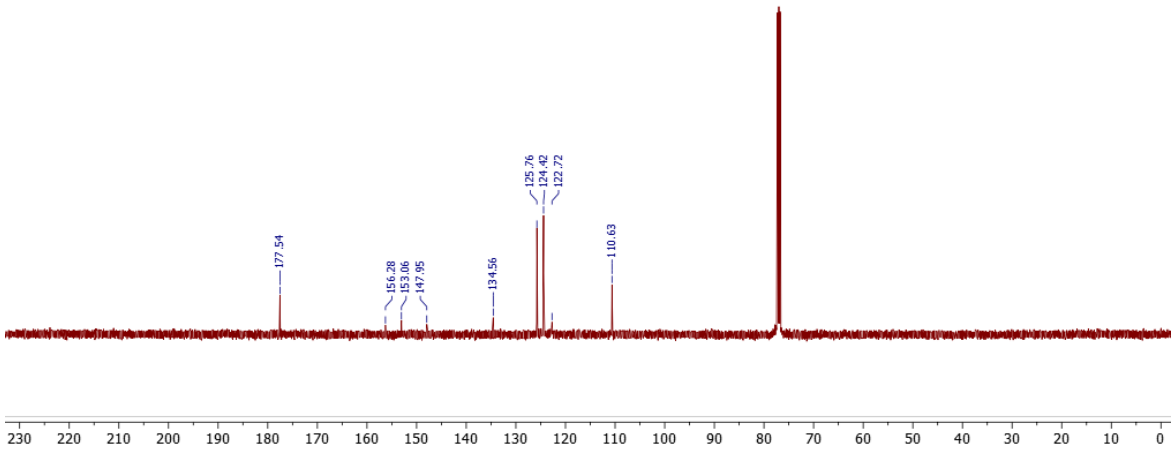

131, 5-(thiophen-2-yl)furan-2-carbonitrile

^{1}H NMR (500 MHz, $CDCl_3$)

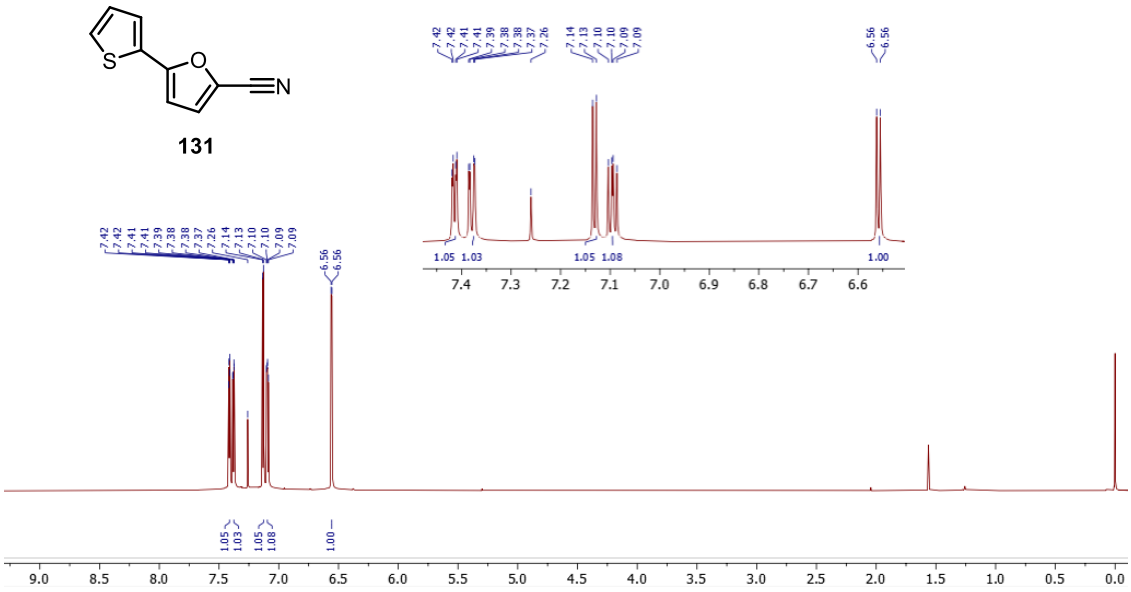

^{13}C NMR (500 MHz, $CDCl_3$)

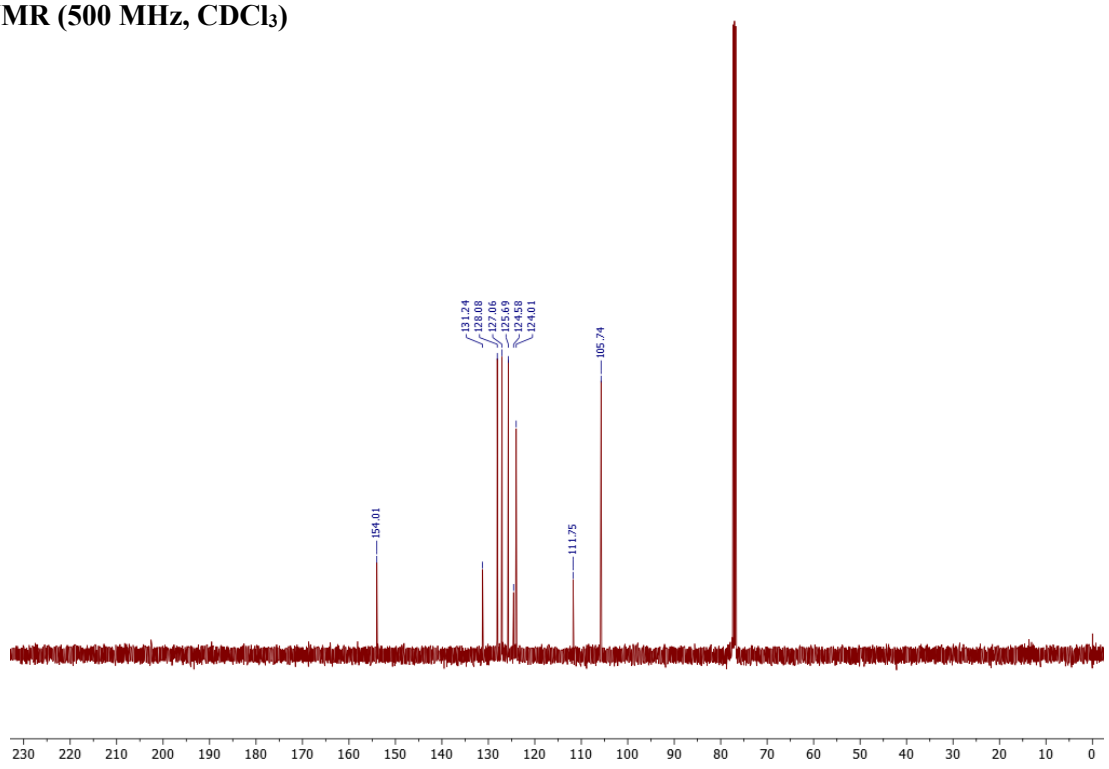

132, 5-phenylfuran-2-carbonitrile

^{1}H NMR (500 MHz, $CDCl_3$)

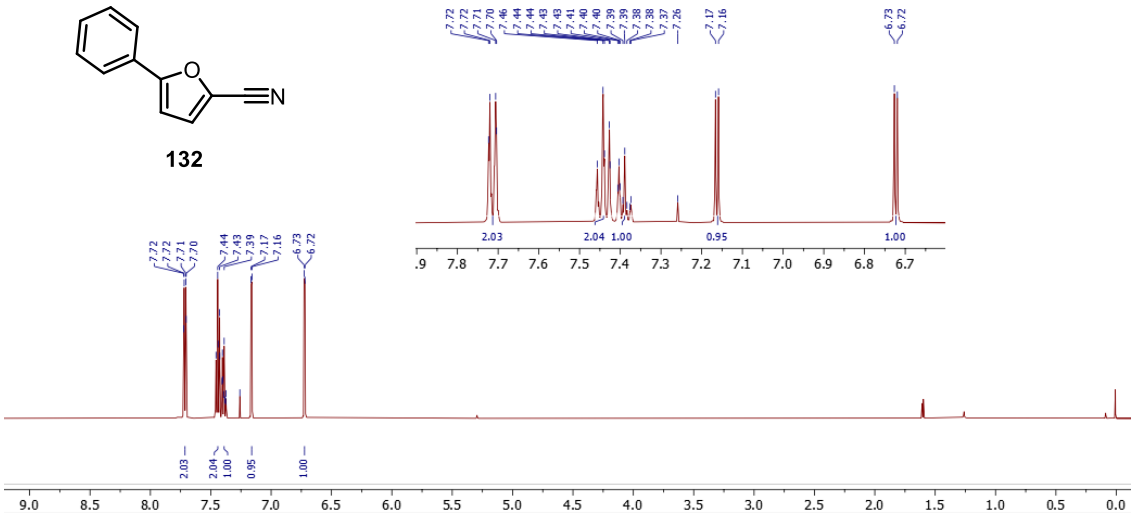

^{13}C NMR (500 MHz, $CDCl_3$)

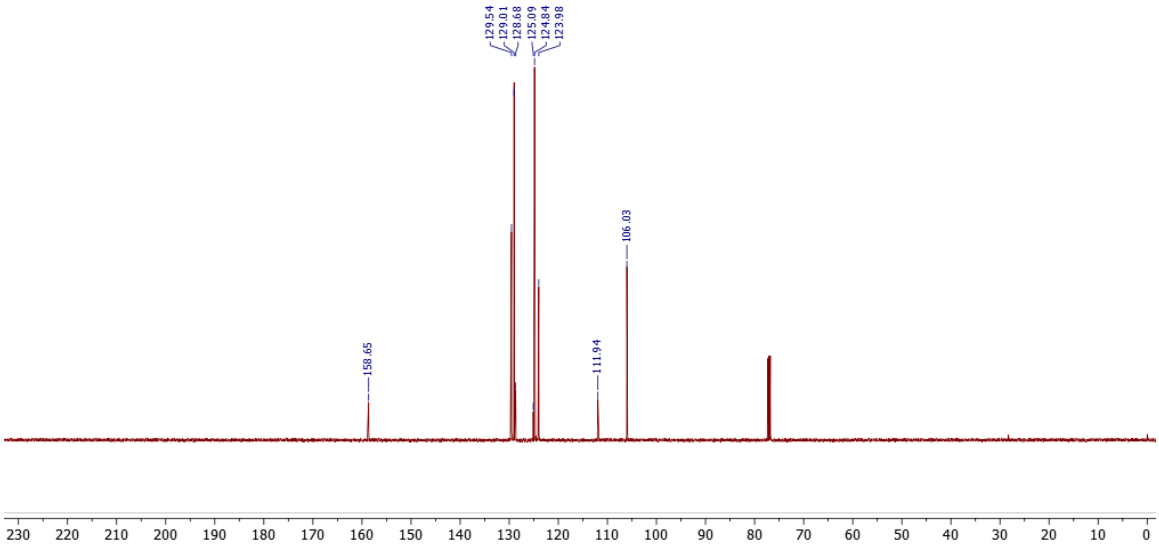

133, 5-(3,5-dimethylphenyl)furan-2-carbonitrile

^{1}H NMR (500 MHz, $CDCl_3$)

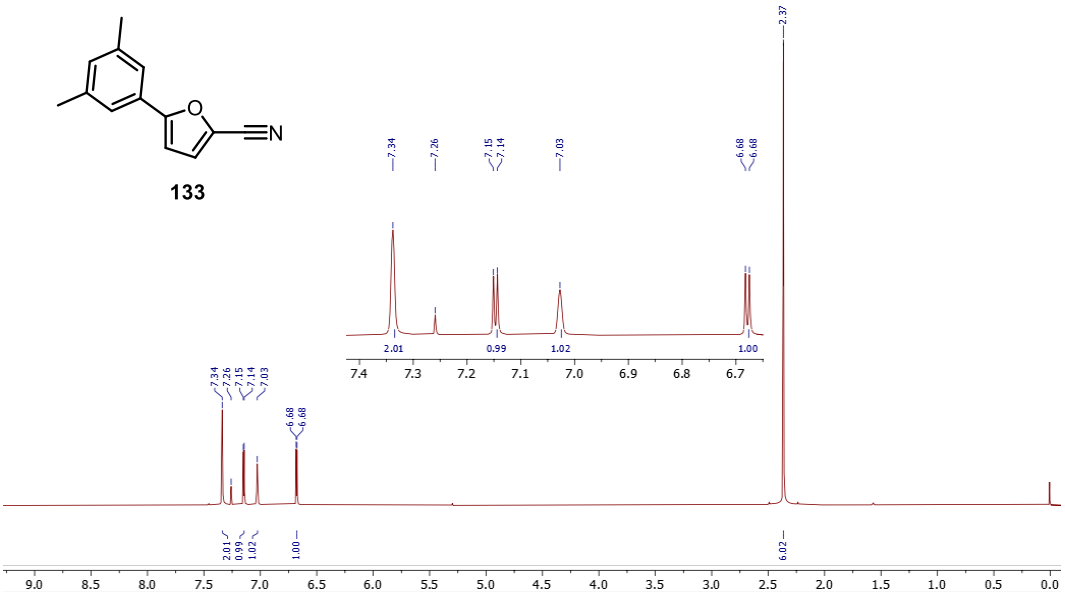

^{13}C NMR (500 MHz, $CDCl_3$)

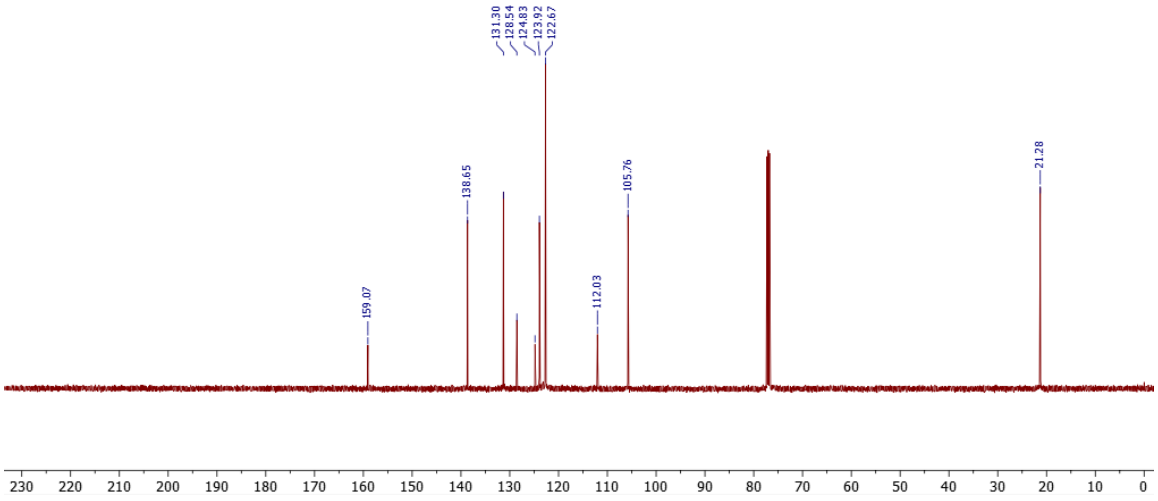

134, 5-(4-(*tert*-butyl)phenyl)furan-2-carbonitrile

^{1}H NMR (500 MHz, $CDCl_3$)

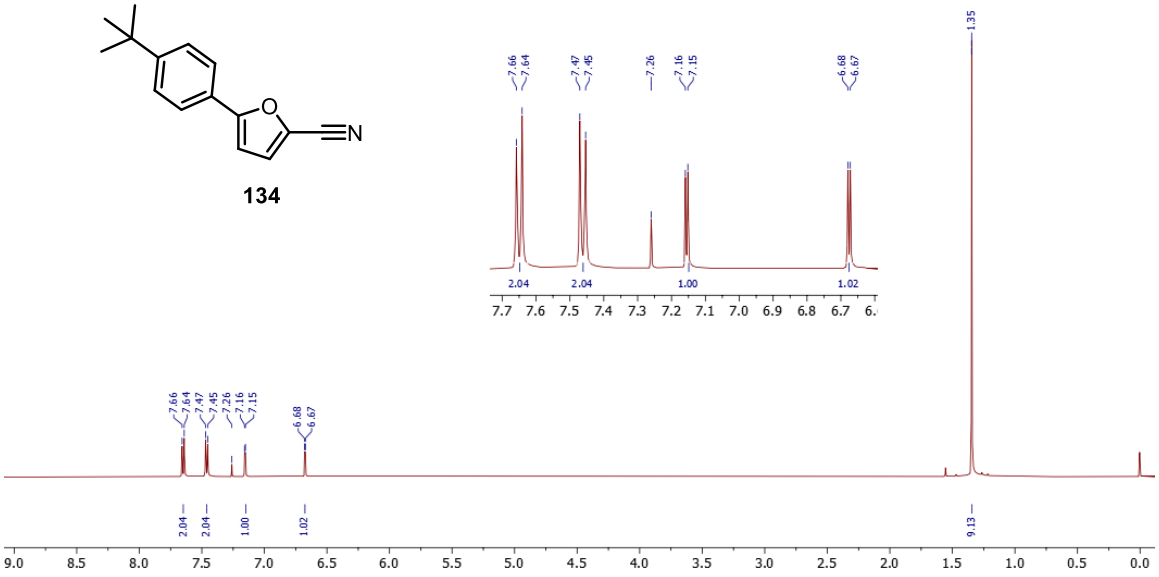

^{13}C NMR (500 MHz, $CDCl_3$)

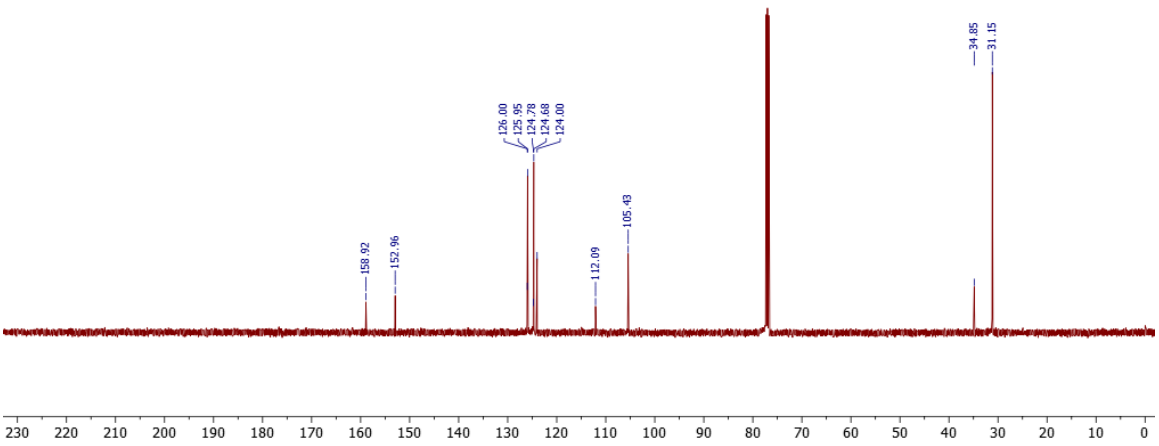

135, 5-(4-methoxyphenyl)furan-2-carbonitrile

^{1}H NMR (500 MHz, $CDCl_3$)

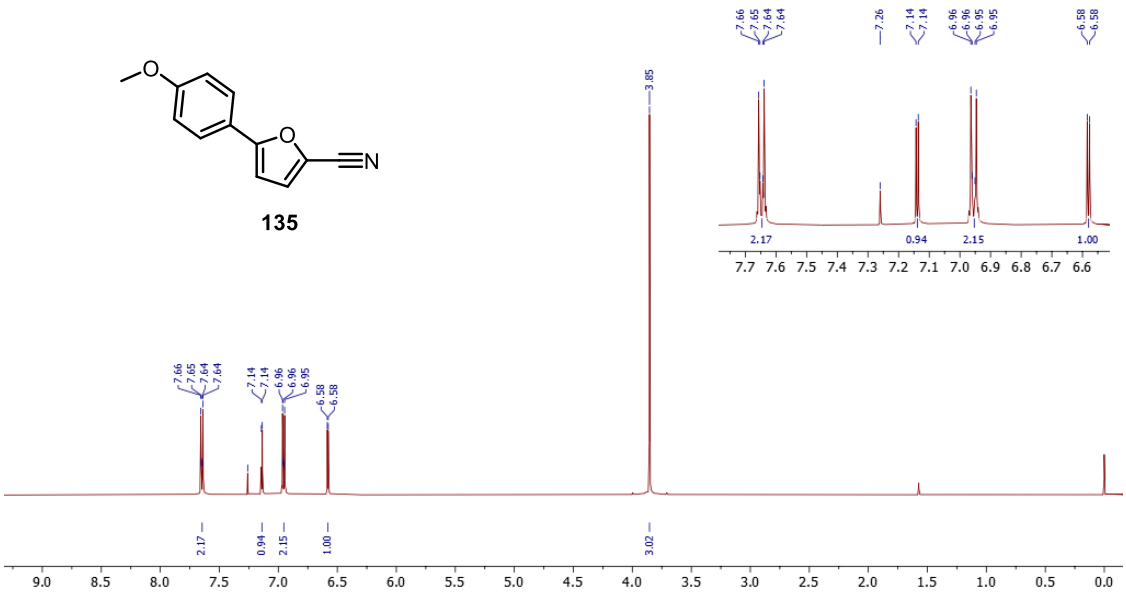

^{13}C NMR (500 MHz, $CDCl_3$)

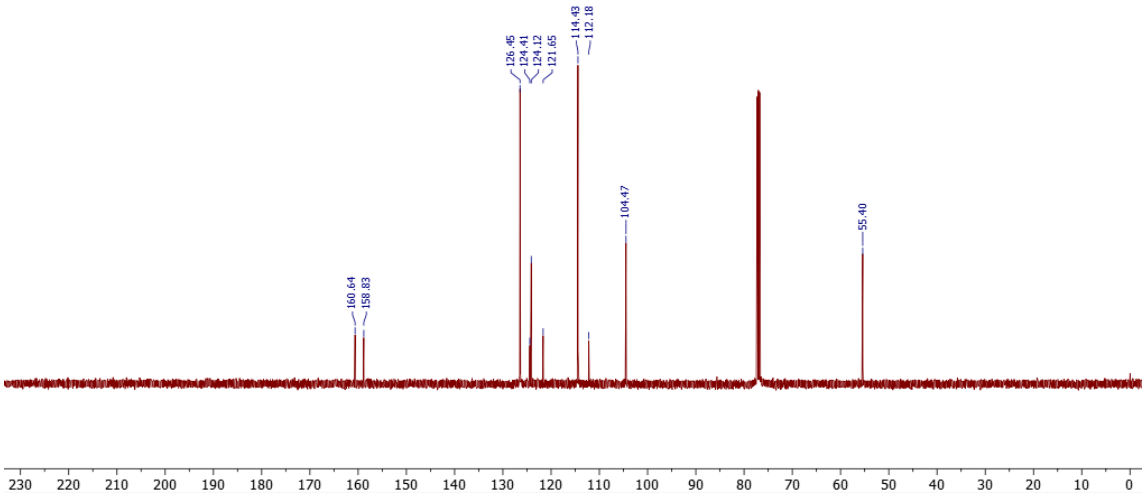

136, 5-(4-(diphenylamino)phenyl)furan-2-carbonitrile

^{1}H NMR (500 MHz, $CDCl_3$)

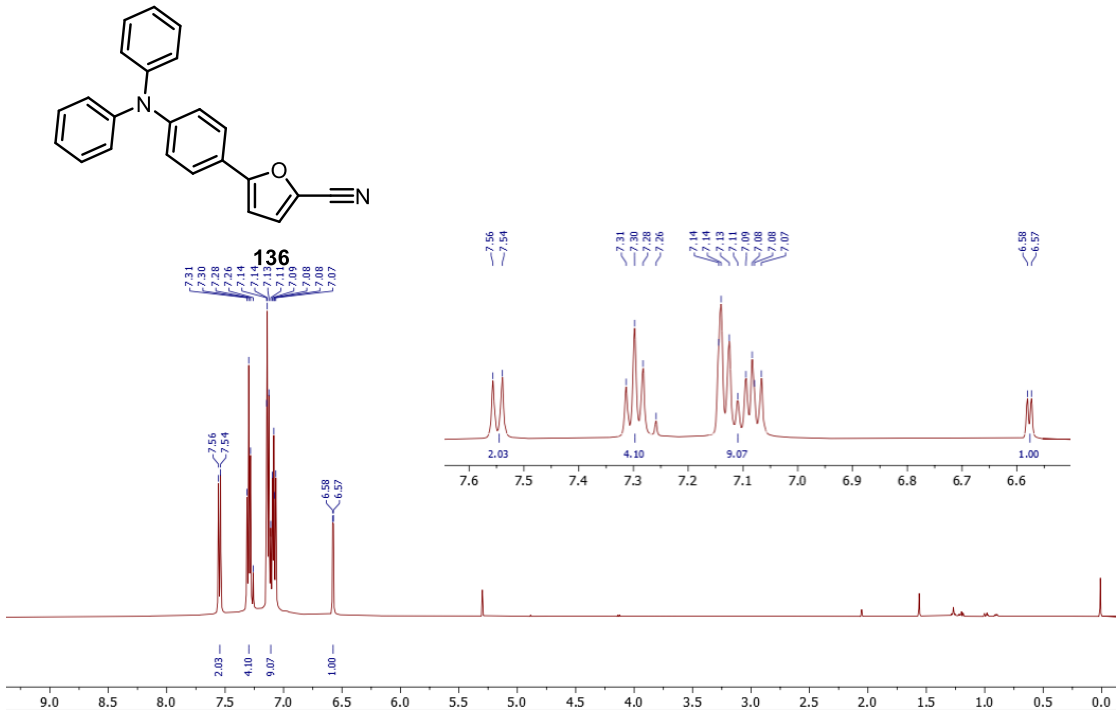

^{13}C NMR (500 MHz, $CDCl_3$)

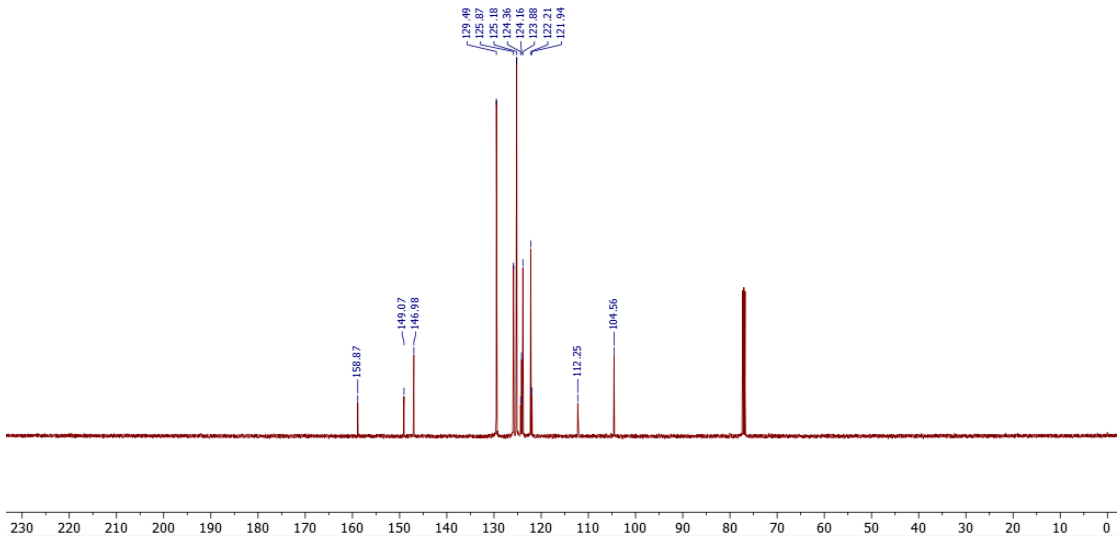

137, 5-(4-(trifluoromethyl)phenyl)furan-2-carbonitrile

^{1}H NMR (500 MHz, $CDCl_3$)

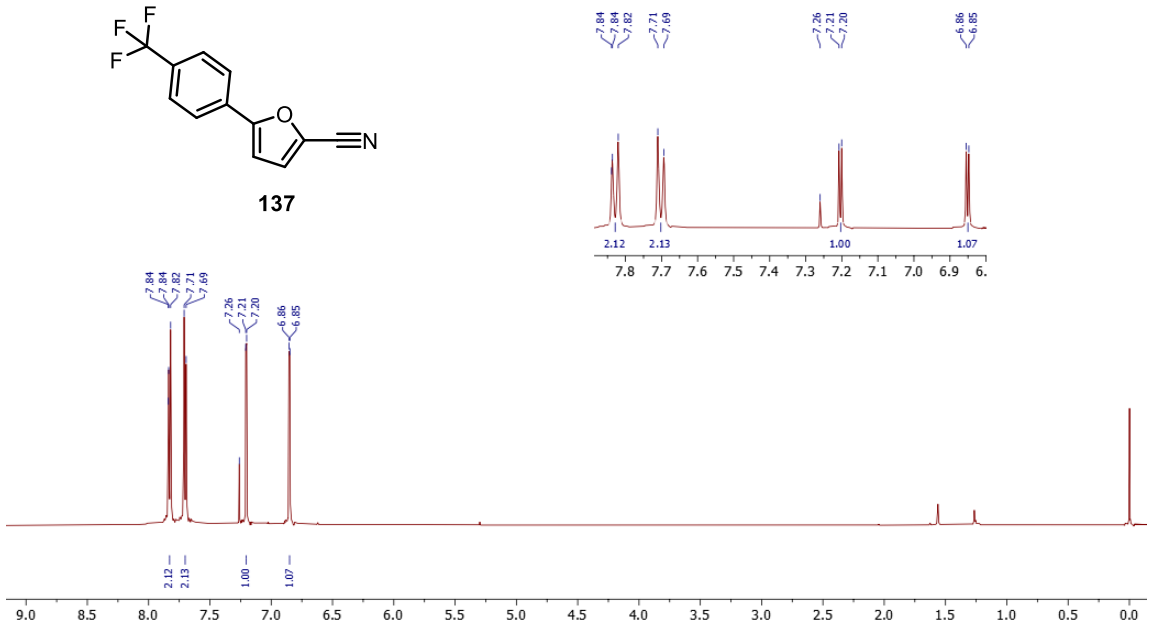

^{13}C NMR (500 MHz, $CDCl_3$)

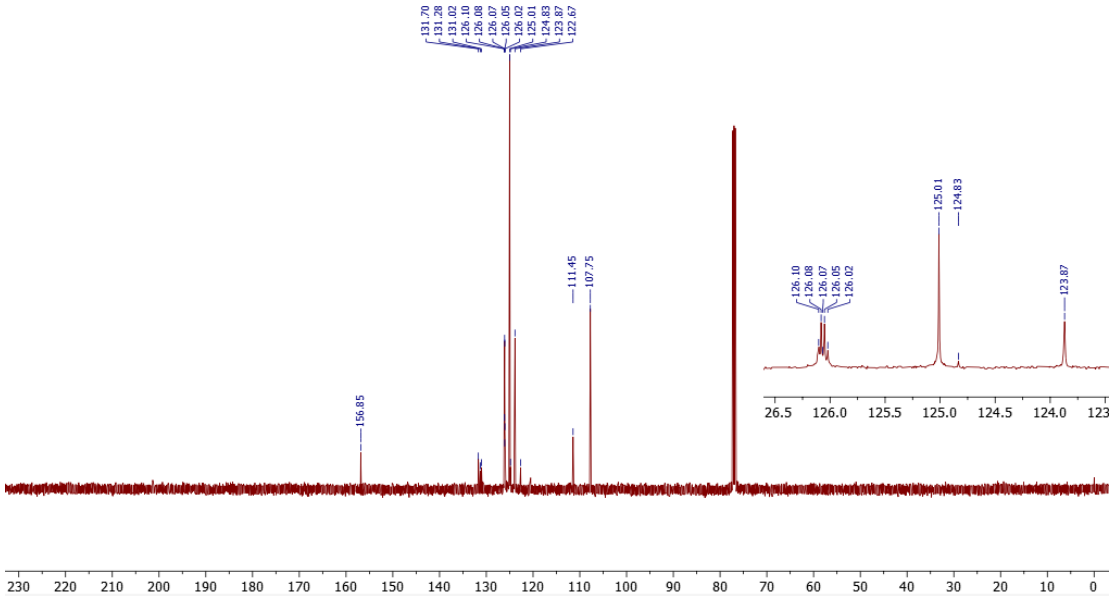

138, 5-(4-nitrophenyl)furan-2-carbonitrile:

^{1}H NMR (500 MHz, $CDCl_3$)

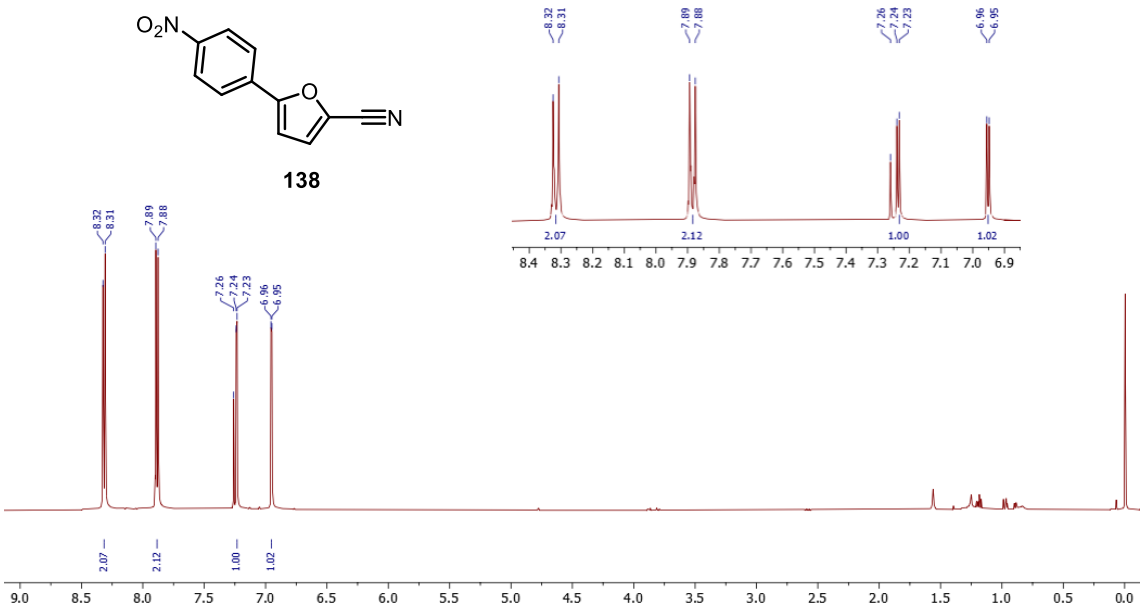

^{13}C NMR (500 MHz, $CDCl_3$)

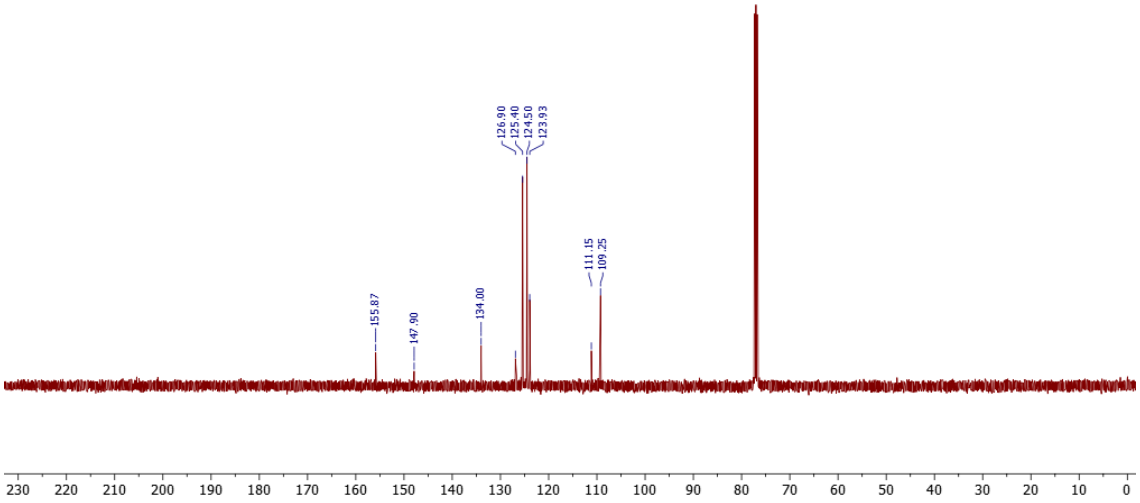

139, 5-(thiophen-2-yl)furan-2-carboxylic acid

^{1}H NMR (500 MHz, DMSO-d6)

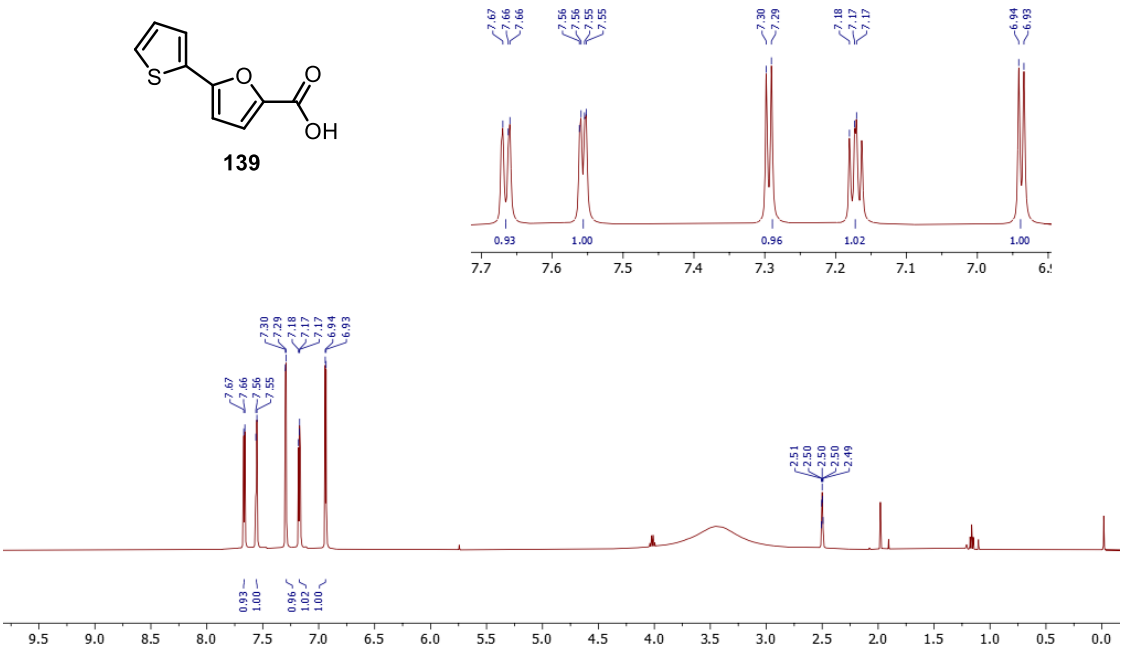

^{13}C NMR (500 MHz, DMSO-d6)

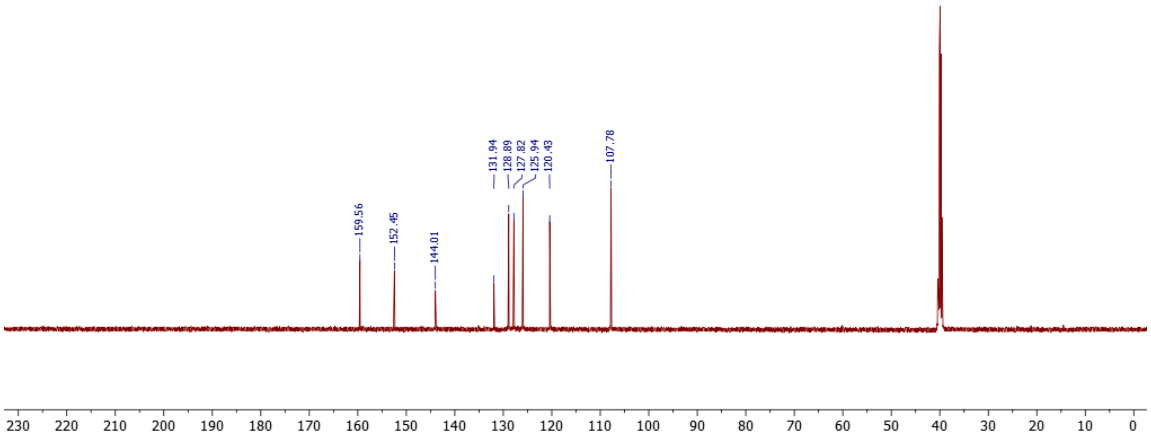

140, 5-phenylfuran-2-carboxylic acid

^{1}H NMR (500 MHz, DMSO-d6)

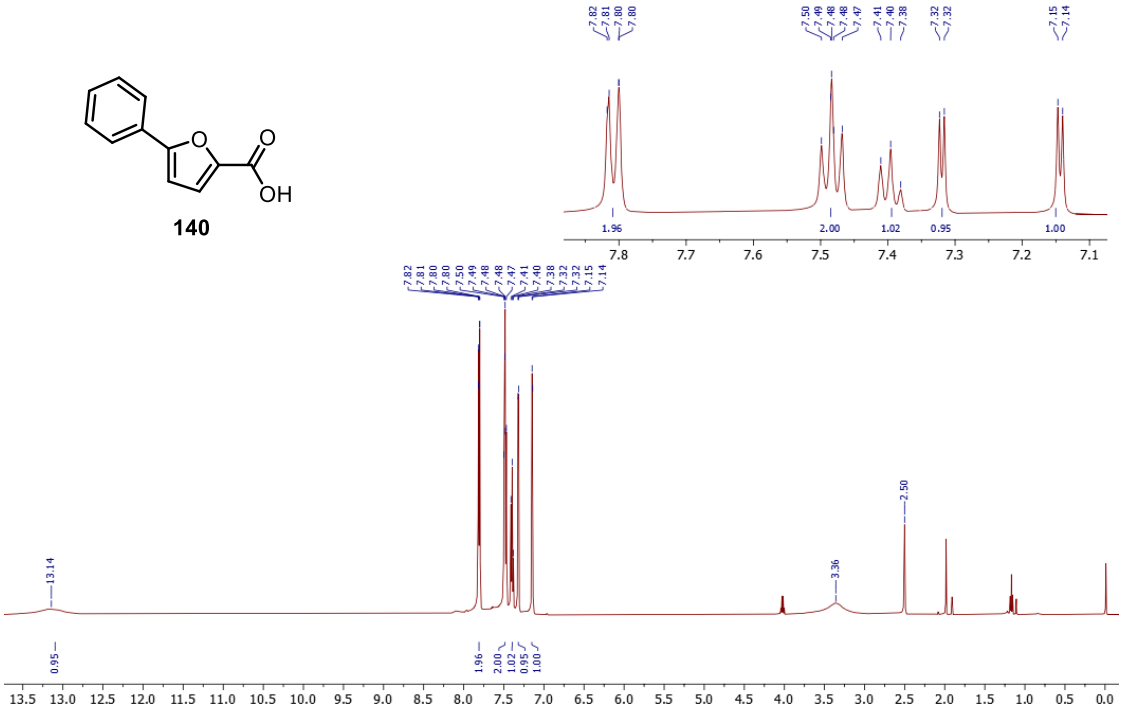

^{13}C NMR (500 MHz, DMSO-d6)

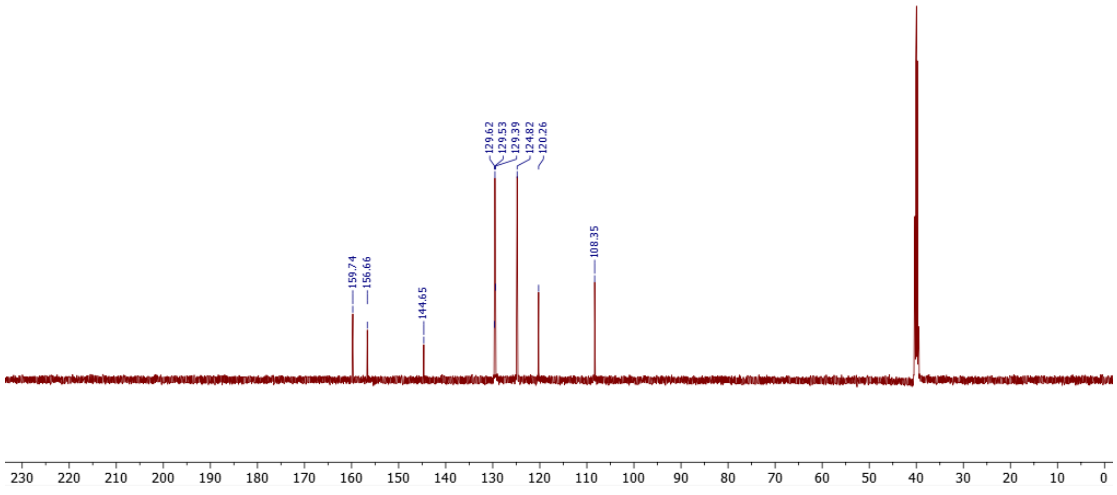

141, 5-(3,5-dimethylphenyl)furan-2-carboxylic acid

^{1}H NMR (500 MHz, DMSO-d6)

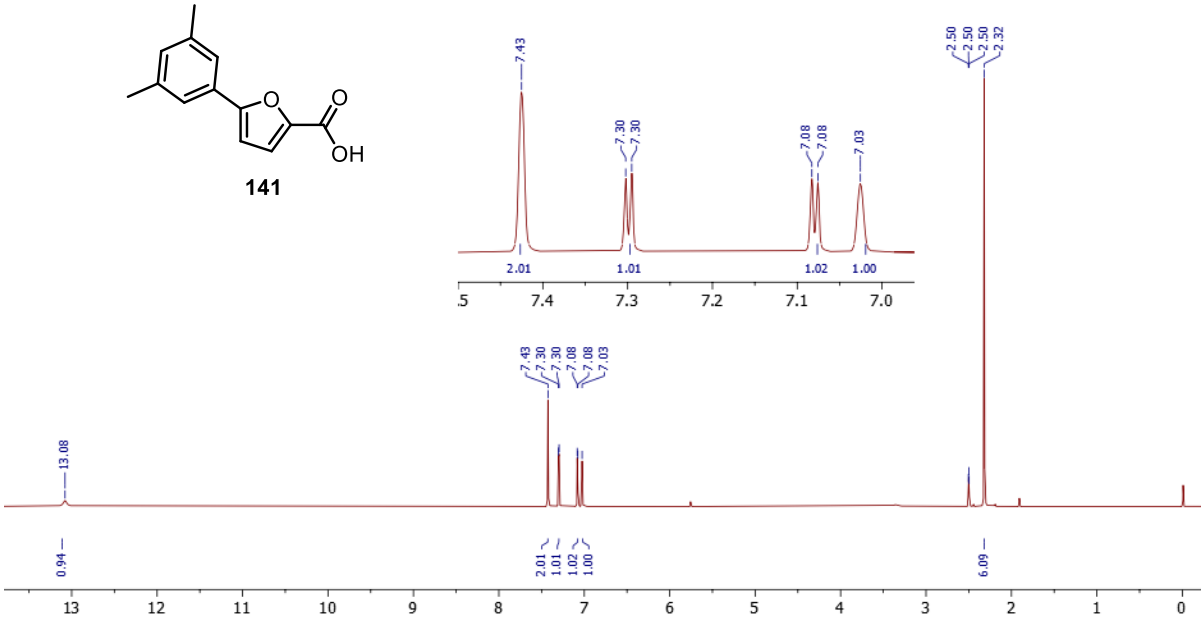

^{13}C NMR (500 MHz, DMSO-d6)

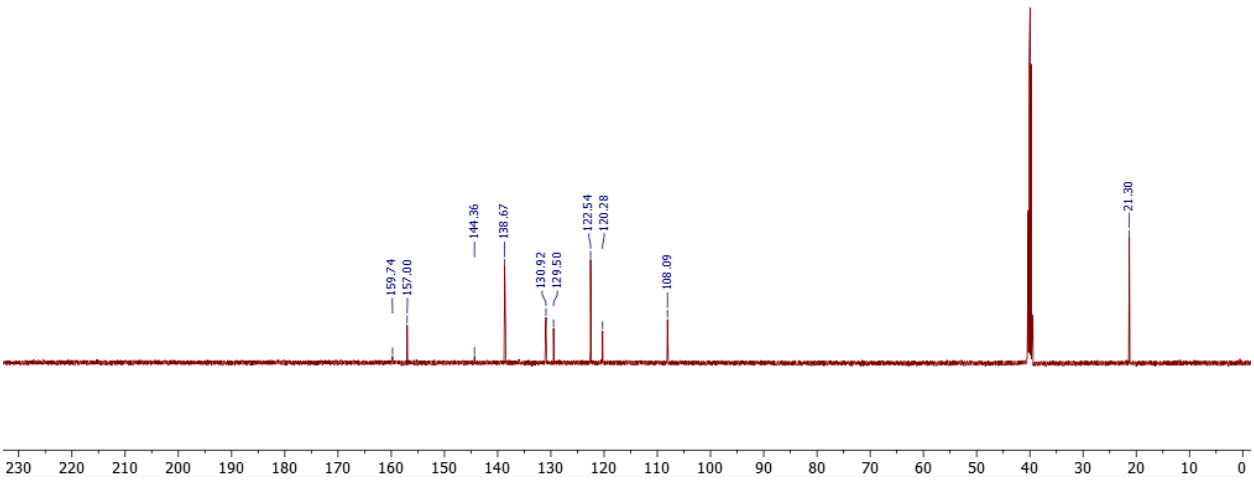

142, 5-(4-(*tert*-butyl)phenyl)furan-2-carboxylic acid

^{1}H NMR (500 MHz, DMSO-d6)

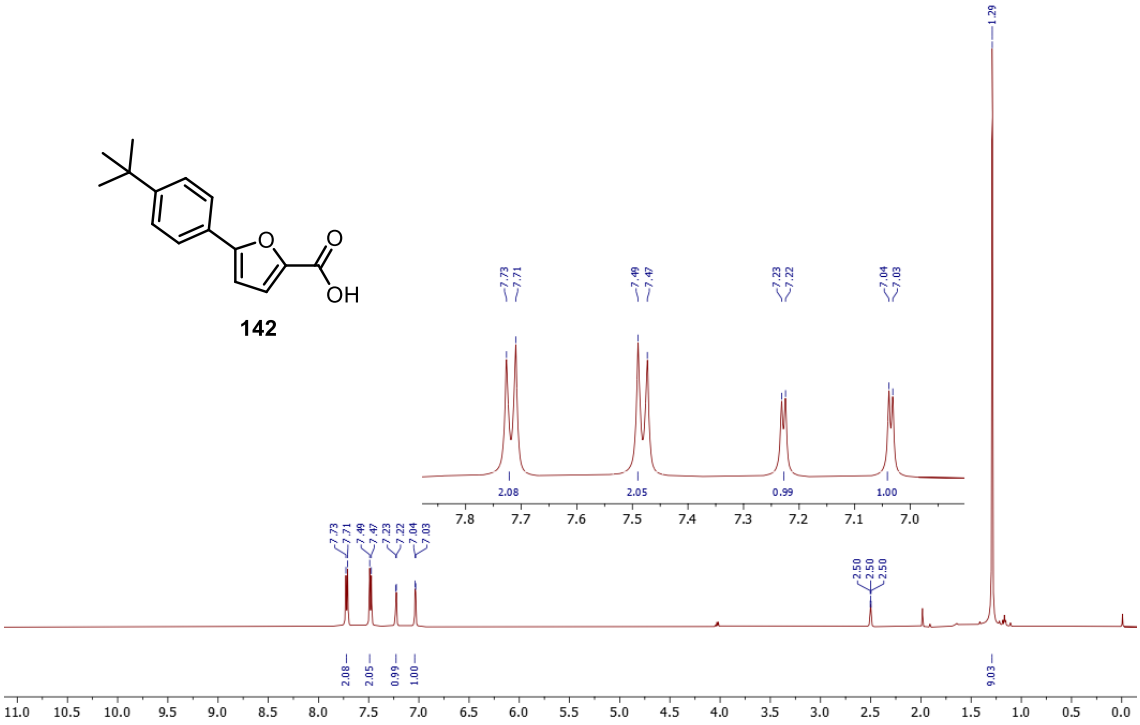

^{13}C NMR (500 MHz, DMSO-d6)

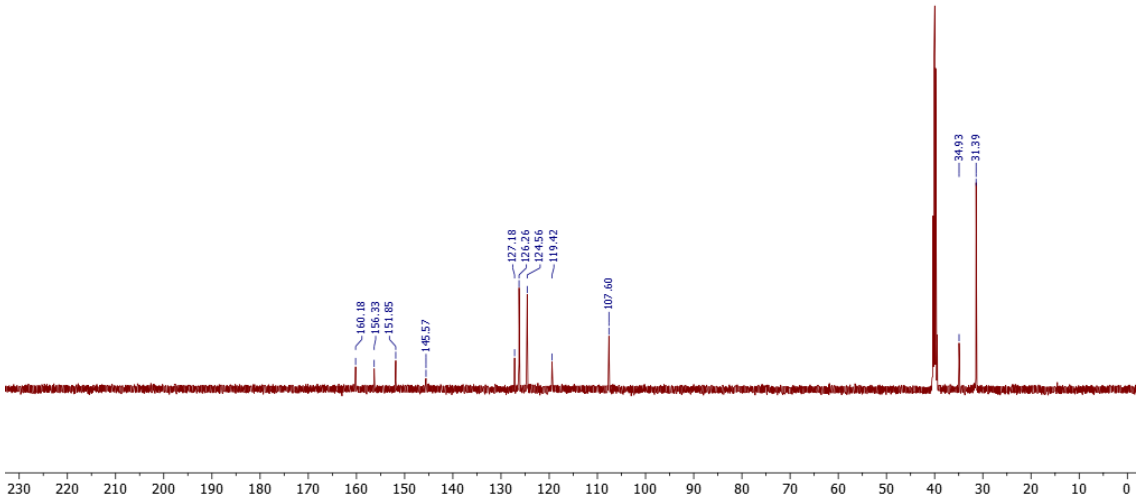

143, 5-(4-methoxyphenyl)furan-2-carboxylic acid

^{1}H NMR (500 MHz, DMSO-d6)

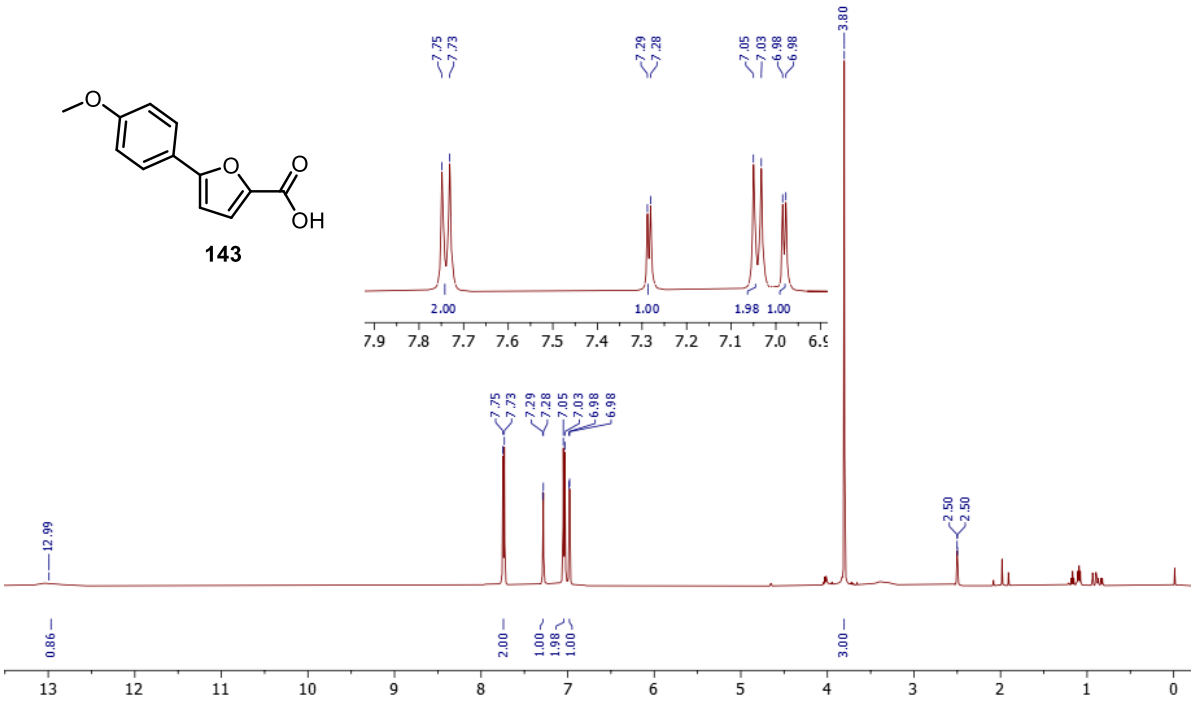

^{13}C NMR (500 MHz, DMSO-d6)

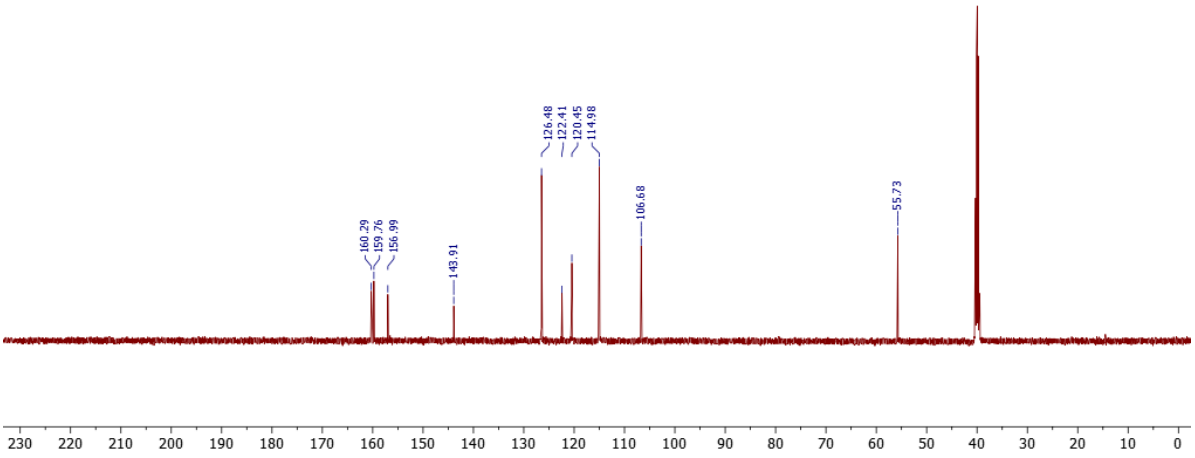

144, 5-(4-(diphenylamino)phenyl)furan-2-carboxylic acid

^{1}H NMR (500 MHz, DMSO-d6)

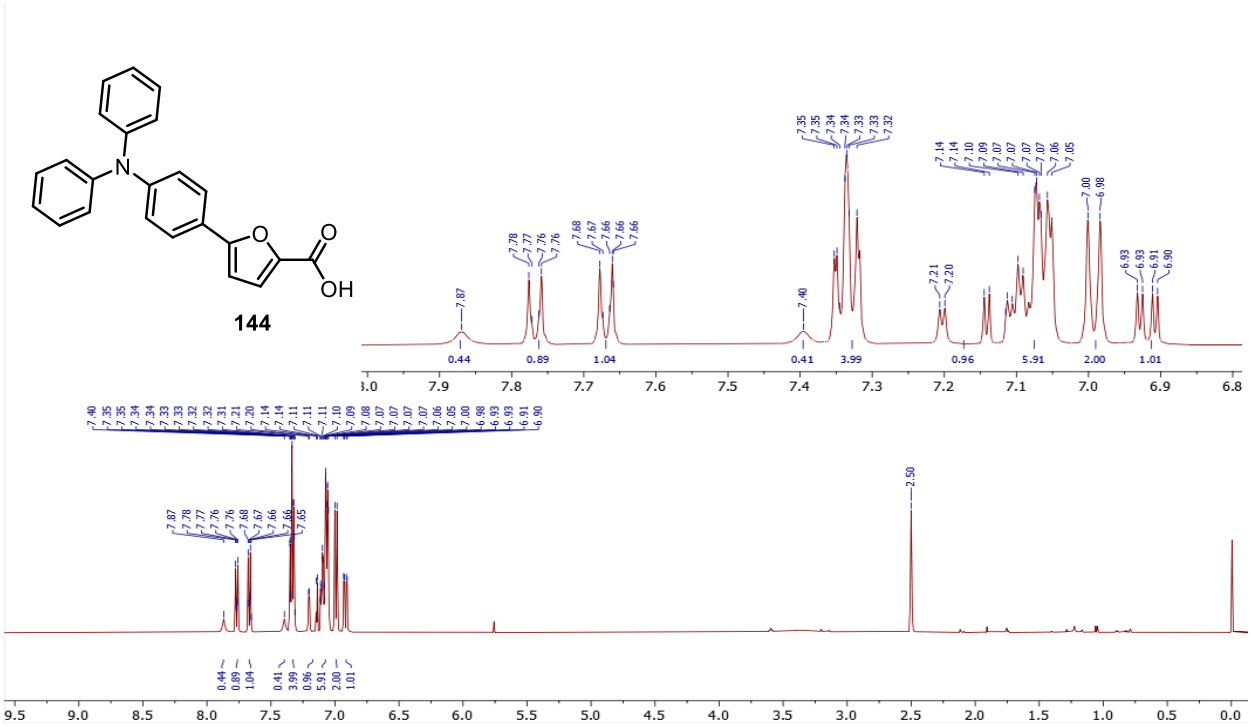

^{13}C NMR (500 MHz, DMSO-d6)

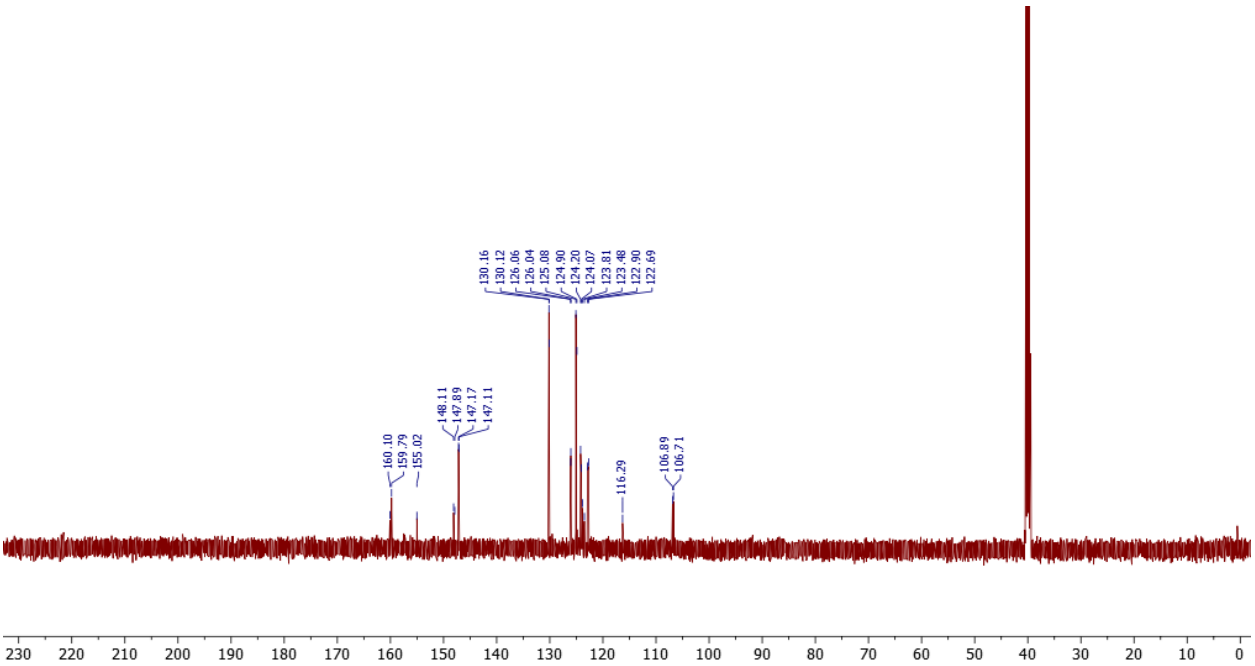

145, 5-(4-(trifluoromethyl)phenyl)furan-2-carboxylic acid

^{1}H NMR (500 MHz, DMSO-d6)*

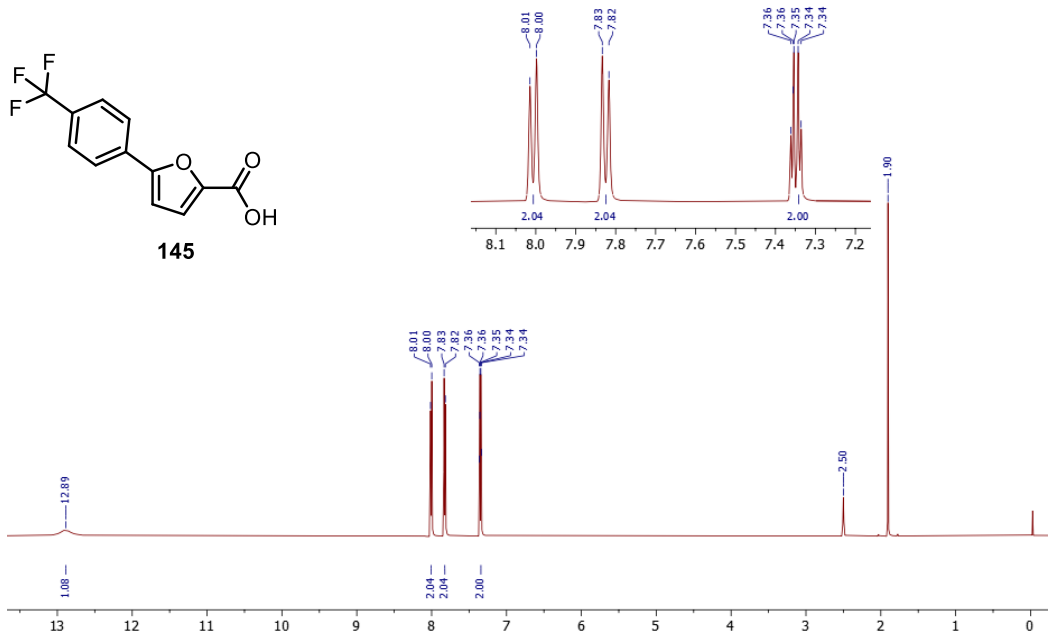

^{13}C NMR (500 MHz, DMSO-d6)*

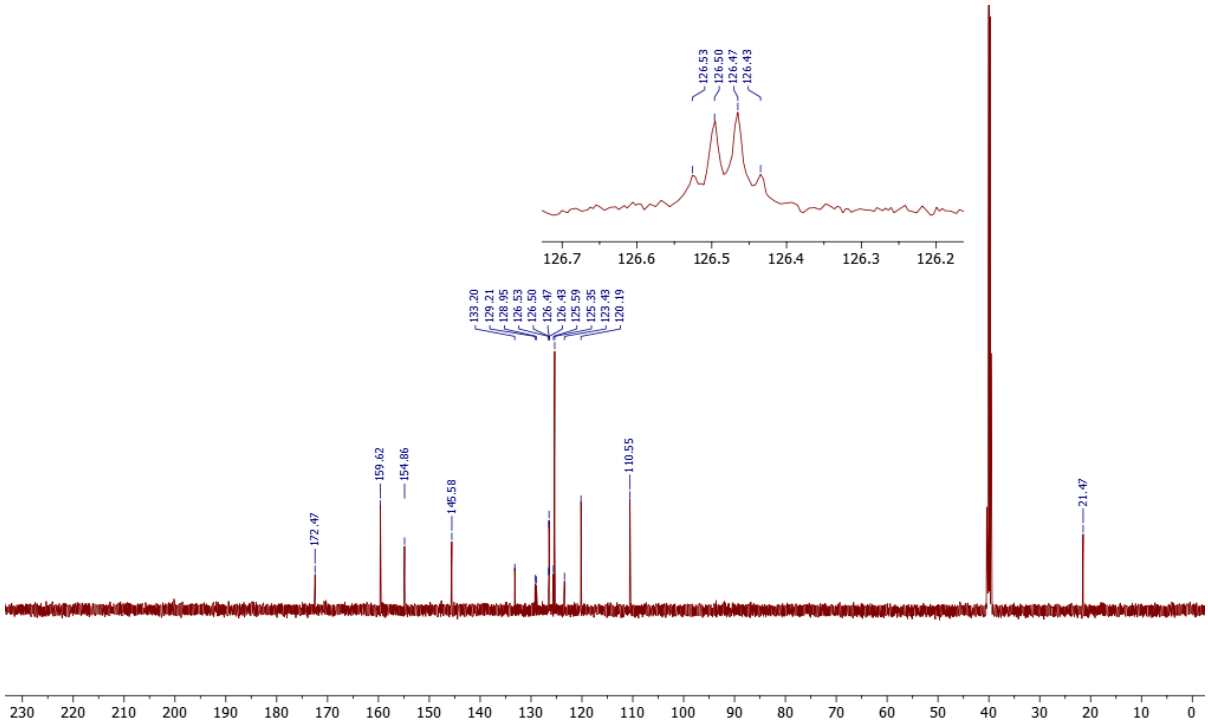

*** ^{1}H NMR peak at 1.90 ppm and ^{13}C NMR peaks at 172.47 and 21.47 ppm relate to acetic acid.**

146, 5-(4-nitrophenyl)furan-2-carboxylic acid

^{1}H NMR (500 MHz, DMSO-d6)

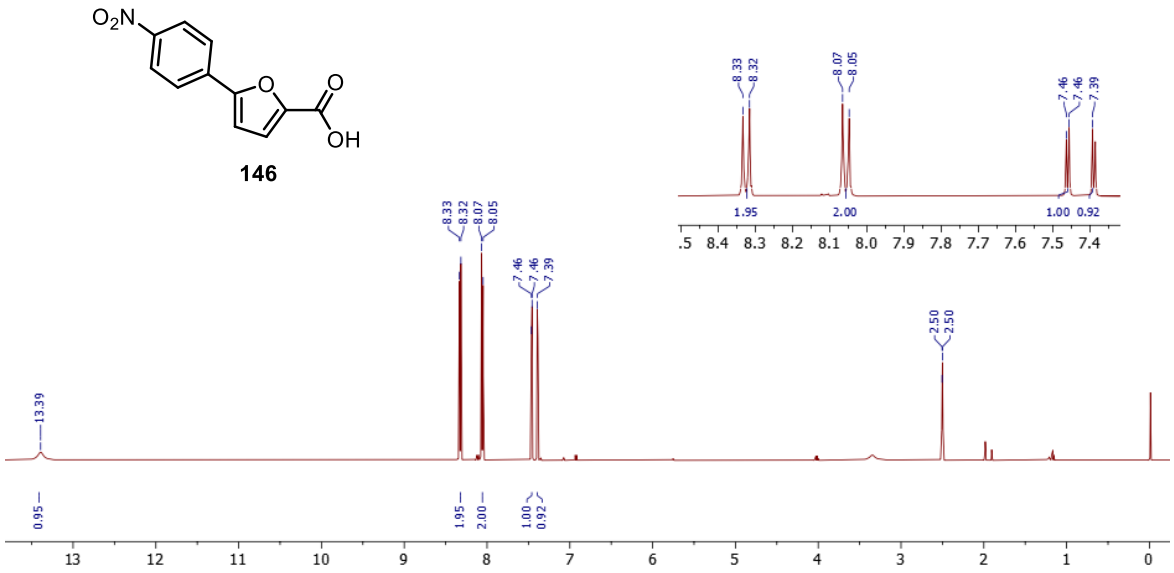

^{13}C NMR (500 MHz, DMSO-d6)

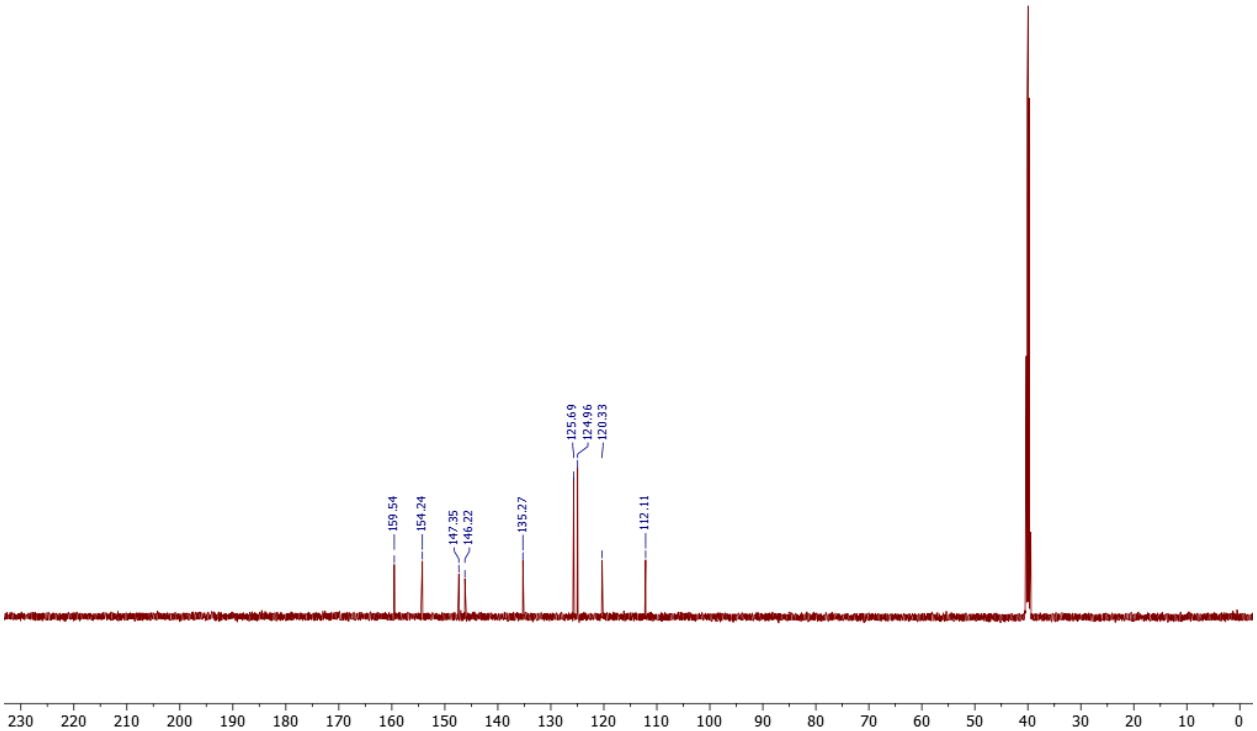

139OH, (5-(thiophen-2-yl)furan-2-yl)methanol:

^{1}H NMR (500 MHz, $CDCl_3$)

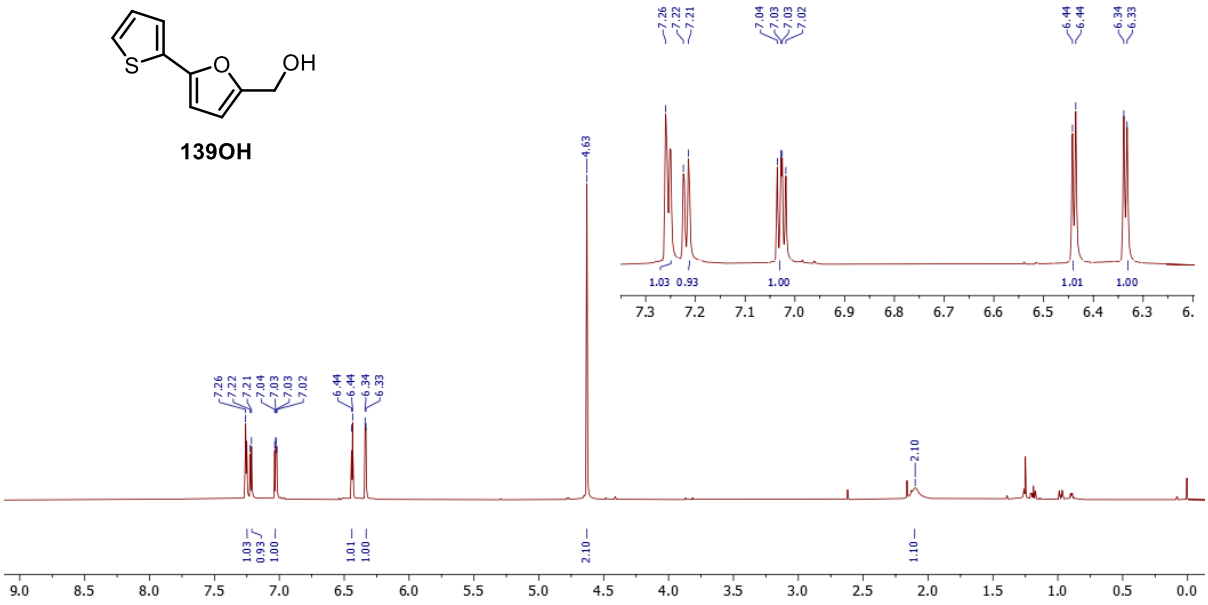

^{13}C NMR (500 MHz, $CDCl_3$)

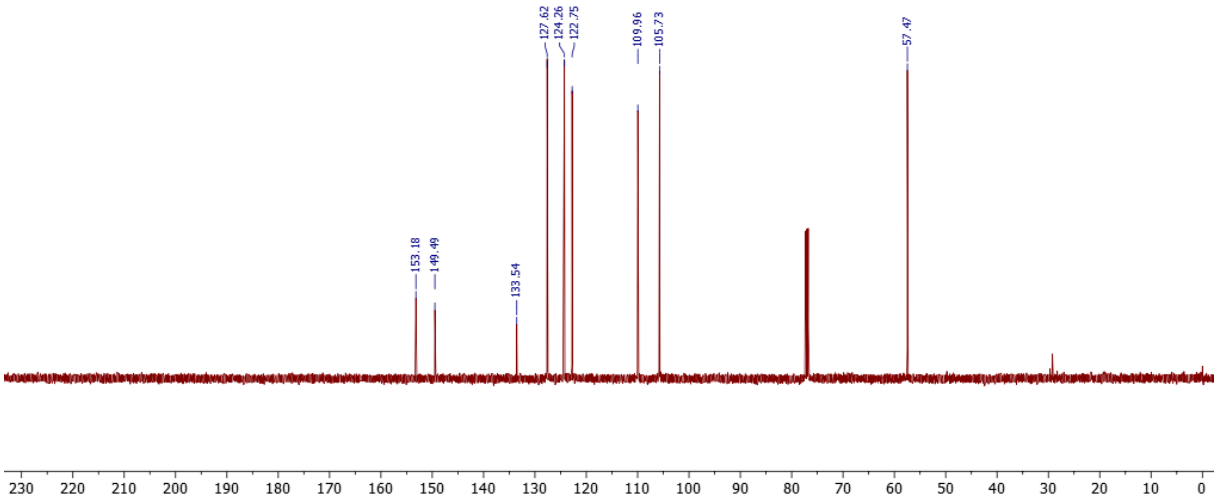

140OH, (5-phenylfuran-2-yl)methanol:

^{1}H NMR (500 MHz, $CDCl_3$)

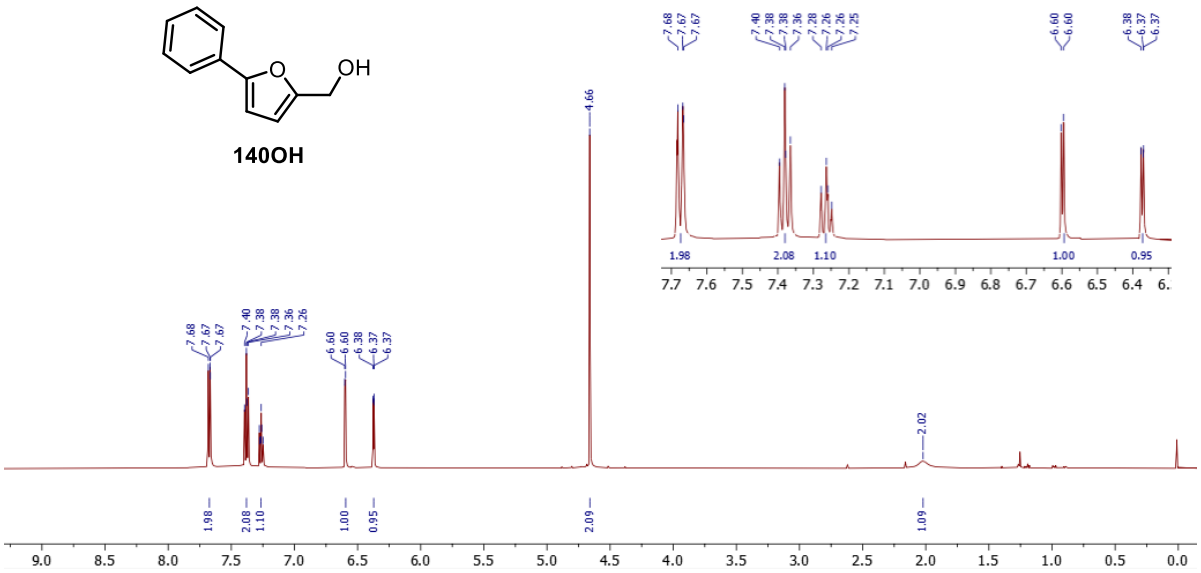

^{13}C NMR (500 MHz, $CDCl_3$)

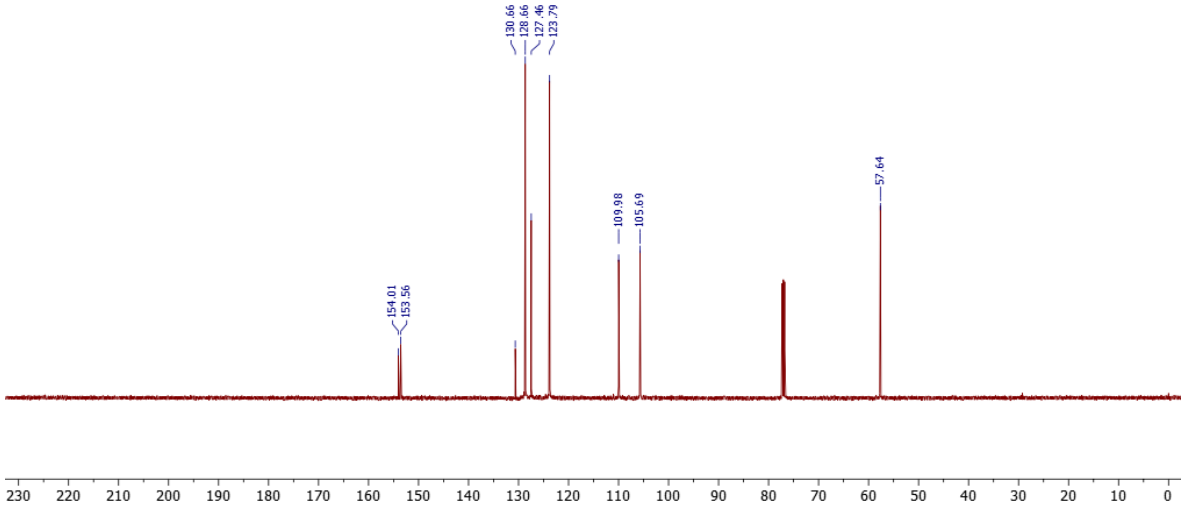

141OH, (5-(3,5-dimethylphenyl)furan-2-yl)methanol:

^{1}H NMR (500 MHz, $CDCl_3$)

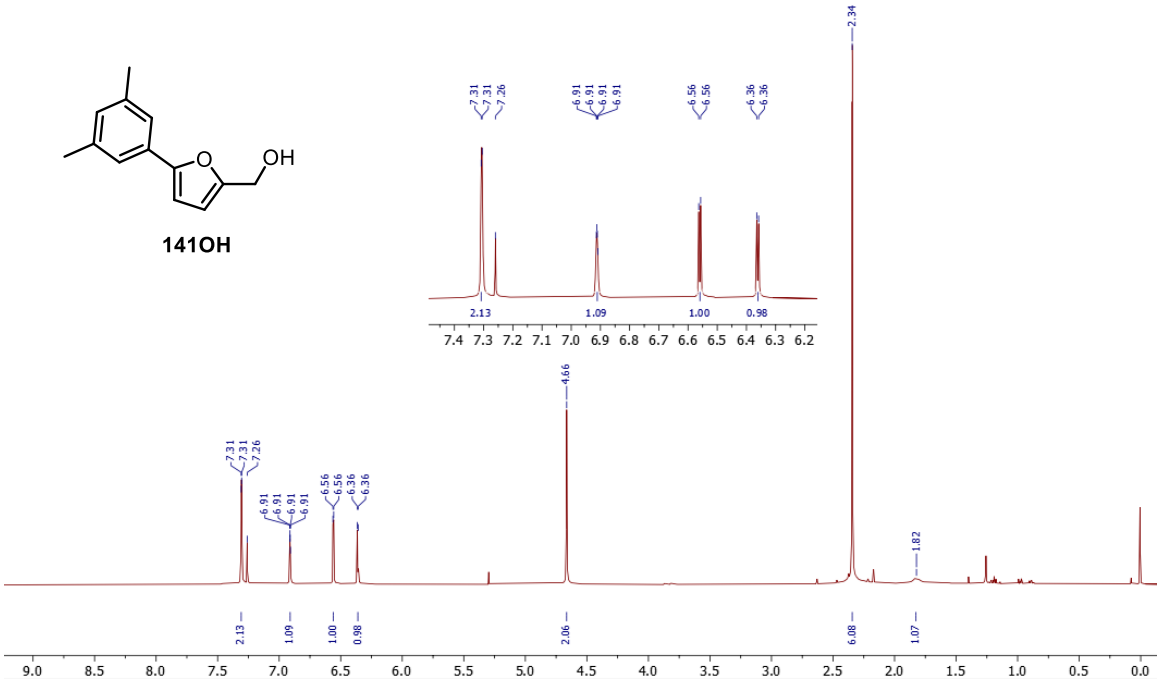

^{13}C NMR (500 MHz, $CDCl_3$)

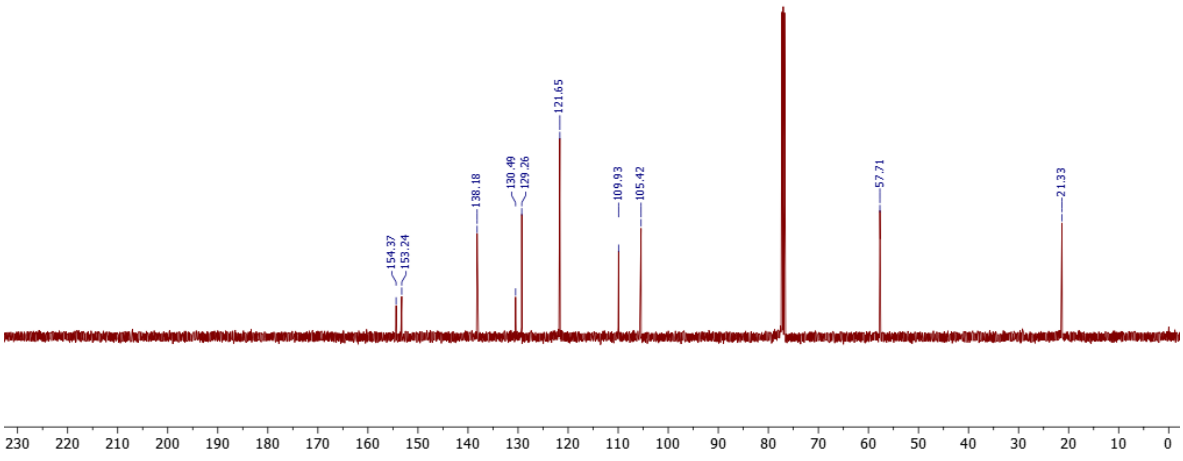

142OH, (5-(4-(*tert*-butyl)phenyl)furan-2-yl)methanol:

^{1}H NMR (500 MHz, $CDCl_3$)

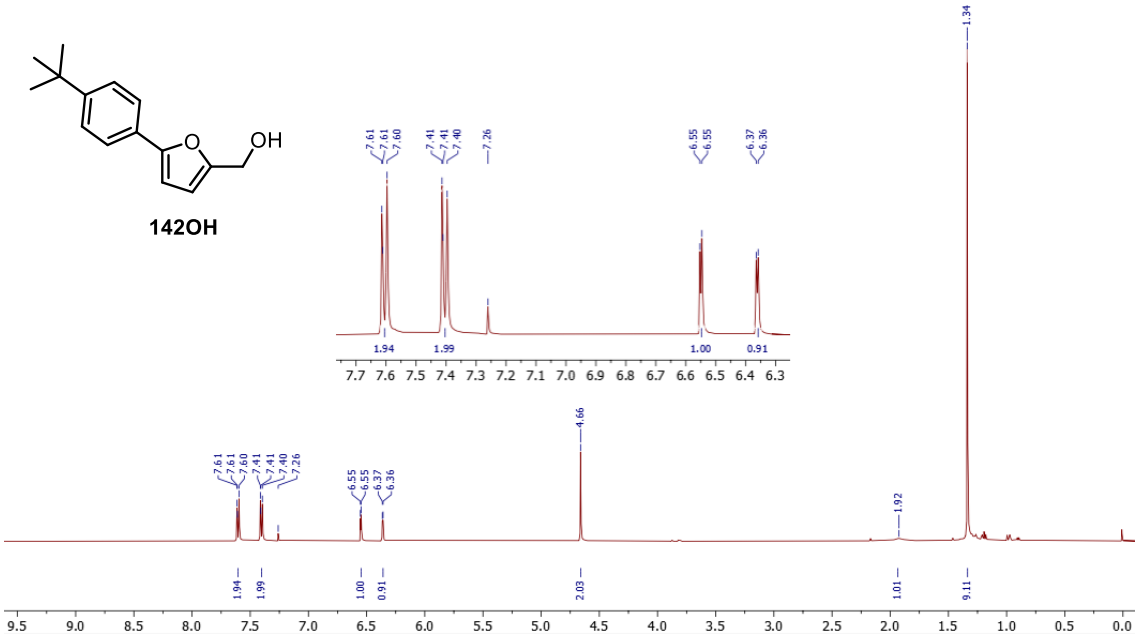

^{13}C NMR (500 MHz, $CDCl_3$)

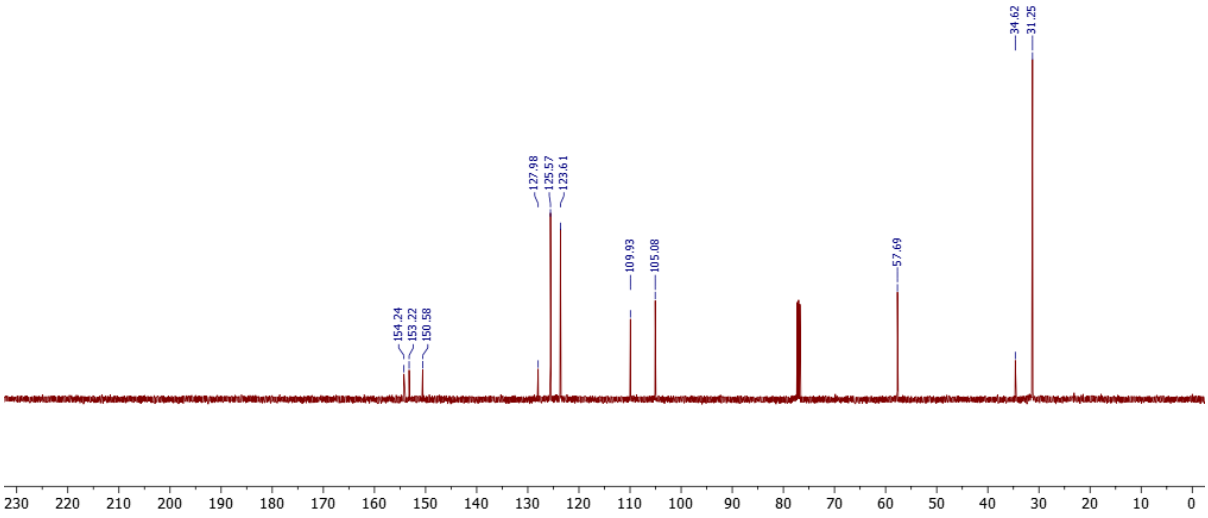

143OH, (5-(4-methoxyphenyl)furan-2-yl)methanol:

^{1}H NMR (500 MHz, $CDCl_3$)

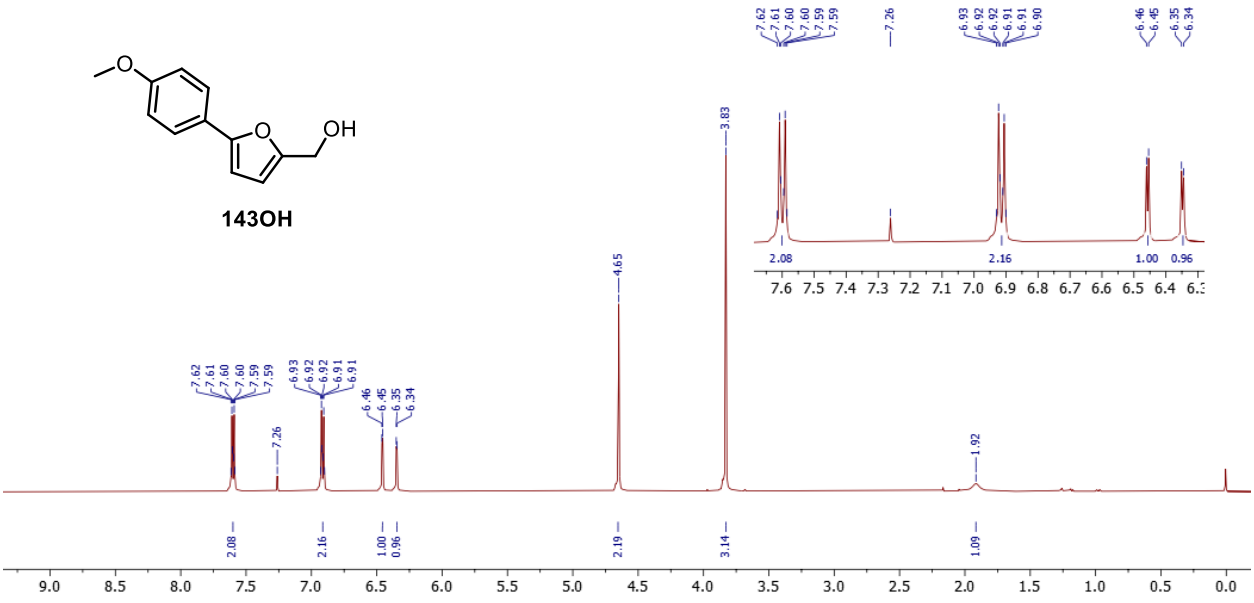

^{13}C NMR (500 MHz, $CDCl_3$)

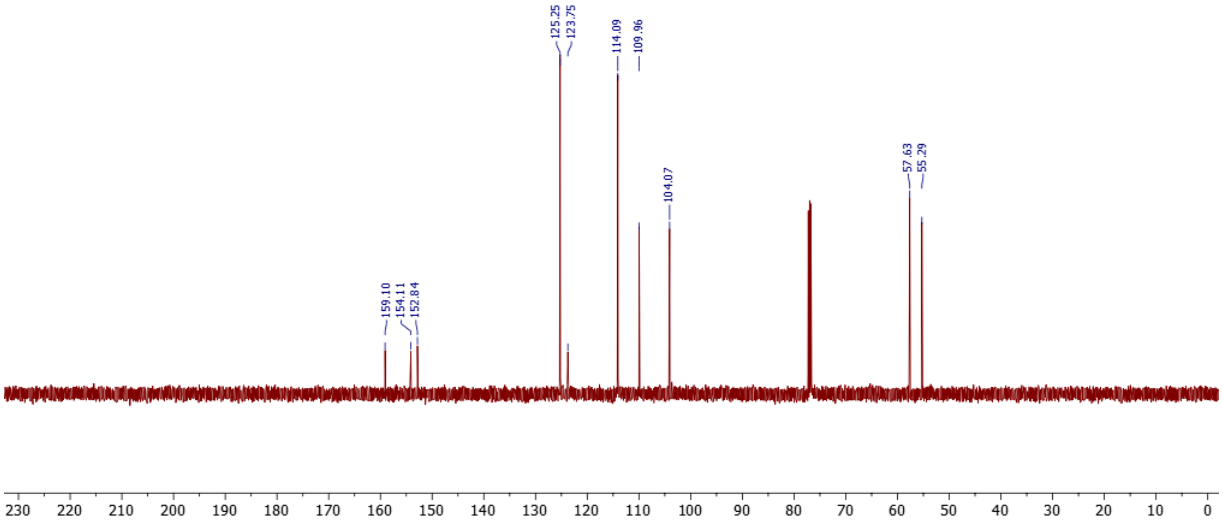

144OH, (5-(4-(diphenylamino)phenyl)furan-2-yl)methanol:

^{1}H NMR (500 MHz, $CDCl_3$)

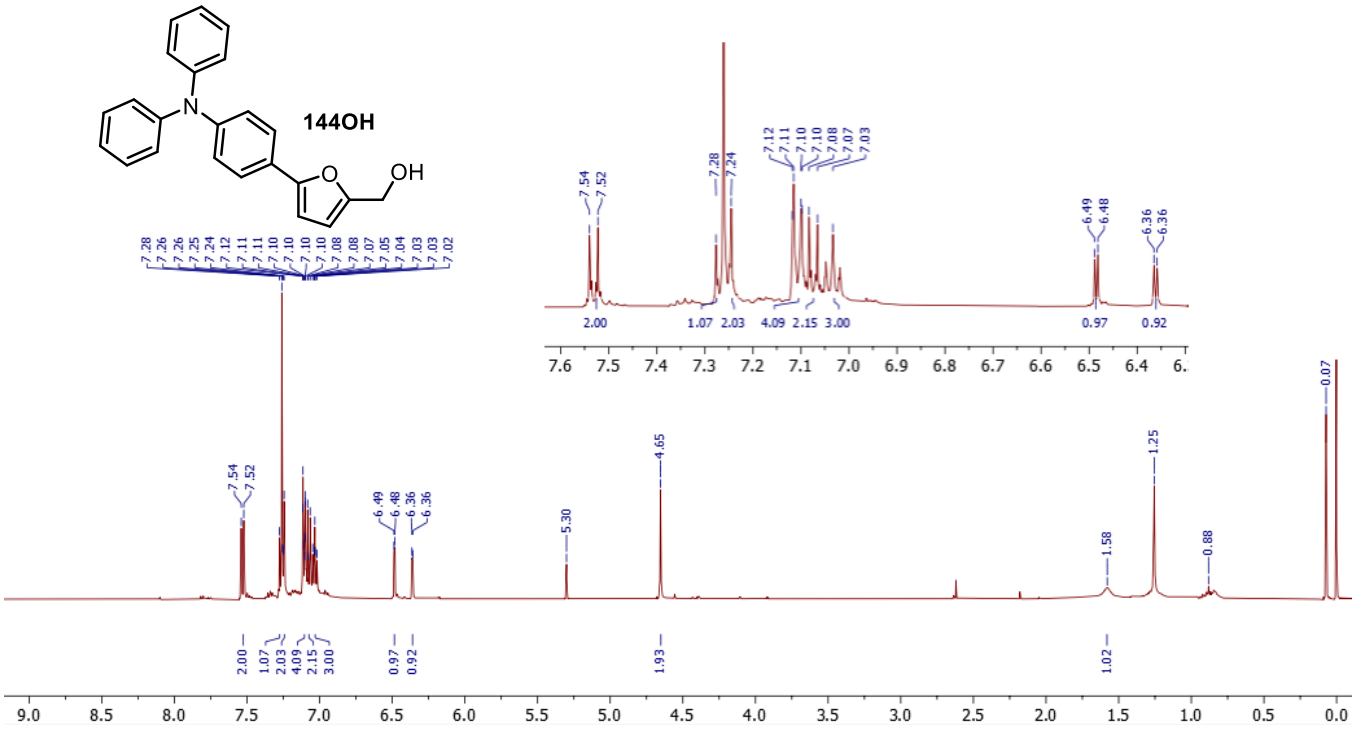

^{13}C NMR (500 MHz, $CDCl_3$)

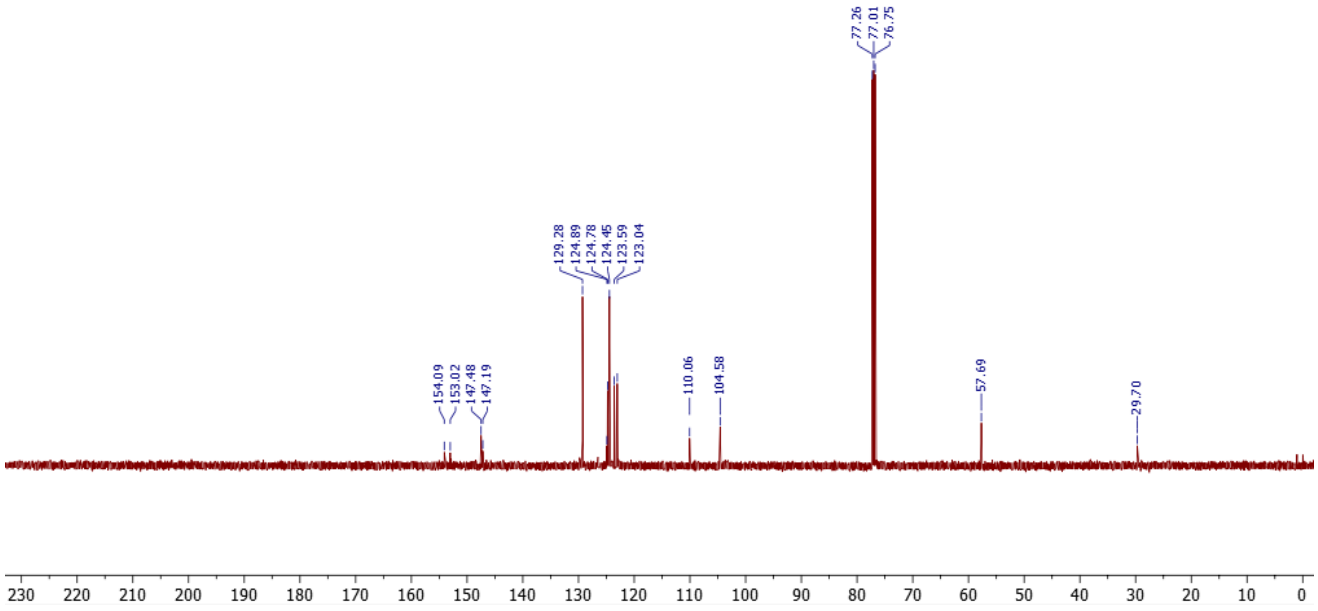

145OH, (5-(4-(trifluoromethyl)phenyl)furan-2-yl)methanol:

^{1}H NMR (500 MHz, $CDCl_3$)

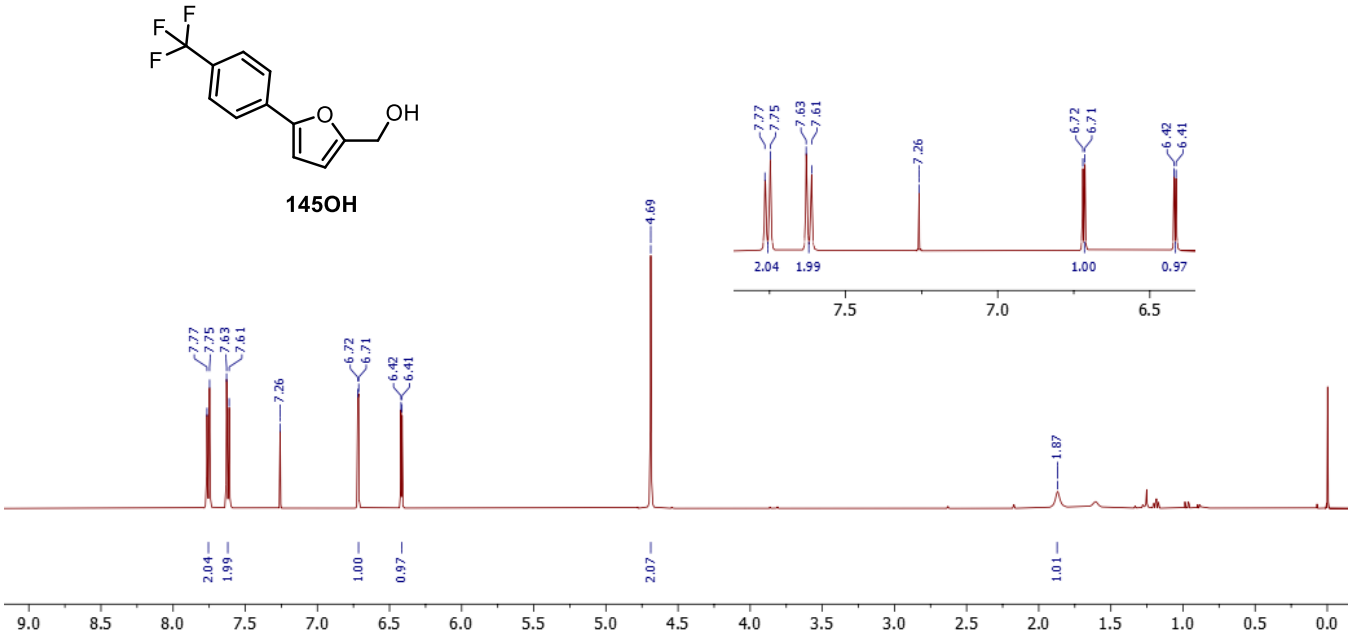

^{13}C NMR (500 MHz, $CDCl_3$)

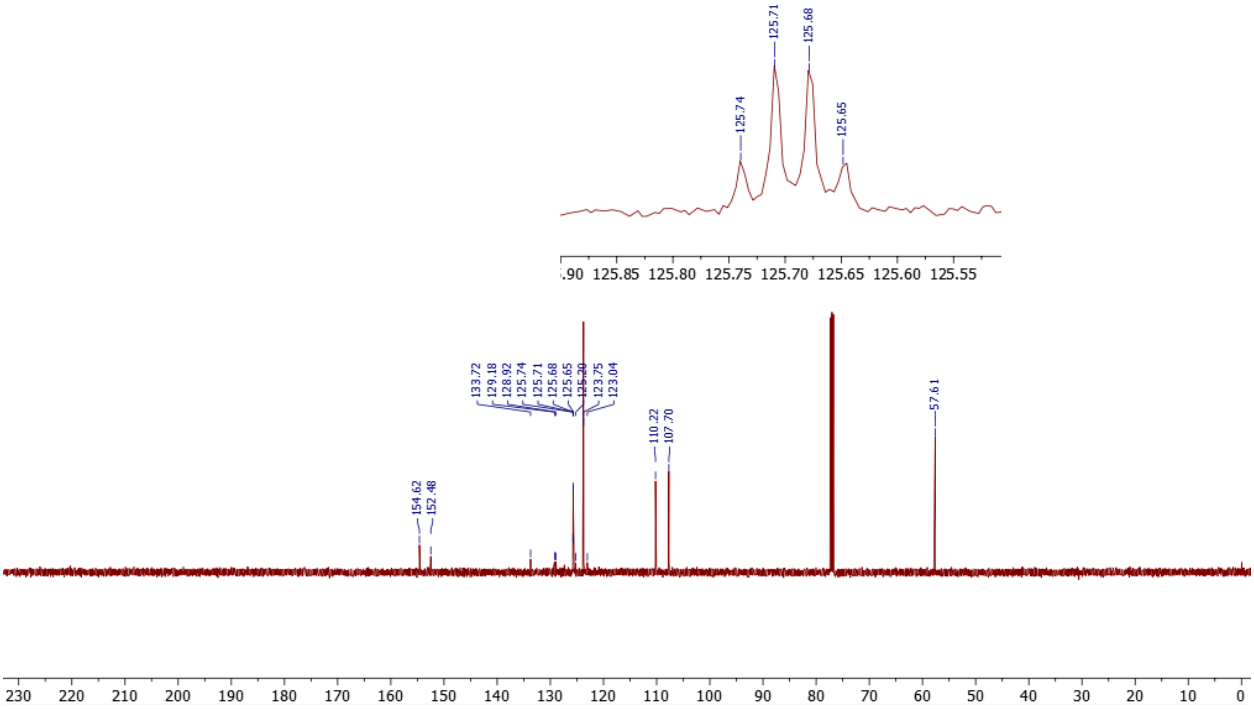

146OH, (5-(4-nitrophenyl)furan-2-yl)methanol:

^{1}H NMR (500 MHz, $CDCl_3$)

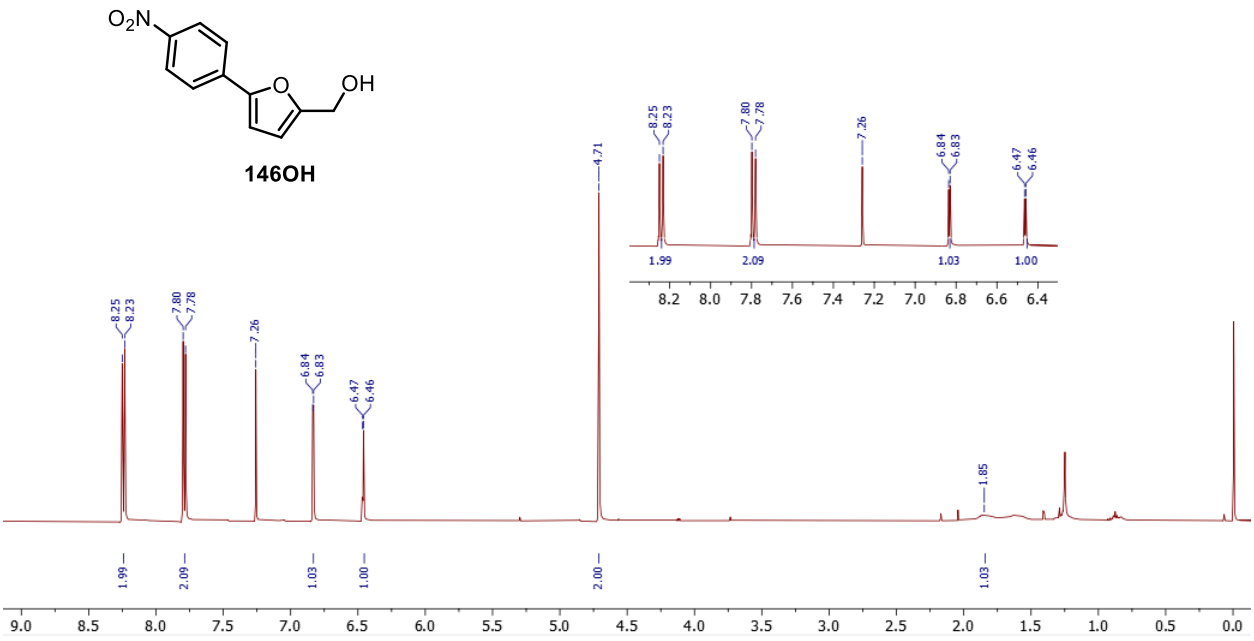

^{13}C NMR (500 MHz, $CDCl_3$)

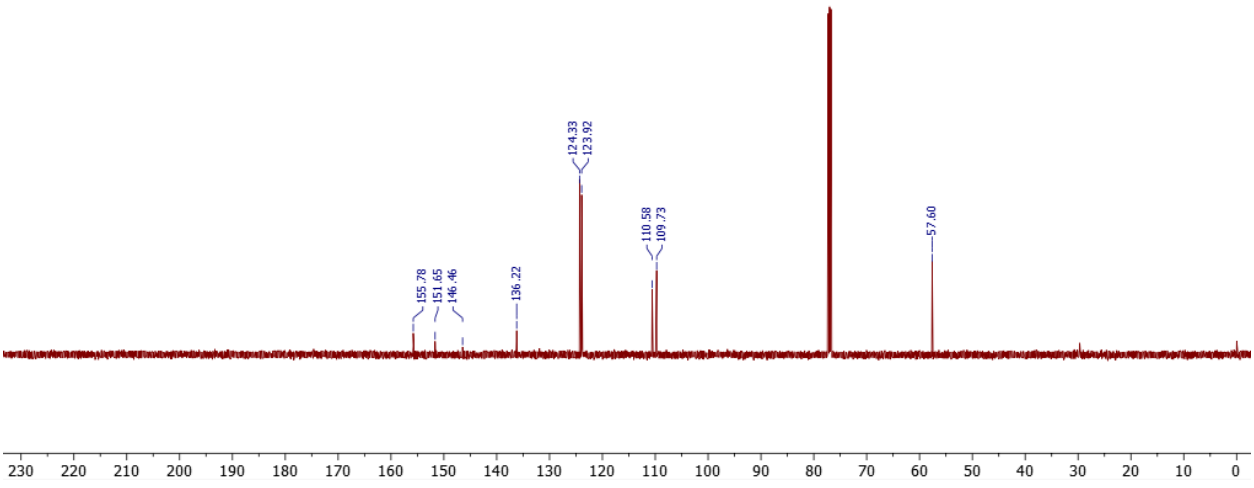

42, 1,4-bis(5-phenylfuran-2-yl)benzene

^{1}H NMR (500 MHz, $CDCl_3$)

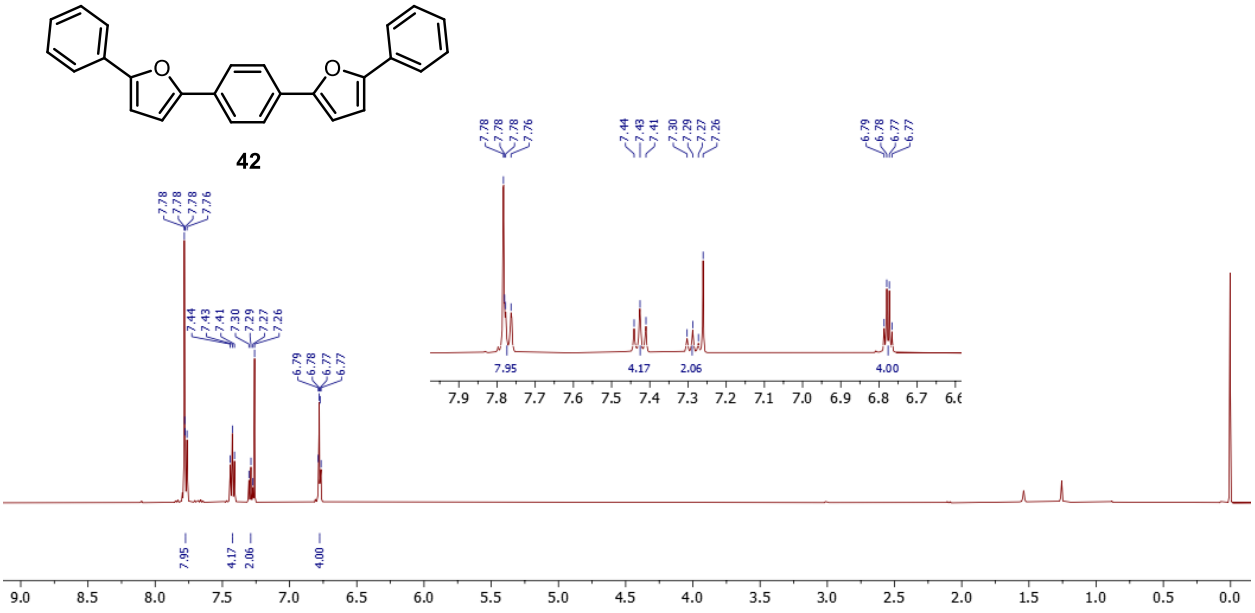

^{13}C NMR (500 MHz, $CDCl_3$)

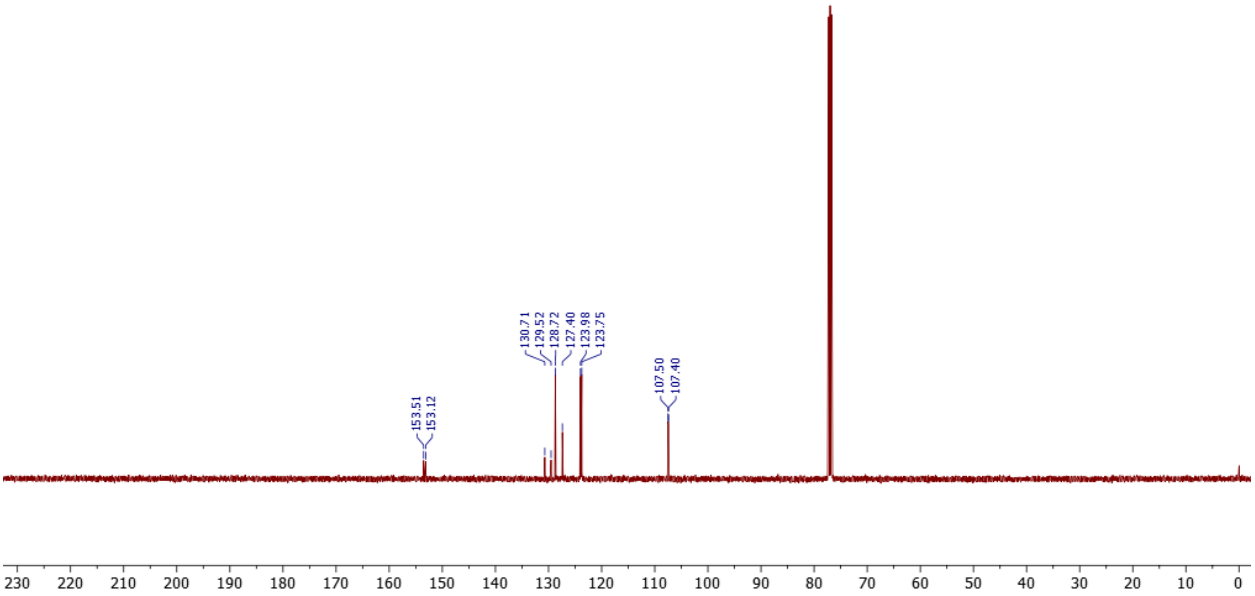

44, 2,5-bis(5-(thiophen-2-yl)furan-2-yl)thiophene

^{1}H NMR (500 MHz, $CDCl_3$)

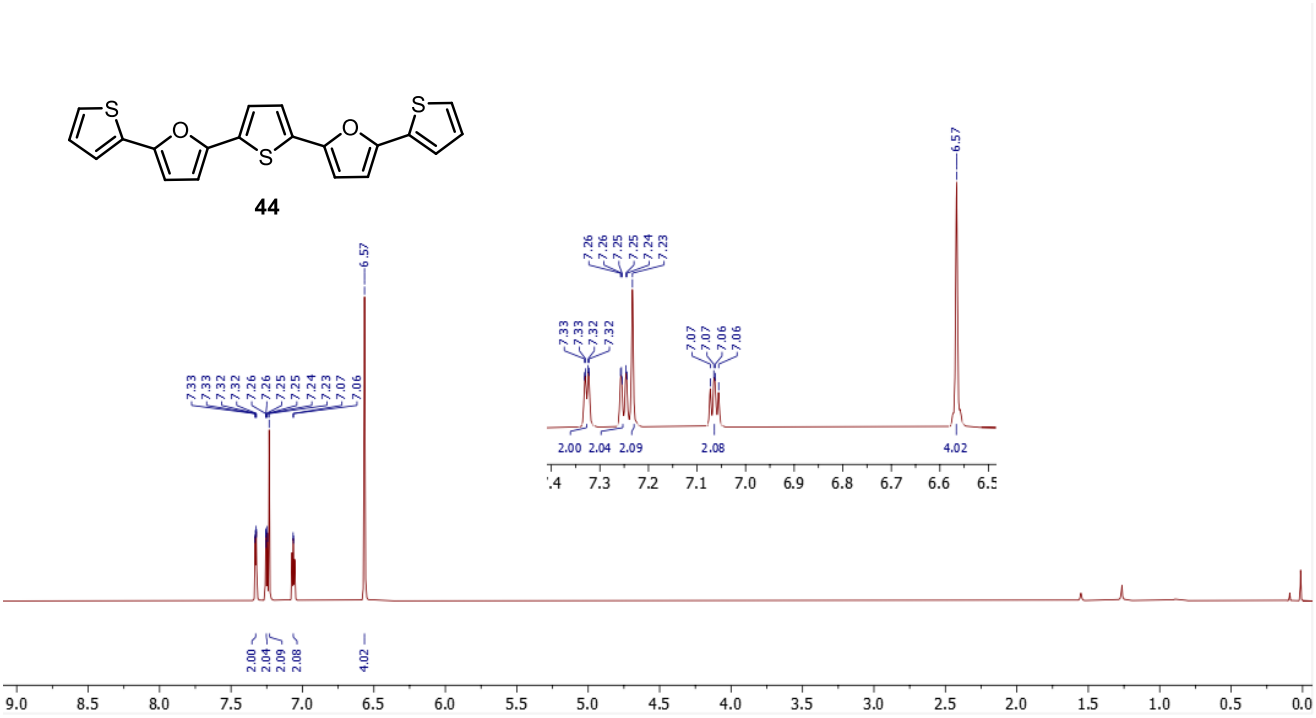

^{13}C NMR (500 MHz, $CDCl_3$)

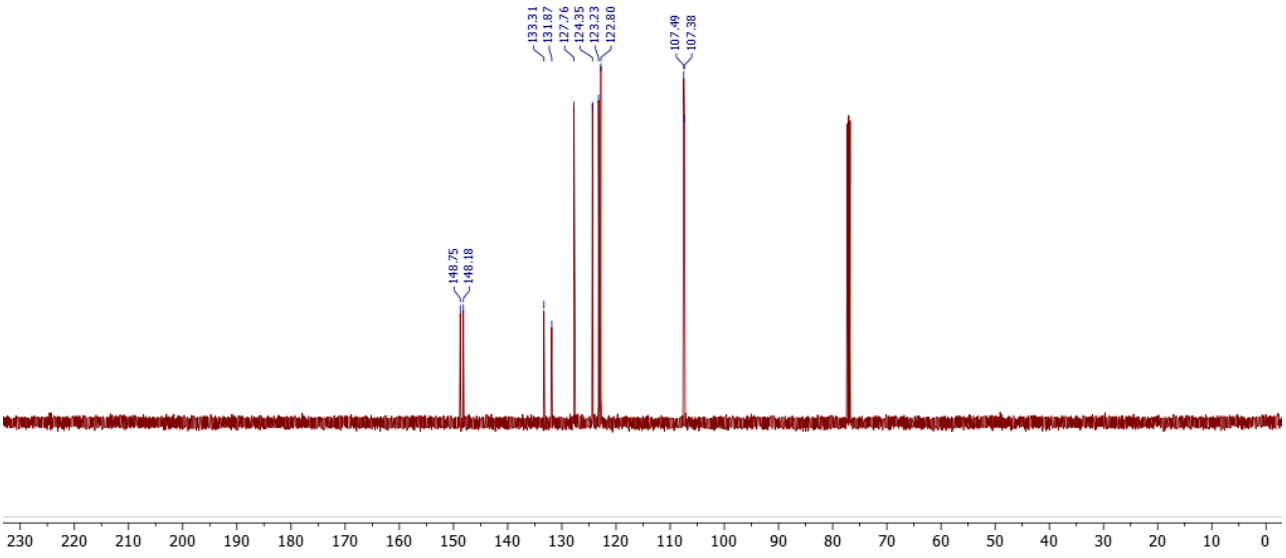

147, 1,4-bis(5-(thiophen-2-yl)furan-2-yl)benzene

^{1}H NMR (500 MHz, $CDCl_3$)

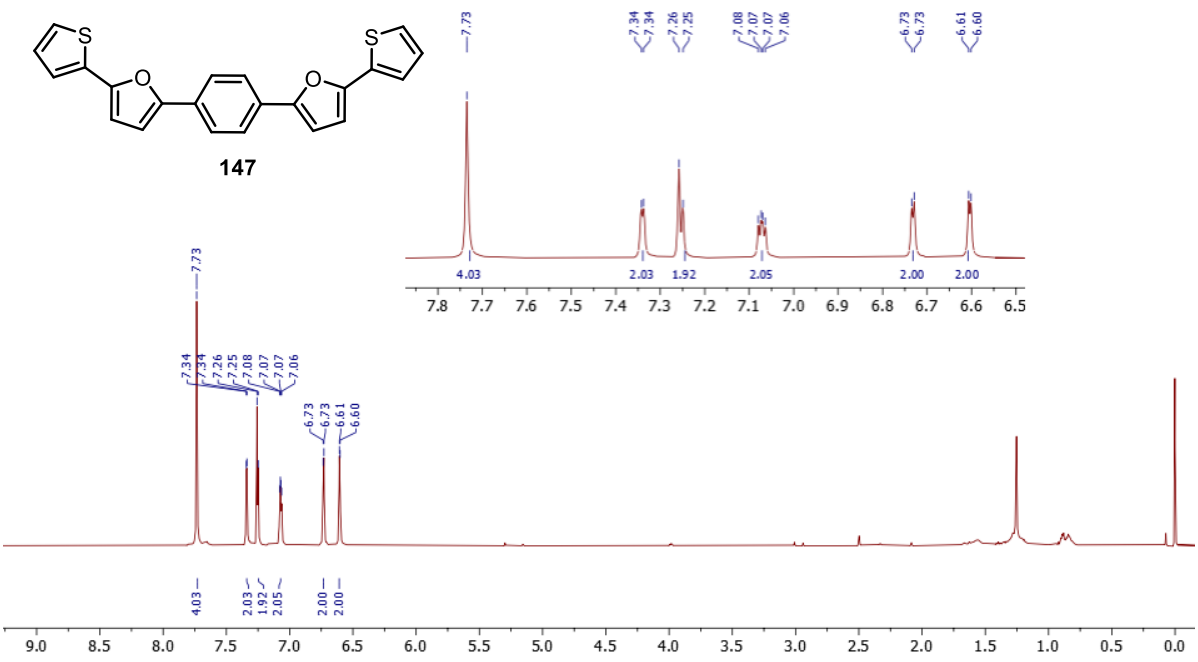

^{13}C NMR (500 MHz, $CDCl_3$)

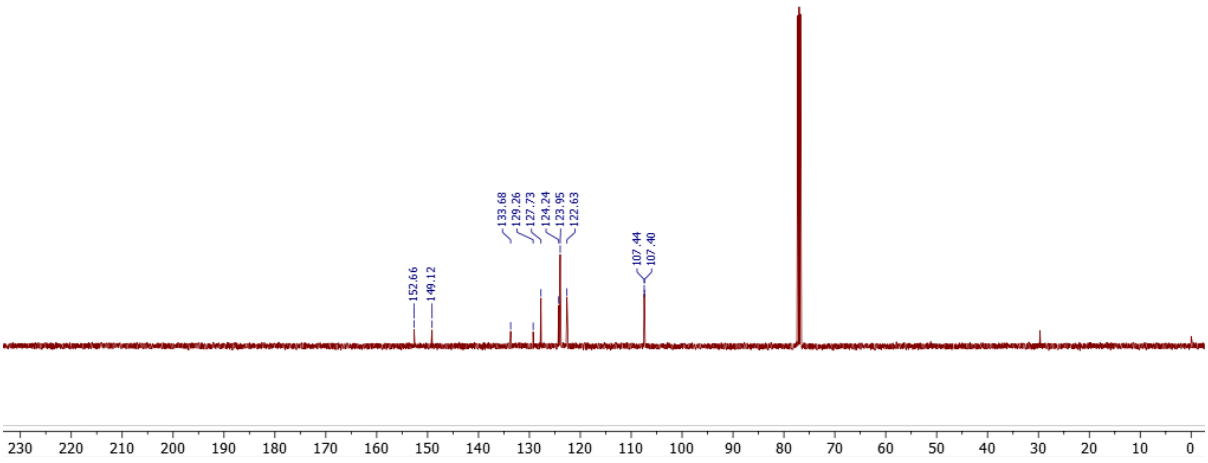

148, 2,5-bis(5-phenylfuran-2-yl)thiophene

^{1}H NMR (500 MHz, $CDCl_3$)

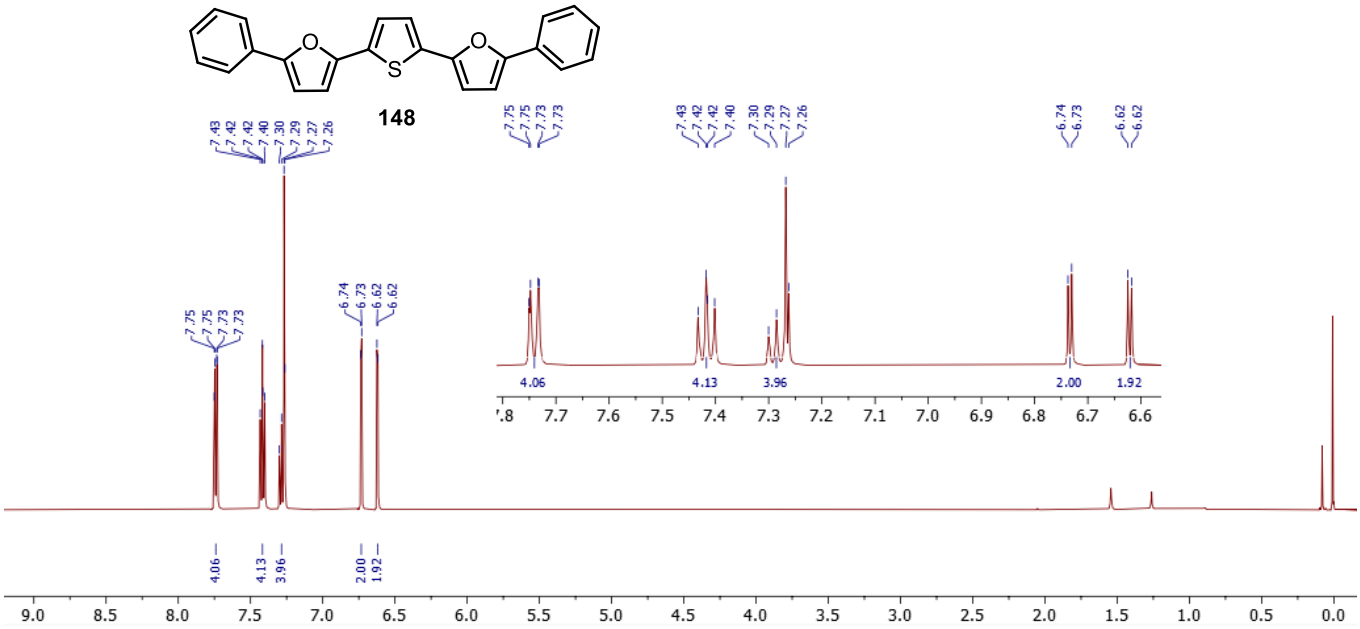

^{13}C NMR (500 MHz, $CDCl_3$)

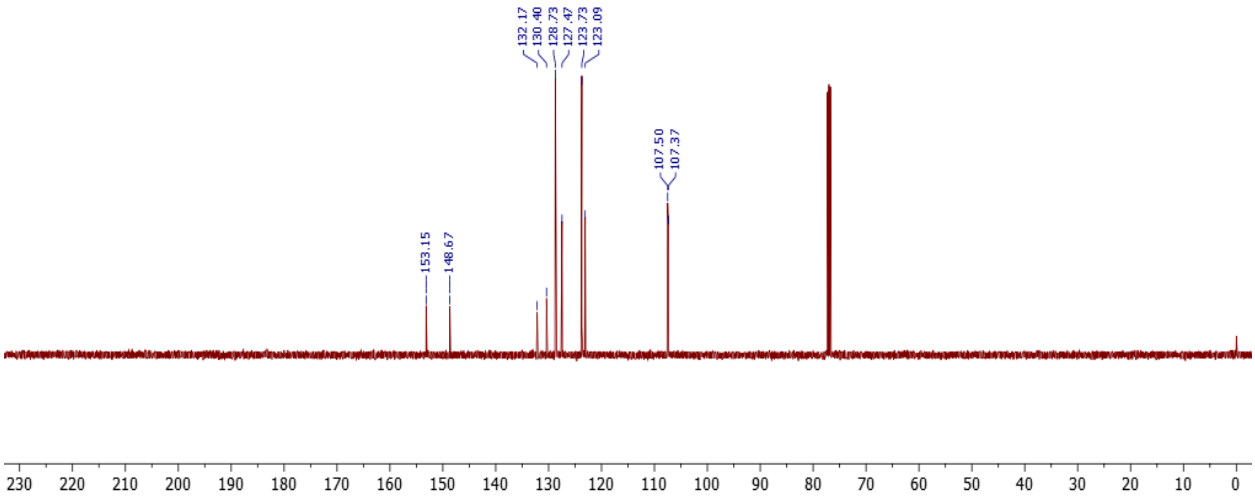

149, 1,4-bis(5-(3,5-dimethylphenyl)furan-2-yl)benzene

^{1}H NMR (500 MHz, $CDCl_3$)

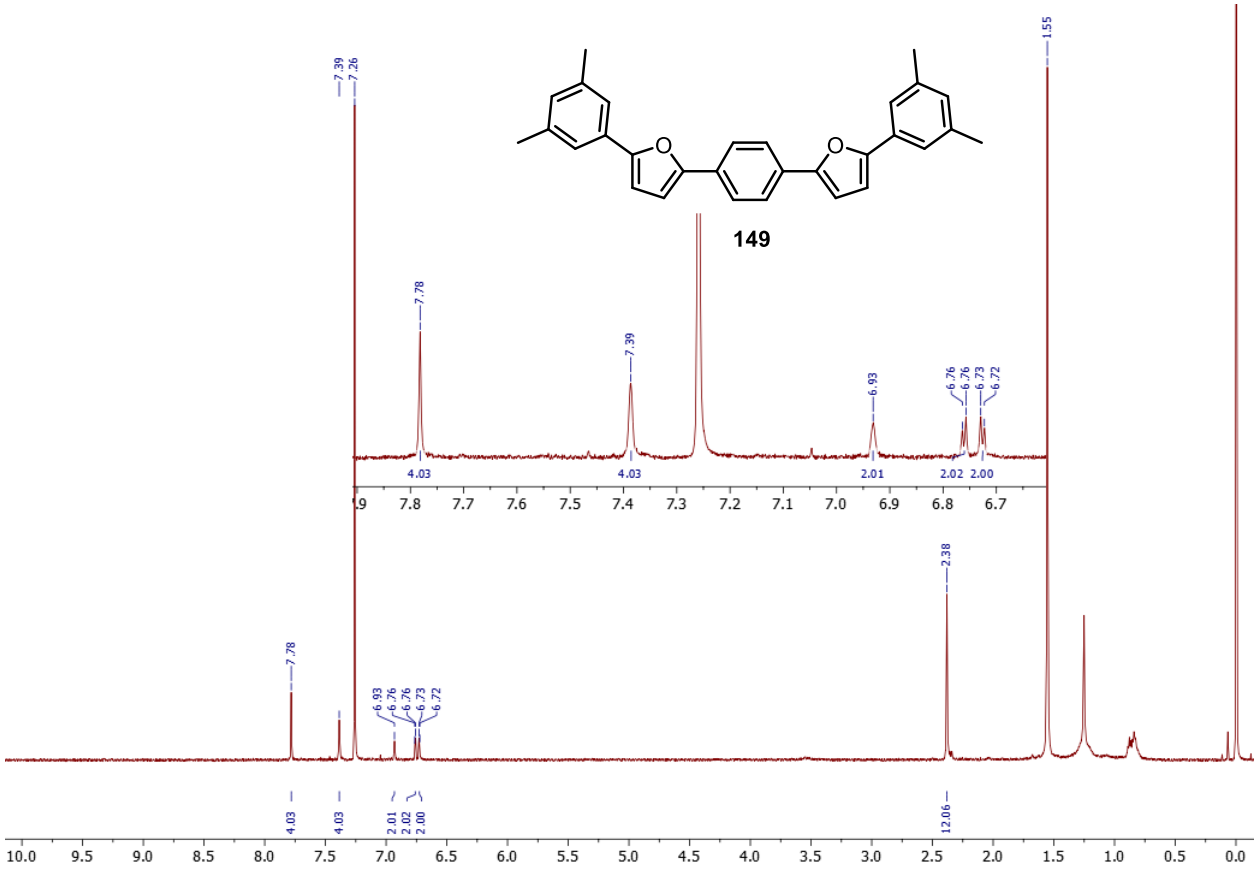

^{13}C NMR (500 MHz, $CDCl_3$)

Note: Compound **149** is too insoluble to record a ^{13}C NMR spectrum.

150, 1,4-bis(5-(4-(tert-butyl)phenyl)furan-2-yl)benzene

^{1}H NMR (500 MHz, $CDCl_3$)

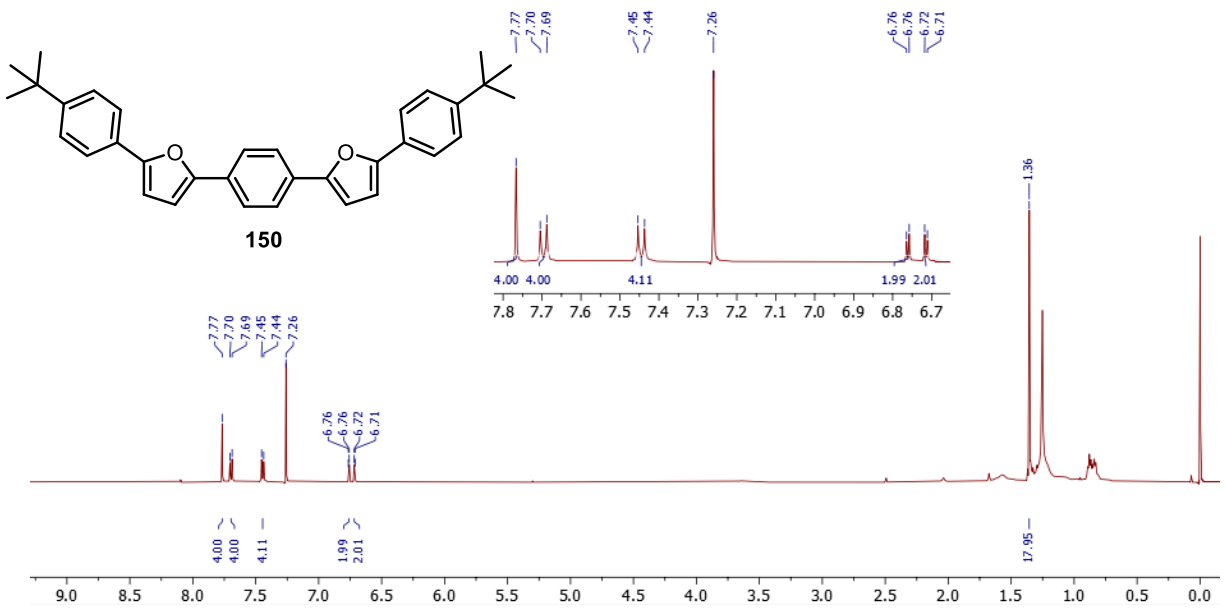

^{13}C NMR (500 MHz, $CDCl_3$)

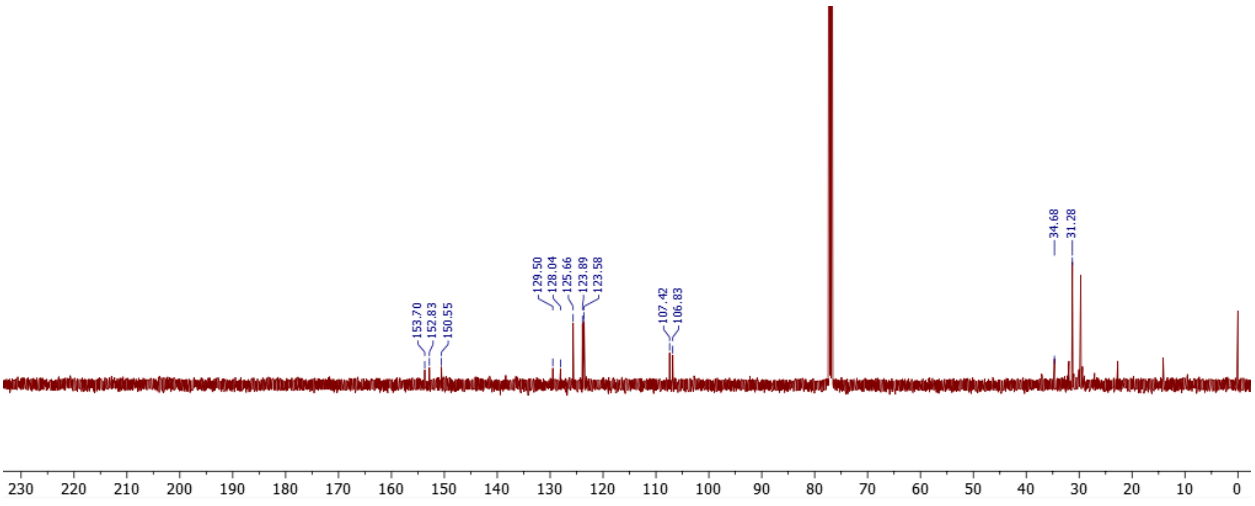

151, 1,4-bis(5-(4-methoxyphenyl)furan-2-yl)benzene

^{1}H NMR (500 MHz, $CDCl_3$)

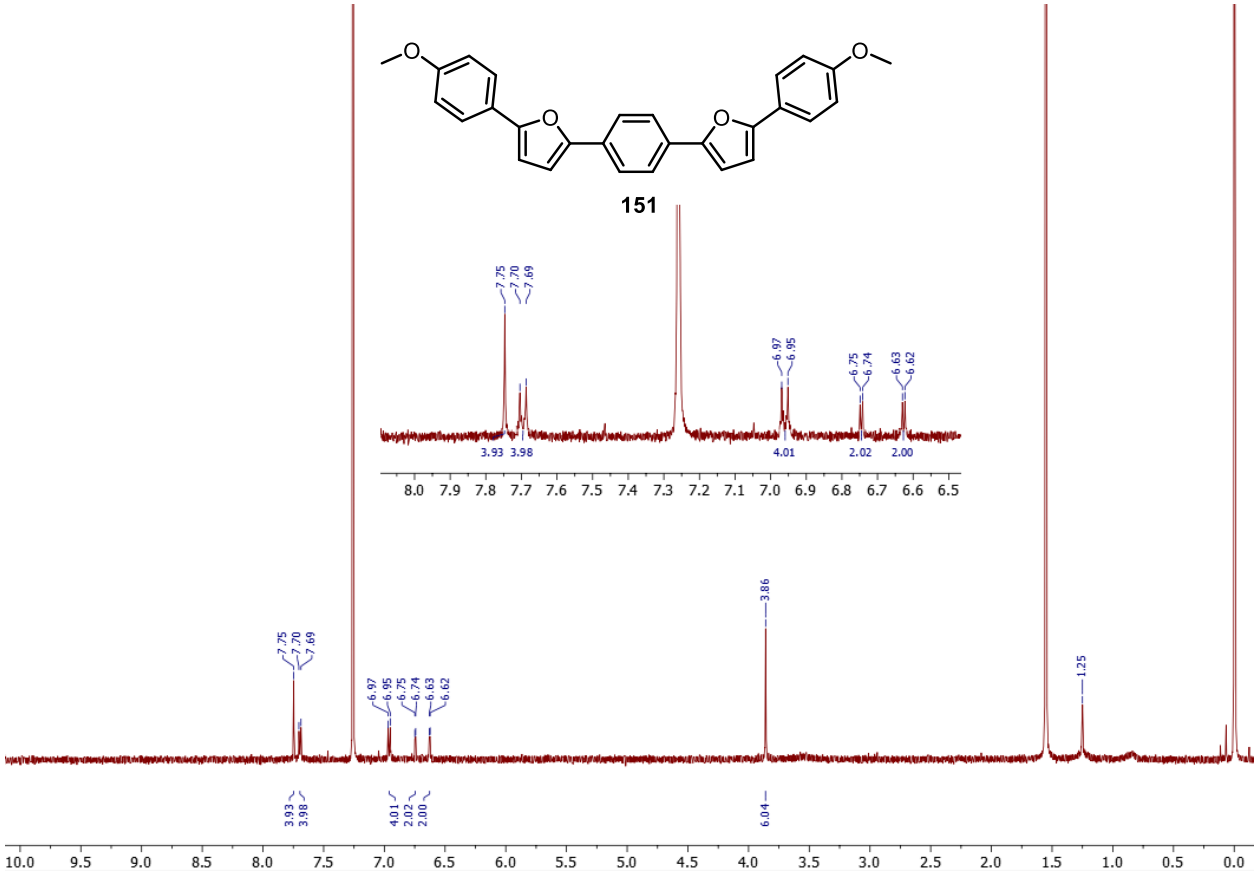

^{13}C NMR (500 MHz, $CDCl_3$)

Note: Compound **151** is too insoluble to record a ^{13}C NMR spectrum.

152, 4,4'-(1,4-phenylenebis(furan-5,2-diyl))bis(N,N-diphenylaniline)

^{1}H NMR (500 MHz, $CDCl_3$)

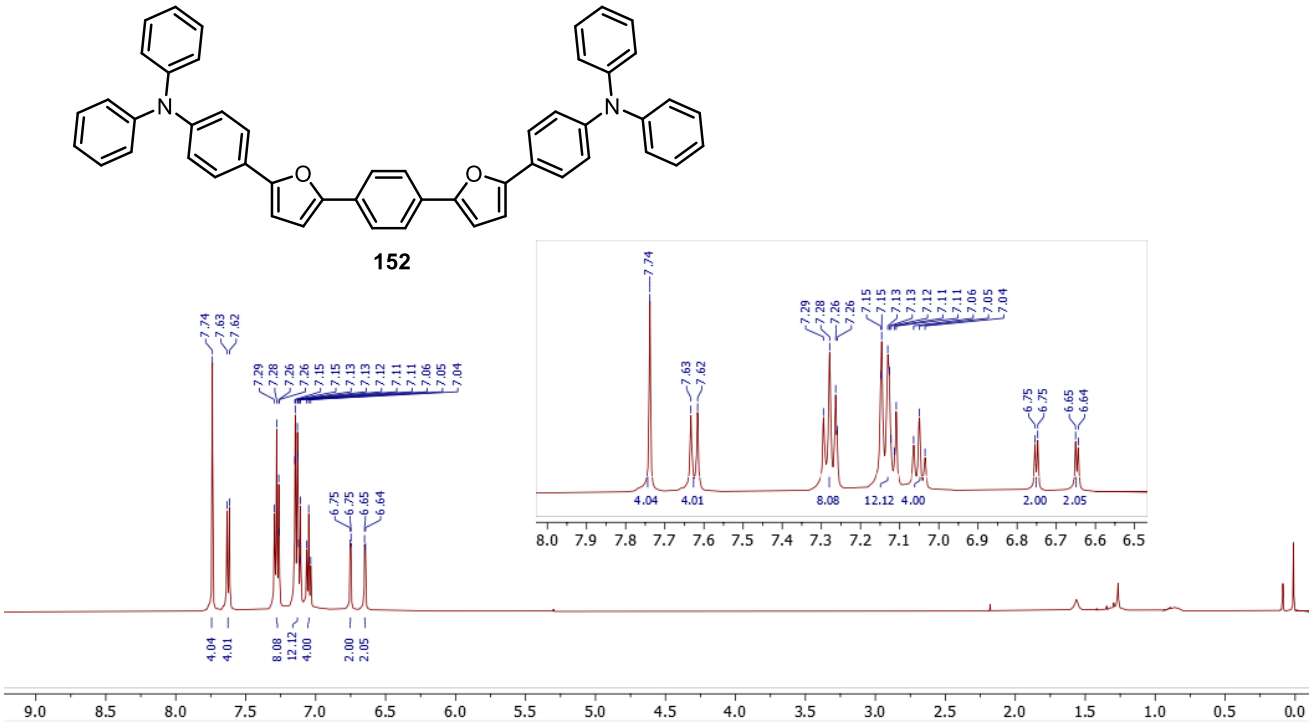

^{13}C NMR (500 MHz, $CDCl_3$)

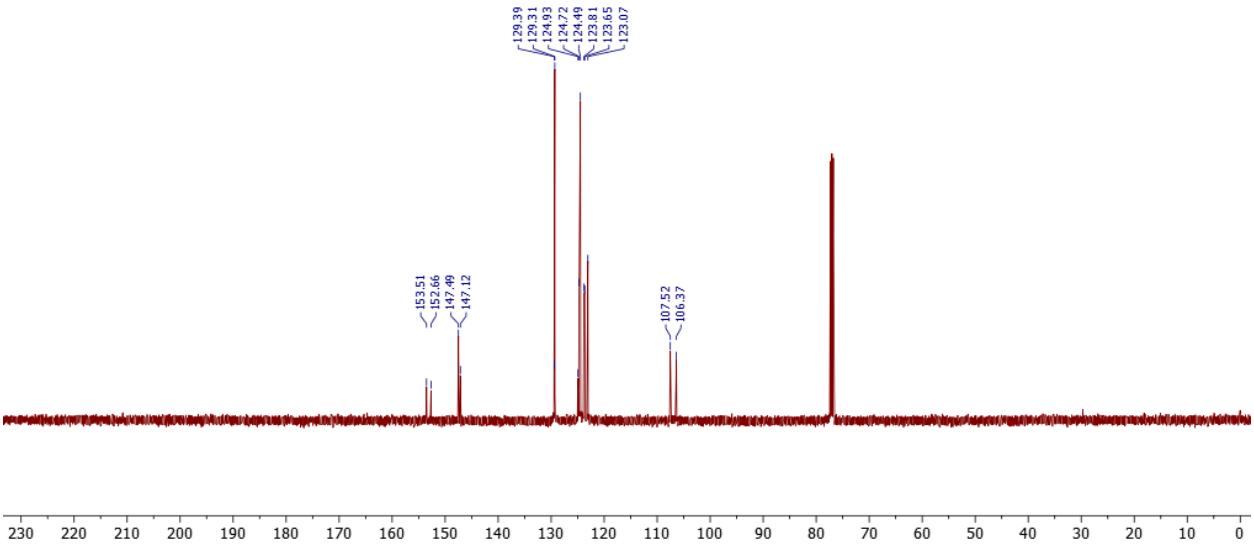

153, 1,4-bis(5-(4-(trifluoromethyl)phenyl)furan-2-yl)benzene

^{1}H NMR (500 MHz, $CDCl_3$)

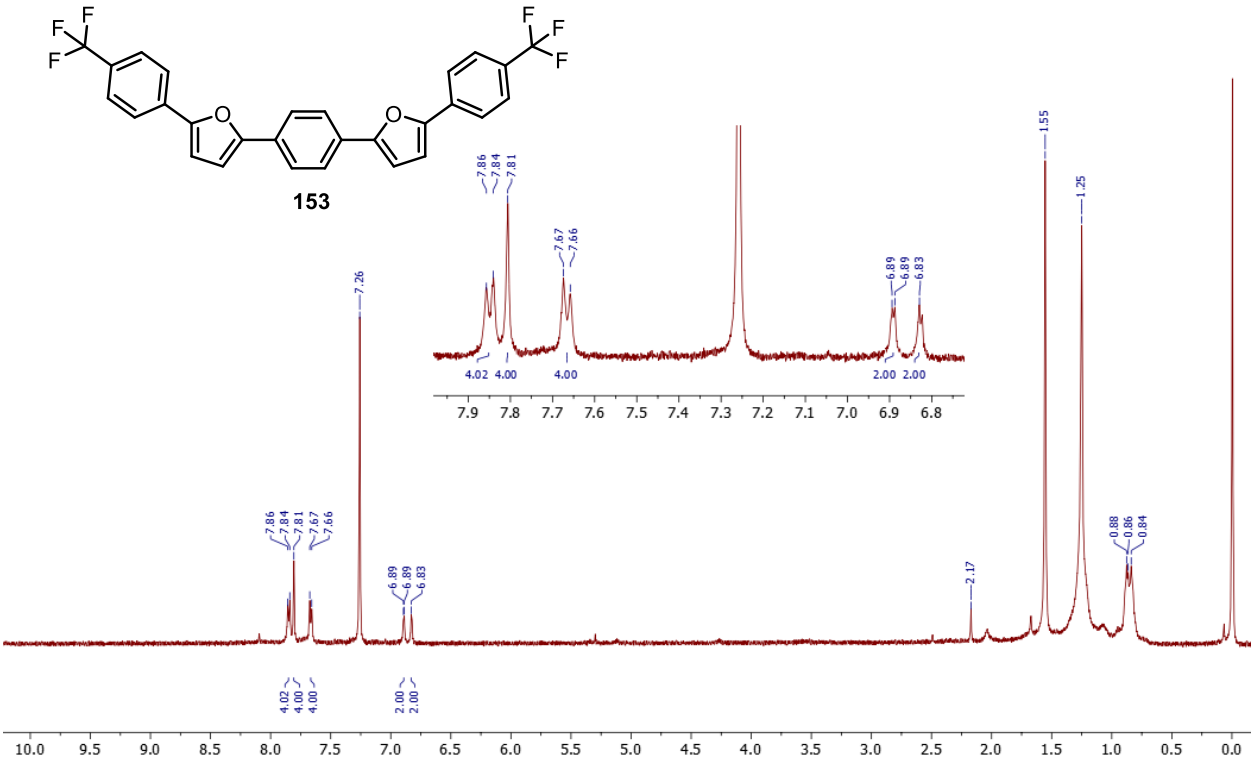

^{13}C NMR (500 MHz, $CDCl_3$)

Note: Compound **153** is too insoluble to record a ^{13}C NMR spectrum.

154, 1,4-bis(5-(4-nitrophenyl)furan-2-yl)benzene

^{1}H NMR (500 MHz, $CDCl_3$)

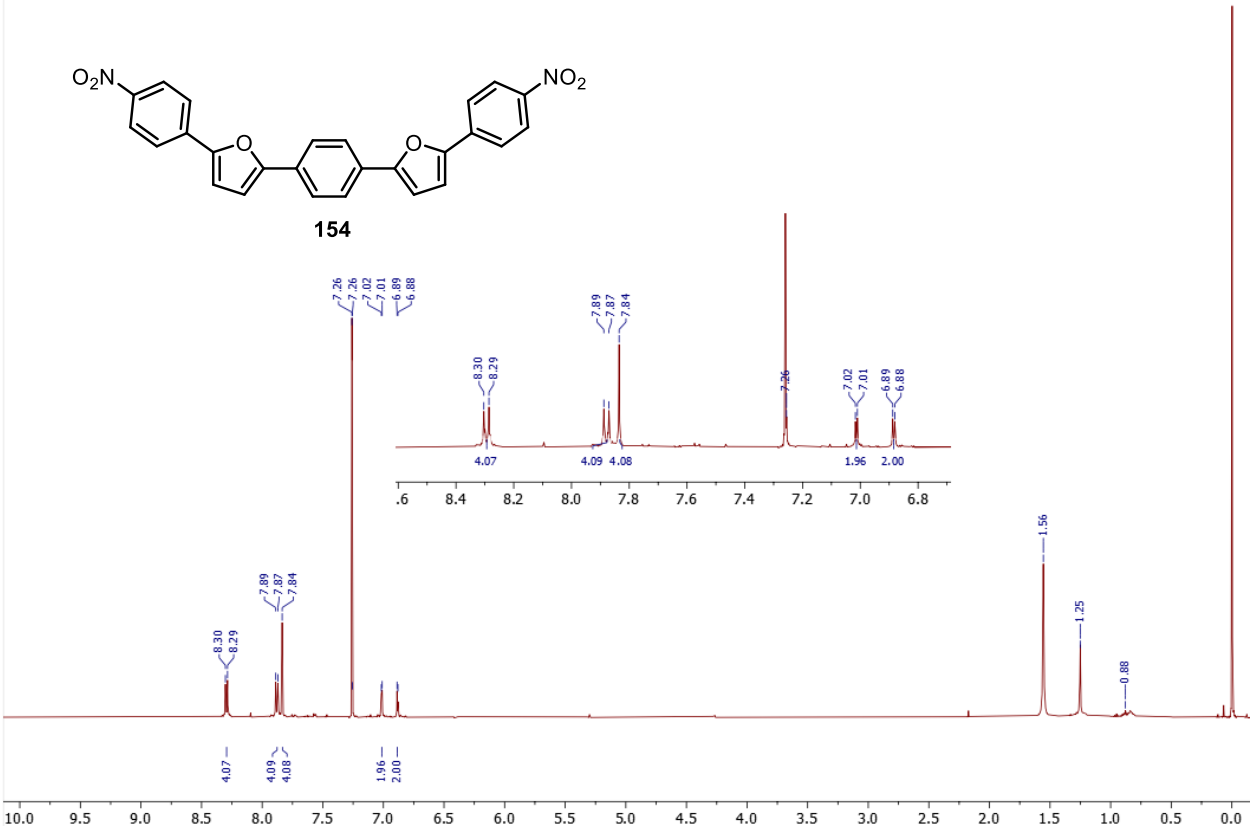

^{13}C NMR (500 MHz, $CDCl_3$)

Note: Compound **154** is too insoluble to record a ^{13}C NMR spectrum.

156, 2-(4-nitrophenyl)-5-(thiophen-2-yl)furan

^{1}H NMR (500 MHz, $CDCl_3$)

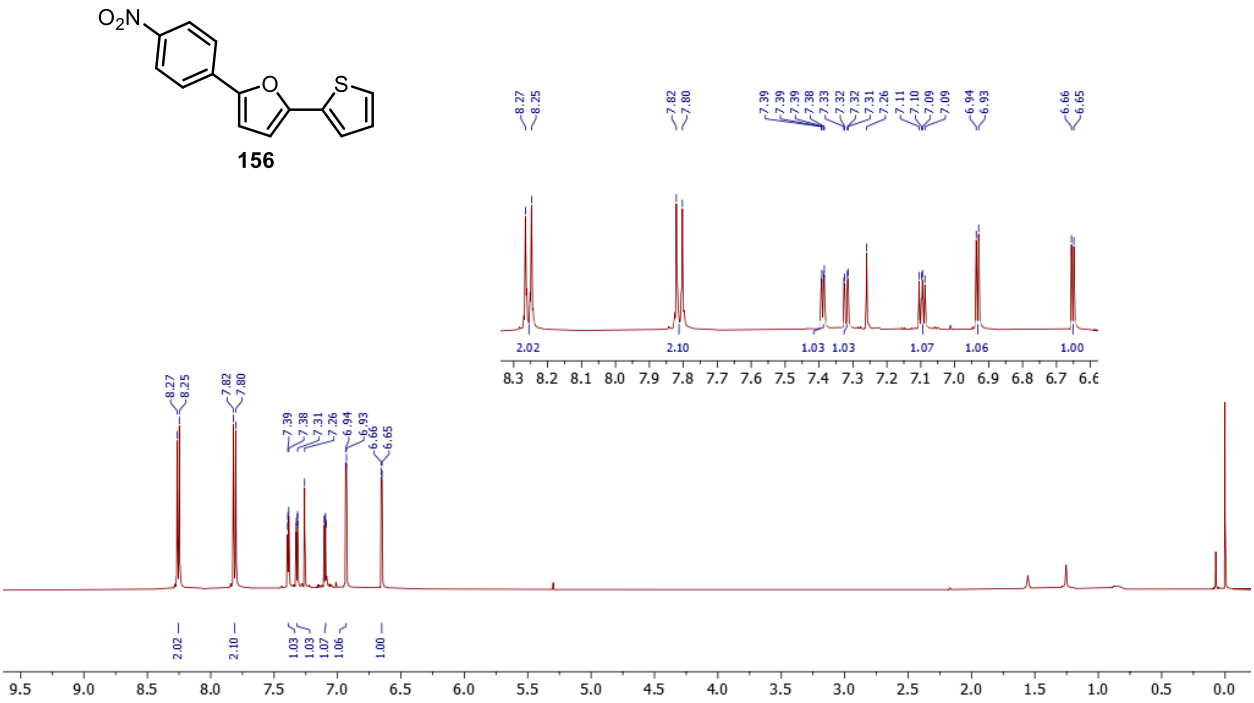

^{13}C NMR (500 MHz, $CDCl_3$)

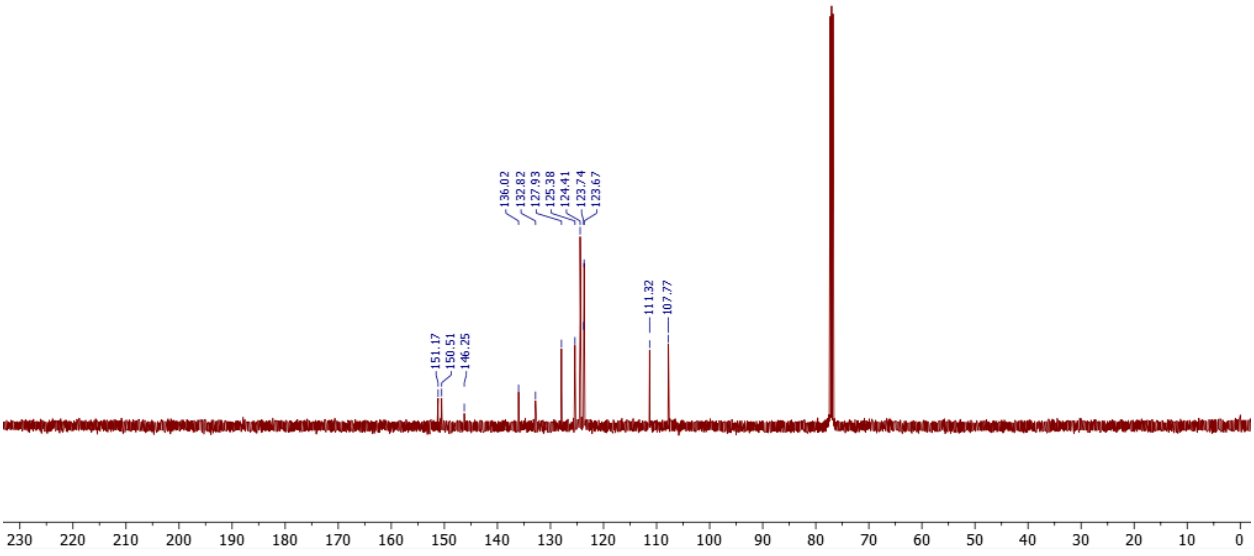

References

(1) Arrhenius, S. *Philosophical Magazine and Journal of Science Series* **1896**, 5, 237–276.

(2) IPCC, 2023: Summary for Policymakers. In: Climate Change **2023**: Synthesis Report. *Contribution of Working Groups I, II and III to the Sixth Assessment Report of the Intergovernmental Panel on Climate Change* [Core Writing Team, H. Lee and J. Romero (Eds.)]. IPCC, Geneva, Switzerland, Pp. 1-34, Doi: 10.59327/IPCC/AR6-9789291691647.001

(3) European Environment Agency. *Trends in atmospheric concentrations of CO2 (ppm), CH4 (ppb) and N2O (ppb), between 1800 and 2017.* https://www.eea.europa.eu/data-and-maps/daviz/atmospheric-concentration-of-carbon-dioxide-5#tab-chart_5_filters=%7B%22rowFilters%22%3A%7B%7D%3B%22columnFilters%22%3A%7B%22pre_config_polutant%22%3A%5B%22CO2%20(ppm)%22%5D%7D%7D (accessed 2024-01-18).

(4) National Oceanic and Atmospheric Administration. *Greenhouse gases continued to increase rapidly in 2022.* https://www.noaa.gov/news-release/greenhouse-gases-continued-to-increase-rapidly-in-2022 (accessed 2024-02-03).

(5) NASA Earth Observatory. *World of Change: Global Temperatures.* https://earthobservatory.nasa.gov/world-of-change/global-temperatures (accessed 2024-02-03).

(6) Graham Steve. *John Tyndall* (1820-1893). https://earthobservatory.nasa.gov/features/Tyndall (accessed 2024-01-18).

(7) Ritchie Hannah; Rosado Pablo. *Energy Mix. Our World in Data.* https://ourworldindata.org/energy-mix (accessed 2024-01-18).

(8) Fernandez Araceli; Levi Peter; Bennett Simon; Elliott Jason; Kim Tae-Yoon; Petrosyan Kristine; Ritchie Joe; Bohemen Aad van; Vass Tiffany; Walton Molly A.; West Kira. **2018**. www.iea.org/t&c/.

(9) Canadian Association of Petroleum Producers. *Uses for Oil.* https://www.capp.ca/oil/uses-for-oil/#:~:text=Many%20of%20our%20personal%20care,%2C%20eyeglasses%2C%20and%20contact%20lenses (accessed 2024-01-18).

(10) U.S. Energy Information Adminstration. *Short-Term Energy Outlook: Global oil markets.* https://www.eia.gov/outlooks/steo/report/global_oil.php#:~:text=Global%20oil%20production%20and%20consumption,and%20slowing%20non%2DOPEC%20growth. (accessed 2024-01-18).

(11) Güleç, F.; Parthiban, A.; Umenweke, G. C.; Musa, U.; Williams, O.; Mortezaei, Y.; Suk-Oh, H.; Lester, E.; Ogbaga, C. C.; Gunes, B.; Okolie, J. A. *Biofuels, Bioprod. Bioref*. **2023**.

(12) Anastas P.T; Warner J.C. (1988), *Green Chemistry: Theory and Practice*; Oxford University Press, England: Oxford University Press.

(13) Trost B. *Science*. **1991**, *254*, 1471–1477.

(14) Sheldon R.A. E-Factor. *Chem. Ind.* **1992**, 903–906.

(15) Tursi, A. *Biofuel Research Journal.* **2019**, *22*, 962–979.

(16) Cherubini, F. *Energy Convers Manag.* **2010**, *51*, 1412–1421.

(17) Dahmen, N.; Lewandowski, I.; Zibek, S.; Weidtmann, A. *GCB Bioenergy*. **2019**, *11*, 107–117.

(18) Trost, B. *Appl. Sci.* **2019**, *9*, 3721.

(19) Zheng, B.; Yu, S.; Chen, Z.; Huo, Y. X. *Front. Microbiol.* **2022**, *13*, 933882.

(20) Liu, Q.; Luo, L.; Zheng, L. *Int. J. Mol. Sci.* **2018**, *19*, 335.

(21) Chaturvedi, T.; Hulkko, L. S. S.; Fredsgaard, M.; Thomsen, M. H. *Processes*. **2022**, *10*, 1752.

(22) Isikgor, F. H.; Becer, C. R. *Polym. Chem.* **2015**, *6*, 4497–4559.

(23) Deng, W.; Feng, Y.; Fu, J.; Guo, H.; Guo, Y.; Han, B.; Jiang, Z.; Kong, L.; Li, C.; Liu, H.; Nguyen, P. T. T.; Ren, P.; Wang, F.; Wang, S.; Wang, Y.; Wang, Y.; Wong, S. S.; Yan, K.; Yan, N.; Yang, X.; Zhang, Y.; Zhang, Z.; Zeng, X.; Zhou, H. *Green Energy and Environment.* **2023**, *8*, 10–114.

(24) Werpy, T.; Petersen, G. Top Value Added Chemicals from Biomass Volume I-Results of Screening for Potential Candidates from Sugars and Synthesis Gas Produced by the Staff at Pacific Northwest National Laboratory (PNNL) National Renewable Energy Laboratory (NREL) Office of Biomass Program (EERE) For the Office of the Energy Efficiency and Renewable Energy; **2004**. http://www.osti.gov/bridge.

(25) Thoma, C.; Konnerth, J.; Sailer-Kronlachner, W.; Rosenau, T.; Potthast, A.; Solt, P.; van Herwijnen, H. W. G. *ChemSusChem*. **2020**, *13*, 5408–5422.

(26) Fan, W.; Verrier, C.; Queneau, Y.; Popowycz, F. *Curr. Org. Synth.* **2019**, *16*, 583–614.

(27) Van Putten, R.-J.; Van Der Waal, J. C.; De Jong, E.; Rasrendra, C. B.; Heeres, H. J.; De Vries, J. G. *Chem. Rev.* **2013**, *113*, 1499–1597.

(28) Gupta, S. S. R.; Vinu, A.; Kantam, M. L. *J. Catal.* **2020**, *389*, 259–269.

(29) Kim, M.; Su, Y.; Aoshima, T.; Fukuoka, A.; Hensen, E. J. M.; Nakajima, K. *ACS. Catal*. **2019**, *9*, 4277–4285.

(30) Prasad, S.; Khalid, A. J.; Narishetty, V.; Kumar, V.; Dutta, S.; Ahmad, E. *Mater. Sci. Energy.* Technol. **2023**, *6*, 502–521.

(31) Corma Canos, A.; Iborra, S.; Velty, A. *Chem. Rev.* **2007**, *107*, 2411–2502.

(32) German, D.; Pakrieva, E.; Kolobova, E.; Carabineiro, S. A. C.; Stucchi, M.; Villa, A.; Prati, L.; Bogdanchikova, N.; Corberán, V. C.; Pestryakov, A. *Catalysts.* **2021**, *11*, 115.

(33) Mishra, D. K.; Lee, H. J.; Kim, J.; Lee, H. S.; Cho, J. K.; Suh, Y. W.; Yi, Y.; Kim, Y. J. *Green Chemistry*. **2017**, *19*, 1619–1623.

(34) Xu, S.; Zhou, P.; Zhang, Z.; Yang, C.; Zhang, B.; Deng, K.; Bottle, S.; Zhu, H. *J. Am. Chem. Soc.* **2017**, *139*, 14775–14782.

(35) Chacón-Huete, F.; Messina, C.; Cigana, B.; Forgione, P. *ChemSusChem*. **2022**, *15*, e202200328.

(36) Zhu, J.; Yin, G. *ACS. Catal.* **2021**, *11*, 10058–10083.

(37) Mariscal, R.; Maireles-Torres, P.; Ojeda, M.; Sádaba, I.; López Granados, M. *Energy Environ. Sci.* **2016**, *9*, 1144–1189.

(38) Kamm, B.; Gerhardt, M.; Dautzenberg, G. (2013), *New and Future Developments in Catalysis*; pp 91–113; Elsevier B. V.

(39) Binder, J. B.; Blank, J. J.; Cefali, A. V.; Raines, R. T. *ChemSusChem*. **2010**, *3*, 1268–1272.

(40) Zhao, Y.; Lu, K.; Xu, H.; Zhu, L.; Wang, S. *Renewable and Sustainable Energy Rev.* **2021**, *139*, 110706.

(41) Slater, J. C. *J. Chem. Phys.* **1964**, *41*, 3199–3204.

(42) Zheng, B.; Huo, L. *Small Methods*. **2021**, *5*, 2100493.

(43) Horner, K. E.; Karadakov, P. B. *J. Org. Chem.* **2013**, *78*, 8037–8043.

(44) Cao, H.; Rupar, P. A. *Chem. Eur. J.* **2017**, *23*, 14670–14675.

(45) Chen, M. S.; Lee, O. P.; Niskala, J. R.; Yiu, A. T.; Tassone, C. J.; Schmidt, K.; Beaujuge, P. M.; Onishi, S. S.; Toney, M. F.; Zettl, A.; Fréchet, J. M. J. *J. Am. Chem. Soc.* **2013**, *135*, 19229–19236.

(46) Lee, S. M.; Lee, H. R.; Han, A. R.; Lee, J.; Oh, J. H.; Yang, C. *ACS Appl. Mater. Interfaces.* **2017**, *9*, 15652–15661.

(47) Gidron, O.; Diskin-Posner, Y.; Bendikov, M. *J. Am. Chem. Soc.* **2010**, *132*, 2148–2150.

(48) Liu, C.; Li, M.; Ma, H.; Hu, Z.; Wang, X.; Ma, R.; Jiang, Y.; Sun, H.; Zhu, S.; Liang, Y. *Research*. **2023**, *6*, 1-11.

(49) Yuan, D.; Sharapov, V.; Liu, X.; Yu, L. *ACS Omega*. **2020**, *5*, 68–74.

(50) Woo, C. H.; Beaujuge, P. M.; Holcombe, T. W.; Lee, O. P.; Fréchet, J. M. J. *J. Am. Chem. Soc.* **2010**, *132*, 15547–15549.

(51) Lin, J. T.; Chen, P. C.; Yen, Y. S.; Hsu, Y. C.; Chou, H. H.; Yeh, M. C. P. *Org. Lett.* **2009**, *11*, 97–100.

(52) Zhao, Z.; Nie, H.; Ge, C.; Cai, Y.; Xiong, Y.; Qi, J.; Wu, W.; Kwok, R. T. K.; Gao, X.; Qin, A.; Lam, J. W. Y.; Tang, B. Z. *Adv. Sci.* **2017**, *4*, 1700005.

(53) Gidron, O.; Dadvand, A.; Wei-Hsin Sun, E.; Chung, I.; Shimon, L. J. W.; Bendikov, M.; Perepichka, D. F. *J. Mater. Chem. C*. **2013**, *1*, 4358–4367.

(54) Kazantsev, M. S.; Frantseva, E. S.; Kudriashova, L. G.; Konstantinov, V. G.; Mannanov, A. A.; Rybalova, T. V.; Karpova, E. V.; Shundrina, I. K.; Kamaev, G. N.; Pshenichnikov, M. S.; Mostovich, E. A.; Paraschuk, D. Y. *RSC Adv.* **2016**, *6*, 92325–92329.

(55) Seixas De Melo, J.; Elisei, F.; Gartner, C.; Aloisi, G. G.; Becker, R. S. *J. Phys. Chem. A*. **2000**, *104*, 6907–6911.

(56) Guijarro, A.; Vergés, J. A.; San-Fabián, E.; Chiappe, G.; Louis, E. *ChemPhysChem*. **2016**, *17*, 3548–3557.

(57) Chen, Y.; Shen, P.; Cao, T.; Chen, H.; Zhao, Z.; Zhu, S. *Nat Commun.* **2021**, *12*, 1-13.

(58) Cordovilla, C.; Bartolomé, C.; Martínez-Ilarduya, J. M.; Espinet, P. *ACS. Catal.* **2015**, *5*, 3040–3053.

(59) The Nobel Prize in Chemistry **2010**. https://www.nobelprize.org/prizes/chemistry/2010/summary/ (accessed 2024-01-30).

(60) Duan, C.; Huang, F.; Cao, Y. *J. Mater. Chem.* **2012**, *22*, 10416–10434.

(61) Sherwood, J.; Albericio, F.; de la Torre, B. G. *ChemSusChem*. **2024**, e202301639.

(62) Messina, C.; Ottenwaelder, X.; Forgione, P. *Org. Lett*. **2021**, *23*, 7348–7352.

(63) Parakka, J. P.; Cava, M. P. *Synth. Met*. **1995**, *68*, 275–279.

(64) Li, W.; Zhang, J. *Chemical Communications*. **2010**, *46*, 8839–8841.

(65) Kondoh, A.; Aita, K.; Ishikawa, S.; Terada, M. *Org. Lett.* **2020**, *22*, 2105–2110.

(66) Wu, J.; Yoshikai, N. *Angew. Chem*. **2015**, *127*, 11259–11263.

(67) D'Alterio, M. C.; Casals-Cruañas, È.; Tzouras, N. V.; Talarico, G.; Nolan, S. P.; Poater, A. *Chem. Eur. J.* **2021**, *27*, 13481–13493.

(68) Shaughnessy, K. H. *Isr. J. Chem*. **2020**, *60*, 180–194.

(69) Milstein, D.; Stille, J. K. *J. Am. Chem. Soc*. **1978**, *100*, 3636–3638.

(70) Che, Y.; Niazi, M. R.; Chan, Q.; Ghamari, P.; Yu, T.; Ruchlin, C.; Yu, H.; Yan, H.; Ma, D.; Xiao, S. S.; Izquierdo, R.; Perepichka, D. F. *Angew. Chem. Int. Ed*. **2023**, *62*, e202309003.

(71) Koskin, I. P.; Becker, C. S.; Sonina, A. A.; Trukhanov, V. A.; Shumilov, N. A.; Kuimov, A. D.; Zhuravleva, Y. S.; Kiseleva, Y. O.; Shundrina, I. K.; Sherin, P. S.; Paraschuk, D. Y.; Kazantsev, M. S. *Adv. Funct. Mater*. **2021**, *31*, 2104638.

(72) Kazantsev, M. S.; Beloborodova, A. A.; Frantseva, E. S.; Rybalova, T. V.; Konstantinov, V. G.; Shundrina, I. K.; Paraschuk, D. Y.; Mostovich, E. A. *CrystEngComm*. **2017**, *19*, 1809–1815.

(73) Steen, A. E.; Ellington, T. L.; Nguyen, S. T.; Balasubramaniam, S.; Chandrasiri, I.; Delcamp, J. H.; Tschumper, G. S.; Hammer, N. I.; Watkins, D. L. *J. Phys. Chem. C*. **2019**, *123*, 15176–15185.

(74) Miyata, Y.; Nishinaga, T.; Komatsu, K. *J. Org. Chem*. **2005**, *70*, 1147–1153.

(75) Kimbrough, R. D. *Environmental Health Perspectives*. **1976**, *14*, 51-56.

(76) Barbosa, C. M. de L.; Ferrão, F. M.; Graceli, J. B. *Frontiers in Endocrinology*. **2018**, *9*, 256.

(77) Miyaura, N.; Yanagi, T.; Suzuki, A. *Synth. Commun*. **1981**, *11*, 513–519.

(78) Lennox, A. J. J.; Lloyd-Jones, G. C. *Chem. Soc. Rev*. **2014**, *43*, 412–443.

(79) Bussolari, J. C.; Rehborn, D. C. *Org. Lett*. **1999**, *1*, 965–967.

(80) Bilodeau, F.; Brochu, M. C.; Guimond, N.; Thesen, K. H.; Forgione, P. *J. Org. Chem*. **2010**, *75*, 1550–1560.

(81) Chacón-Huete, F.; Lasso, J. D.; Szavay, P.; Covone, J.; Forgione, P. *J. Org. Chem*. **2021**, 86, 515–524.

(82) Liu, J. T.; Hase, H.; Taylor, S.; Salzmann, I.; Forgione, P. *Angew. Chem. Int. Ed*. **2020**, *59*, 7146–7153.

(83) Dalcanale, E.; Montanari, F. *J. Org. Chem*. **1986**, *51*, 567–569.

(84) Jöbstl, D.; Husøy, T.; Alexander, J.; Bjellaas, T.; Leitner, E.; Murkovic, M. *Food Chem*. **2010**, *123*, 814–818.

(85) Liu, S.; Zhu, Y.; Liao, Y.; Wang, H.; Liu, Q.; Ma, L.; Wang, C. *Applications in Energy and Combustion Science.* **2022**, *10*, 1-13.

(86) Coumans, F. J. A. G.; Overchenko, Z.; Wiesfeld, J. J.; Kosinov, N.; Nakajima, K.; Hensen, E. J. M. *ACS Sustainable Chem. Eng.* **2022**, *10*, 3116–3130.

(87) Chang, H.; Motagamwala, A. H.; Huber, G. W.; Dumesic, J. A. *Green Chemistry.* **2019**, *21*, 5532–5540.

(88) Warlin, N.; Garcia Gonzalez, M. N.; Mankar, S.; Valsange, N. G.; Sayed, M.; Pyo, S. H.; Rehnberg, N.; Lundmark, S.; Hatti-Kaul, R.; Jannasch, P.; Zhang, B. *Green Chemistry.* **2019**, *21*, 6667–6684.

(89) Koskin, I. P.; Mostovich, E. A.; Benassi, E.; Kazantsev, M. S. *J. Phys. Chem. C*. **2017**, *121*, 23359–23369.

(90) Mannanov, A. A.; Kazantsev, M. S.; Kuimov, A. D.; Konstantinov, V. G.; Dominskiy, D. I.; Trukhanov, V. A.; Anisimov, D. S.; Gultikov, N. V.; Bruevich, V. V.; Koskin, I. P.; Sonina, A. A.; Rybalova, T. V.; Shundrina, I. K.; Mostovich, E. A.; Paraschuk, D. Y.; Pshenichnikov, M. S. *J. Mater. Chem. C*. **2019**, *7*, 60–68.

(91) Fitton, P.; Rick, E. A. *J. Organometal. Chem*. **1971**, *28*, 287–291.

(92) McDonald, I. M.; Black, J. W.; Buck, I. M.; Dunstone, D. J.; Griffin, E. P.; Harper, E. A.; Hull, R. A. D.; Kalindjian, S. B.; Lilley, E. J.; Linney, I. D.; Pether, M. J.; Roberts, S. P.; Shaxted, M. E.; Spencer, J.; Steel, K. I. M.; Sykes, D. A.; Walker, M. K.; Watt, G. F.; Wright, L.; Wright, P. T.; Xun, W. *J. Med. Chem*. **2007**, *50*, 3101–3112.

(93) Krasovskiy, A.; Krasovskaya, V.; Knochel, P. *Angew. Chem. Int. Ed*. **2006**, *45*, 2958–2961.

(94) Etherington, M. K.; Franchello, F.; Gibson, J.; Northey, T.; Santos, J.; Ward, J. S.; Higginbotham, H. F.; Data, P.; Kurowska, A.; Dos Santos, P. L.; Graves, D. R.; Batsanov, A. S.; DIas, F. B.; Bryce, M. R.; Penfold, T. J.; Monkman, A. P. *Nat Commun.* **2017**, *8*, 1-11.

(95) Praveen, P. A.; Muthuraja, P.; Gopinath, P.; Kanagasekaran, T. *J. Phys. Chem. A* **2022**, *126*, 600–607.

(96) Kowada, T.; Ohe, K. *Bull. Korean Chem. Soc*. **2010**, *31*, 577–581.

(97) Sonina, A. A.; Koskin, I. P.; Sherin, P. S.; Rybalova, T. V.; Shundrina, I. K.; Mostovich, E. A.; Kazantsev, M. S. *Acta Cryst.* **2018**, *74* , 450–457.

(98) Kazantsev, M. S.; Beloborodova, A. A.; Kuimov, A. D.; Koskin, I. P.; Frantseva, E. S.; Rybalova, T. V.; Shundrina, I. K.; Becker, C. S.; Mostovich, E. A. *Org Electron*. **2018**, *56*, 208–215.

(99) Wu, X.; Peng, X.; Dong, X.; Dai, Z. *Asian J. Chem.* **2012**, *24*, 927–928.

(100) Nejrotti, S.; Marra, F.; Priola, E.; Maranzana, A.; Prandi, C. *J. Org. Chem*. **2021**, *86*, 8295–8307.

(101) Talukdar, S.; Hsu, J.-L.; Chou, T.-C.; Fang, J.-M. *Tetrahedron Lett*. **2001**, *42*, 1103–1105.

(102) Do, J. L.; Friščić, T. *ACS. Cent. Sci.* **2017**, *3*, 13–19.

(103) Chacón-Huete, F.; Messina, C.; Chen, F.; Cuccia, L.; Ottenwaelder, X.; Forgione, P. *Green Chemistry*. **2018**, *20*, 5261–5265.

(104) Seixas De Melo, J.; Elisei, F.; Becker, R. S. *J. Chem. Phys.* **2002**, *117*, 4428–4435.

(105) Becker, R. S.; Seixas De Melo, J.; Maçanita, A. L.; Elisei, F. *J. Phys. Chem.* **1996**, *100*, 18683–18695.

(106) Zhao, C. X.; Liu, T.; Xu, M.; Lin, H.; Zhang, C. J. *Chinese Chemical Letters*. **2021**, *32*, 1925–1928.

(107) Constable, D. J. C.; Curzons, A. D.; Cunningham, V. L. *Green Chemistry*. **2002**, *4*, 521–527.